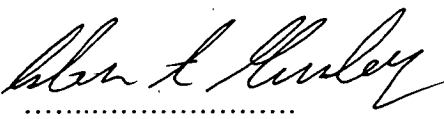


This thesis is not to be made available for loan or copying for two years following the date this statement was signed. Following that time the thesis may be made available for loan and limited copying in accordance with the Copyright Act 1968.

Signed 

February 1996

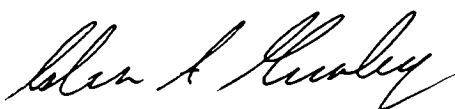
For Chas and Eve Hurley,
and especially for Espe.

"Learning without thought is labour lost; thought without learning is
perilous."

Confucius.

Declaration

To the best of my knowledge, this thesis contains no material which has been
accepted for the award of any other degree or diploma in any tertiary institution, or
which has been previously published or written by another person, except where
due reference is made in the text.

A handwritten signature in black ink, appearing to read 'Colin A. Hurley', written in a cursive style.

Colin A. Hurley

August, 1995

A spectroscopic analysis of carbons derived from heat treated phenolic-resins.

by

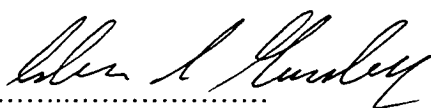
Colin A. Hurley, B.Eng. (RMIT)

**Submitted in fulfilment of the requirements for the degree
of**

**Doctor of Philosophy
University of Tasmania**

August, 1995.

This thesis is not to be made available for loan or copying for two years following the date this statement was signed. Following that time the thesis may be made available for loan and limited copying in accordance with the Copyright Act 1968.

Signed 

February 1996

For Chas and Eve Hurley,
and especially for Espe.

"Learning without thought is labour lost; thought without learning is
perilous."

Confucius.

Declaration

To the best of my knowledge, this thesis contains no material which has been
accepted for the award of any other degree or diploma in any tertiary institution, or
which has been previously published or written by another person, except where
due reference is made in the text.



Colin A. Hurley

August, 1995

Abstract

The aim of this study is to determine the degree to which the aromaticity of carbons produced from heat-treated (to 1000°C) acid-catalysed phenolic resins is altered when the resin precursors are combined with furfuryl-alcohol, paraformaldehyde and hexamine. Of fundamental importance to the research was the use of four novel techniques to provide the required information; Fourier Transform Infrared Spectroscopy, Solid State Nuclear Magnetic Resonance Spectroscopy, Laser Raman Spectroscopy and X-ray Photoelectron Spectroscopy. To this end, the techniques themselves are described in great detail to indicate their importance as analytical tools.

Between 180 and 350°C, paraformaldehyde is seen to provide a linearised *ortho-ortho* resin structure which greatly assists in cross-linking, and lattice formation at higher temperatures. In the 350 - 750°C range, the release of water is seen as the predominant pyrolysis reaction mechanism, followed by CH aliphatic bridge formation to 400°C. Below 400°C, a combination of furfuryl alcohol and paraformaldehyde creates the most cross-linked structure due to both resin additives providing methyl groups to the phenolic rings, thereby aiding cross-polymerisation. The cross-linking of the furfuryl-paraformaldehyde system is aided by the rapid removal of phenolic hydroxyl groups near 400°C. Double bonded carbon-carbon formation commences in all resins at ca. 550°C, and extensive polycondensation occurs at 600°C due to the removal of the CH and CH₂ aliphatic bridges. Rapid ring condensation occurs between 600 and 700°C and is mostly facilitated by the release of aromatic unsubstituted hydrogens (ring protons) below 700°C.

A more extensively formed poly-aromatic lattice exists in the furfuryl-paraformaldehyde system, than in the other resins at 700°C, as shown by the ring cluster diameter, D ; $D_{700} \approx 125 \text{ \AA}$ for LFP, $D_{700} \approx 50 \text{ \AA}$ for LFH, and $D_{700} \approx 20 -$

40 Å for HFH, HFP, NFH and NFP. As many functional groups are retained in the non-furfuryl containing resins, NFH and NFP, the poly-aromatic nuclei of these particular resins are observed as being small and poorly formed.

The surface chemistry of all the resins to 1000°C suggests that the surface reactions were very similar to the bulk reactions, such that there were no specific surface phenomena on these resins, and therefore these carbons show surface behaviour similar to glassy carbons. Between 900 and 1000°C the proportion of structural (lattice twisting) defects present in all resins is reduced, although an increase in defects due to the presence of hetero-atoms is shown. To 1600°C, the degree of lattice refinement is marginally favoured by the level of furfuryl-alcohol and paraformaldehyde, and by a higher pyrolysis heating rate. Between 1600 and 2200°C, these factors have little effect on degree of lattice refinement.

The recommendation is that a combination of paraformaldehyde and furfuryl-alcohol in a phenolic novolac resin matrix will provide for a highly cross-linked polymeric structure. Although non-graphitising, this furfuryl-paraformaldehyde-phenolic system will achieve a greater degree of lattice ring formation when heat treated to temperatures of at least 1000°C, than will a novolac cured resin containing only hexamine or paraformaldehyde.

Acknowledgments

The author would like to express his appreciation to the following people for their help and encouragement throughout the progress of this study; Dr Michael Ridd, Dr Barry O'Grady and Prof. Frank Larkins for their supervision and advice; Dr Paul Greenhill and Comalco Limited for their financial and technical assistance and the use of their library and laboratory facilities; Dr Graham Robottom and Mr Evan Peacock of the Central Science Laboratories of the University of Tasmania for their technical assistance with Raman, FT-Infrared and NMR Spectroscopy; Mr Marshall Hughes for his advice and assistance with the X-ray Photoelectron Spectrometer and various computer problems and Mr Peter Dove (mechanical technician), Mr John Davis (electronic technician), and Mr Michael Brandon (glassblower), all of the Chemistry Department of the University of Tasmania, for their technical assistance and advice in their respective fields; Dr Terry Mernagh of the Bureau of Mineral Resources for his assistance and advice with the BMR Laser Raman Microprobe Spectrometer; and not least of all, Ms Supanee Peschombut and Mr Scott Stark for their friendship and support.

Table of Contents

Chapter	Page
1. Introduction and Project Aim.	1
2. Literature Review.	6
Material Science of Carbon.	7
Phenol-Formaldehyde Resins	9
The Analytical Techniques used for the Characterisation of Phenolic Resin Pyrolysis Products.	13
<i>Thermal and Gas Phase Analysis</i>	13
<i>Infrared Spectroscopy</i>	14
<i>¹³C Nuclear Magnetic Resonance Spectroscopy</i>	21
<i>Laser Raman Spectroscopy</i>	29
<i>X-Ray Photoelectron Spectroscopy</i>	38
3. Experimental Procedure.	43
Sample Preparation.	44
Carbon Analyses Experimental Procedures.	48
<i>Thermo-Gravimetric Analysis</i>	48
<i>Elemental Analyses</i>	48
<i>Liquid Volatiles Analysis</i>	50
<i>Fourier Transform Infrared Spectroscopy</i>	53
<i>Solid-State ¹³C Nuclear Magnetic Resonance Spectroscopy</i>	54
<i>Laser Raman Spectroscopy</i>	57
<i>X-ray Photoelectron Spectroscopy</i>	59

	Chapter	Page
4.	An overview of the Phenolic Resin Pyrolysis Process (25-1000°C) by Thermo-Gravimetric, Elemental and Liquid Volatiles Analyses.	64
	Thermo-Gravimetric Analysis	65
	Elemental Analyses	71
	Liquid Volatiles Analysis	79
5.	The determination of the specific Phenolic Resin Pyrolysis Reaction Mechanisms (25-750°C) by Fourier Transform Infrared Spectroscopy.	88
	Fourier Transform Infrared Spectroscopy	89
6.	The determination of specific Phenolic Resin chemical and structural modifications during Pyrolysis (25-750°C) by Solid-State ¹³C Nuclear Magnetic Resonance Spectroscopy.	108
	Solid-State ¹³ C Nuclear Magnetic Resonance Spectroscopy.	109
7.	The determination of crystallite formation in the Phenolic Resin Chars during Pyrolysis (600-2200°C) by Raman Spectroscopy.	147
	Raman Spectroscopy	148
8.	The observation of alterations in the Surface Chemistry of the Phenolic Resin Chars during Pyrolysis (25-1000°C) by X-ray Photoelectron Spectroscopy.	166
	X-ray Photoelectron Spectroscopy	167

Chapter	Page
9 . The comparison of experimental data for the determination of the Phenolic Resin Pyrolysis Reaction Mechanism.	184
Pyrolysis Reaction Mechanisms of Novolac Phenolic Resins.	185
Further Study and Experimentation.	200
Bibliography	201

Chapter One

Introduction and Project Aim.

Glassy and other forms of partially ordered carbons are used extensively in a variety of electrochemical systems. There is a need to understand the chemical and crystallographic nature of solid carbons to relate the physical properties (mechanical wear, electrical conductivity, etc.) to the chemistry of the carbonaceous precursor materials (resins, low-rank coals, pitches, etc.). Of particular interest to this study is phenol-formaldehyde resin, a common precursor material for making high-temperature/high-toughness glassy carbons, which has found wide commercial application [Knop and Pilato,1985; Segal,1967].

When thermally degraded and carbonised, at heating rates lower than 20°C/min., to temperatures approaching 1000°C, phenolic resins can provide partially ordered glassy carbons that have micro-structural properties capable of withstanding chemically corrosive and physically erosive working environments [Kinoshita,1988]. As phenolic resins often incorporate cross-linking agents within their formulations to assist hardening of the as-cured resins at relatively low temperatures, the carbon produced can be greatly effected by the choice and amount of such hardening agents [Fitzer *et al*,1969; Fitzer and Schaefer,1970].

Because of the chemically inert nature of heat treated phenolic resins and their insolubility in most common solvents, many traditional methods of analysis, such as Gas or Liquid Chromatography, Mass Spectrometry, or the solution form of Fourier Transform Infrared- and Nuclear Magnetic Resonance- Spectroscopies, are found to be largely uninformative. The complexity and heterogeneity of the pyrolysis products of phenolic resins, which display similar chemical characteristics to high-rank coals [Ouchi and Honda,1959], cause these chars to be difficult to study, and impose limitations on any generalisations made about their properties and structural features.

Prior to 1980, the majority of research conducted on phenolic resins and their heat treatment products provided information derived from the chemical structures of the

liquid and volatile products of phenolic resin pyrolysis. The techniques previously employed include pyrolysis-gas chromatography [Christu *et al*,1969; Jackson and Conley,1964], mass spectrometry [Ouchi and Honda,1959; Shulman and Lochte, 1966], infrared spectroscopy [Conley and Bieron, 1963a, 1963b ; Conley,1970; Czuchajowski,1961; Ouchi,1966], thermo-gravimetric analyses [Lochte *et al*,1965] elemental analyses [Lochte *et al*,1965], diamagnetic susceptibility [Honda and Ouchi, 1955c,1955d; Honda and Sanada,1957; Ouchi,1955], electrical resistance [Honda and Ouchi,1955e; Ouchi,1955] and mechanical properties [Lausevic and Marinkovic,1986]. The major difficulty in using the above techniques is the speculative nature of the conclusions arising from the analyses.

During the 1980's more efficient analysis techniques were used to determine the structural parameters of pyrolysed phenolic resins. Improvements in the design and operation of solids analytical instruments, particularly with regard to more efficient detection electronics and computer technology, have provided better elucidation of the changes in chemistry taking place as the resins are heat treated.

Among the techniques now being used, Fourier Transform Infrared (FTIR), ^{13}C Solid State Nuclear Magnetic Resonance (^{13}C NMR), Laser Raman, and X-ray Photoelectron Spectroscopies (XPS) can be applied directly to analyse solid resin pyrolysis products in a non-destructive manner. The FTIR and ^{13}C NMR techniques are used as complementary methods and have become essential techniques in studying the chemistry of phenolic resins as they are heat treated to 1000°C. Laser Raman is useful in characterising the fully carbonised chars by detecting fundamental lattice vibrations and identifying the corresponding graphitic lattice and defect modes within the micro-structure. The technique of XPS is used to identify and, possibly, quantify the chemical species associated with the carbon surfaces.

Although the potential benefits of these techniques are well recognised and

documented, the majority of previous research in the chemistry of phenolic resin derived carbons has concentrated on the alteration of a particular chemical species within the resin over the heat treatment temperature range, or in the characterisation of the crystal structure of the high temperature chars. There has been particularly little research conducted on the effect that the cross-linking agents in the pre-cured resin have on the final carbon product.

It was, therefore, the objective of this project to identify and characterise the chemical mechanisms involved in the heat treatment of an acid catalysed phenolic resin as it was transformed into an isotropic partially-ordered carbon. This was undertaken with particular interest in the effect of the curing agents in the pre-cured resin formulation on the resultant carbons. Due to the uncertainty of the effect of the curing agents, three different groups of resins were used containing a conventional novolac (acid catalysed) pre-polymer with furfuryl-alcohol incorporated in the resin formulations to levels of 0%, 28.04% and 68.00% . Each of the three furfuryl-alcohol resin classes were also formulated containing either hexamethylenetetramine (hexamine) or paraformaldehyde in differing proportions.

Each of the six resin formulations were initially characterised by the traditional methods of thermo-gravimetric analysis and differential thermal analysis (TGA and DTA) to resolve the regions in the 25-1000°C temperature range where the major pyrolysis chemical reactions occur. Each resin was heat treated in an inert atmosphere in 50°C stages to 1000°C, and volatiles analysis by GC/MS was used to characterise the liquid organic species produced as a by-product of pyrolysis. The elemental carbon, hydrogen, oxygen and nitrogen compositions of solid pyrolysis products were determined as a function of heat treatment temperature to provide a general chemical analysis of the pyrolysis mechanism.

The FTIR analyses were performed to identify and qualitatively describe the degradation in the polymeric structure of the resins as the hydroxyl groups and

methylene aliphatic chains are broken to allow condensation of the benzene rings present in the phenolic polymer structure. Solid-state ^{13}C NMR experiments were conducted to quantitatively measure the proportion of aromatic and aliphatic components within the solid pyrolysis products, and to describe the condensation mechanism of the benzene rings by the measurement of several polymeric structural parameters. These experiments were undertaken using the techniques of cross-polarisation magic-angle-spinning (CP-MAS) and total suppression of spinning sidebands (TOSS) to obtain the high-resolution spectra of the resin chars. Cross-polarisation dynamics, and the pulse technique of dipolar dephasing were implemented with the TOSS sequence to provide the complex structural information.

The 1000°C carbons were additionally heat treated to 1600°C and 2200°C, and these carbons were analysed by Laser Raman spectroscopy. The ratio of the graphite lattice vibration to the defect bands was determined to semi-quantitatively describe the development of any ordered lattice formation in the resin chars. A near complete pyrolysis mechanism is then established for the six resins, and the effect of the furfuryl-alcohol as a hardening agent is explained.

Although a high error relative to the other analyses was found, the alteration of the elemental surface carbon, oxygen and nitrogen components of the resin chars over the 25-1000°C range was determined by XPS. Surface oxidation of the carbons species was investigated by deconvolution of the C1s envelope into the graphite and oxide components, and comparing the relative areas of each band.

Chapter Two

Literature Review.

Material Science of Carbon

Carbon as an element has the unique ability to bond with itself principally via sp^3 (diamond-like) and sp^2 (graphite-like) hybridisation. The resultant structures have a wide range of possibilities, but for most of the materials used in carbon science these structures can be considered as being composed of mainly graphitic sub-units, with more or less structural order, joined together by less ordered regions [Edwards,1989].

The bulk structures of the more ordered carbons are essentially graphitic, with small volumes having an almost perfect graphite lattice. As the volume increases, the presence of defects, distortions and hetero-atoms destroys the regularity, hence providing for a very disordered material. All graphites contain defects within their structures, i.e. stacking faults, dislocations, vacancies and interstitial atoms [Amelinckx *et al*,1965].

Most carbon materials are composites of ordered graphite-like regions with a high degree of anisotropy, and regions of lower order where the structure is, for most analyses, isotropic. The process of conversion of less ordered into more ordered material via heat treatment, known as carbonisation or graphitisation, is of major concern to the carbon industry. The range of structures encountered in this increase in order during the carbonisation process is wide and varied [Marsh and Griffiths,1982].

Not all disordered carbon forms can be easily graphitised, even though the degree of graphitisation is determined by the temperature of the heat treatment and the annealing time. Non-graphitisable carbons are defined as those which cannot be transformed into graphitic carbon solely by heat treatment up to 3000K under atmospheric or lower pressure, and graphitisable carbons are those which are so converted [Marsh and Menedez,1989].

Non-graphitisable carbons are generally produced from wood, nut-shells and non-fusing coals. The macro molecular (polymeric) structure of these materials remains during heat treatment only losing small molecules by degradation, and developing even more cross-linking so that fusion cannot take place. The loss of small molecules and retention of the complex macromolecular structure leads to high micro porosity, with surface areas in the order of $1000 \text{ m}^2\text{g}^{-1}$ [Edwards,1989]. Isotropic, non-graphitisable carbons originate from materials which are already macromolecular in nature. Apart from those already stated, they include the specific cross-linked structures (C-O-C bondings) of low rank coals such as peats, lignites, brown coals and non-caking bituminous coals. Of more relevance to this study, synthetic resins of the chemical industry, such as phenolic resins, polyfurfuryl-alcohol and polyvinylidene chloride are of a similar nature [Marsh and Menedez,1989].

Although not fully understood, in the early stages of carbonisation the thermal collapse of macromolecular systems is known to involve the elimination of small molecules as volatile material in the form of water, methanol, methane and carbon dioxide [Fitzer *et al*,1969; Fitzer and Schaefer,1970]. This elimination of volatiles creates space or micro-porosity within the rigid macromolecular system and, simultaneously, the radicals generated at the surface either combine with each other or abstract hydrogen from the system. Industrial carbons are obtained from materials such as cellulose and resins because a cross-linked, and possibly heterocyclic polymer already exists in the parent material.

Phenol-formaldehyde Resins

Because of their good ablative properties, phenolic resins are often used as high temperature polymers [Schmidt,1971; Segal,1967], as well as in other commercial applications [Whitehouse *et al*,1967].

Phenols are a family of aromatic compounds with the hydroxyl group bonded directly to the aromatic nucleus. Although they have been used for many decades, detailed chemical understanding of their formation and cure has been speculative and not fully elucidated [Keutgen,1968; Knop and Scheib,1979; Martin,1956; Megson,1958]. Formaldehyde is virtually the only carbonyl component for the synthesis of technically relevant phenolic resins, although special resins can also be produced from other aldehydes, such as acetaldehyde, furfural or glyoxyl, but these have yet to receive commercial attention. A detailed description of the production and physical properties of both phenol and aldehydes has been given [Knop and Pilato,1985].

Phenolic resins are obtained by step-growth polymerisation of di-functional monomers (aldehydes) with monomers of functionality greater than 2 (phenol). Phenols as monomers possess a functionality of 1 to 3 depending on substitution. The temperature and pH conditions under which reactions of phenols with formaldehyde are carried out have a profound effect on the characteristics of the resulting product. Three reaction stages for the production of phenol-formaldehyde resins are considered as follows; (i) formaldehyde addition to phenol, (ii) chain growth or pre-polymer formation, and, finally, (iii) the cross-linking or curing reaction. Two pre-polymer types are obtained depending on pH, with the rate of reaction at pH 1 to 4 being proportional to the H^+ concentration, and above pH 5 being proportional to OH^- concentration, indicating a change in reaction mechanism.

Polymerisation of phenol-formaldehyde in the presence of an acid catalyst results in a linear chain condensation product which contains methylene linkages almost quantitatively, and this product is referred to commercially as *novolac* [Conley,1970; Ishida *et al*,1981; Kumar *et al*,1980]. This form of phenolic resin is obtained by the reaction of phenol and formaldehyde in a strongly acidic pH range and molar ratio of 1 mol phenol to 0.75 - 0.85 mol formaldehyde. The resins are linear or slightly branched condensation products linked with methylene bridges, having relatively low molecular weights up to approximately 2000. These resins are soluble and permanently fusible (thermoplastic), and can only be cured to insoluble and infusible (thermosetting) products by the addition of a hardening agent. This is almost always provided as hexamethylenetetramine (HMTA, or *hexamine*, as it is more commonly known.)

Resoles are produced by alkaline reaction of phenols and aldehydes, with the aldehyde being used in excess. Typical phenol/formaldehyde ratios are between 1:1.0 and 1:3.0. These are mono- or poly- nuclear hydroxy methyl phenols (HMP) which are stable at room temperature, but are transformed into three dimensional, cross-linked, insoluble and infusible polymers by the application of heat.

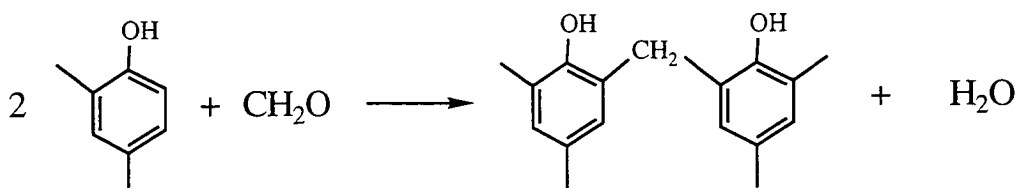
The methylene bridge is thermodynamically the most stable cross-link site, and is prevalent in both *ortho* and *para* positions in cured phenolic resins. Theoretically, 1.5 mol of formaldehyde is required for the complete three dimensional cross-linking of 1 mol of phenol. Because of possible molecular shielding, or for other steric reasons, as the oligomer increases in size not all reactive sites are accessible to formaldehyde, so generally an excess of formaldehyde is supplied in resin manufacture to meet product specifications. Only the production of novolac resins, i.e. those produced under acidic conditions, will be discussed in this report. Mechanisms of resole formation can be found in many studies [Knop and Pilato,1985; Zinke,1951].

Normal resins formed in strongly acidic pH ranges show methylol substitution and methylene bridge formation favouring the *para* position, with no *meta* substitution and the extent of *ortho* substitution being further reduced by high acidity. In contrast, novolacs favour high-*ortho* substitution in pre-polymer formation, with the accessibility of the vacant *para* position enhancing cure rate.

Curing of the thermoplastic novolac pre-polymer resins requires the addition of a cross-linking agent, which is usually hexamine, but in rare cases paraformaldehyde or trioxane. Novolacs, which are generally made at a phenol/formaldehyde ratio of 1:0.8, are cured by the addition of between 8 and 15 % hexamine, with the most commonly employed level being 9 - 10 %. The cross-linking reaction, which is enhanced by the presence of free phenol and water, is accompanied by the liberation of a considerable amount of gas phase material. This gas is shown to consist of at least 95% ammonia, leaving a cured resin which may contain up to 6% chemically bound nitrogen. Products containing the azomethine group $-\text{CH}=\text{N}-$, amongst others, are formed. This accounts for the yellow colour of the oligomers [Knop and Pilato,1985].

The assembly of phenolic units that are connected by methylene groups is conducted primarily by two reactions;

a) The direct condensation with formaldehyde, leading to symmetrical structures:



b) The condensation of hydroxymethyl derivatives with other phenols, which can generate non symmetrical structures.

These two reaction mechanisms provide for four general types of phenolic compounds if more than three phenolic units are connected by methylene bridges, as shown in Figure 2.1.

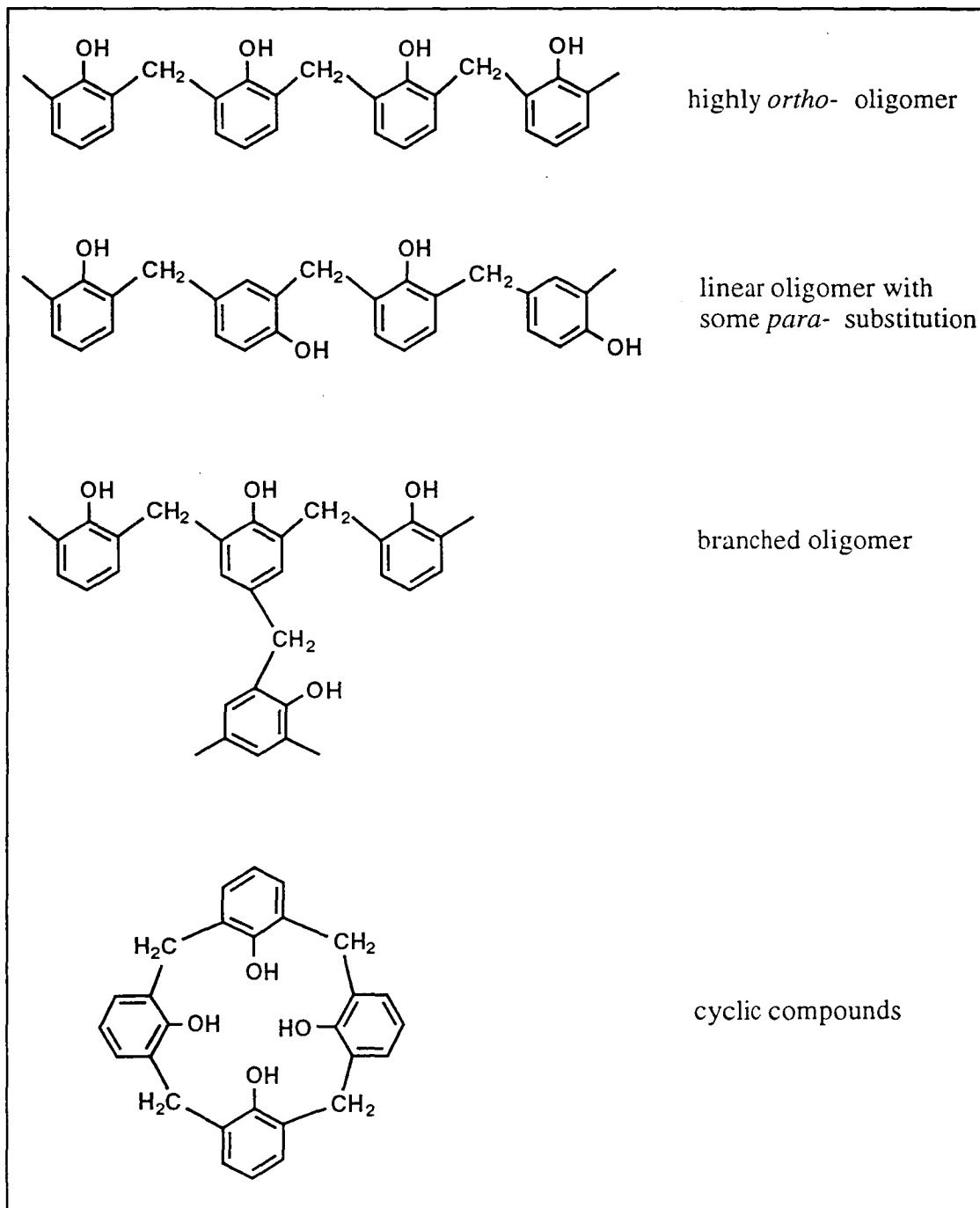


Figure 2.1 The four general types of novolac phenolic compounds produced when greater than three phenolic units are connected by methylene bridges.

The Analytical Techniques for Characterisation of Phenolic Pyrolysis Products

Thermal and Gas Phase Analysis:

Useful information regarding the mechanism of pyrolysis can be obtained by a combination of thermogravimetric and differential thermal analysis. There are several good reviews available for TGA, DTA and also TVA (thermal-volumetric analysis) methods [Slade and Jenkins,1966; Wendlandt,1964], particularly for the TGA pyrolysis of important polymers [Madorsky,1964; Perkins *et al*,1966; Fitzer *et al*,1969; Fitzer and Schaefer,1970; Shulman and Lochte,1966].

It was discovered from TGA/DTA that, basically, three temperature regions exist for pyrolysis of phenolic type resins; 25-250°C, 250-560°C and 560-1000°C, with the middle region being that where the main volatile evolution processes exist [Simitzis,1991; Lochte *et al*,1965]. The use of gas chromatography for pyrolysis analysis is reported in several reviews [Lausevic and Marinkovic, 1986; Levy,1967], and the use of elemental analyses by Ouchi [Ouchi,1955] and Honda [Honda and Ouchi,1955e] provided some information about the pyrolysis of resole chars.

The function of carbon black to lower volatile evolution from novolac pyrolysis was discussed in relation to the nature of partially ordered carbon as a complex organic material [Bansal and Dhami,1980; Coughlin *et al*,1968; Mattson *et al*,1969], with effective adsorbent properties for organic liquids and gases [Rivin and Illinger,1969]. This is suggested to be due to the surface groups being more stable and providing surface condensation reactions that are less reversible than the van der Waal's bonds of the less functionalised graphite surface [Given and Hill,1969].

Infrared Spectroscopy:

Infrared spectroscopy (i.r.) is useful in the analysis of solid carbonaceous pyrolysis products due to its ability to describe the solid product itself, rather than by indirect analysis of the volatile residuals. Czuchajowski [1961] provided a discussion of limited detail describing the changes observed in the i.r. spectrum of a phenol-formaldehyde resin during pyrolysis, and Ouchi [1966] used i.r. to postulate a mechanism for the structural changes during the pyrolysis of a resole resin, and to confirm his results from other techniques [Honda and Ouchi 1955a, 1955c, 1955d, 1955e; Ouchi, 1955; Ouchi and Honda, 1956, 1959]. Infrared spectroscopy has elucidated degradation mechanisms of cured novolacs as well as structural features [Conley, 1970; Lindberg *et al*, 1975; Mukoyama and Tanno, 1973; Secrest, 1965].

From a study by Morterra and Low, the i.r. technique of photothermal beam deflection spectroscopy was used to determine the degradation mechanism for the pyrolysis of a novolac type resin to a char [Morterra and Low, 1985a]. There was a particular interest in the comparison between pyrolysis *in vacuo*, and under a stream of N₂. As their study represented similar findings to the FTIR work of this report, the band assignments used were seen to be useful for the assignment of the i.r. spectra of the six cross-linked novolac resins in this study (Table 5.1). There was the suggestion of disagreement of some of the major bands, although most of the previous work had been conducted on resole resins and therefore were considered as being different to some of the infrared bands found in novolac resins.

It was shown that the pyrolysis of a novolac can be placed into three temperature regions; pyrolysis up to 350°C; between 350 and 520°C; and pyrolysis above 560°C [Morterra and Low, 1985a]. Generally, up to 350°C there is an elimination of water from the starting material, shown by the analysis of bands at 3340 and 1650 cm⁻¹, the latter being the scissor deformation of a water impurity. Also the evaporation of oligomers present in the starting material is shown by the similarity in infrared

spectra between the solid and volatile residues up to 350°C. It was also observed that in the pyrolysis of a resole, *in vacuo*, up to 350°C, adjacent phenolic hydroxyl groups are seen to react forming diphenyl-ether linkages and evolving water. Fragmentation of oligomers was likely to be caused by the cleavage of some methylene bridges, the process of which was seen to compete with branching and cross-linking of the chains in the residue at the active ring position [Winkler and Parker, 1971]. A decrease in the concentration of 1,4- and 1,2,4- tri-substitution was matched by an increase in 1,2,4,6- tetra-substitution, as shown by the ring stretch vibration 1480 cm⁻¹ and the out-of-plane CH deformation band at 880 cm⁻¹. This shows that thermal branching and cross-linking of novolacs happens at low temperatures without cross-linking agents, and which suggests that the diphenyl-ether structures at this stage have great significance. The greater degree in dehydration and fragmentation evolution of the pyrolysis *in vacuo* up to 350°C was considered to be likely as the vacuum is considered to be more efficient in removing evolved material than an N₂ stream.

Up to heat treatment temperatures of 500 - 520°C the results of Morterra and Low [1985a] show no difference between pyrolysis *in vacuo* or in an N₂ stream, and this spectroscopic observation has been confirmed by the work of Camino *et al* [1982]. Towards 500°C the N₂ pyrolysed resin develops diphenyl-ether linkages from OH-HO condensation, as well as triphenyl-methane formation from the reaction between adjacent hydroxyl groups and methylene bridges, with water as a by-product [Ouchi, 1966]. Occuring simultaneously is increased poly-substitution of the aromatic system as shown by the increased complexity of the 900 - 800 cm⁻¹ absorptions, ascribable to the wagging of isolated aromatic CH groups. The formation of a highly conjugated carbonyl group at ca. 1650 cm⁻¹ was attributed by Morterra as a benzophenone bridge replacing a methylene bridge [Morterra and Low, 1985a]. In contrast to the i.r. resole studies of Conley [Conley and Bieron, 1963a, 1963b; Conley, 1965] and Ouchi [1966], this wasn't considered an important pathway in novolac pyrolysis.

Above 560°C, Morterra describes a single symmetrical band formed at 1600 cm⁻¹, with a band width of approximately 100 cm⁻¹. This band, which had been reported to exist with all oxidised carbons [Morterra and Low,1983,1985b] was shown to be due to the C=C stretch in poly-aromatic systems made i.r. active by an oxidic layer. Aromatic CH groups were considered to be the only detectable vibrations, as seen in the 900 - 700 cm⁻¹ region. The novolac chars of Morterra were shown to be indistinguishable from chars of cellulosic and other ternary (C,H,O) compounds [Morterra and Low,1983]. This was suggested to show complete elimination of aliphatic residues, which is in part due to the oxygen ether bridges entering into the poly-nuclear system by transformation into pyran/furan rings [Fitzer and Schaefer,1970]. The existence of a semicircle ring stretching vibration at 1435 cm⁻¹, as a shoulder of a much broader ether-like band, suggested the possibility of short ranged order or small domain size of the poly-aromatics. The chars produced at and above 700°C show no elemental oxygen or hydrogen [Delhaes *et al*,1981] and no residual i.r. structure between 2000 and 500 cm⁻¹, similar to the strong continuum absorption of most high temperature carbons. Therefore, Morterra and Low [1985a] suggested that the pyrolysis technique, i.e. the heating rate and carrier gas, had little effect on the pyrolysis mechanism as demonstrated by Conley [Conley and Bieron,1963a,1963b; Conley,1965]. Unlike these studies and others [Fitzer *et al*,1971] it was put forward that auto-oxidation wasn't a major degradation pathway and that the condensation of phenolic groups with methylene bridges to form diphenylmethane structures [Fitzer and Schaefer,1970] and the formation of diphenyl-ether type linkages between benzene nuclei with the elimination of water was equally if not more important [Ouchi,1966]. Working with a novolac resin, Camino *et al* concluded that, during pyrolysis, thermal cross-linking occurred without significant modification of the main chemical structure of the polymer and especially did not involve oxidative reactions [Camino *et al* ,1982]. It was suggested by Morterra that the preparation conditions of the polymer, and therefore its nature, is at least as important as the pyrolysis conditions in

determining the degradation mechanism [Morterra and Low,1985a].

From the volatiles and infrared analyses of the solid resin pyrolysis products, it was suggested that hindered diffusion in the bulk samples provided for the formation of a variety of unstable structures with unsaturated bonds, as supported in a previous study [Yamashita and Ouchi,1981]. Due to the complex and unstable structure, and the creation of high pressures within the polymer, the following reactions were considered to further exist in the bulk sample. The H_2O produced by the dewatering reaction between hydroxyl and methylene groups is likely to react further with methylene bridges to form ether type bonds, thereby evolving CO and H_2 . This is seen as the first H_2 evolution reaction. Methane is formed by the reaction of H_2 with the methylene bridge to cause scission of the chain, and H_2 is evolved above $500^\circ C$ due to the aromatisation of the polymeric structure. This information was considered to be important when deciding the correct procedure for the fabrication of glassy carbons from either bulk or powdered phenolic resins.

Simitzis used FTIR to observe the structural changes of cellulose/polyfurfuryl-alcohol and cellulose/furfuryl-alcohol-formaldehyde resin composites during inert atmosphere pyrolysis [Simitzis,1991]. The curing and pyrolysis of these systems was reported as being similar to phenolic resins [Fitzer *et al*,1971]. The i.r. spectra for the initial as-cured resins show similar information for polyfurfuryl-alcohol (PFA) and furfuryl-alcohol/formaldehyde (FA-F) resins, but that the FA-F contains more hydroxyl groups. From the furan ring peak assignments at 3126, 1564 and 1357 cm^{-1} , it was found that a PFA/cellulose composite contained little residual furfuryl-alcohol in the cured system. The spectra generally showed no change for either PFA, FA-F or their cellulosic composites up to $300^\circ C$. Between 300 and $400^\circ C$ it was found that the methylene bridges (at ca. 2920 cm^{-1}) were removed to form methane, and the furan C-O-C bonds (1710 cm^{-1}) were being destroyed due to the breaking of the furan rings in this temperature range. The unfilled PFA resin at $500^\circ C$ was seen to have a strong absorbance at 1613 and 1428 cm^{-1} due to the

C=C double bonds of the initial furan ring being ruptured at such high temperatures to form poly-aromatics. In comparison the pyrolysis of cellulose in the 400-500°C range gives little evidence of OH and CH bands above 400°C, and C=O, which is very weak at 450°C, diminishes at higher temperatures. In the cellulose the band at 1613 cm⁻¹ (the skeletal vibrations of aromatic rings) dominates the 400 - 500°C spectra due to the conjugated C=C bonds, suggesting the formation and growth of aromatic systems [Tang and Bacon,1964]. As a further comparison it was shown [Perkins *et al*,1966] by infrared spectroscopy that chars of cotton fabric begin to show a typical pyrolysis pattern at 360°C by formation of bands near 1720 cm⁻¹ (carbonyl) and at 1620 cm⁻¹ due to C=C bonds.

From the diffuse reflectance FTIR (DRIFT) studies of Young, the characterisation was made of the alteration of a polyimide/carbon composite due to thermal cycling up to 250°C in air [Young and Chang,1988]. As with other studies [Conley and Bieron,1963a,1963b; Conley,1965], the oxidation of the methylene bridges to carbonyl groups on the composite surface was discovered. Evidence for incomplete cross-linking was also shown. This was suggested by the relative increase of the carbonyl group between two phenyl rings at 1660 cm⁻¹ and 930 cm⁻¹ in relation to a decrease in the methylene bridges at 1500 cm⁻¹. From previous work with the DRIFT technique [Young and Chang,1988], and polyimides [Jewell and Sykes,1977], it was found that the carbonyl conjugation between phenyl rings is typical of these systems, although it is only found at the surface of the polymer with no evidence of methylene bridge oxidation in the interior.

Using the complementary techniques of FTIR and ¹³C nmr to elucidate the reaction mechanism of the curing process between phenol and hexamethylenetetramine (hexamine), it was discovered that during the reaction, primary, secondary and tertiary hydroxybenzylamines were produced as reaction intermediates [Sojka *et al*,1979]. The growth and decay of these intermediates was monitored in association to the formation of methylene bridges. The disappearance of hexamine

was discovered by both nmr and FTIR to occur early in the reaction, although a difference in *detectability* between the two techniques was shown by the observation of two different hexamine rates of decay. The phenolic ring was observed to find preference for the reaction at the *ortho* position, and further cross-linking was found to occur late in the reaction.

Chiu used a combined GC/FTIR technique known as matrix-isolation FTIR to isolate and identify poly-cyclic aromatic compounds in pollutant streams [Chiu and Biemann,1984]. The i.r. band assignments from that work were used to confirm some of those used in this study.

FTIR was used by Solomon to determine the hydroxyl concentration of coals and related chars [Solomon and Carangelo,1988]. Quantitative reproduction of spectra was found to be within $\pm 5\%$ and Beers Law was followed for concentrations in the range of 0.3-1.3 mg of coal/cm². Although a broad absorbance may appear in the range of 2000-3600 cm⁻¹ as a result of H-bonded OH from spurious water, the correct preparative techniques of drying the sample is shown to provide a simple method of estimating the hydroxyl content of a coal quantitatively. Therefore good results can be obtained despite the problem of water interference, by using the 3200 cm⁻¹ band, and the problem of scattering can be minimised by the use of rectilinear baseline subtraction. From quantitative FTIR, the hydroxyl oxygen concentration could be determined to an accuracy of $\pm 10\%$.

Solomon also used quantitative FTIR for the determination of aliphatic and aromatic hydrogen in coals [Solomon and Carangelo,1988]. Mathematical and regression analysis were used to determine absorptivity (relating concentration to peak areas in the FTIR spectra) for coals and chars. The aromatic C-H stretching region at 3100 cm⁻¹ was suggested to be particularly sensitive to oxygen concentration, and therefore the 800 cm⁻¹ wagging mode was used. A similarity of results between FTIR and nmr existed for the determination of aliphatic hydrogen for coals of all

rank, although the similarity between the two techniques for the determination of aromatic hydrogen existed for coals of above 85% carbon, with discrepancies remaining for those below 85% carbon concentration. This similarity between techniques was supported for high rank coals by the work of Supaluknari [1989].

Painter *et al* [1981b] conducted a critical assessment of the FTIR technique in its application of the characterisation of coal structures. Disagreement of band assignments were considered with the conclusion that a strong 1600 cm^{-1} band was discovered and assigned to an aromatic ring stretching mode in coals, enhanced by phenolic rings. Computer routines were used to determine the concentration of OH and CH groups, and established criteria for curve fitting was applied to the problem. Qualitative identification of functional groups was achieved, although consistent quantitative measurements were suggested to require a determination of the relationship between extinction coefficients of resolved bands. An earlier study by Painter had used a similar quantitative technique of least-squares fitting of FTIR spectra to determine the mineral matter in coals [Painter *et al*, 1981a].

Meldrum *et al* used various FTIR band assignments to determine the carbon/oxygen surface species found on carbonaceous materials oxidised in air [Meldrum and Rochester, 1990]. A similar study was undertaken by Ianniello using the DRIFT technique to determine the surface species on chemically modified carbonaceous materials [Ianniello *et al*, 1983]. Comparisons were made between graphite, graphitic oxide and activated carbon and these were found to be responsive to the technique only if the materials had high surface area and relatively high surface oxide concentration.

Solid State ^{13}C Nuclear Magnetic Resonance Spectroscopy:

The application of ^{13}C NMR to the study of carbonaceous solids has only come about relatively recently by the advent of the modern spectrometers with their ability to operate with very high speed switching radiofrequency electronics. The pioneering work of Shaefer *et al* combined the techniques of High Power proton dipolar decoupling (DD), magic angle sample spinning (MAS) and cross-polarisation (CP), thereby providing high resolution solid state ^{13}C nmr, which has subsequently been widely used [Schaefer and Stejskal,1976; Schaefer *et al*,1977].

Laupretre has discussed the combined application of these techniques in depth as an investigative tool into the structure of polymeric systems; with many related studies being cited [Laupretre,1990]. From this work an attempt was made to indicate the principles on which the solid state nmr experimental method is based. The resolution enhancing capabilities of High Power proton decoupling, magic angle spinning and cross-polarisation are discussed in detail, with particular reference to their mathematical derivations.

The value of High Power proton decoupling was explained relatively early, such that by irradiating protons with a strong radio frequency field in the neighbourhood of their Larmor frequency, the heteronuclear ^{13}C - ^1H dipolar broadening, which is a problem with protonated carbon species, can be removed [Bloch,1959].

The theory of magic angle spinning has been described well [Andrew,1971; Yannoni,1982]. In this technique it is found mathematically that by spinning the sample at sufficient angular frequency at the magic angle of 54.7° , there is a zero averaging of chemical shift contributions to each carbon in a solid matrix from its neighbouring orientations. The problem with this method of line narrowing is that the spinning itself can create side bands which may confuse or distort the value of the 'real' peaks. If the spinning speed is large relative to the chemical shift

anisotropy, the side bands can be spread out and the spectrum will consist of one peak per magnetically non-equivalent carbon.

By the use of an appropriate pulse sequence, such as the TOSS sequence designed by Dixon [1981,1982], it is possible to suppress the spinning side bands artificially and to recover easily tractable spectra. Calculations by Olejniczac and co-workers have shown that the TOSS sequence provides low error when the side bands are small, but when they are large the TOSS sequence cannot provide any quantitative estimate of the chemical structure of an unknown sample [Olejniczac *et al*,1984].

A further problem found in the solid state nmr of rare spins such as ^{13}C nuclei is the lack of sensitivity. A method, which is known as cross-polarisation, of increasing the ^{13}C magnetisation by transferring a small fraction of the proton magnetisation to the carbon spin system, has previously been described [Pines *et al*,1973]. This technique is achieved by spin-locking the protons with an radiofrequency (r.f.) field, parallel to the proton rotating frame magnetisation. During the proton spin-lock time, a second r.f. field is applied at the carbon resonance frequency under the Hartmann-Hahn condition [Hartman and Hahn,1962], establishing thermal contact so that the energy levels of the protons and carbons become equal in the doubly rotating frame. After transfer of proton magnetisation it is possible to multiply the carbon magnetisation by a factor of four at most.

The cross-polarisation experiment can be used to quantify carbon species in a carbonaceous solid by variation of the spin contact time, and the quantitative character of such determinations has been evaluated by several authors [Fyfe *et al*,1979; Maciel *et al*,1979; Resing *et al*,1978; Retcofsky and Vanderhart,1978]. Problems from this experiment arise when studying heterogeneous materials where the proton spin-lattice relaxation in the rotating frame is not simply described by a simple relaxation time [Earl and Vanderhart,1979]. Various studies exist explaining

general examples of the use of the CP/MAS technique [Fyfe *et al*,1978; Lyerla and Yannoni,1982; Schaefer and Stejskal,1976; Yannoni,1982].

The work of Fyfe outlines in various studies the use of these line narrowing techniques in solid state ^{13}C nmr for the investigation of the thermal decomposition of a cured resole [Fyfe *et al*,1983a,1983b]. A resole formulated with 5% ^{13}C enriched formaldehyde was used to follow the mechanism of air and vacuum pyrolysis of such a resin [Fyfe *et al*,1983a,1983b]. Using a 1 millisecond contact time and 1 second delay between each acquisition, quantitatively reliable spectra were achieved. A nonprotonated carbon selection experiment was used to discriminate between the unsubstituted *meta* and substituted *ortho* and *para* methylene bridge positions on the phenolic ring. In this experiment, a 50 μs decoupler-off delay was applied between the cross-polarisation contact time and the acquisition of the free induction decay (FID) signal. As only non-protonated carbons were observed in such spectra, subtraction of the dipolar decoupled spectra presented the signals representing directly bonded protons. The dipolar dephasing experiment is well described in other studies [Opella *et al*,1979].

It was shown that the spectra discriminate in favour of functionalities derived from the formaldehyde-based portion of the resin and against such species as quinones derived from the phenol, although evidence from the unenriched samples show that the carbonyl/acid reaction mechanism is not the major reaction pathway [Fyfe *et al*,1983b]. From a comparative experiment, it was seen that approximately 10% of the aromatics are formed from the linking aliphatic groups, and from a confirmation by i.r. data it was suggested that much of the char heated to temperatures greater than 400°C was made up of poly-cyclic structures. It was also shown by nmr that the C=O bridges were eliminated with the biphenyl-type units remaining.

Further studies showed that when a resole is pyrolysed under vacuum to 400°C it suffers a loss of methylol groups, followed by complete methylene bridge

formation, although there is largely no change in the polymer structure [Fyfe *et al.*, 1983b]. The sample was seen as more stable under vacuum, and when reheated in air at 300°C it was seen to follow the same previously described oxidation sequence of acidic and ketonic carbonyl functionalities, confirming that these oxidised functionalities are not from methylol groups.

From the study of Amram, a resole resin was carbonised by laser pyrolysis at 50W/cm², and the chars analysed by solid state ¹³C nmr [Amram and Laval, 1989]. As no direct temperature measurement could be made, laser heating times were varied to approximate an increase in degree of pyrolysis. Two experiments were conducted using the nmr with the first experiment using a normal CP/MAS pulse sequence but varying the contact time between 0.25 and 10 ms. This technique was used to mathematically determine a theoretical carbon magnetisation such that there was no cross-polarisation, M_0 . As M_0 is found to be proportional to the number of carbons of its kind, and as it was considered that there were only aromatic and aliphatic carbons present in the chars, the fraction of aromatic carbons, f_a , was determined.

The second experiment used by Amram and Laval [1989] was to analyse the chars by the dipolar dephasing technique, which is similar to the conventional cross-polarisation experiment except for the introduction of a delay between the contact time and acquisition of the FID [Opella *et al.*, 1979]. In this experiment protonated and non-protonated carbons species could be discriminated by their relaxation properties and the ratio of quaternary to tertiary carbons, $f_{q/t}$, was determined for the chars.

The assignment of the described peaks [Amram and Laval, 1989] was made to those of a solution-state reference [DeBreet *et al.*, 1977], and calculations from empirical parameters [Wehrli and Wirthlin, 1976]. For the unpyrolysed resin, the aliphatic peak was shown due to methylene bridges, and the aromatic peaks were assigned

as due to hydroxyl carbons, C_{ar} -OH (152 ppm) and ring carbons, C_{ar} (130 and 116 ppm). There was a noted absence of unsubstituted *para* aromatic carbons (no resonance at 120 ppm). For the unpyrolysed resin, the structural parameters were found to be $f_a = 0.85$, and $f_{q/t} = 0.82$. As the theoretical values for a highly cross-linked resin would be $f_a=0.86$ and $f_{q/t}=1.00$, it was considered that the unpyrolysed resin had a linear structure.

Although it was found that f_a was enhanced from the unpyrolysed ($f_a=0.85$) to the fully pyrolysed resin ($f_a=0.90$), the values remained constant with a pyrolysis time range of 1 to 10 minutes. The proton spin-lattice relaxation time, $T_{1\rho}^H$, which can be also be determined from the variable contact time experiment, was seen to increase significantly with time of pyrolysis with an approximately linear relationship. This showed an increase in structural regularity due to the formation of a graphitic lattice during pyrolysis. From the variable dephasing delay experiment, it was shown that $f_{q/t}$ increased with pyrolysis duration, therefore in the aromatic rings there are more quaternary carbons during the pyrolysis.

From the model of DuBois-Murphy *et al* [1982] for the pericondensation of aromatic units in coals, a one parameter model was developed consisting of a two-dimensional aromatic cluster growing isotropically during pyrolysis, without estimating the stacking of the graphitic layers [Amram and Laval, 1989]. From this model the number of benzene rings per aromatic cluster, r , and the cluster diameter, D , could be determined from the $f_{q/t}$ values. These char parameters were found to be approximately increasing linearly with time of pyrolysis, with the average cluster diameter varying between 9 and 14 Å, and the number of condensed rings, r , ranging from 10 to 23 units. The ring condensation index of Van Krevelen [1961], F_{rci} , was calculated such that the theoretical F_{rci} equals zero for benzene and F_{rci} equals unity for graphite. The F_{rci} was shown to increase from 0.5 to 0.7 and was therefore characteristic of an important pseudo crystalline condensation. As a comparison with other studies, the XRD analysis of high rank coals (95% C) of

Hirsch [1954] estimated r to be approximately 30 and D to be 16 Å, and the high resolution TEM studies of Oberlin and Terriere [1975] gave parameter values for anthracites of $D = 10$ Å and $r < 10$ aromatic rings.

The CP/MAS solid state ^{13}C nmr experiment was used to study a highly-*ortho* and *random* novolac resin [Bryson *et al*,1983]. The band assignments for the observed and fitted peaks came from solution spectrum data from other literature [Dradi *et al*,1978; Siling *et al*,1977; Sojka *et al*,1979]. The relative peak intensities were seen not to be affected by contact time, although the sensitivity was shown to increase with an increase in the magnetic field strength, although this had no effect on resolution. The sideband suppression method of Dixon [1981,1982], TOSS, was used to remove sidebands from the highest field strength of 4.7T. From the spin-echo method of Earl, the values of T_2 for the carbons were determined as $T_2 = 0.03 - 0.06$ s for aromatic carbons, and $T_2 = 0.015$ s for the aliphatic carbons, and these values were found to remain constant with time of cure [Earl and Vanderhart,1979]. Because of the removal of the low T_2 signals (aliphatics) by the use of the TOSS method, and the confusion of the spectrum with the sideband suppression, Bryson chose to rely on the lower field of 2.35 T to acquire further spectra [Bryson *et al*,1983].

A different CP/MAS experiment was used by Fyfe *et al* [1980] to confirm cross-linking modes in resoles. It was suggested that the difference between resole and novolac resins is the presence in the resole of some methylol and dibenzyl-ether links between the phenolic groups, in addition to the methylene bridges which are the only type of linkages in novolacs. In both cases the resins are considered to be highly cross-linked. The band assignments chosen by Fyfe *et al* for the resole correspond to solution assignments for stage-A resins [Sojka *et al*,1979]. The aliphatic assignments associated with methylene groups from formaldehyde were confirmed by using an identical resole cured with 5% ^{13}C enriched formaldehyde. The spectra, while representing structures typical of a cross-linked resole,

displayed band widths (150-250 Hz) that were found to be greater than those from other forms of polymeric material. It was suggested that this was due to the existence of closely related isomeric forms of a given species of carbon unit, and also possibly due to variations of spatial arrangements in the disordered three-dimensional network, which leads to the limited resolution of the cross-linked two component resin.

Schaefer *et al* used the dipolar-decoupled CP/MAS experiment to analyse various glassy polymers, most of which contained aromatic rings joined by aliphatic chain groups [Schaefer *et al*, 1977]. The combination of the various line narrowing techniques provided solid state spectra that closely resembled the corresponding solution spectra for the polymers, such that individual bands could be assigned to chemically unique carbons both in the side and main polymeric chain groups. Various relaxation parameters were measured for the individual bands at room temperature, and the ^{13}C rotating frame relaxation time ($T_{1\rho}$) was shown to be dominated by spin-lattice rather than spin-spin processes. Therefore, the $T_{1\rho}$ values were seen to contain information about the motions of the polymers in the 10-50 kHz region of the spectra, while the cross-polarisation relaxation times (T_{CH}) contained information about the near static interactions within the polymers. Interpretation of the $T_{1\rho}$ values of these polymers emphasised the dynamic heterogeneity of the glassy state. Relaxation processes established the short range nature of the low-frequency side group motions, while defining the long range nature of some of the main chain motions. The ratio of T_{CH} to $T_{1\rho}$ for protonated carbons in the main chain of the polymers was found to have a direct correlation with the toughness or impact strength for the polymers. This was explained in terms of the energy dissipated throughout the chains in the amorphous state in which the low-frequency motions are determined by the same *inter*- and *intra*- steric interactions which influence the nmr relaxation parameters.

Laupretre also used the various available line narrowing techniques associated with

the CP/MAS experiment to analyse a polystyrylpyridine thermosetting resin [Laupretre,1990]. By the use of the variable contact time experiment, a quantitative estimation of the chemical structure and curing mechanism of the reaction pathway between terephthalic aldehyde and pyridine to form the polymer system could be established. Decreasing amounts of aldehyde and methyl groups corresponded to the development of the network cross-linked structure, and the different reactivities of the *ortho*- and *para*- methyl substituents of the collidine molecule were shown such that the *p*-methyl reaction occurred only when most of the *o*-methyl functions had disappeared.

Botto and Winans [1983] used CP-MAS with the PASS technique of sideband suppression [Dixon,1981] to determine aromatic carbon content, f_a , in three different coals, and the PASS technique was seen to correspond well with the normal CP/MAS spectra. The spectra of whole coals showed resonances at ca. 30 ppm due to several aliphatic structures in different steric environments, a main aromatic peak at ca. 120 ppm, with absorptions for substituted aromatic carbons at ca. 140 and 155 ppm.

Supaluknari *et al* [1990] used CP/MAS/HPPD with the TOSS sequence of Dixon *et al* [1982] to analyse Australian coals varying in rank from semi-anthracite to brown coals. An analysis of the cross-polarisation dynamics in the coals, and a further analysis by dipolar dephasing provided structural parameters which could be elucidated due to the use of such a high field (7.05 T) spectrometer. The degree of substitution of the aromatic ring and the average size of the aromatic clusters were parameters of particular interest. Wilson *et al* [1984] also used conventional and dipolar dephasing CP/MAS experiments to determine the degree of aromaticity and various other structural parameters in reference to the changes in protonation of the carbonaceous ring systems. A more concise and less accurate method of determining these parameters was also described. Further studies are also reported on coals using the normal CP/MAS experiment for the determination of cross-

polarisation dynamics [Sullivan *et al*,1982] and the dipolar dephasing experiment [Theriault *et al*,1988]. An extensive nmr study of coal and coal products by Meiler *et al* [1991] uses analytical methods that relate well to the structural determination of phenolic resins .

Many reports exist on the study by solution state ^{13}C nmr of the curing of phenolic resins [Aranguren *et al*,1982; Casiraghi *et al*,1981; DeBreet *et al*,1977; Dradi *et al*,1978; Kamide and Miyakawa,1978; Mukoyama and Tanno,1973; Siling *et al*,1977; Sojka *et al*,1979], including the curing of furfuryl-alcohol resins [Maciel *et al*,1982; Chuang *et al*,1984].

Laser Raman Spectroscopy:

The general advantage of the laser Raman spectrometer in the analysis of carbon materials is its non-destructive nature and its ability to distinguish between different carbons types. It is one of the preferred methods of analysis of graphitic structures, since it provides structural information second only to x-ray diffraction. The spectra obtained from Raman spectroscopy are very sensitive to changes that disrupt the translational symmetry of the material studied, i.e., those that occur in small-dimensional crystals [Dillon *et al*,1984], and to the changes in basal plane separation [Bowling *et al*,1989].

There are many reports that deal with the analysis of carbon materials by Raman Spectroscopy, including diamond structures [Knight and White,1989; Nemanich *et al*,1988], graphite [Tuinstra and Koenig,1970; Vidano *et al*,1981] and partially ordered carbon [Ramsteiner *et al*,1987].

Tuinstra and Koenig [1970] provided an extensive explanation of the appointment of the Raman vibrations associated with crystalline and defective graphite. The

microprobe laser Raman technique was suggested as being useful for the determination of graphite lattice dynamics without the need for large single crystals. The Raman line found in natural graphite was at 1575 cm^{-1} with no polarisation detected. A second line was found at 1355 cm^{-1} for activated charcoal, carbon black and vitreous carbon. The relative intensities of the two bands, I_{1355}/I_{1575} , were suggested to depend on the type of graphitic material. The intensity of the 1355 cm^{-1} band was seen to increase from that of a stress annealed pyrolytic graphite to a commercial graphite to a carbon black. The increase was suggested to correspond to an increase in the proportion of disorganised carbon, and a decrease in the graphite crystal size.

The graphite structure, as represented by its hexagonal D_{6h}^4 space group, and the interatomic in-plane distance of 1.42 Å , remain largely unaffected by the carbon type, whereas the interplanar distance of 3.354 Å for a pure graphitic lattice can be seen to increase to 3.7 Å [Tuinstra and Koenig, 1970]. The loss of density is suggested to correspond to a loss of 3 dimensional crystallinity. The layers are shown to stay perfectly parallel, but their mutual orientation in the plane direction is seen to be random (turbostratic). The Raman line was seen at 1575 cm^{-1} for all of the graphite samples analysed, and a frequency shift of up to 15 cm^{-1} towards higher wavenumbers was suggested to occur in the samples of smaller crystallite sizes. The band is shown not to depend on the mutual arrangement of the graphite planes as it appears at the same frequency in the graphite samples with only two-dimensional crystallinity. From the space rules for the four atom unit cell of graphite it was shown that only the two E_{2g} modes are expected to be Raman active as fundamentals frequencies. The two different E_{2g} modes in the 3 dimensional analysis occur because adjacent planes can vibrate in phase or with opposite phase. It was suggested that in single crystals of graphite, the two E_{2g} modes are unlikely to show a large frequency separation and therefore appear as one single band in the Raman spectrum. This is mostly due to the small difference in energy between the two E_{2g} modes because of the weak interlayer forces and the Raman band observed

in single crystals of graphite can be assigned to these E_{2g} modes. From theoretical considerations, using approximate force constants, the approximate frequency of the E_{2g} mode is 1588 cm^{-1} [Tuinstra and Koenig, 1970]. This calculated frequency is in reasonable agreement with the single line observed at 1575 cm^{-1} , and this calculation gives additional evidence for assignment of the band at 1575 cm^{-1} to the degenerate E_{2g} mode.

The line at 1355 cm^{-1} is shown not to be due to either impurities in the graphite, or to the presence of diamond like tetrahedral bonding in the lattice. The explanation put forward for the existence of this line is as a particle size effect. The intensity of the 1355 cm^{-1} line shows a linear relationship to the inverse of the crystallite size, L_a , such that the intensity of the peak is proportional to the percentage of grain boundary in the sample. Therefore the 1355 cm^{-1} line is due to a change in the selection rules for Raman activity of certain phonons which were inactive in the infinite lattice. From this it was suggested that the 1355 cm^{-1} band is due to the A_{1g} mode of small crystallites, or boundaries of larger crystallites, corresponding to a longitudinal acoustic mode for the infinite lattice. It is shown that this mode isn't effected by changes in bond angles so the force constant involving deformation of the angle is not involved [Tuinstra and Koenig, 1970].

Lespade and Marchand [1984] used a Raman microprobe to observe the graphitisation of carbon fibre composites heated to 2700°C . It was shown that the advantage of the microprobe analysis was its ability to examine areas of the sample down to the order of $1\text{ }\mu\text{m}^2$. Various graphitising and non-graphitising carbons were heat treated to 3000°C for different time periods. Their depth of Raman penetration was found to be about 100 nm , and so it was considered that there must be a degree of surface sensitivity associated with the Raman analysis of pyrolytic carbons. The lines of interest found in the spectra were the defect band at 1350 cm^{-1} , the first order graphite (E_{2g}) band at ca. 1580 cm^{-1} and the second order graphite band at ca. 2700 cm^{-1} . A fourth band of interest was found at $1600 - 1620$

cm^{-1} as a shoulder of the E_{2g} band, and it was considered to be due to further disorder in the lattice. After characterisation of the graphitisation of the carbons by determination of the d_{002} spacing from X-ray diffraction, four parameters derived from the Raman spectra were used to provide 'graphitisation indices'. These parameters were the frequency shift and the line width of the graphitic E_{2g} band, the ratio, R , of the intensities of the 1350 cm^{-1} and E_{2g} lines, and the line width of the second order graphite band near 2700 cm^{-1} . A good correlation was found between these indices and the d_{002} , although both the position and line width of the E_{2g} band was seen to remain constant when compared to d_{002} values below 3.38 \AA . The relationship between the line width of the 2700 cm^{-1} band to that of the E_{2g} band was shown to provide a graphical representation of the 'graphitisation path', about which any carbon can be described regardless of its degree of graphitisation.

Cottinet *et al* [1988] used laser Raman microprobe spectroscopy to study the changes in the microstructure of mesophase pitches during heat treatment. The microprobe was useful in discriminating between the mesophase and isotropic phase of the pitch, as the laser spot could be resolved to $1\text{ }\mu\text{m}^2$. The spectra from the isotropic phase of the pitches showed a wide asymmetric band near 1600 cm^{-1} which is characteristic of amorphous carbon materials. The mesophase component of the pitch showed two distinct bands at ca. 1580 and 1360 cm^{-1} which were characteristic of a pre-graphitic structure. The 1580 cm^{-1} band was assigned to the E_{2g} vibrational mode, and the 1360 cm^{-1} band was assigned to a graphitic defect mode. Two Raman indices were defined for each of the pitch regions being analysed, such that for the isotropic phase the R_1 index was defined as the normalised area of the 1600 cm^{-1} band, and for the mesophase the R_2 index was defined as the area ratio of the 1360 to 1580 cm^{-1} bands. The two indices were considered to be characteristic of the structural order of the two phases due to their tendency to decrease with an increase in the structural order of the carbons. From the changes in the Raman indices with heat treatment, a model for the alteration in structural order of a heat treated pitch was established such that the role of the

coalescence process in the degradation of the order of a mesophase pitch corresponds to an increase in the Raman R_2 index [Cottinet *et al*,1984].

From Doll *et al* [1988] an investigation of carbon/carbon composites was made by way of Raman microprobe so that the graphitic characteristics of the heat treated carbon fibres could be examined independently from that of the matrix. All of the carbon species were heat treated to temperatures of 2680°C, 2820°C and 3015°C, and they all were seen to display a well resolved E_{2g} band at $\approx 1585\text{ cm}^{-1}$. It was also shown that there was an absence of an order induced mode in the spectra for both the carbon fibre and the matrix, which implied that large in-plane crystallite sizes ($L_a \geq 1000\text{ \AA}$) were shown for both the matrix and the fibres. The observed E_{2g} peaks were fitted with Lorentzian lineshapes, and from these the disorder in the carbon structures was shown to cause the E_{2g} line to broaden and shift to higher frequencies due to a higher density of phonon states near 1620 cm^{-1} . There was no spectral evidence of the 1620 cm^{-1} disordered graphite band for the matrix and fibres above 2000°C. All the frequencies of the E_{2g} band were within the experimental error of $\pm 2\text{ cm}^{-1}$ of the theoretical frequency at 1585 cm^{-1} for highly ordered pyrolytic graphite.

Raman spectroscopy was used complementarily with scanning tunneling microscopy (STM) to observe the effect of electrolysis time and current on the surface of highly ordered pyrolytic graphite electrodes [Siperko,1990]. As was expected, the main Raman band for the unelectrolysed control electrode was seen at 1580 cm^{-1} , representing the E_{2g2} graphite vibration, with no defect band. It was suggested that the defect band could be increased with a decrease in crystallite size of a graphite surface, and that this band will appear in the spectrum of graphites possessing significant edge plane density, although the E_{2g2} band was not likely to change position or width.

In addition to other techniques, Tither *et al* [1990] used Raman spectroscopy to

analyse a thin carbon film produced by the ion source deposition of hydrocarbon gases. The Raman spectrum of such a carbon showed a broad band centred at ca. 1540 cm^{-1} associated with the graphitic 1575 cm^{-1} E_{2g2} graphite (G) vibration, and a broad band shoulder at ca. 1275 cm^{-1} due to the defect (D) vibration of disordered sp^2 bonded carbon species. A very weak band at ca. 850 cm^{-1} was observed and couldn't be accounted for, but its existence was discussed by Nemanich and Lucovsky [1977]. From another study it was suggested that the ratio of the intensities of the defect to E_{2g2} bands, I_{1350}/I_{1575} was inversely proportional to the graphite crystallite size [Tuinstra and Koenig, 1970]. The poorly resolved spectrum was deconvolved to give a value for the I_D/I_G ratio of 0.82 which corresponded to a crystallite size of 50 \AA . Although it was suggested that the G and D bands are expected to shift to higher frequencies (up to 20 cm^{-1}) with increasing disorder, the bands in the study of Tither *et al* (203) were seen to be shifted to lower wave numbers. A similar observation in the Raman spectra of Dillon *et al* [1984] was made for carbon films produced by radio frequency discharge and ion beam deposition, and computer model calculations [Beeman *et al*, 1984] showed that disorder in carbon films may involve bond angle disorder with some tetrahedral (sp^3) bonding in addition to (sp^2) bonds, that would cause shifts to lower wavenumbers for the G and D bands and also produce greater band widths.

Mernagh *et al* [1984] discussed the existence of the defect (1360 cm^{-1}) and graphite (1580 cm^{-1}) bands in terms of their respective space groupings. From Brillson *et al* [1971] the D^4_{6h} space group is at first considered for the single line spectrum of crystalline graphite, although the Wyckoff [1963] space group, C^4_{6v} , could explain the observed spectrum of Mernagh *et al* if weak interlayer interaction and no coupling of vibrational modes is assumed. For partially ordered carbons, such as graphitised carbon blacks, it was suggested that the D^4_{6h} space group is less likely to provide a suitable model. Layer stacking disorder in microstructures of carbon blacks [Medalia and Rivin, 1976] tended to eliminate interlayer centres of symmetry invoked for crystalline graphite. All the bands observed for graphite and carbons

are suggested to be in-plane vibrations [Vidano *et al*,1981].

From the angular dependence studies of the Raman interaction of a Graphon carbon (a channel black graphitised to ca. 3000°C) a model was established for the change in space group symmetry from a D^4_{6h} for graphite to C^4_{6v} for disordered carbons and a prediction of changes in the spectrum [Mernagh *et al*,1984]. The A_1 (C^4_{6v}) mode for carbons is shown to coincide with the out-of-plane i.r. active A_{2u} (D^4_{6h}) vibration assigned to an absorption at 868 cm^{-1} [Nemanich and Lucovsky,1977]. As the intensity of the 1360 cm^{-1} defect band was seen to be independent of the incident angle of the laser beam to the sample, unlike the 1580 and 2700 cm^{-1} graphite bands, that vibration was suggested to be associated with the non-planar zones of microstructure distortion (zones of curvature) as shown by high resolution transmission electron microscopy of graphitised carbons. This distortion band, along with that at 1620 cm^{-1} , was interpreted as arising from the non-degenerate components of the degenerate layer modes. The displacement of the split 1360 cm^{-1} component from the original degenerate layer mode at 1580 cm^{-1} was suggested as being indicative of major changes in the carbon-ring force constants. This displacement was explained in terms of a disruption of the delocalised electronic structure at the point of deviation from planarity, or at the edge layer, and this localised electronic structure was suggested as having alkene-type characteristics. The I_{1350}/I_{1580} band ratio was shown to decrease smoothly with laser excitation frequency, and this information was suggested to be useful as a characteristic of the carbon type. Following this, the spectrum was suggested to arise from vibronic enhancement, with the interaction being different for the D and G bands, particularly as the G line is shown to be relatively insensitive to changes in excitation frequency. A band was also found at 1470 cm^{-1} due to carboxylates or related oxidised species. The depth of laser was shown to be of the order of tens of nanometres, which, in combination with the angular dependence information, suggested that the intensity of the 1580 and 1360 cm^{-1} bands are not optical skin depth dependent.

Laser Raman microprobe was used with TEM and optical microscopy by Rouzaud *et al* [1983] to investigate the graphitisation of thick (500 Å) and thin (150 Å) carbon films prepared by carbon vapour deposition. Initially, it was considered that during the coalification and carbonisation processes the basic structural units in a carbonaceous material become poly-aromatic molecules of less than 12 rings. The Raman spectra of the carbon films heat treated in 100°C steps to 2700°C at 20°C/min in argon show the appearance of the E_{2g} graphite mode at 1350 cm^{-1} and the defect band at 1500 cm^{-1} . The spectra were fitted based on a two and three band hypothesis, and a comparison of the differences between the experimental and deconvolved spectra suggested that a three band fit gave the least residual error. The bands were therefore shown to exist at 1580, 1500 and 1350 cm^{-1} .

From the error analysis of the spectra of Rouzaud *et al* [1983], the data showed good reproducibility. The E_{2g} band at 1350 cm^{-1} showed a general tendency to increase with heat treatment temperature and become the only band present in the spectra of the carbons between 2120 and 2500°C. The 1500 cm^{-1} band was found to be due to in-plane defects located between adjacent basic structural units (BSU's), causing tilt and twist boundaries between the planes. The 1580 cm^{-1} band was shown to be due to interstitial defects from hetero-atoms, existing either between the layers or at the boundaries of the BSU's. The observed shift of the 1580 cm^{-1} band was considered as being due to interstitial defects. The spectrum of the room temperature carbon film, which was likely to have the greatest proportion of hetero-atoms contained in its microstructure, corresponded to the maximum band intensity at 1500 cm^{-1} . The most energetic interstitial atoms were released at $\text{HTT}=1375^\circ\text{C}$, and completely removed at 1670°C, which corresponded to the disappearance of the this band. The first series of in-plane defects were removed at the tilt and twist boundaries between 1500 and 1670°C. The intensity of the 1350 cm^{-1} band was seen to decrease steadily above 1500°C, and then to disappear above 2120°C, with the L_a increasing gradually. A second series of in-plane defects were

removed between 2120 and 2500°C, and the aromatic layers were shown to become perfectly ordered with L_a increasing rapidly.

In a related study, Beny-Bassez and Rouzaud [1985] compared the pyrolysis of thick (500 Å) and thin (150 Å) carbon films, anthracene ($C_{14}H_{10}$) and saccharose ($C_{12}H_{22}O_{11}$) cokes, and various ranks of coals (semi-bituminous to anthracitic) by microprobe laser Raman spectroscopy. It was first suggested that the oxygen rich materials, such as the saccharose cokes, exhibit only small molecular orientation (≈ 50 Å), whereas the oxygen free materials, such as an anthracite coke, show crystallite sizes of up to several microns. As the crystallite size is shown to determine the graphitisability of the carbonaceous material, the larger molecules provide a graphitisable carbon structure, whereas the lattice containing small molecules remain non-graphitised up to 3000°C.

Beny-Bassez and Rouzaud [1985] found only two Raman bands existing for saccharose-cokes at 1350 and 1580 cm^{-1} . The S_{1350} and S_{1350}/S_{1580} parameters were shown to remain approximately constant over the heat treatment of the saccharose cokes, and the nature of their defects were shown to be similar to other cokes. In the Raman spectra of coals, only two bands were found; one at 1350 cm^{-1} and the other at 1600 cm^{-1} , red shifted in relation to graphite. The band-width of the 1600 cm^{-1} band, Γ_{1600} , was shown to decrease with an increase in coal rank.

A comparison was made between the S_{1350} and the crystallite diameter, L_a , as derived from $\langle 11 \rangle$ dark field measurements obtained from TEM [Beny-Bassez and Rouzaud, 1985]. Their L_a values were found to differ from different values derived by XRD [Nakamizo et al, 1974], although the S_{1350} parameter was shown to have a good linear dependence with $1/L_a$, the slope of which depended on the reference graphitisable carbon series. This linear dependence showed three distinct stages of crystallite growth according to the specific mode of defect removal. For anthracene

cokes the stages were shown to correspond; first to the release of out of plane defects up to 1600°C with little change in L_a ; followed by in-plane defect removal up to 2000°C with an increased rate of L_a growth; and finally above 2000°C the removal of the defects at the joints between graphitic grains, with a very rapid rate of crystallite growth.

X-Ray Photoelectron Spectroscopy:

X-ray photoelectron spectroscopy (XPS) is a technique for elemental analysis which can probe, qualitatively to semi quantitatively, the first 1-5 nm thickness of the outer layer of a sample. All elements except hydrogen can be monitored with an ultimate sensitivity approaching 10^{-9} g.cm⁻² of surface [Brown *et al*,1981]. It is also often possible to confirm chemical environment (oxidation state and coordination number) of an element from chemical shift information [Bancroft *et al*,1979a]. The usefulness of the XPS technique was established for the chemical surface analysis of amorphous carbons and graphite [Evans *et al*,1975]. For a simple surface elemental analysis XPS was used to determine the change in relative atomic carbon and oxygen concentration of carbon fibres after exposure to atomic oxygen [Pattabiraman *et al*,1990].

Yoshida *et al* [1990] used the technique of XPS to analyse the surface of activated carbons produced by the 'moist' pyrolysis of novolac phenolic resins. A wet chemical method was used to determine the concentration of surface acidic groups, and XPS used to determine the surface O/C ratio. The novolac fibres were initially carbonised in a water vapour enriched N₂ stream to 1000°C, and then 'dry' heat treated in N₂ at 1000°C for 1 hour. The O/C ratio for the heat treated activated carbon was seen to be reduced from 0.3 to 0.1 with the time of heat treatment. The O1s peak was identified within the spectra, and the carbon-oxygen bonding species were resolved into the C-O band at 534.7 eV and the C=O band at 532.9 eV. The

heat treatment of the activated carbon was shown to have converted the surface carboxy and ester groups to phenolic hydroxy and quinone groups, which corresponded to a decrease in the acid functionality concentration, resulting in a suppression of electrochemical interactions of activated carbon with the electrolytic solution.

Kozlowski and Sherwood [1986] used the XPS technique to analyse the surface of carbon fibres that had been electrochemically treated in the ammonium salts of strong acids. The chemical shifts of the surface species were assigned in relation to the C1s 'graphite' peak at 284.6 eV, and the peaks were fitted by using a non-linear least squares curve fitting algorithm. In the C1s spectrum, in addition to the main graphite peak, oxide species were observed for keto/enol and carboxyl/ester groups at 286.8 and 288.8 eV respectively. The relative intensity of the satellite peak at ca. 291 eV was seen to remain unchanged with increasing potential. At low potentials (< 0.5 V), the O1s spectra were shown to have oxygen species at 533.3 eV for the =O, and 531.8 eV for the -O- groups. The N1s spectrum was resolved into two bands assigned as amine groups at 401 eV and amide groups at 399 eV.

Wandass *et al* [1987] analysed the electrolytically modified surfaces of graphite electrode material by XPS to determine their degree of oxidation. The model used for the selection of band assignments assumed a constant and tightly constrained binding energy for the main graphite band at 284.6 eV when being mathematically fitted. A combined Gaussian-Lorentzian fitting algorithm was used with the Gaussian component being varied between 65% and 90% for each spectrum. The other carbon species were assigned as the CH_x , C-O and C=O peaks at 284.8, 286.1 and 287.5 eV respectively, although these assignments varied slightly between spectra due to their less severe fitting constraints of 0.1 - 0.2 eV. The C-O species were suggested as being due to C-OH surface groups. The unelectrolysed (blank) graphite showed no C=O species on its surface, although an approximate correlation was made between the saturation of oxygen functionalities and the

depletion of the surface CH_x groups. An angular dependence study was made of the XPS signals, and from that the average depth of surface oxidation was estimated to be approximately 50 Å.

Galsuska *et al* [1988] used core-level XPS to determine the change in the surface chemistry of compression annealed pyrolytic graphite. Although the graphite surfaces were prepared for analysis in air, the XPS surface oxygen concentration was estimated as less than 2 atomic %, suggesting that the material was inert to oxygen-bearing species in air, with no other impurities being detected. The graphite samples were analysed for surface oxidation and crystal alteration by treatment in a mixture of anhydrous sulphuric acid, sodium nitrate and potassium permanganate and xenon ion etching to provide a good model for an amorphous carbon surface. For the basal and edge planes of the unoxidised pyrolytic graphite, oxygen was found as the only contaminant and the oxygen concentration was determined as 1.3 and 1.6 atomic % for the basal and edge planes, respectively. The surface oxygen concentration of the xenon ion bombarded graphite was shown to be 1 atomic %, and that of the oxidised sample was 38 atomic %. The band width of the C1s peak centred at 284.5 eV was shown to be 1.7 eV for both the basal and edge plane graphite spectra, although the spectra of the graphite oxide showed an additional peak component at ca. 288 eV associated with oxygen-carbon bonding, such as those described previously [Kozlowski and Sherwood, 1986; Evans *et al*, 1975]. The C1s band width for the graphite oxide spectra was shown to be 2.5 eV, which was likely due to the structural disordering that accompanies the oxidation of graphite. The partial O-C bonds themselves may also have contributed to the peak broadening effect. The xenon ion bombardment of the surface of one graphite sample caused its C1s spectrum band to broaden to 2.1 - 2.2 eV due to the induced increase in surface defects, although the main 'graphitic' peaks of the C1s spectra for all the samples showed no shifting in position due either to surface oxidation or ion damage.

The XPS technique was used in the study of coal derived steam activated carbons to determine the mechanism of potassium and iodine impregnation into the carbon surface after chemical treatment with a potassium iodide solution [Gai *et al*,1989]. The binding energies of the various detected bands were referenced to the main carbon peak at 285 eV. Four peaks were identified in the C1s spectra for the carbons at 285 eV (aromatic/aliphatic hydrocarbon), 286.6 eV (ether/hydroxyl), 287.7 eV (carbonyl) and 288.9 eV (carboxyl), with two additional peaks suggested as being due to 'shakeup' processes associated with aromatic surface species. From the O1s spectrum, two oxygen peaks were fitted at 533.1 eV and 535.5 eV, although their assignments were considered to be speculative. Surface elemental analyses were calculated from peak areas corrected for atomic sensitivity, and it was found that the total surface oxygen concentration was 6.3 atomic %.

Hu *et al* [1988] used XPS and other related techniques to determine the structural changes associated with the high temperature pyrolysis of a polyimide sample in Argon to 2100°C. The C1s spectrum of the raw polyimide showed bands at 284.6 eV (aromatic), 286.0 eV (C-O, C-N) and 288.4 eV (C=O), whereas the C1s spectrum of the heat treated polyimide showed a single peak at 284.6 eV corresponding to the *graphitic* carbon species. The surface analyses were shown to be the same for the raw polyimide and heat treated sample (2 atomic %) suggesting that surface oxidation did not occur in the polymer during heat treatment.

Brown *et al* [1981] determined the surface elemental composition of several North American coal samples using XPS following the methods of other studies [Frost *et al*,1974,1977] in analysing coal surfaces for carbon, oxygen and sulphur. The binding energies were calibrated using the gold Au4f_{7/2} peak at $E_b = 84.0$ eV. A quantitative analysis of the surface species was possible as a result of adopting the method of Bancroft *et al* [1979b], where the ratio of the elemental concentrations are seen to be proportional to the ratio of their corresponding peak intensities, with a factor of proportionality which is itself a function of the spectrometer and the

'cross-section' of the core level of the elements examined. The depth of analysis was determined to be ≈ 5 nm, with a bulk detection limit of ≈ 1000 ppm (0.1 wt%), suggesting that only surface concentrations of greater than 0.1% could be detected by XPS. From the coal spectra, C1s peaks were observed at 285 eV (hydrocarbons), 287 eV (carbonyl), 289 eV (carboxyl) and for a high rank coal sample a peak at 285 eV being assigned as a *graphite* C1s band. The quantitative analyses were shown to give reasonable results, although it was shown that there was a difference between the bulk and surface elemental analyses.

Chapter Three

Experimental Procedure.

Sample Preparation

Resin Heat Treatment; 25 - 1000°C :

Six samples of cured (polymerised) phenol-formaldehyde resins were received from the Comalco Research Centre of Comalco Ltd., Melbourne, Australia. The curing cycle for the resins is the proprietary knowledge of Comalco Limited, although it is known that the maximum curing temperature of the resins was approximately 180°C, such that a resin sample heated to this temperature was used throughout this research to denote a fully cured, unpyrolysed resin. All post-cured resin samples had been ground to less than 106 µm particle size prior to pyrolysis. The phenol-formaldehyde resin used in each of the six cured resins was of an acid catalysed novolac type with a phenol to formaldehyde ratio of approximately 0.85. The resin contained approximately 16 phenolic units per oligomer and had a molecular weight of approximately 1600 atomic mass units.

A three letter nomenclature for each resin was used throughout the research program to indicate the respective level of resin formulation furfuryl-alcohol as either high, low or none, given equal proportions of either hexamethylenetetramine (named as *hexamine* throughout this thesis) or paraformaldehyde. This is explained as follows: the first letter being H, L, or N indicates a High, Low or No furfuryl-alcohol level, the F indicates furfuryl-alcohol, and the final letter being H or P indicates hexamine or paraformaldehyde, for example 'HFH' indicates a High Furfuryl-alcohol Hexamine cured resin. A number following the resin name indicates the pyrolysis heat treatment temperature, such that HFH500 indicates a High Furfuryl-alcohol Hexamine cured resin heat treated to 500°C. This naming convention, and the pre- and post- cure constituent compositions for the six resins, stated in weight percent, are shown in Table 3.1. The pre-cure compositions quoted in Table 3.1 are for the actual proportions of the constituents as they were mixed into the resin formulation.

The post-cure resin composition of the same constituents was calculated by adjusting the weight-loss after curing for the chemistry of the curing reaction which liberates 1 mole of NH_3 per mole of $\text{C}_6\text{H}_{12}\text{N}_4$ (hexamine cured) and 1 mole of H_2O per mole of CH_2O (paraformaldehyde cured) and assuming that most of the remaining weight-loss is due to furfuryl-alcohol volatilising [proprietary information supplied by Comalco Limited]. This is a valid assumption as it can be shown that the weight-losses in the furfuryl-alcohol free resins are almost completely accounted for by the evolution of ammonia (hexamine cured) and water (paraformaldehyde cured) respectively.

Resin	Constituents	Composition (wt %)		^a Weight Loss (%)
		Pre-Cure	Post-Cure	
HFH	phenol formaldehyde	29.10	62.5	53.45
	furfuryl-alcohol	68.00	32.0	
	hexamine	2.90	5.5	
HFP	phenol formaldehyde	29.10	64.6	54.98
	furfuryl-alcohol	68.00	32.8	
	paraformaldehyde	2.90	2.6	
LFH	phenol formaldehyde	65.42	70.7	7.41
	furfuryl-alcohol	28.04	23.1	
	hexamine	6.54	6.2	
LFP	phenol formaldehyde	65.42	73.8	11.33
	furfuryl-alcohol	28.04	23.3	
	paraformaldehyde	6.54	2.9	
NFH	phenol formaldehyde	90.00	91.3	1.57
	hexamine	10.00	8.7	
NFP	phenol formaldehyde	90.00	96.4	7.39
	paraformaldehyde	10.00	3.6	

^a Weight loss (%) of the resins after curing.

Table 3.1 The naming convention and constituent compositions of the six phenolic resins in their pre-cured and 'as-received' post-cured conditions.

Each resin was carbonised by heating within an Argon atmosphere in a 32 mm (28 mm internal diameter) quartz glass reactor tube. The heating system is shown diagrammatically in Figure 3.1. The reactor tube was placed inside a 36 mm internal diameter tube furnace. The furnace heating cycles were controlled by using a 'feedback' proportional-integral-derivative control loop using 'Work Bench' electronic control software and data acquisition hardware. The control software was operated using an IBM-compatible 8086 XT personal computer. The temperature of the furnace was observed using 'K'-type thermocouples; one placed inside a quartz sheath, the end of which could be positioned in the centre of the sample boat; the other situated at the centre of the furnace on the outside surface of the glass reaction tube.

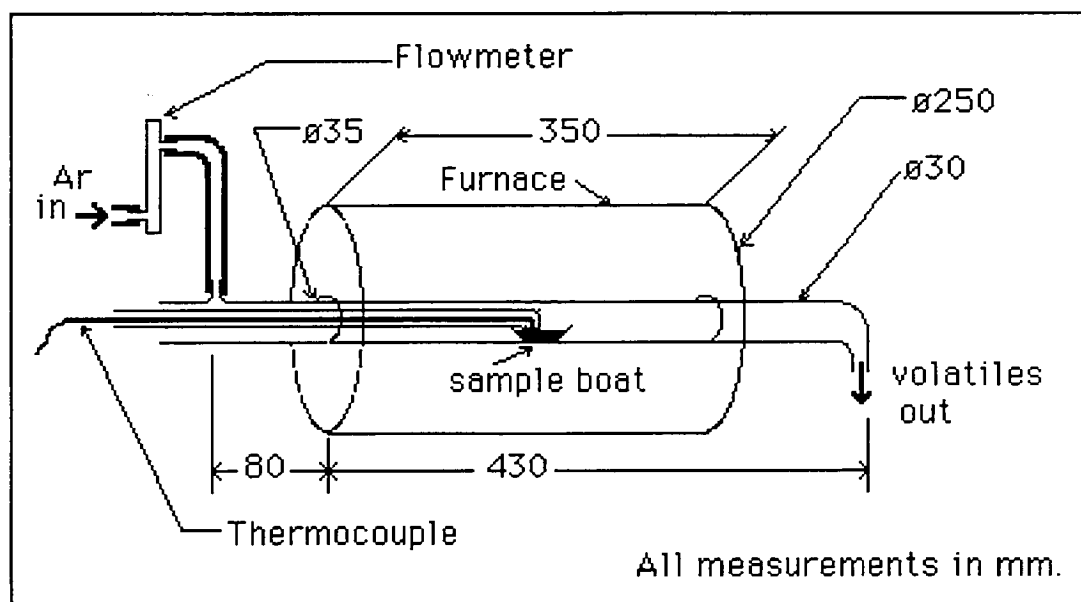


Figure 3.1 Diagram of the resin heat treatment pyrolysis system.

The pyrolysis of each sample was conducted by placing the powdered resins in quartz glass boats of approximately 24 mm wide x 80 mm long, each holding approximately 1 to 3 grams of resin. All pyrolysis experiments were conducted in an inert atmosphere with high purity argon used as an inert carrier gas at flow rates of between 0.5 and 1.5 ml/sec. The argon flow rate was measured using a 1 mm internal diameter 'floating-ball' type graduated flow-rate tube which had been

calibrated for argon and nitrogen using a Hewlett-Packard Gas-Chromatograph 'bubble' type flow-rate meter.

Initially, all six resins were heated at a ramp rate of $10^{\circ}\text{C}/\text{min}$ from 25°C to 1000°C with a dwell time at 1000°C of 10 minutes. A dwell time of 10 minutes was used to allow for temperature equilibration of the sample due to a temperature variation in the sample boat of $10 - 15^{\circ}\text{C}$. The initial ramp rate of $10^{\circ}\text{C}/\text{min}$ was used to determine the effect of heating rate of the resins on various structural parameters.

Following these experiments, samples of all six resins were pyrolysed at $3^{\circ}\text{C}/\text{min}$ from 25°C to 200°C , and then additional samples from 25°C to successively higher temperatures in 50°C increments up to 1000°C , so that there were pyrolysed resin samples of heat treatments from 180°C (cured resin) to 1000°C (fully carbonised resin). Each sample was held at the maximum temperature for 5 minutes so as to facilitate as complete a pyrolysis of the sample as possible at the particular temperature, in a similar way to the pyrolysis at $10^{\circ}\text{C}/\text{min}$. Following this dwell time at temperature, the furnace tube was cooled with air to reduce the sample temperature to 25°C within 5 minutes. This was considered sufficient to stop any back reactions in the resins as they were cooled to room temperature. Upon removal from the sample tube, and therefore the argon shield, a small amount of sample (approximately 100 mg) was immediately contained in argon filled sample tubes for the purpose of conducting XPS surface analyses at a later stage in the research program. This was done so as to reduce the possibility of surface contamination from atmospheric oxygen, which would affect the XPS results.

Although there was an observed overall temperature variation in the sample boat of 10°C between the centre and the extreme ends of the resin sample, a furnace length of 350 mm and diameter of 250 mm was sufficient to sustain the recorded temperature of the thermocouple throughout the resin sample so that the observed temperature was closely representative of the whole sample. The combination of long heating

times, continuous argon flow, and a large free space in the reaction tube provided for all pyrolysis gases to freely leave the sample heating chamber during resin carbonisation.

Analyses Experimental Procedures

Thermo-Gravimetric Analysis:

A series of thermo-gravimetric analyses experiments was conducted on each of the six resins. A Setaram TAG 24 thermo-gravimetric analyser was used to determine rates of volatiles evolution and to observe any phase changes during the pyrolysis of the phenolic resins. The six resins were all analysed gravimetrically by heating approximately 50 mg of each sample in an Al₂O₃ crucible from 20°C to 1000°C at two heating rates, the first of 3°C/min and the second of 10°C/min, and, subsequently, observing the weight loss, rate of weight loss (differential thermal gravimetry) and heat flow. Initially the TGA furnace was evacuated to 0.2 mbar, and then filled with ultra high purity argon to 1 bar pressure. The resin samples were heated in alumina crucibles of ≈0.1 ml with ultra high purity argon as the carrier gas. The raw data for each experiment was stored on personal computer for subsequent analysis.

Elemental Analyses:

Each resin, and its solid pyrolysis product, was analysed for its weight percent content of carbon, hydrogen, nitrogen and oxygen (by difference). These analyses were conducted using a Carlo Erba CHNOS EA1108 Elemental Analyser. An acetanilide standard (C₆H₉NO - 71.09%C, 6.71%H, 10.36%N and 11.84%O) was

analysed after every 10 samples to compensate for machine drift. The level of accuracy achieved for these analyses were found to be dependent on several factors. Firstly, the machine error was quoted by the operator [Dr G. Robbottom - Central Science Laboratory, University of Tasmania] to be no greater than 0.5% due to the regularity of calibration of the instrument. The sampling of the resin chars introduced a larger error due to the inhomogeneity of the carbonised samples. The inherent difficulty in fully 'burning' the highly carbonised samples to CO₂ during analysis was also a source of error. The elemental analysis errors for triplicate analyses of six *typical* resin samples are shown in Table 3.2.

Resin Sample	Triplicate Error (wt%)			
	C	H	O	N
HFH450	0.7	0.6	3.6	6.2
HFP400	0.6	1.3	3.7	^a 83.3
LFH200	0.7	1.0	3.8	7.9
LFP250	0.5	9.9	3.8	^a 27.6
NFH300	1.0	1.3	5.3	34.4
NFP350	0.8	0.9	2.4	^a 64.3

a. Initially nitrogen-free resin formulations.

Table 3.2 Elemental analysis errors for six typical carbonised resin samples.

This inhomogeneity was partly due to a temperature gradient in the sample boat of showing an end temperature of up to 15°C less than the reported central temperature of the sample. At the critical heat treatment range of 250-700°C, where all of the important pyrolysis reactions were taking place, there could be several carbon structural phases existing in the one sample. The nitrogen analysis errors for the non-hexamine containing resins (HFP, LFP, NFP) are unimportant as the levels of nitrogen discovered for these samples were assumed to be zero, especially after the nitrogen results for all the samples were corrected for base line nitrogen

contamination from the atmosphere during sample preparation. The nitrogen error for NFH was also seen as insignificant above 300°C due to the low retention of nitrogen observed in that resin above that temperature. The fully charred samples were also found to have highly variable results due to their inability to be fully burnt in the furnace of the analyser, and therefore provide a complete CO₂ peak in the gas-chromatograph. Finally, as the oxygen analyses were taken as the difference of the three detected species (C, H and N), the errors for those results would be compounded by the combination of all the other errors. Therefore the elemental analysis figures for all the chars are reduced to two significant figures.

Liquid Volatiles Analysis:

An analysis of the liquid pyrolysis products was conducted on each resin by collecting samples from the volatiles off-gas stream every 50°C during the resin pyrolysis program as it was heat treated in argon from 20°C to 1000°C at 3°C/min in the furnace tube, as shown in Figure 3.1. A diagram of the off-gas volatiles sampling apparatus is shown in Figure 3.2. The sampling device consisted of a glass tube with a bulb to condense the heavy organic volatiles. A water trap, filled with anhydrous calcium chloride as a desiccant, was placed at the end of the tube, with an outlet to release any pyrolysis gases from the furnace reactor tube.

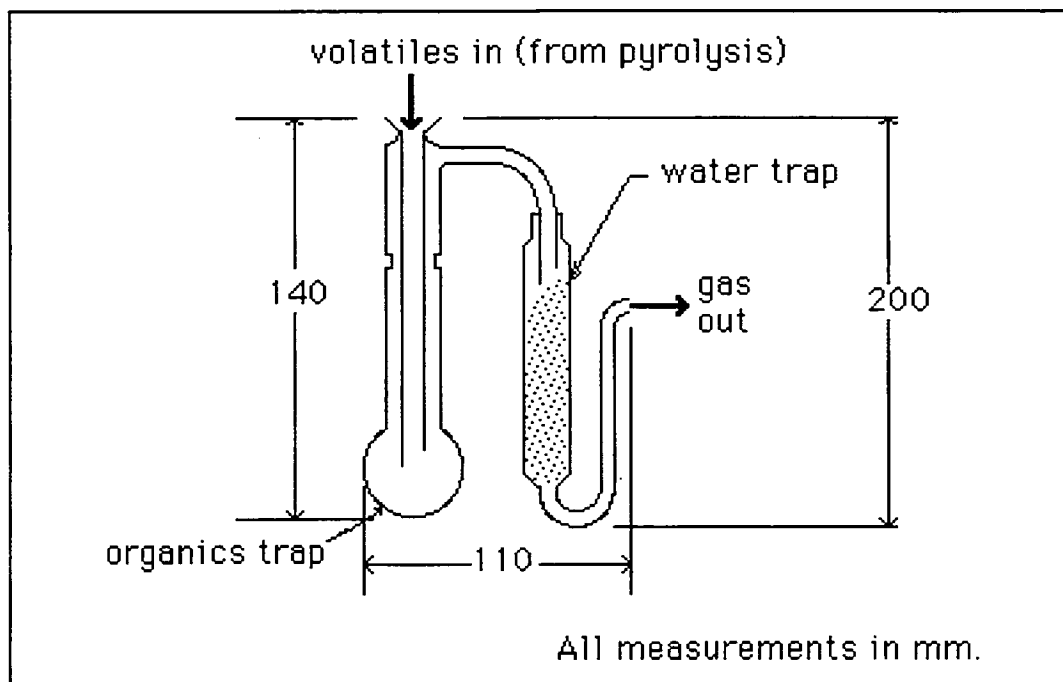


Figure 3.2 Diagram of the pyrolysis volatiles sampling apparatus.

A preliminary experiment on resin LFH was conducted to test the pyrolysis system. After washing the desiccant with acetone and conducting a GC/MS analysis of the washings, it was discovered that the desiccant remains relatively uncontaminated with organics. Therefore it can be assumed that the heavy organics were all condensed in the bulb before the remaining volatile stream entered the water trap. Some of the very heavy organics were seen to be condensed or pyrolysed inside the end of the furnace tube, and acetone washings of the tube residue revealed the presence mainly of bis-cresols and other two-ringed phenolic compounds. As these residual organics in the furnace tube amounted to no more than approximately 10 mg for each resin over the whole temperature range (ca. 0.05% per temperature interval) the loss was considered to be negligible, particularly when relative differences between resins are being considered.

In each experiment, two entrapment tubes were used such that while one tube was used for collecting the volatile sample, the other tube was taken for analysis, and the water trap was weighed. As the organics were seen to begin evolution at

approximately 150°C and to cease evolution at approximately 650°C (which relatively corresponds to the TGA and elemental analyses trends for the lower and upper limits of the major weight loss mechanism during pyrolysis) only 12 bulbs were required to collect the organic volatile samples. The first and second bulbs were repeatedly used every 50°C from 50°C to 250°C to measure low temperature water evolution, as it was observed that some water was evolved from the resins at these below 250°C. From 300°C each successive bulb was used to contain the volatile organic sample from each successive 50°C interval until the final bulb was used at 700°C. As organic evolution had ceased by this temperature, the last two bulbs were used to collect any water remaining in the volatile stream.

Each bulb was dried over silica gel in a desiccator for 15 hours to measure water loss and remove water impurities before GC/MS analysis. The bulbs were weighed to determine the total organic weight for the particular temperature interval. Each organic sample was diluted with a known amount of an acetone solution with 0.6% dodecanol as an internal standard. Each of the two water traps were weighed after their temperature interval to determine water content. The water traps were dried in an oven at 200°C for approximately 12 hours between experiments to precondition the desiccant.

The Gas-Chromatography/Mass-Spectrometry analysis was conducted for each organic volatile sample using a Hewlett Packard HP5890 GC and HP5970 Mass Selective Detector. For the GC analyses a capillary column of dimensions 0.32 mm x 25 metre x 0.17 µm film thickness was used, with a 'HP1' polymethyl-siloxane stationary phase. Helium was used as the carrier gas at a pressure of 12 psi, and the heating cycle of the column was as follows. The column was held initially at a temperature of 40°C for 2 minutes, and then ramped at 10°C/min to 290°C. The initial low temperature dwell was to slowly remove the more volatile molecules such as phenol and furfuryl-alcohol, and the high temperature ramp was to remove the larger molecules such as xanthene. The injector temperature was held at 260°C and the GC-

MS interface at 290°C. The mass/charge (m/z) scan range of the mass selective detector was from 500 to 35 at a rate of 1 scan per second.

Fourier Transform Infrared Spectroscopy:

All of the solid resin pyrolysis samples were investigated by FTIR to establish the relative alteration of the organic species within the resins over the pyrolysis temperature range. The resins' analyses were undertaken using finely ground samples pressed in KBr pellets. For each spectrum a small 1.00 - 3.00 mg (± 0.01 mg) sample of the pyrolysed carbon was weighed with a Mettler AT250 electronic balance, and added to approximately 250 mg of KBr containing a known amount of $K_3Fe(CN)_6$ reference (0.2%). The KBr and carbon sample were ground together in mortar and pestle for approximately 5 minutes, and pressed into a 13 mm pellet in an evacuated die at 8000 kg pressure. The pellet was weighed and dried at 105°C under nitrogen for at least 24 hours, and immediately analysed.

Due to the intensity dependence of infrared spectroscopy on the degree of grind (particle size), and therefore grinding time of the sample, it was found necessary to vary the integrated absorption of a large i.r. frequency band with the time of hand-grinding in a mortar and pestle. The integrated absorption of the CN stretching frequency at 2150 - 2000 cm^{-1} , as measured from the internal cyanide standard, varied with grinding times between 0 and 5 minutes. It was found that a constant optimum absorption was achieved with a grinding time of approximately 5 minutes, or greater. This grinding time was used for all FTIR experiments.

All FTIR spectra were recorded on a Digilab FTS-20E system at a resolution of 4 cm^{-1} with 260 co-adding interferograms. All spectra were adjusted for baseline drift [Painter *et al*, 1981a] and normalised to 1.00 mg of sample in 100.00 mg of KBr [Solomon and Carangelo, 1982]. Software packages on the Digilab computer system

were utilised for spectral data analyses. All spectra were baseline corrected using a weighted correcting routine with reference to three points on the spectrum being fitted to zero. Although the pellets had been dried, spurious water was found to adversely affect the OH stretching region near 3000 cm^{-1} , and therefore the $4000\text{--}2500\text{ cm}^{-1}$ region was considered of no quantitative significance to this study. The points of interest for baseline correcting were taken as 2200 , 1750 and 864 cm^{-1} , which corresponded to points of local minimum absorption in these spectra. Due to the complex nature of the spectra, and the extent to which frequency bands of importance overlapped, a quantitative analysis of the i.r. spectral information was avoided, as reliance on this type of information could have led to false conclusions. Also, as the CN stretching region of the internal standard can be shown to lie between 2140 and 2000 cm^{-1} , and below 600 cm^{-1} , it was considered to have no effect on the vibration frequencies of the resins' chemical species, and therefore could have no effect on the semi-quantitative analysis.

Solid-State ^{13}C Nuclear Magnetic Resonance Spectroscopy:

All solid-state ^{13}C nmr experiments were undertaken at a carbon frequency of 75.46 MHz on a Bruker AM300 spectrometer equipped with a 7.05 T superconducting magnet and a Spectrospin single-coil double-tuned solid-state probe. During magic-angle spinning of the sample, a double-air-bearing system was used to alter the spin rate, and a micrometer was used to hold the sample mounting at the magic-angle.

An alumina rotor ($99.5\%\text{ Al}_2\text{O}_3$) capped with a Kel-F spinner was used as the sample holder, and in all nmr experiments a resin or char sample of approximately 0.2 grams was spun at a MAS speed of $3010 \pm 5\text{ Hz}$. The magic-angle was set by monitoring ^{79}Br FID (Free Induction Decay) from a mixture of KBr and adamantane. The Hartmann-Hahn matching condition for the $^1\text{H}\text{--}^{13}\text{C}$ cross-

polarisation was obtained by adjusting the power of the ^1H channel for a maximum ^{13}C signal from adamantane [Hartmann and Hahn,1962].

The general acquisition parameters were as follows:

- quadrature detection for 1K and zero-filled to 16K
- 29.4 kHz spectral width and 36.8 kHz filter width
- 1000-2000 signal averages
- 5-6 μs 90° ^1H pulse width and 2 s repetition time
- 2 ms contact time

All FID were recorded on the Bruker Aspect computer and transferred to a Sun workstation, and using the nmr spectral analysis software *Felix* (Hare Corporation), the FID's were line broadened with a Gaussian window function of 25 Hz and then Fourier Transformed, phased, and baseline corrected. Chemical shifts had previously been calibrated with respect to tetramethylsilane by using hexamethylbenzene as a secondary standard.

The nmr pulse sequence used in this study is shown in Figure 3.3. After the initial 90° ^1H pulse, the spin-lock period consists of a long ^1H irradiation that is phase shifted from the initial pulse to spin-lock the protons. The ^{13}C contact time irradiation (t_{cp}) is applied to allow for the Hartmann-Hahn cross-polarisation condition between the two spin systems : $\gamma_{\text{H}}H_{\text{H}}=\gamma_{\text{C}}H_{\text{C}}$, such that γ_{I} is the I spin gyromagnetic ratio and H_{I} is the I spin magnetic field in the rotating frame for both ^1H and ^{13}C spins.[Hartmann and Hahn,1962]

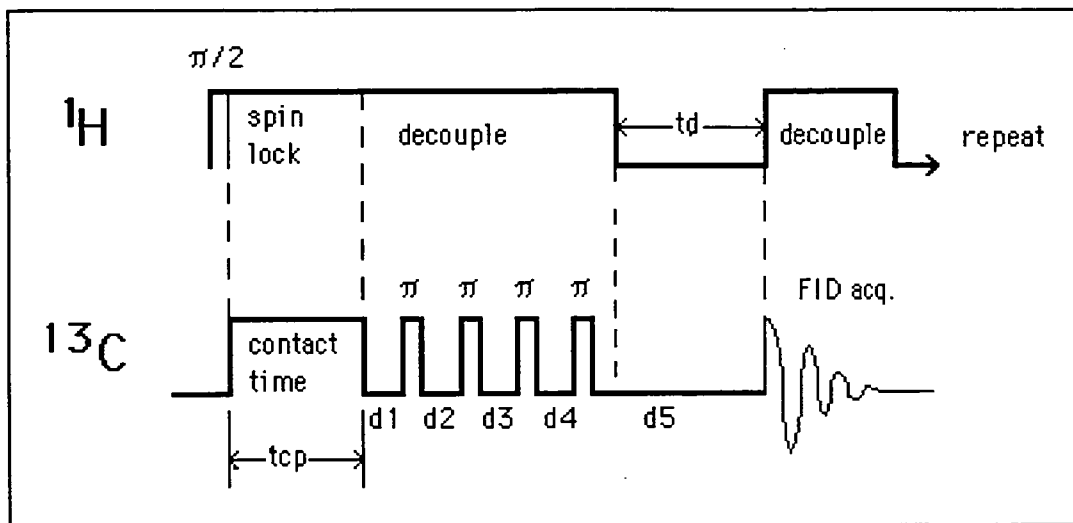


Figure 3.3 The nmr pulse sequence for a cross-polarisation (CP) and dipolar-dephasing(DD) experiment using the total suppression of spinning sidebands (TOSS) technique.

Following the contact time pulse, the TOSS sequence of Dixon [1982] was used to reduce the effects of sideband resonances on the nmr spectra. In the TOSS sequence, four 180° ^{13}C pulses of mismatched amplitudes are applied during proton decoupling so as to phase-alter spinning sidebands and, therefore, cancel the unwanted bands from the nmr spectra. As the TOSS result is very sensitive to pulse errors and delays, the 180°C pulse width and the delay between the last pulse and acquisition time were adjusted by monitoring the sidebands of aromatic carbons in the hexamethylbenzene sample for minimal intensities. The pulse widths are also determined by the proton power [Dixon,1982]. This procedure was conducted at the commencement of every weekly experiment period (usually several days). The pulse width of each of the four 180° pulses was normally in the range 10.5 - 12 μs .

The dipolar-dephasing (DD) experiment was implemented in the TOSS sequence by introducing a decoupler-off period (t_d) in the last TOSS delay before the ^{13}C acquisition time (d_5 in Figure 3.3) [DuBois-Murphy *et al*,1982; Opella *et al*,1979]. During the decoupler-off delay interval there is no applied r.f. irradiation in either the ^{13}C or ^1H channels to allow the ^{13}C spins to precess in their local ^1H dipolar fields. Following this delay, the ^1H decoupling pulse was again applied during the ^{13}C FID

acquisition to provide the decoupled carbon signals [Opella *et al.*, 1979]. As can be seen in the pulse diagram (Figure 3.3), within the five delays around the four 180°C ^{13}C pulses, there are two delays designated D_3 and D_4 that are sufficiently long for a typical DD observation ($> 40\ \mu\text{s}$). In all DD experiments, a single contact time of 2 ms was used.

Two series of spectra were obtained for each sample. Normal CP/MAS experiments with variable contact time, t_{cp} (0.25 - 10 ms), were conducted in order to obtain the aromatic fraction, f_a , and the proton spin-lattice relaxation time in the rotating frame $T_{1\rho}^{\text{H}}$. Dipolar-dephasing (DD) experiments with a contact time of 2 ms and a variable decoupler-off delay, t_d (0.5 - 100 μs), were conducted in order to obtain the quaternary-to-tertiary aromatic fraction, $f_{\text{q/t}}$, of the chars.

Laser Raman Spectroscopy:

The degree of carbonisation of the resins was examined with the aid of Laser Raman spectroscopy on those resin samples heated to temperatures of 600, 700, 800, 900, 1000, 1600 and 2200°C . For the examination of the 1600°C and 2200°C pyrolyses samples, char samples were prepared from each of the 1000°C chars for the six resins (of both the 3 and $10^{\circ}\text{C}/\text{min}$ heating rates) by pyrolysis to 1600°C and 2200°C using the methods described below. The chars were first dampened with isopropanol and uniaxially pressed into 10 mm pellets at a pressure of approximately 150 MPa. The pressed samples were dried at 110°C prior to firing. The char samples were contained in individual graphite crucibles during firing. Two firings, each of 12 samples, were conducted using a graphite resistance furnace with an atmosphere of Argon gas at 1 atm. The firing programs are described as follows.

1600°C Heat Treatment : For each of the six resins, approximately 0.5-0.8 g of the chars formed by heat treatment to 1000°C (at ramp rates of both 3 and $10^{\circ}\text{C}/\text{min}$)

were heated from 25°C to 300°C at 20°C/min. The furnace was held at 300°C until the internal pressure was reduced to a sufficient vacuum of less than 200 $\mu\text{m Hg}$, and then backfilled to atmosphere with high purity argon. The sample was then heated from 300°C to 1600°C at 20°C/min, and held at 1600°C for 6 minutes, prior to cooling to 25°C at 20°C/min.

2200°C Heat Treatment : The 2200°C heating cycle was similar to that of the 1600°C heat treatment program, except that the heating ramp after evacuation and argon back filling was taken from 300°C to 2200°C at 20°C/min, followed by cooling to 25°C at 20°C/min.

Laser Raman spectra were recorded on a Dilor Microdil 28 spectrometer. Each spectrum was collected with the detector in multichannel mode (512 diodes). A slit width of 3.09 cm^{-1} was utilised, without spectral filtering, for each spectrum. A Spectraphysics 164 laser was used as the monochromatic light source, with an Ar^+ excitation wavelength of 514.5 nm (the green line), at a nominal power of approximately 30 mW (+/- 1 mW). For each sample, spectra centred at 1600 and 1250 cm^{-1} were collected separately on the spectrometer, and concatenated later prior to mathematical manipulation of the total 1000 - 1800 cm^{-1} spectrum.

Due to the spectrometer's ability to function as a *microprobe* instrument, its laser beam, which falls at normal incidence with a spot of approximately 2 μm diameter, was positioned such that a certain particle surface of the powdered sample could be selected specifically for its optimal surface topography. Both the optical sample observation, and the laser spectroscopy itself, were conducted through the same microscope at 100X magnification (10X eyepiece, 50X objective lens). The power was adjusted for each sample, depending on the susceptibility of the sample to laser ablation. For each sample, 30 co-adding accumulations were taken with 10 s integration time for each accumulation. The spectrometer was calibrated each day by

using spectroscopic grade silica as a standard. The position of the laser was also adjusted each day.

After the spectral data were collected on to computer disk, the spectra were baseline corrected and deconvolved for the particular vibrational bands using the nmr spectral software Felix (Hare Corp.)

X-Ray Photoelectron Spectroscopy:

The surface technique of X-ray photoelectron spectroscopy (XPS) was used in this study to observe the changes in surface chemistry of the resin chars as they are heated to 1000°C. This technique, also known as Electron Spectroscopy for Chemical Analysis (ESCA), is used to provide chemical and elemental information about the surfaces of solid samples by bombarding the sample with 'soft' X-rays, and collecting and analysing the energy of the ejected photoelectrons to determine their electronic environment, and therefore the atomic species to which they correspond. As the electrons can only escape to the surface from a depth of less than approximately 40 Å, XPS is seen to be a highly surface sensitive technique, and is considered to cause little, if any, surface damage to the sample. Because XPS can only provide chemical and elemental information from lithium onwards in the periodic table, the surface hydrogen content of these resin chars cannot be established [Gasser,1985]. The X-rays used to produce photoelectrons are themselves produced by electron bombardment of metal targets, generally Mg or Al, held at a potential of 15 - 20 kV. A thin foil window, (usually Al or Be) separates the X-ray source and sample, preventing electron escape from the source region.

The spectrum of the X-rays produced contains the characteristic $K\alpha$ emission lines, and also a component known as the Bremsstrahlung emission which accounts for approximately 50% of the observed X-ray intensity, but does not have a significant

effect on photoelectron emission. The $K\alpha_{1,2}$ line has a full width at half maximum peak height (FWHM) of approximately 1 eV for Mg and Al sources with greater energy resolution achievable if a monochromated X-ray source is used. Standard unmonochromated X-ray sources are sufficient to determine core level binding energies to within 0.2 eV [Feldman and Mayer, 1986].

The X-rays produced from the source are then used to eject core level electrons from the surface atoms and deeper atoms of the sample material. Electrons are generally ejected from a range of core levels and as a result emerge with different kinetic energies, which allows the fingerprints of individual elemental constituents to be identified. The resulting energies of the photoelectrons are analysed to determine their distribution, and therefore to display characteristic peaks corresponding to the surface constituents. The kinetic energy of the photoelectrons arising from an atomic species is determined by the following equation;

$$E_k = h\nu - E_b - \phi \quad \text{.....(i)}$$

where $h\nu$ is the energy of the incident radiation, E_b is the characteristic atomic binding energy of the ejected electron and ϕ is the work function term. The binding energy of the electrons can then be calculated automatically (by computer) from the detected kinetic energy by assuming a work function value for the spectrometer [Lubenfeld, 1977].

For the X-ray source, a standard Elliot hospital Al $K\alpha_{1,2}$ (1487 eV) X-ray generator was used with an aluminium window to filter scattered incident electrons. Approximately 10% of the X-ray intensity was due to the $K\alpha_{3,4}$ satellite line. The accelerating current was at 15 mA and 15 kV potential. The spectrometer was regularly calibrated by comparing a gold spectrum against the theoretical spectrum of the $Au4f_{7/2}$ peak which has a sharp peak at a kinetic energy of 1402.6 eV. The spectrometer used was a modified A.E.I. ES100, with a hemispherical analyser and

multichannel detector held at 2000 V with 255 channeltrons in the detector plate allowing for an 8 eV scan width. The detector was interfaced to a dedicated IBM compatible AT 80386 computer. The computer was used for control of the X-ray source and spectrometer, and for data acquisition and storage. The software needed for these processes was written in the *Turbo-Pascal* computer language. The stored spectra were converted to ASCII files and transferred to a SUN computer such that the data could be later manipulated for spectral resolution and peak integration. The software to undertake these functions was written in the *Fortran* computer language, and modified by the author to suit the format of the XPS spectral files.

The resin char samples to be analysed had been stored in high purity argon after pyrolysis and removed only minutes prior to XPS analysis. This was done to minimise possible surface oxidation of the chars from atmospheric oxygen or water. The samples were mounted and pressed on a gold support which had been cleaned with acetone and zirconia paste just prior to each analysis. The mounted sample was then placed inside a VG high vacuum sample chamber, whose internal pressure, after closing, was reduced to a vacuum of 10^{-8} Torr. When this vacuum was achieved, the sample was passed through a butterfly valve opening into the spectrometer chamber which always remained at a vacuum of 10^{-10} Torr. This low vacuum was sustained by a diffusion pump system such that the time taken to form a monolayer of contamination on the surface of the sample would be in the order of several hours, which was several orders of magnitude longer than the time taken to acquire each spectrum. Considering all contributing factors, the scaling of the binding energies for the elements was such that a binding energy range of 0 - 1200 eV corresponded to a kinetic energy range of 1476 - 274 eV respectively. For each char sample the acquisition conditions are shown in Table 3.3. Four different binding energy ranges were observed such that each range was analysed by acquiring signal counts for the acquisition time period at each binding energy step in the binding energy range.

Scan Region	B.E. (eV)		Acquisition Time (ms)	Step (eV)
	Start	Finish		
Wide	200	800	500	0.5
C1s	265	305	500	0.1
O1s	515	555	4000	0.1
N1s	380	420	4000	0.1

Table 3.3 Acquisition conditions for the XPS analyses of each resin sample.

The wide scan of 600 eV width was conducted as an indication of the approximate proportions of the different elemental peaks for each sample. The three elements likely to be detected on the surface of the chars, i.e., carbon, oxygen and nitrogen, are observed by the ranges centred at 284.6 (C1s), 532.7 (O1s) and 400.5 (N1s) respectively [Gai *et al*,1989; Hu *et al*,1988; Kozlowski and Sherwood,1986]. The acquisition time is the length of time (in milliseconds) during which the detector is held at a particular binding energy (eV) step, which is analogous to the number of scans. Because the C1s peak is likely to be more intense than the O1s or N1s peaks due to the nature of the sample, an acquisition time of 500 ms at each 0.1 eV step was considered sufficient to collect the C1s spectrum, as compared to 4000 ms for the O1s and N1s spectra. The carbon surface was itself used as a secondary standard such that all the peaks were shifted to compensate for any drift of the C1s peak away from the theoretical 284.6 eV peak centre.

For the determination of the relative concentrations of the three surface species, the following equation is used [Brown *et al*,1981];

$$n_1/n_2 = K.(I_1/I_2) \quad \text{.....(ii)}$$

where n_1 and n_2 are elemental concentrations and I_1 and I_2 are XPS peak areas of elements 1 and 2 respectively, and K is a function of the spectrometer and the elements examined [Brown *et al.*,1981]. Details of the function K are reported in the literature [Bancroft *et al.*,1979a,1979b], and it is shown that this factor is related to the probability of exiting a photoelectron, or *cross-section* as calculated by Scofield [1976]. As the calculation of the K factor is relatively complicated and out of the scope of this study, it was found that a comparison of the ratios of the elemental peaks within each sample was a satisfactory substitute, and useful in eliminating the need for such calculations. The XPS results therefore represent a relative, rather than absolute, change in concentration of the surface oxygen and nitrogen species as a ratio of the concentration of surface carbon, being the most abundant species. For the purpose of analysis, the chemical nature of the surface elements was determined quantitatively by comparing the areas of each peak within the same sample. This form of analysis has been used in other studies [Kozlowski and Sherwood,1986; Wandass *et al.*,1987; Yoshida *et al.*,1990]. This was also done to eliminate the effects of the sample surface roughness, and orientation in the spectrometer, on the signal to noise ratio of the spectrum, as these factors are seen to affect each element equally within the same sample. The effect of any spectrometer peak broadening function is also removed by this method [Briggs, 1978].

Chapter Four

**An overview of the Phenolic
Resin pyrolysis process (25 -
1000°C) by Thermo-Gravimetric,
Elemental and Liquid Volatiles
Analyses.**

Thermo -Gravimetric Analysis.

An initial series of thermo-gravimetric analyses was conducted on each of the six resins to determine differences in their thermal properties according to the temperatures and rates at which the greatest degree of volatiles weight loss occurs.

Figures 4.1 and 4.2 show the TGA results for the six resins at the two ramp rates of 3°C/min and 10°C/min respectively. The results for the 3°C/min experiments show that NFH sustains the greatest retention of its mass over the heat treatment temperature range, losing approximately 35% of its mass to volatilisation of organics. The resin NFP appears to have a slightly lower mass retention with a weight loss of 38% at 1000°C, with the other four resins displaying similar thermo-gravimetric properties with final mass losses of approximately 50% to 55% at 1000°C.

The results for the 10°C/min experiments show that for NFH and the furfuryl-alcohol containing resins there is no appreciable difference, although for NFP there is a slight increase in weight loss to 42% at 1000°C. These results show evidence of a lack of sufficient cross-polymerisation in the furfuryl-alcohol free resins in their post cured state and their subsequent ability to form a low temperature *meso*-phase at approximately 200°C (also observed visually). The *meso*-phase creates a surface barrier through which the organic volatiles from the pyrolysing bulk cannot pass at higher temperatures.

From Figures 4.3 and 4.4 the differential thermo-gravimetric analysis (DTG) shows from the rates of mass loss for each resin that three ranges of mass loss can generally be distinguished for all resins, as follows;

a) 50°C to 250°C; b) 250°C to 600°C; c) 600°C to 1000°C.

Two anomalies to this observation are; i) the DTG peaks for NFH for the 3°C/min and 10°C/min heating rates are centred at temperatures approximately 100°C higher than the average for the five remaining resins at approximately 400°C; ii) for both heating rates, NFP has two DTG peaks, at 350°C and 550°C which suggests two modes of weight loss within the 250°C to 600°C range.

The TGA curves for these resins show similar trends to the highly cross-linked phenol-formaldehyde resins of Fitzer and Schaefer [1970] as the continuous curve shape suggests that there are no further cross-linking or polymerisation processes taking place. From the TGA studies of Dollimore and Head [1967] it is shown that these resins are seen to behave in an exothermic nature with the slower reaction occurring between 104 and 406°C and the faster reaction occurring at 560°C with up to 50% of its original mass being removed due to gas evolution. Compared to TGA results of Simitzis [1991], the above temperature ranges suggest that these resins also exhibit similar thermal degradation properties to a furfuryl-alcohol - formaldehyde composite. The only exception is NFH which has a lower weight loss and whose thermal activity appears to occur at higher temperatures. This suggests that NFH inhibits weight loss to a much greater degree than the other resins. As has been suggested, it is possible that the degradation mechanism of the other resins allows for a relatively free evolution of volatiles through micropores, whereas that mechanism in NFH is opposed by the formation of a barrier to volatiles evolution.

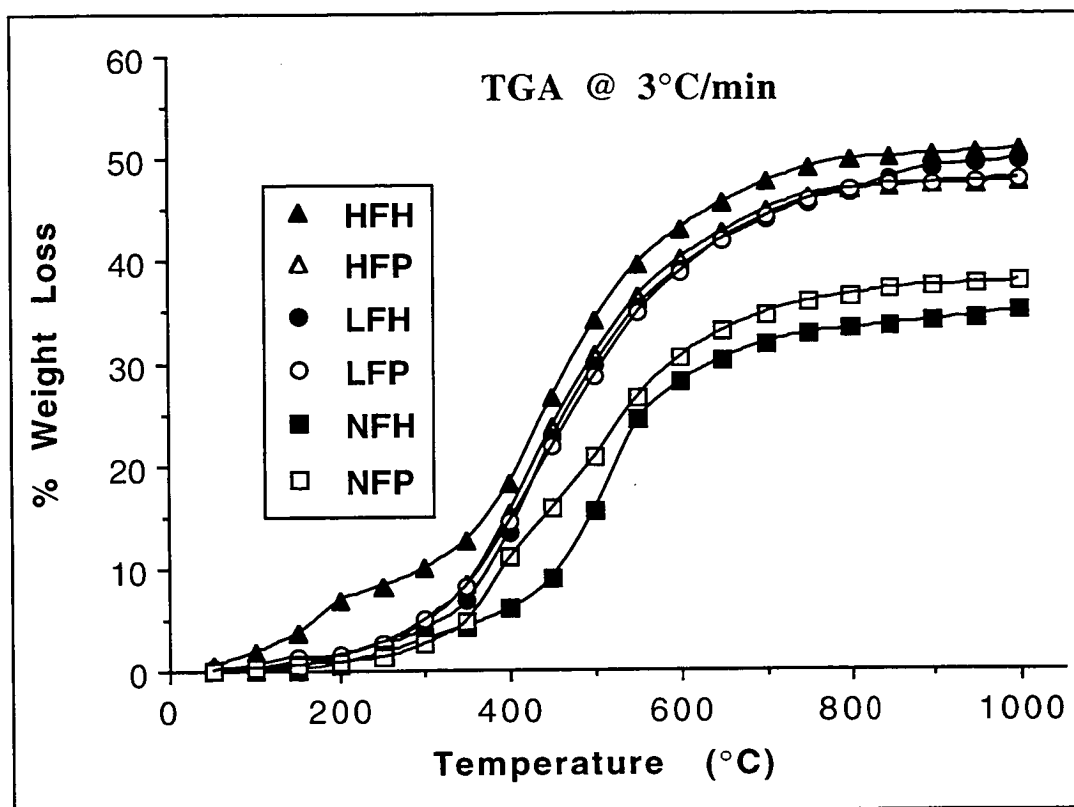


Figure 4.1 The TGA curves for the 3°C/min ramp rate.

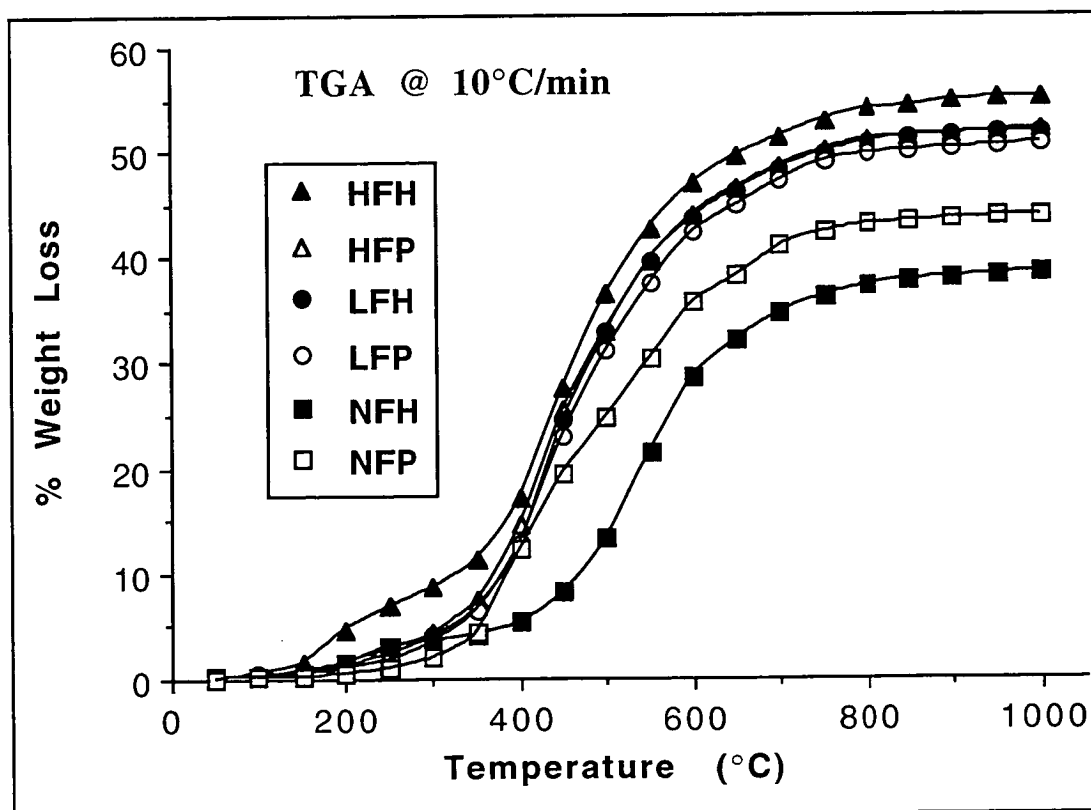


Figure 4.2 The TGA curves for the 10°C/min ramp rate.

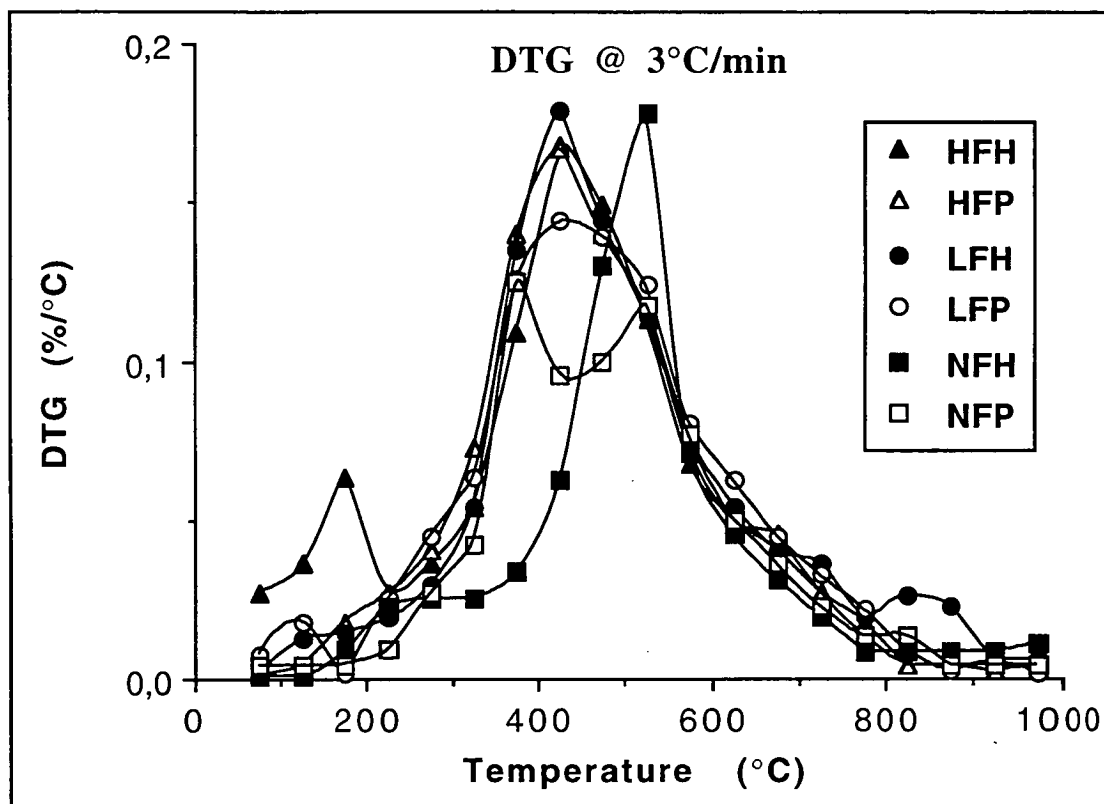


Figure 4.3 The DTG curves for the 3°C/min ramp rate.

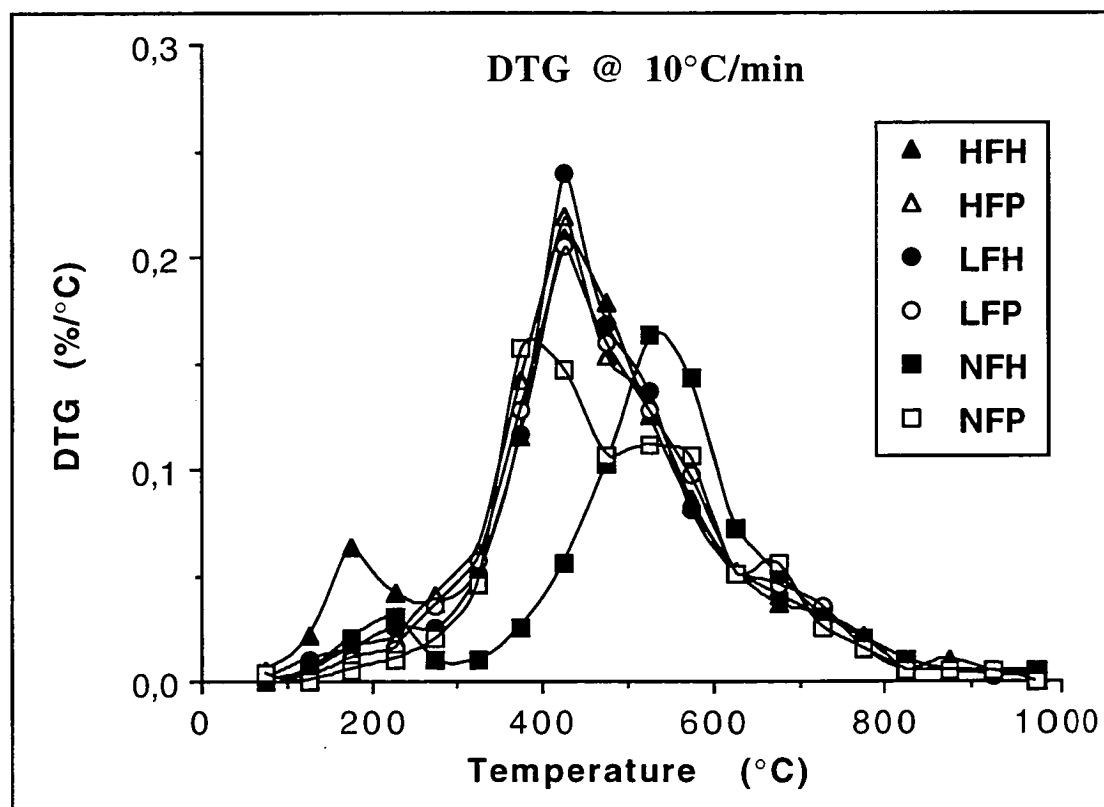


Figure 4.4 The DTG curves for the 10°C/min ramp rate.

As the powdered sample for NFH is visually observed to be fused after pyrolysis to 200°C, the barrier to volatiles evolution could be due to the repolymerisation of the resin upon subsequent heating. In the TGA experiments of HFH at both 3°C/min and 10°C/min (Figures 4.1 and 4.2), it is seen that a slight discontinuity exists at approximately 200°C which suggests a predominant loss of excess furfuryl-alcohol before the major degradation processes begin (also shown in Figure 4.15).

The bimodal characteristics shown by NFP in the differential thermo-gravimetric analyses of Figures 4.3 and 4.4 suggest that this resin lacks the continuous volatile evolution patterns of the other resins, and that it may have a series of events in its pyrolysis process where volatiles are seen to build up due to the *meso*-phase formation, and then be released due to the excess back-pressure. This phenomenon is shown most severely in the higher heating rate of 10°C/min.

In general, it is suggested from Dollimore and Heal [1967] that these TGA curves follow a similar trend to those of a group of carbon precursors which includes polyacrilamide, polyfurfuryl-alcohol, cellulose and cellulose acetate, which are also seen to show mainly exothermic DTA peaks. To qualify the ideal TGA experiments from the Setaram thermo-gravimetric analyser, the weight loss of each bulk pyrolysis sample, after heating to each successive heat treatment temperature during the production of the bulk carbon samples at 3°C/min, was calculated as a percentage of the original sample weight for each resin and presented as a discontinuous Thermogravimetric Analysis (DTGA) in Figure 4.5. It is shown from Figure 4.5 that in the weight loss results of the pyrolysis experiments, the greater sample mass of 1 to 3 grams, as compared to approximately 50 milligrams in the TGA experiments, has provided for a slight increase in weight loss of the DTGA bulk samples for all the resins, although, least of all for NFH, which has an approximate ultimate bulk weight loss (i.e. as the temperature approaches 1000°C) of 35%. From this it is suggested that the 5 min dwell time at temperature for the

bulk pyrolysis samples causes a continued isothermal weight loss in the resins. The greater variance shown in the DTGA curves of NFH and NFP is likely due to the previously suggested volatile transport barrier, present at or near 200°C, which may cause some inconsistencies in the relative weight loss with temperature, particularly as this phenomenon would also be a function of other varying factors such as bulk sample geometry, sample mass, etc. The general relative trends of the DTGA curves of Figure 4.5 follow closely to those of the TGA curves in Figure 4.1 in that NFH, again, shows the lowest weight loss at approximately at 1000°C, followed by NFP at approximately 50%, with the remaining resins all at approximately 55% after the 1000°C heat treatment. Therefore, the pyrolysis experiment for each resin follows the TGA experiments relatively closely, and in addition, the method adopted in this research program of taking representative *snap-shot* samples of the resins at 50°C intervals during heat treatment to 1000°C is valid in modelling the true continuous pyrolysis of these resins.

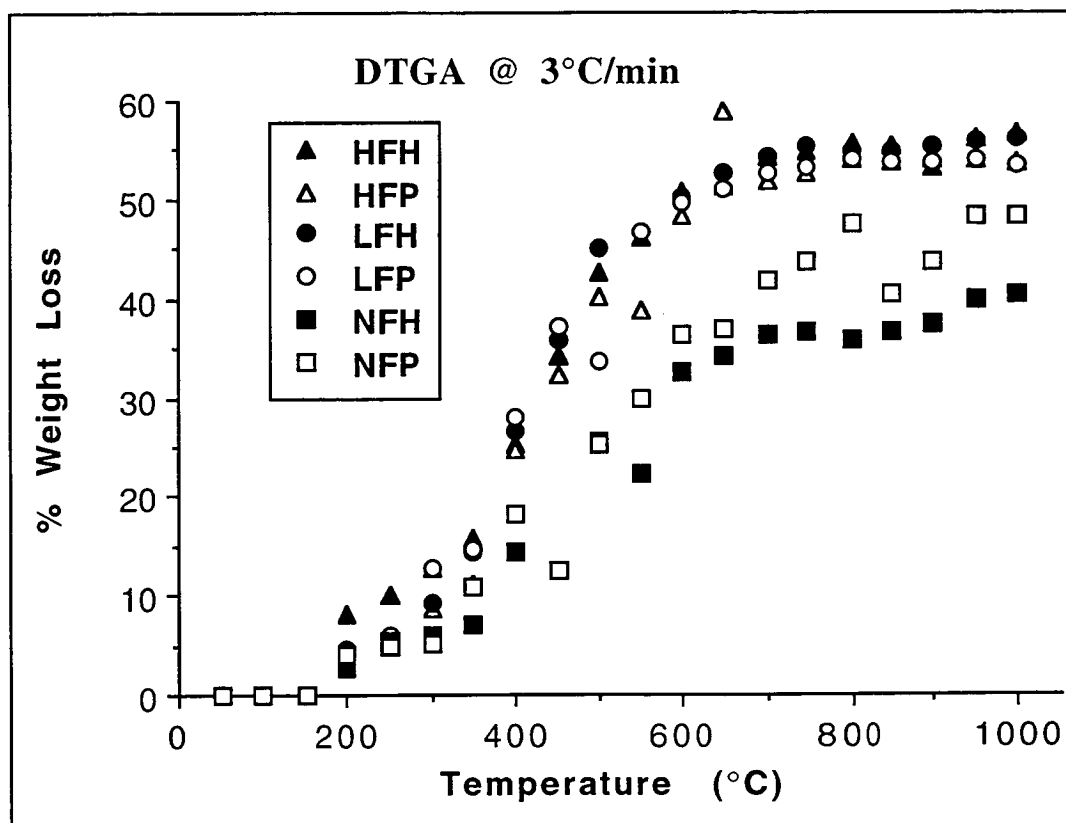


Figure 4.5 The Discontinuous Thermo-gravimetric Analysis curves for the resins pyrolysed at 3°C/min.

Elemental Analyses

The resins, and their solid pyrolysis products, were analysed for their weight percent contents of carbon, hydrogen, nitrogen and oxygen (by difference). The analyses were converted to atomic % and the changes in elemental species over the pyrolysis temperature range are presented in Figure 4.6 (at% carbon), Figure 4.7 (at% hydrogen), Figure 4.8 (at% nitrogen) and Figure 4.9 (at% oxygen). The theoretical elemental analyses from the constituent composition of the resins were calculated from the molecular weights and the molecular formulae of the resin's organic compound precursors. These data are compared with the experimental data and presented in Table 4.1.

Resin	N			C			H			O		
	Theor.		Exp.	Theor.		Exp.	Theor.		Exp.	Theor.		Exp.
	Pre ^a	Post ^b		Pre	Post		Pre	Post		Pre	Post	
HFH	0.62	1.17	1	41.41	44.87	47	45.48	44.65	43	12.47	9.31	9
HFP	0.00	0.00	0	41.41	45.56	48	45.30	44.12	42	13.27	10.32	9
LFH	1.39	1.32	1	45.05	45.69	46	44.66	44.47	44	8.88	8.52	9
LFP	0.00	0.00	0	45.11	46.56	48	44.25	43.84	43	10.63	9.60	9
NFH	2.12	1.86	2	47.34	47.67	47	44.22	44.05	45	6.30	6.42	7
NFP	0.00	0.00	0	47.48	49.10	49	43.57	43.11	43	8.94	7.79	8

Table 4.1 The comparison between the theoretical atomic % elemental analysis of the six resins (theoretical) in the (a) pre-cured, and (b) post-cured (pre-pyrolysis) condition and the experimental analyses (exp) of the post-cured resins.

The differences between the theoretical elemental analyses of the pre- and post-cured resins are due to solvent loss of the various constituents (proprietary knowledge of the sponsoring company). The experimental elemental analyses of

the unpyrolysed post-cured resins display a reasonable accuracy to the associated theoretical results.

The variation of elemental carbon content of the resins as they are pyrolysed is shown in Figure 4.6, and it is shown that the carbon yields of the resins are as expected [Fitzer *et al*,1971], with no major differences between the resins. The release of volatiles above 350°C causes the carbon content to rise significantly and then to plateau near 750°C at approximately 90 atom%. The similarity between the resins suggest that the volatile loss mechanisms are similar for all resins, despite the different starting chemistry, hence carbon loss cannot be used as a criterion for resin differentiation.

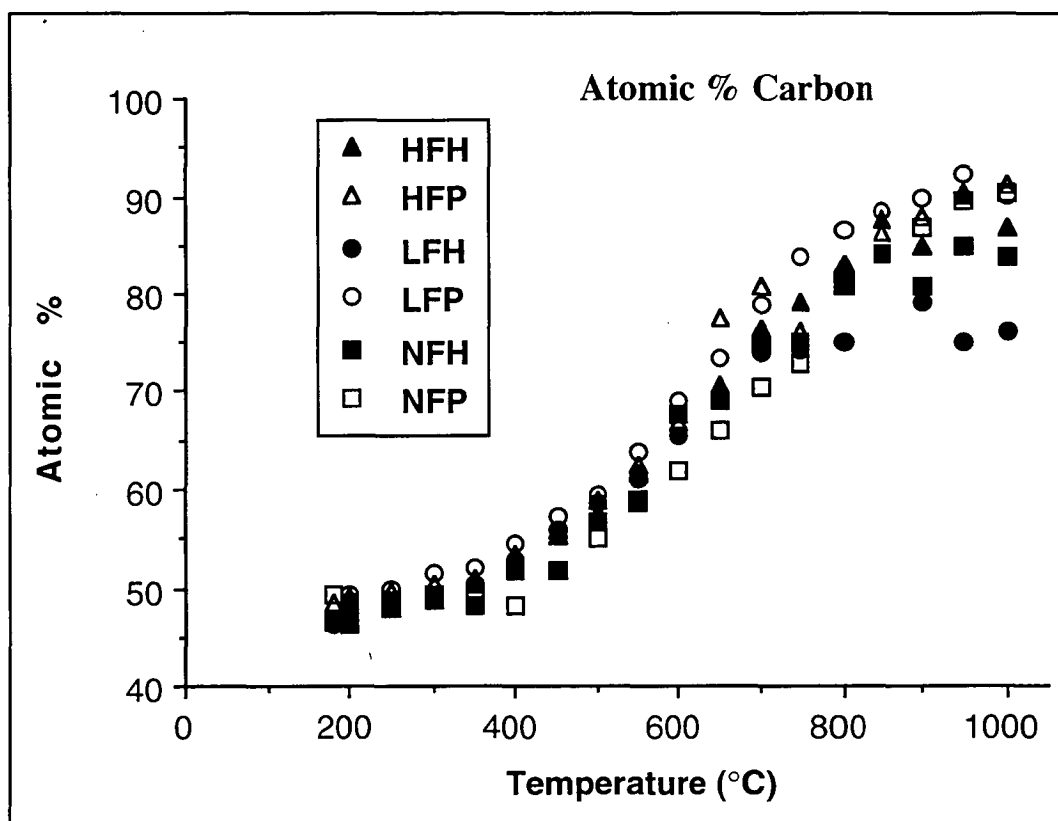


Figure 4.6 Variation of atomic % carbon of resin chars over the heat treatment temperature range.

The variation of elemental hydrogen content of the resins (Figure 4.7) shows that the curves for each resin are seen to parallel each other over the pyrolysis temperature range which suggests that the hydrogen loss mechanisms for all of the resins are similar.

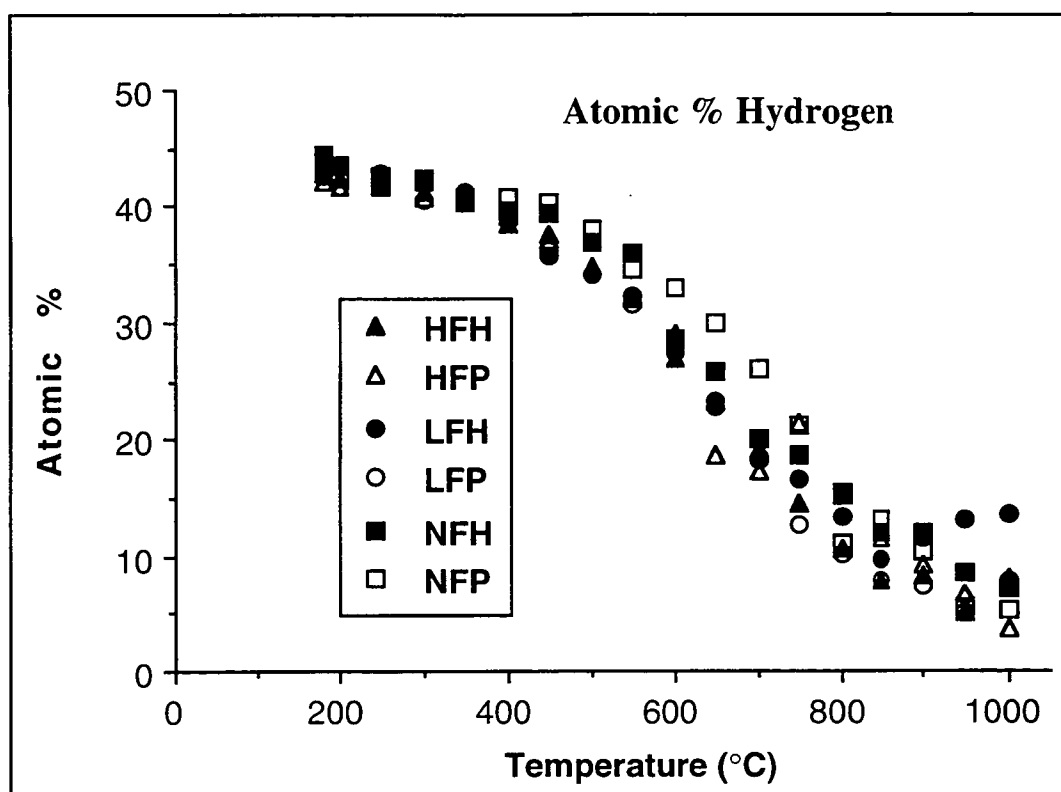


Figure 4.7 Atomic % hydrogen of resin chars over the heat treatment temperature range.

The nitrogen elemental analyses of the three hexamine containing resins over the heat treatment temperature are shown in Figure 4.8. The curve for HFH shows no significant change in nitrogen content during pyrolysis, and the low level of approximately 1 atom% suggests that the nitrogen is capable of remaining as a hetero-atom in the carbon lattice, or as surface species. The nitrogen curve for LFH shows a similar pattern to that of HFH, although there is an anomaly shown between 400 and 600°C which represents a sudden rise in nitrogen level. This is possibly due to random error, as this increase is within the observed error between the theoretical and experimental results. The flat and linear nature of the curve would agree with this hypothesis. The nitrogen curve for NFH shows a significant

difference to that of the other two nitrogen containing resins in that the nitrogen content of NFH decreases markedly with temperature from the cured analysis at 180°C to 350°C where it can be assumed to be zero. Combined with TGA results, this suggests that the major weight loss mechanism of NFH up to 350°C is via the volatilisation of nitrogen species.

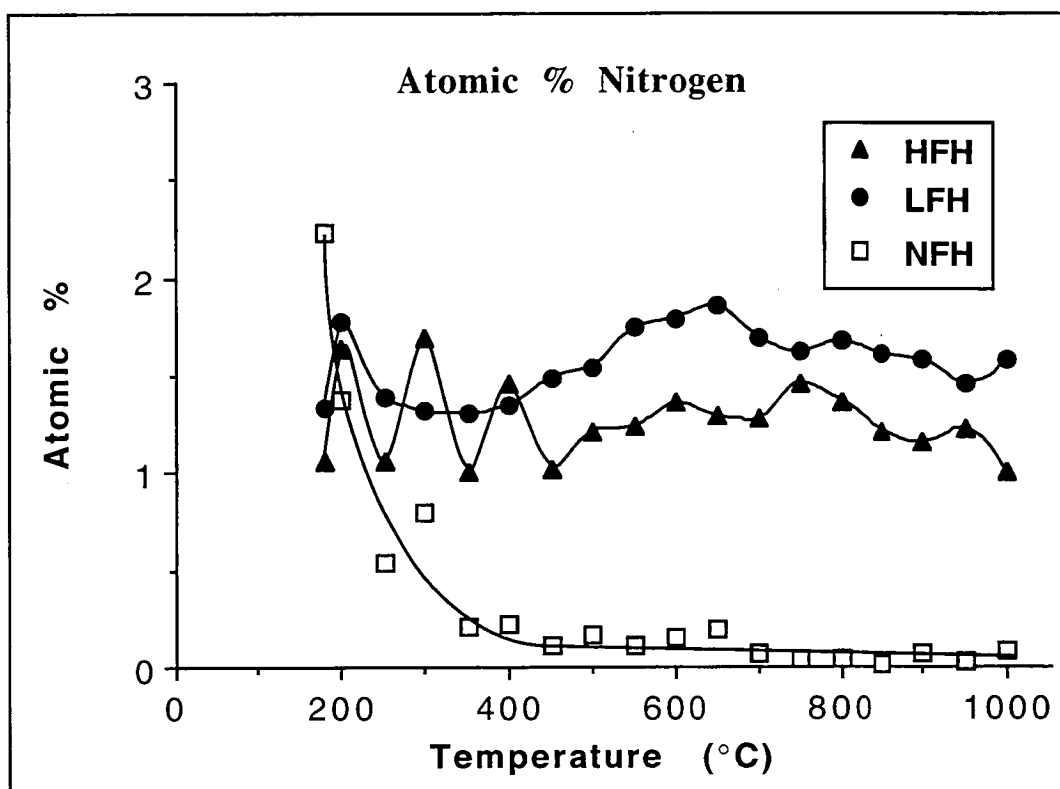


Figure 4.8 Atomic % nitrogen of resin chars over the heat treatment temperature range.

The oxygen elemental analyses are shown in Figure 4.9. As is expected, the bulk oxygen composition of the chars is shown to decrease with increasing heat treatment as this species is removed with the volatile organics. The variation of atomic oxygen content of the resins over the temperature range follows the trends of hydrogen for most resins, although LFH, and to a lesser extent NFP, show an increased oxygen content above 750°C. It is possible that the morphology and chemical nature of the carbons at the higher temperatures (>750°C) creates difficulty in collecting true data from the elemental analyses in that these carbons could not be completely oxidised to CO₂ in the elemental analyser furnace tube, and therefore,

they provided a great error in their oxygen analyses. A large error for the oxygen composition is due to its calculation as the difference between the experimentally derived elemental compositions (C, N, H) and 100%. Because of this error the curves show a large variance in values and this is most obvious in the case of NFH and NFP. Therefore, it is possible that the lack of furfuryl-alcohol in the initial resin formulation of these two resins provides for a greater retention of oxygenated functional groups to higher pyrolysis temperatures, which create large crystallites in the char structure that are difficult to fully oxidise to CO_2 at high temperatures, and which therefore cause a greater source of error in the elemental analyses.

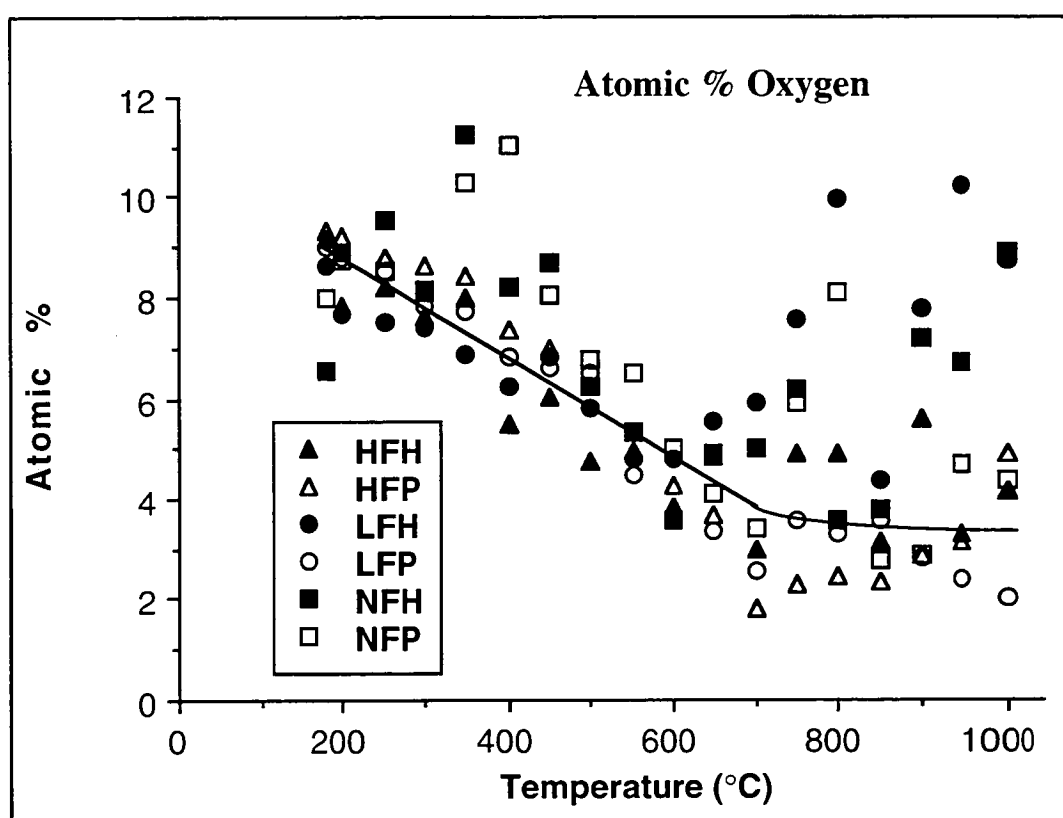


Figure 4.9 Atomic % oxygen of resin chars over the heat treatment temperature range.

The residual molar compositions of the resins over the pyrolysis temperature range are shown in Figure 4.10 (carbon), Figure 4.11 (hydrogen), Figure 4.12 (nitrogen) and Figure 4.13 (oxygen). These data were calculated by correcting the amount of resin in the initial 25°C pyrolysis sample to 100 mols and multiplying the weight

loss (Discontinuous TGA from the pyrolysis experiments) for each 50°C temperature interval by its corresponding elemental analyses. For residual carbon it can be seen from the curves in Figure 4.10 that the resins show a similar and constant degree of carbon loss between 150 and 350°C, although, above 400°C there is shown a wide variation in the degree of absolute elemental loss of carbon in the resins. NFH is shown to retain the greatest amount of carbon by only losing 18% of its original carbon up to 1000°C and the carbon loss process for this resin is effectively terminated above 400°C. Resins LFH and NFP are seen to lose 37% of their original carbon, LFP and HFH 43% and HFH 48%, and these five resins exhibit carbon loss up to 600°C with a sharp increase in the rate of carbon loss between 400 and 500°C. As the absolute hydrogen (Figure 4.11) and oxygen (Figure 4.13) content of the resin systems decrease over the pyrolysis temperature range up to 700°C at a constant empirical molar ratio of 5 hydrogens to 1 oxygen atom (H_5O), it is possible that the major volatile species are water and hydrogen [Lausevic and Marinkovic, 1986]. The spread of results in the high temperature tail of the residual oxygen composition of the resins in Figure 4.13 is likely due to error in the oxygen elemental analyses as described earlier.

The nitrogen profile for the three nitrogen bearing resins (Figure 4.12) is similar to those of the individual atom % elemental analyses of nitrogen in Figure 4.8. The profiles for HFH and NFH show great similarity, suggesting that the nitrogen loss process isn't greatly dependent on the level of furfuryl-alcohol in the initial uncured resin, although the total loss of nitrogen in NFH above 400°C again suggests that the furfuryl-alcohol plays a role in nitrogen retention of the resins up to 1000°C. In the residual composition profile, HFH and LFH also show a tendency to decrease in absolute nitrogen content rather than remain constant above 200°C, as in Figure 4.8, which suggests that a nitrogen loss process exists in all three resins to 1000°C.

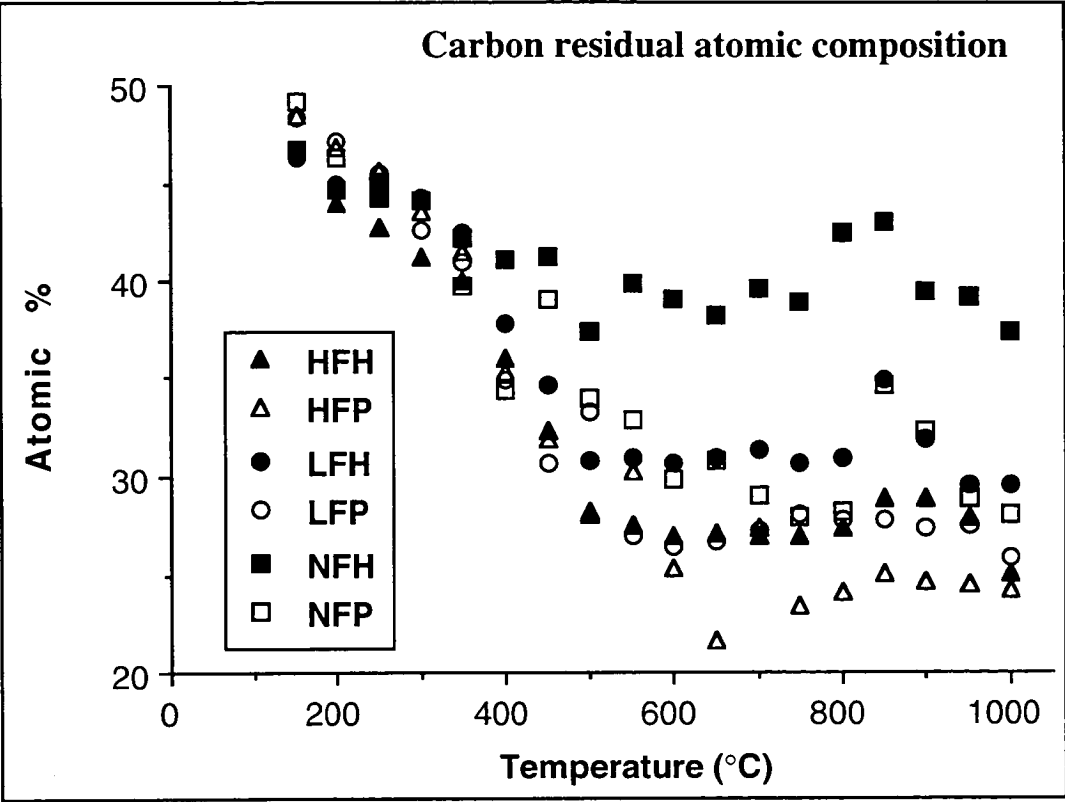


Figure 4.10 Carbon residual molar composition over the heat treatment temperature range.

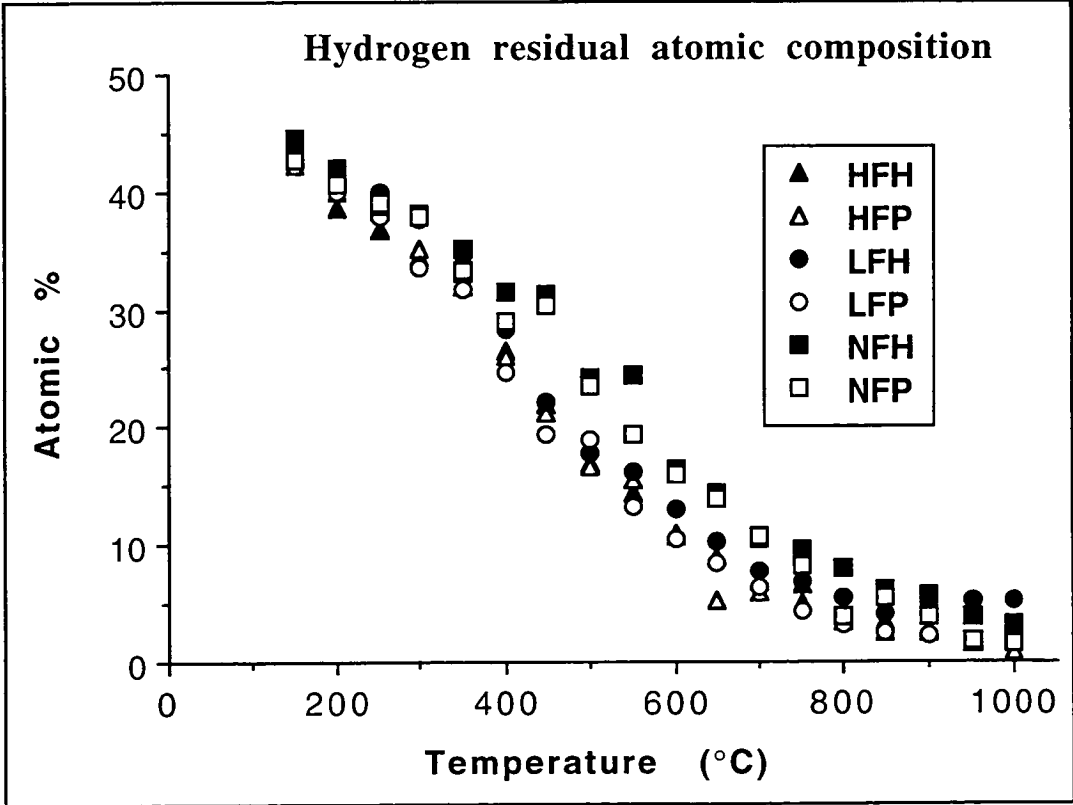


Figure 4.11 Hydrogen residual molar composition over the heat treatment temperature range.

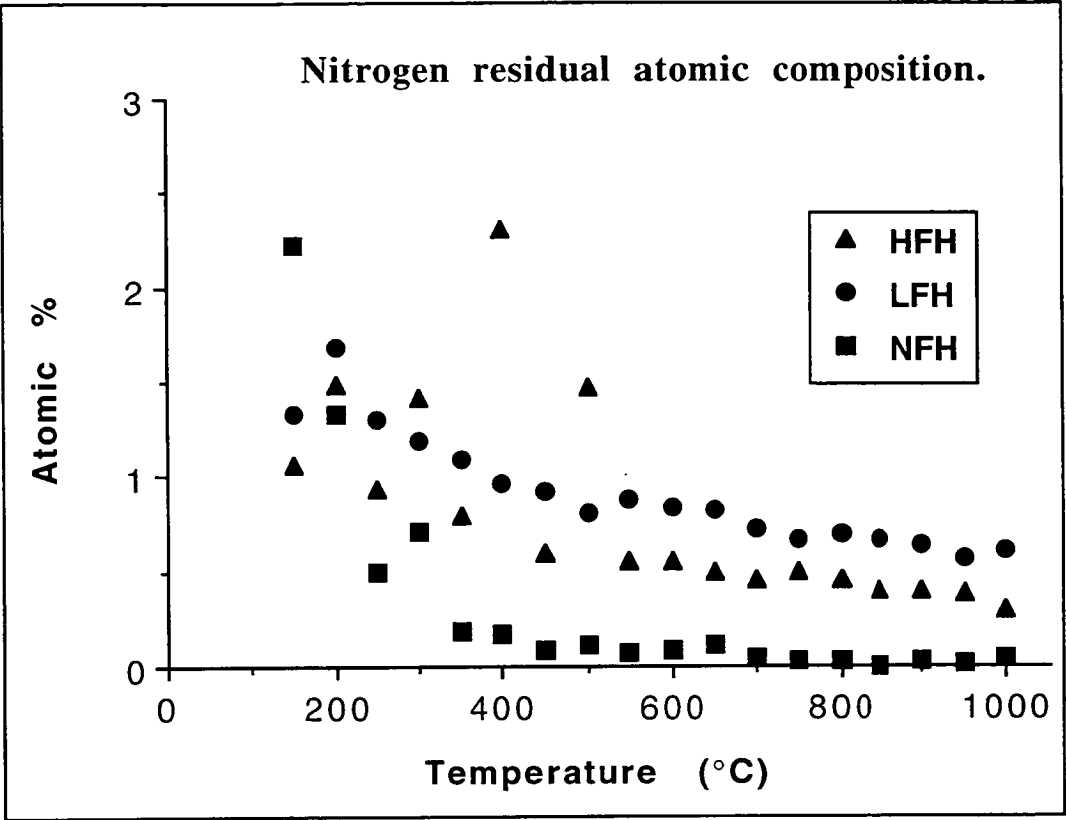


Figure 4.12 Nitrogen residual molar composition over the heat treatment temperature range.

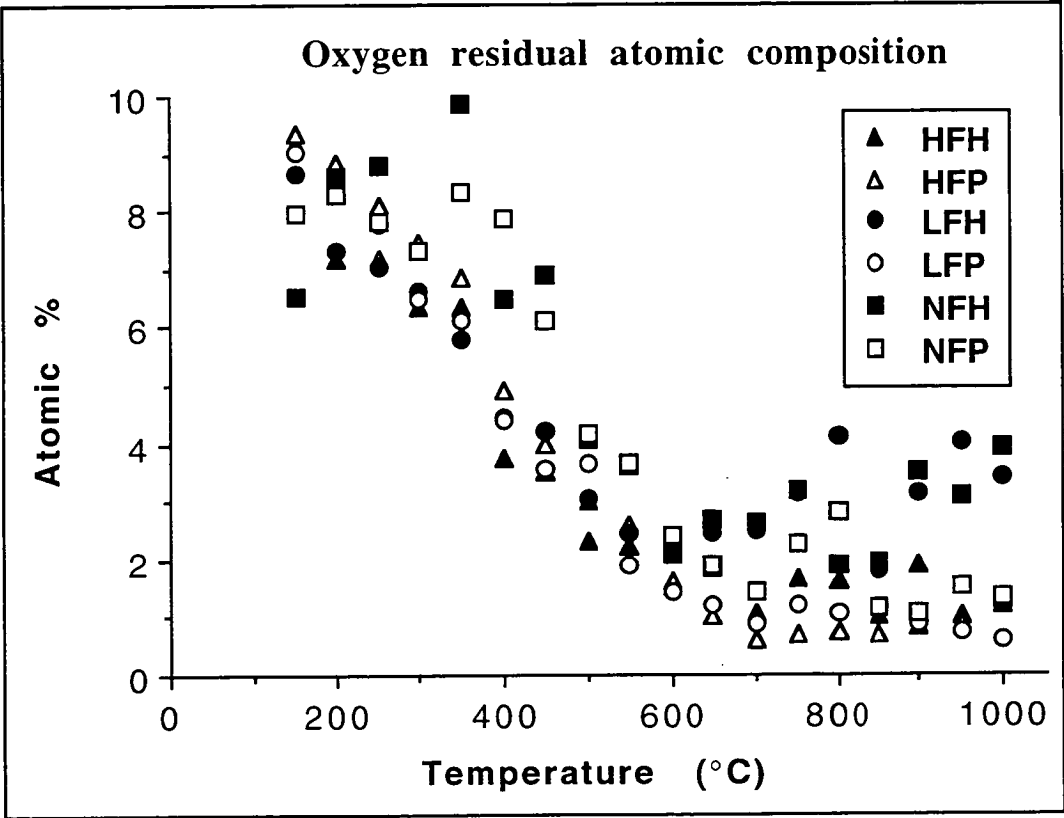


Figure 4.13 Oxygen residual molar composition over the heat treatment temperature range.

Liquid Volatiles Analysis

An analysis of the condensed volatiles from the pyrolysis process was conducted so as to determine approximately the stages at which certain reactions take place during the carbonisation process of the phenolic resins. The term *relative evolution* is used here because the amounts of the volatiles species produced are calculated relative to the mass of the as-cured resin sample just prior to pyrolysis. The relative evolution of water from the resins over the pyrolysis temperature range is shown in Figure 4.14. It can be seen that the main temperature range for the production of water during pyrolysis is from 300 to 750°C. The maximum water losses appear to be similar for all resins, although the maximum water evolution for NFH is seen to occur at a temperature approximately 100°C higher than the other resins. Another water loss peak between 100 and 300°C suggests the presence of two water production mechanisms in the resins. This phenomenon is most obvious in HFH.

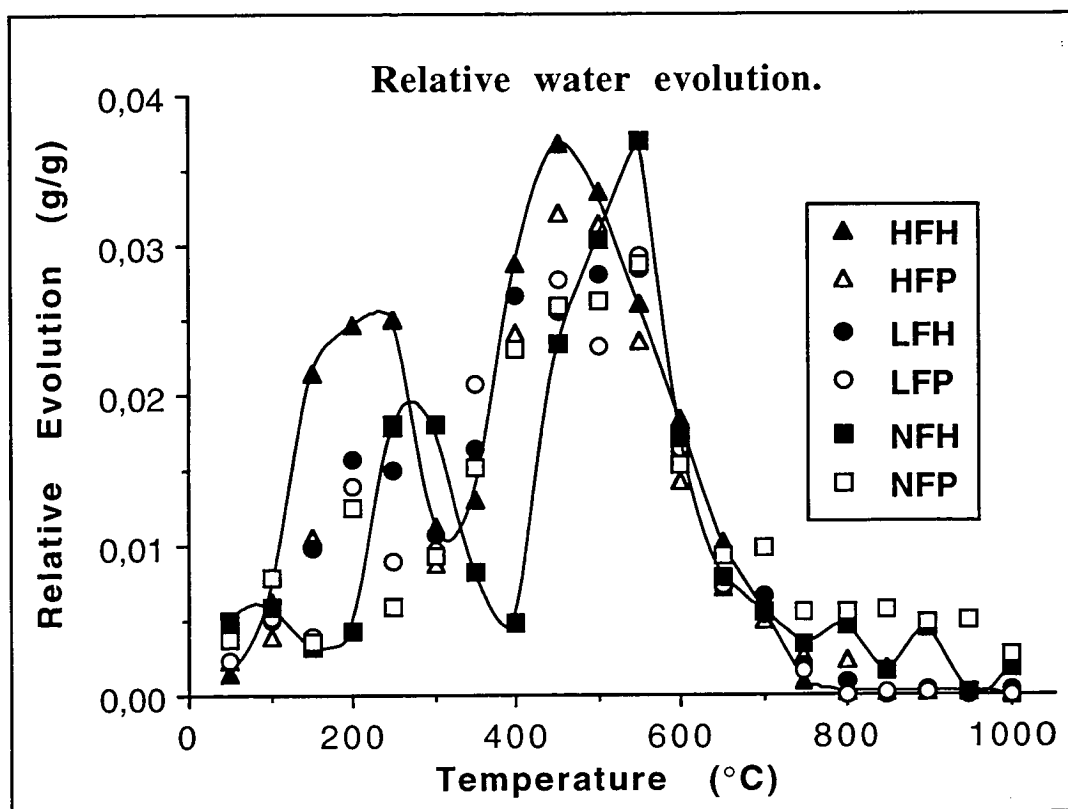


Figure 4.14 The relative evolution of water from the resins over the heat treatment temperature range.

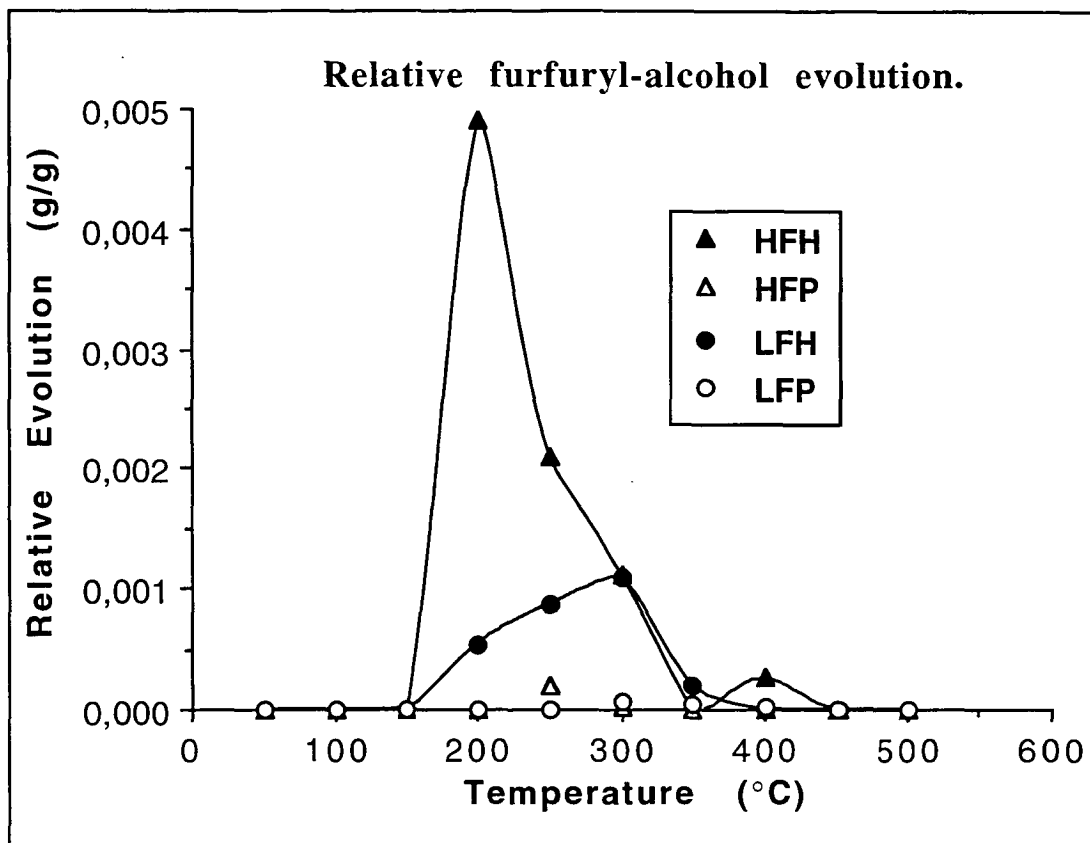


Figure 4.15 The relative evolution of furfuryl-alcohol from the furfuryl-alcohol containing resins over the heat treatment temperature range.

The relative amounts of volatilised organics from the resins are shown in Figures 4.15 to 4.23. The molecular species detected by GC/MS could not easily be determined isomerically and therefore the relative amounts of the species reported in this study are by total abundance of their various isomeric forms. From Figure 4.15 it is shown that HFH evolves the greatest amount of furfuryl-alcohol of those resins which had been cured with furfuryl-alcohol. As this loss is also seen in LFH, except to a lesser degree, it is possible that the hexamine used in the curing of HFH and LFH has the effect of promoting the evolution of furfuryl-alcohol. The relative amount of furfuryl-alcohol lost from HFH, which is approximately 5 times that of LFH, doesn't compare closely to HFH having approximately 1.5 times the starting content of furfuryl-alcohol as LFH. Therefore, the lower hexamine content in HFH fails to retain furfuryl-alcohol to the same degree as LFH. The paraformaldehyde in HFP and LFP assists the furfuryl-alcohol in cross-linking the

phenolic chains with the effect that the furfuryl-alcohol is not available for volatilisation. The GC/MS analysis of the volatiles from HFH and LFH also show the presence of difurfuryl-ether in approximately the same proportions and at the same temperatures as that of furfuryl-alcohol. This is an additional indicator of the evolution of free furfuryl-alcohol, and therefore its inability to react sufficiently with the phenolic resin in the hexamine cured HFH and LFH.

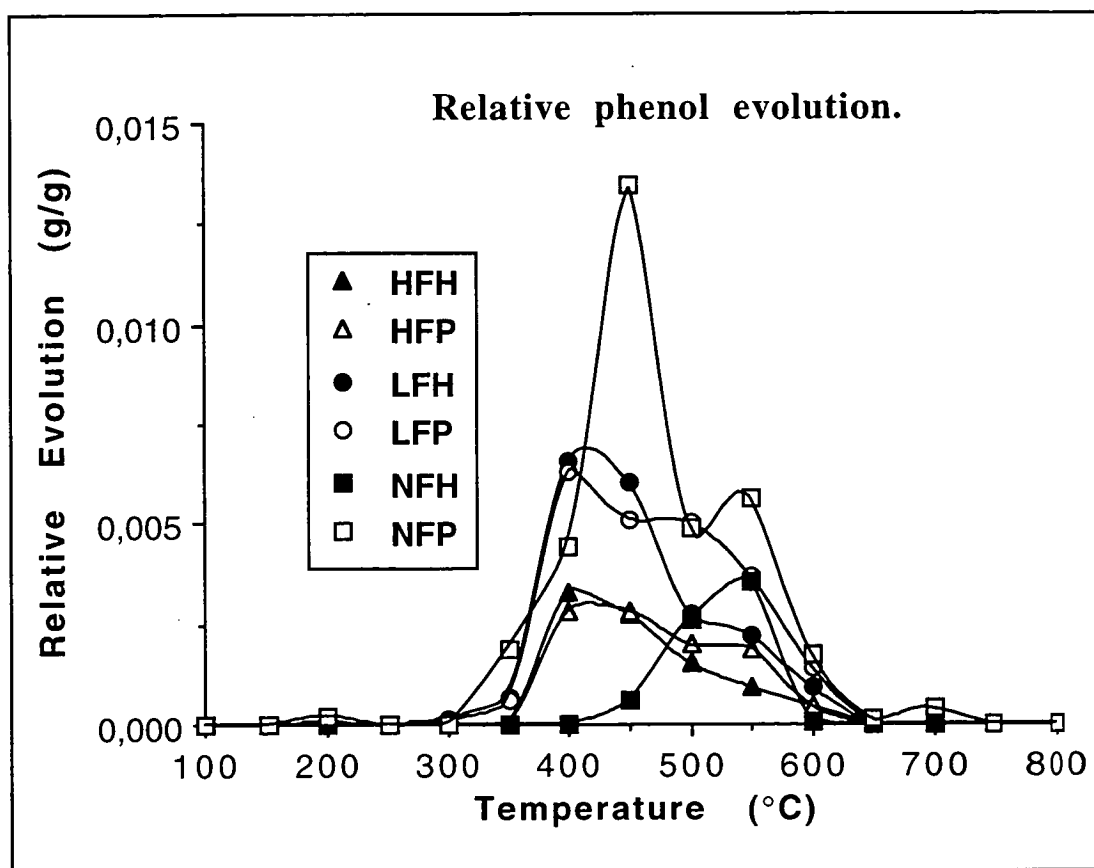


Figure 4.16 The relative evolution of phenol from the resins over the heat treatment temperature range.

From Figure 4.16 it can be seen that the evolution of phenol is greatest at approximately 400°C. The amounts evolved correspond generally with the amounts of phenol-formaldehyde in the starting resins. NFP, with 96% phenol-formaldehyde, has the greatest evolution of phenol, followed by LFH and LFP ($\approx 70\%$ phenol-formaldehyde) with approximately half the amount of phenol evolution as NFP, and HFH and HFP ($\approx 63\%$ phenol-formaldehyde) with half

again the degree of phenol evolution. NFH is an exception to the close relationship between the phenol-formaldehyde content and phenol evolution. Resin NFH, which contains 90% phenol-formaldehyde as a cured resin, loses approximately the same amount of its phenol as the low phenol bearing HFH and HFP. Resin NFH also shows a delayed loss of phenol as the maximum phenol loss for this resin occurs at approximately 550°C, rather than at 450°C for the other resins. This phenomenon of delayed volatile evolution for NFH, which is also shown in the water evolution for the six resins (Figure 4.14), further adds to the theory of NFH delaying its pyrolysis mechanisms due to a restriction of volatiles evolution.

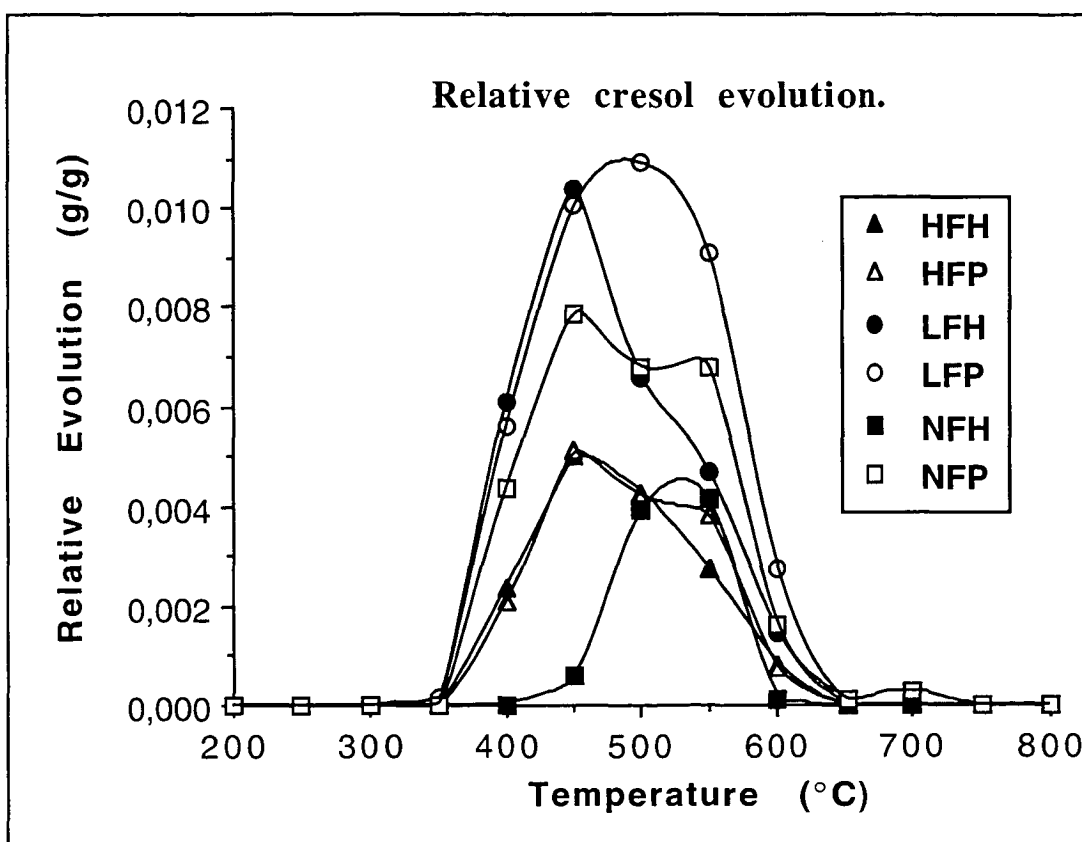


Figure 4.17 The relative evolution of cresol from the resins over the heat treatment temperature range.

The relative evolution of cresol is shown in Figure 4.17. To a certain degree this follows a similar trend to that for phenol evolution such that LFH and LFP contain approximately 1.1 times the phenol-formaldehyde of HFH and HFP, but display approximately twice the cresol evolution of those two resins. Resins NFH and

NFP go against this trend which suggests that the furfuryl-alcohol in LFH and LFP assist in methylating the phenolic groups to form cresols, which subsequently leave the system. In comparison, it can be shown that the paraformaldehyde cured NFP releases approximately 30 % more cresol than the hexamine cured NFH which suggests that hexamine is a poor agent for cross linking as it impedes the evolution of methylated phenols, which are good indicators of such polymerisation when evolved. Again, the late appearance of maximum cresol evolution in NFH at approximately 550°C, as opposed to approximately 450°C for the other resins, suggests the restriction of evolution of cresols.

The evolution of methyl-cresol, as shown in Figure 4.18, is very similar to that of cresol for all the resins, which suggests that the resins are indeed cross-linked. As the evolution of all the phenolic species (regardless of their degree of methylation) is seen to commence at approximately 350°C for all except NFH, which commences at approximately 450°C, it can be assumed that the degradation mechanisms of the five like resins commence at approximately the same temperature.

The relative evolution of bis-cresol and methyl-bis-cresol is shown in Figures 4.19 and 4.20 respectively. As the evolution of these species is a strong indicator of prior cross-linking in the resin, it is shown that the paraformaldehyde cured resins HFP, LFP and NFP have the most cross-linked polymeric structures due to their greater evolution of the bis-cresol species, particularly methyl-bis-cresol. The greater evolution of bis-cresol from LFP is most likely as a result of the greater proportion of phenol-formaldehyde initially in that resin. The hexamine/furfuryl-alcohol cured HFH and LFH evolve the two bis-cresol species at low levels, with LFH evolving a slightly greater amount of both species than HFH. This suggests that the cross-linking ability of furfuryl-alcohol, although largely reduced by the addition of hexamine, is only mildly affected by the proportion of phenol-formaldehyde. NFH is seen to evolve no bis-cresol species.

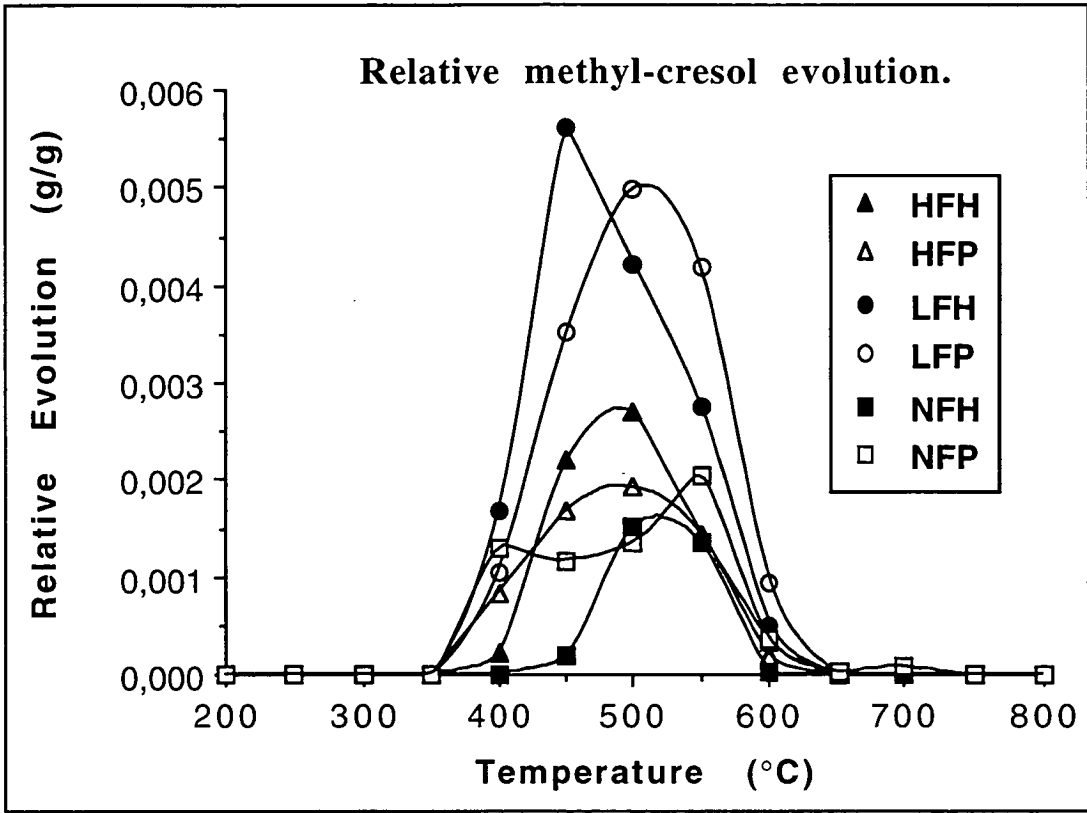


Figure 4.18 The relative evolution of methyl-cresol from the resins over the heat treatment temperature range.

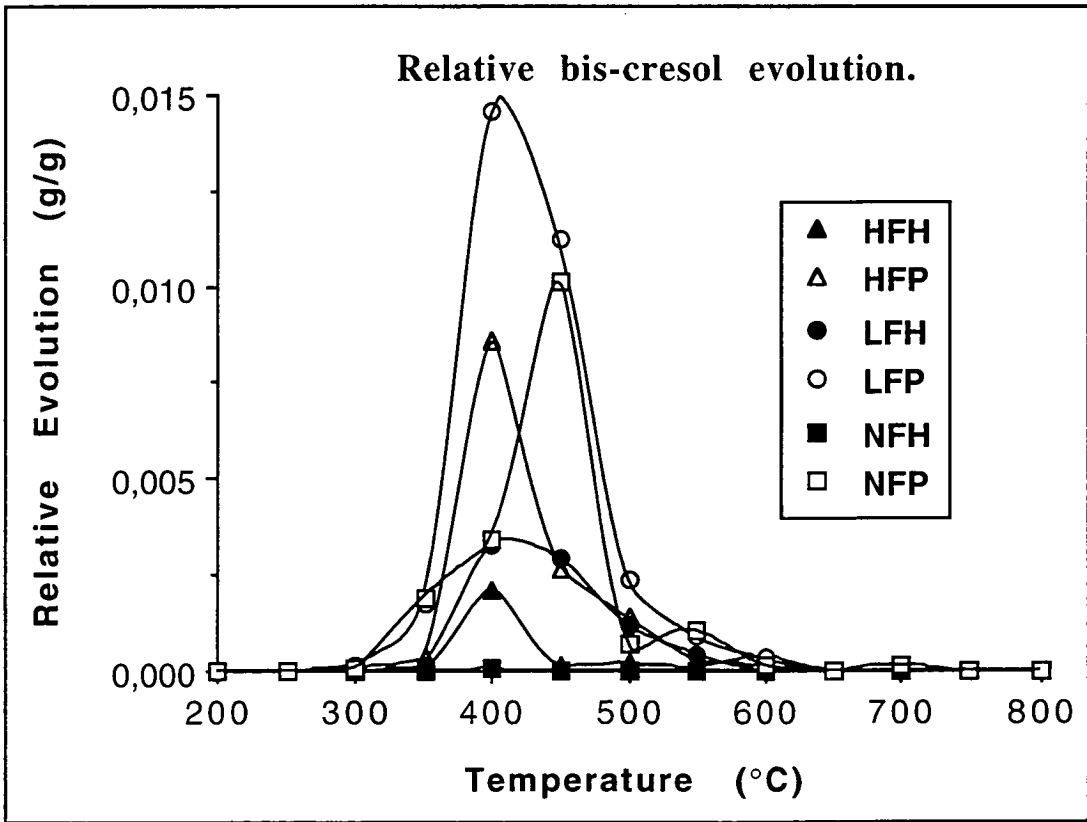


Figure 4.19 The relative evolution of bis-cresol from the resins over the heat treatment temperature range.

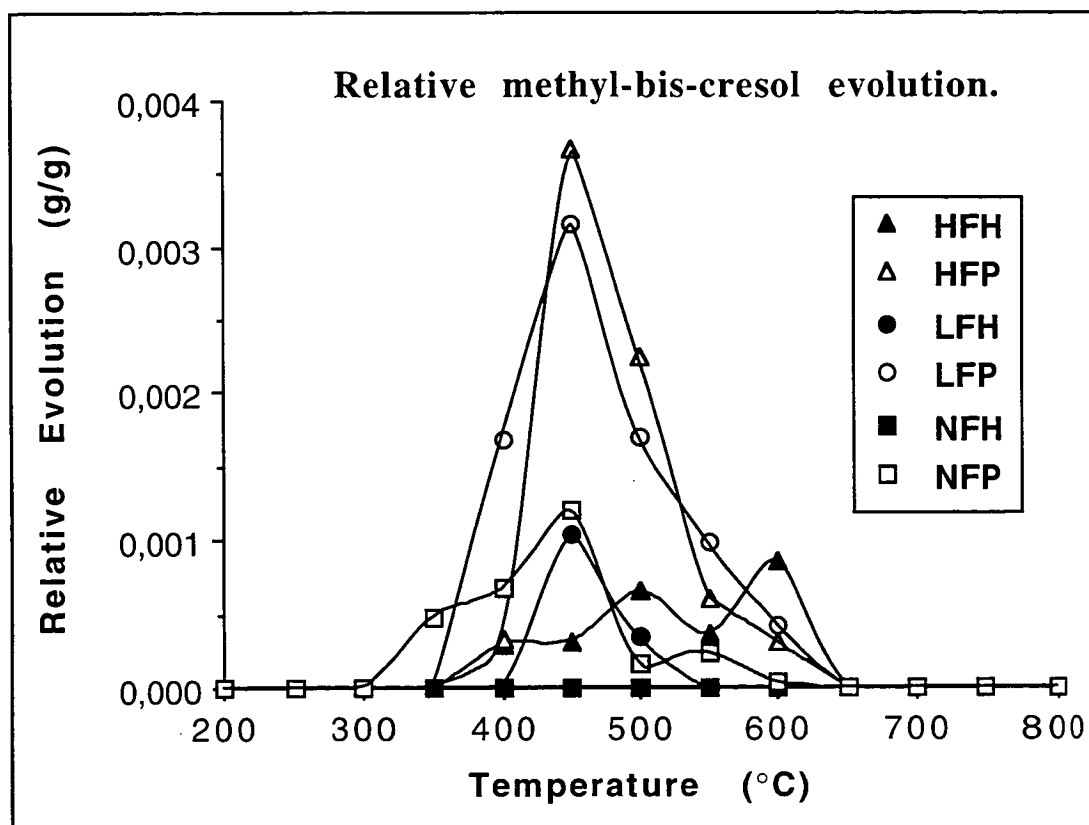


Figure 4.20 The relative evolution of methyl-bis-cresol from the resins over the heat treatment temperature range.

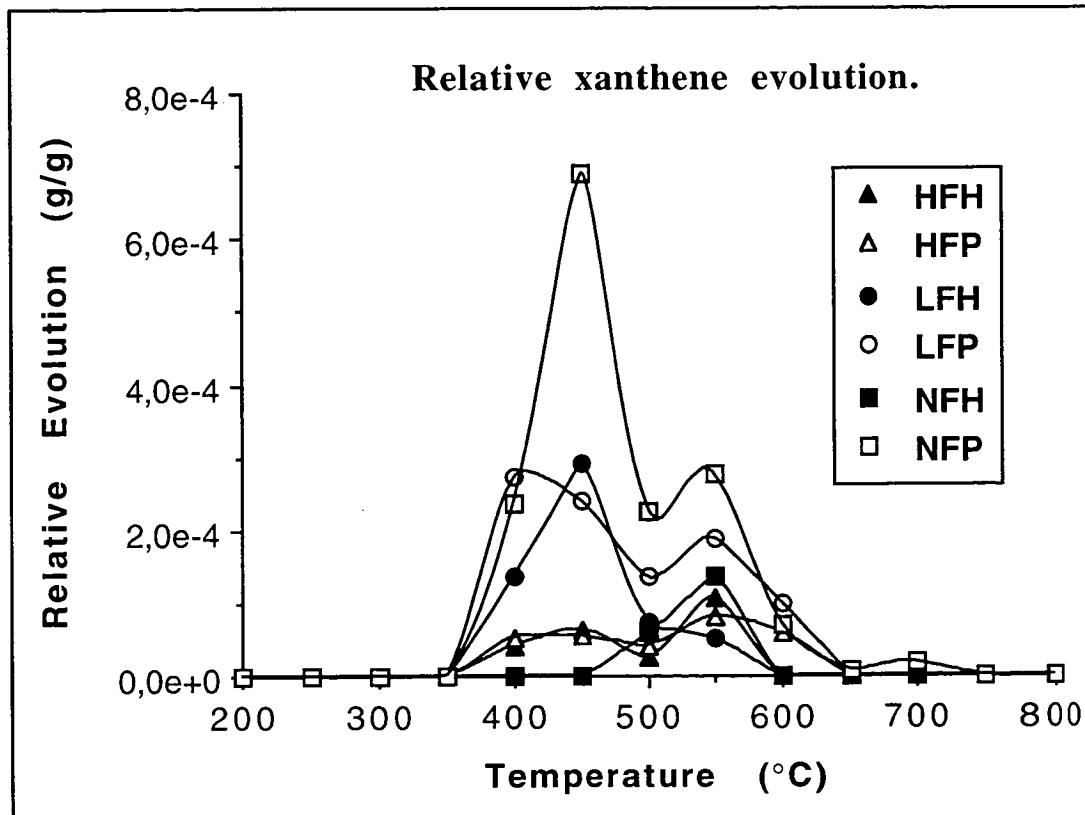


Figure 4.21 The relative evolution of xanthene from the resins over the heat treatment temperature range.

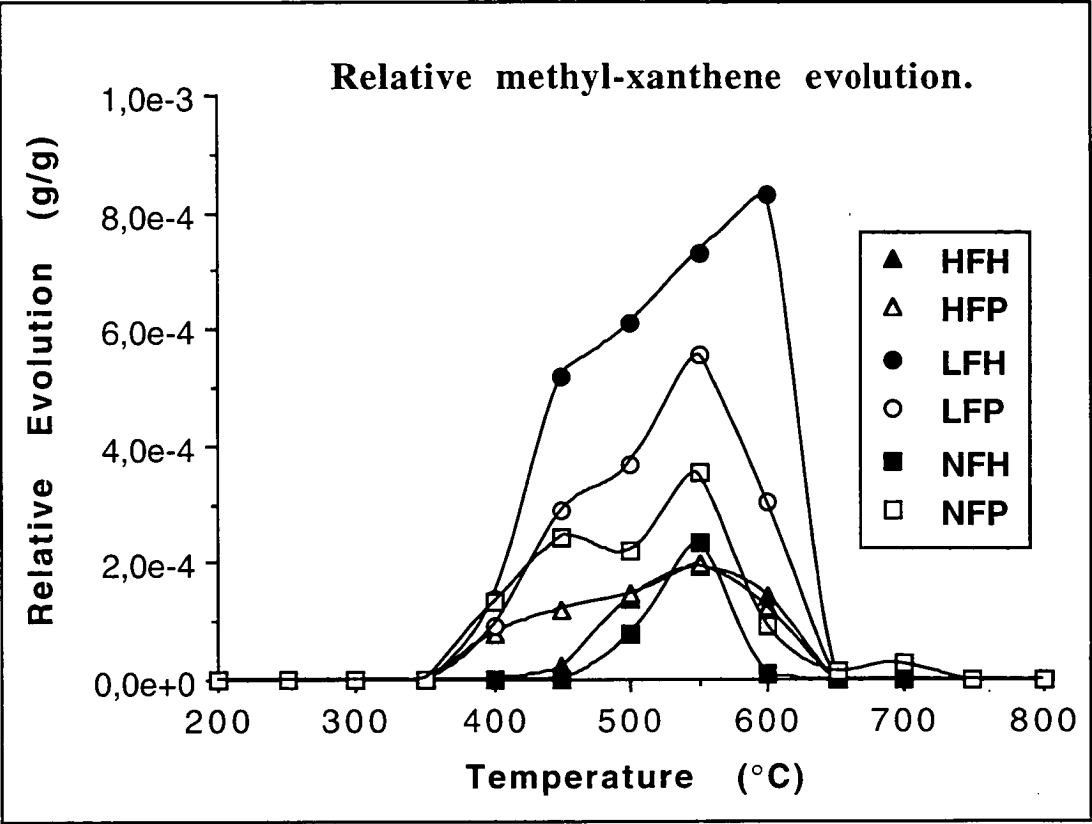


Figure 4.22 The relative evolution of methyl-xanthine from the resins over the heat treatment temperature range.

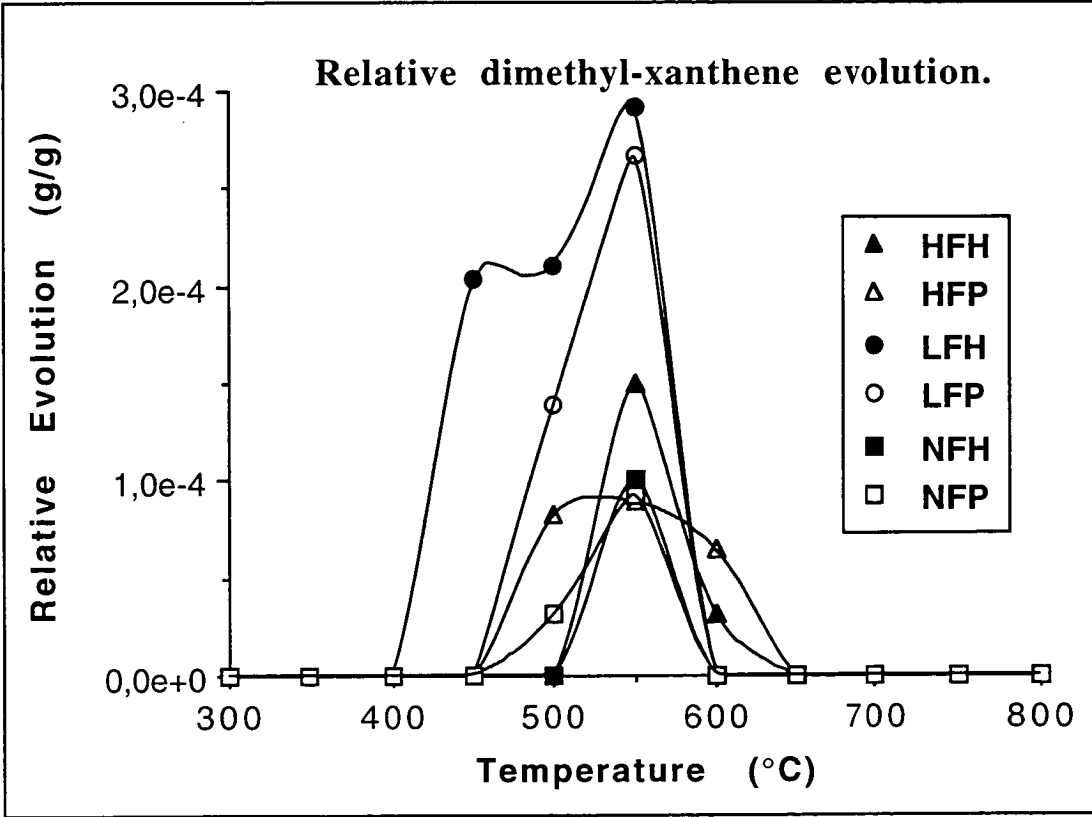


Figure 4.23 The relative evolution of dimethyl-xanthine from the resins over the heat treatment temperature range.

The relative evolution of xanthene, methyl-xanthene and dimethyl-xanthene is shown in Figures 4.21, 4.22 and 4.23 respectively. Generally, the amounts of xanthene species evolved from the resins are low compared to the other volatilised organics, although it is possible to relate these trends to resin chemistry in a broad sense. It is seen that the xanthene evolution of NFP is greater than the other resins, which suggests that the presence of paraformaldehyde provides ether linkages with the phenolic ring carbons *ortho* to the methylene bridge carbons in the bis-cresol, followed by the loss of the phenolic hydroxyl groups to water, and further ether linkages between the rings.

The maximum evolutions of the three xanthene species from HFH, HFP and NFH are of similar value, and all at 550°C. This parallels the previous theory of NFH as being incompletely cross-linked, and HFH and HFP as having the lowest proportion of phenol-formaldehyde. The shift in maxima between the bis-cresol and xanthene species suggests that the first cross-linking mechanism of the resins is by methylene bridging, and then a further cross-linking exists by ether linkages, as shown by xanthene formation at approximately 550°C. This is also shown by the maximum water evolution of the resins at approximately 500°C which is as a result of the reaction between hydroxyl groups on adjacent phenolic rings.

Chapter Five

**The determination of the specific
Phenolic Resin pyrolysis reaction
mechanisms (25 - 750°C) by Fourier
Transform Infrared Spectroscopy.**

Fourier Transform Infrared Spectroscopy.

Fourier Transform Infrared Spectroscopy was used in this study to monitor the degradation process of the phenolic resins until the residual functionalities of the chars could no longer be observed spectroscopically. From this it is possible to describe a *pseudo* reaction path for the resin pyrolysis process. The infrared spectrum for each resin and its subsequent pyrolysis char is shown in Figures 5.1 to 5.6. The number shown on each spectrum indicates the temperature (in °C) to which the resin was heat treated. The i.r. band assignments used as a basis for this study are reported in Table 5.1, along with the appropriate references. The band assignments in Table 5.1 are as for poly-aromatic and phenolic resin materials. As was suggested by Morterra and Low [1985a], most i.r. modes of poly-atomic carbonaceous systems, and especially those incorporating aromatic rings, are likely to have mixed character. Consequently, the proposed assignments of Table 5.1 are only representative of the character of each mode believed to be the most prominent. As the resolution of the acquired spectra is $\pm 4\text{ cm}^{-1}$, it can be assumed that the exact band positions of the reference assignments in Table 5.1 are within the error of the band positions in the experimental spectra of this study.

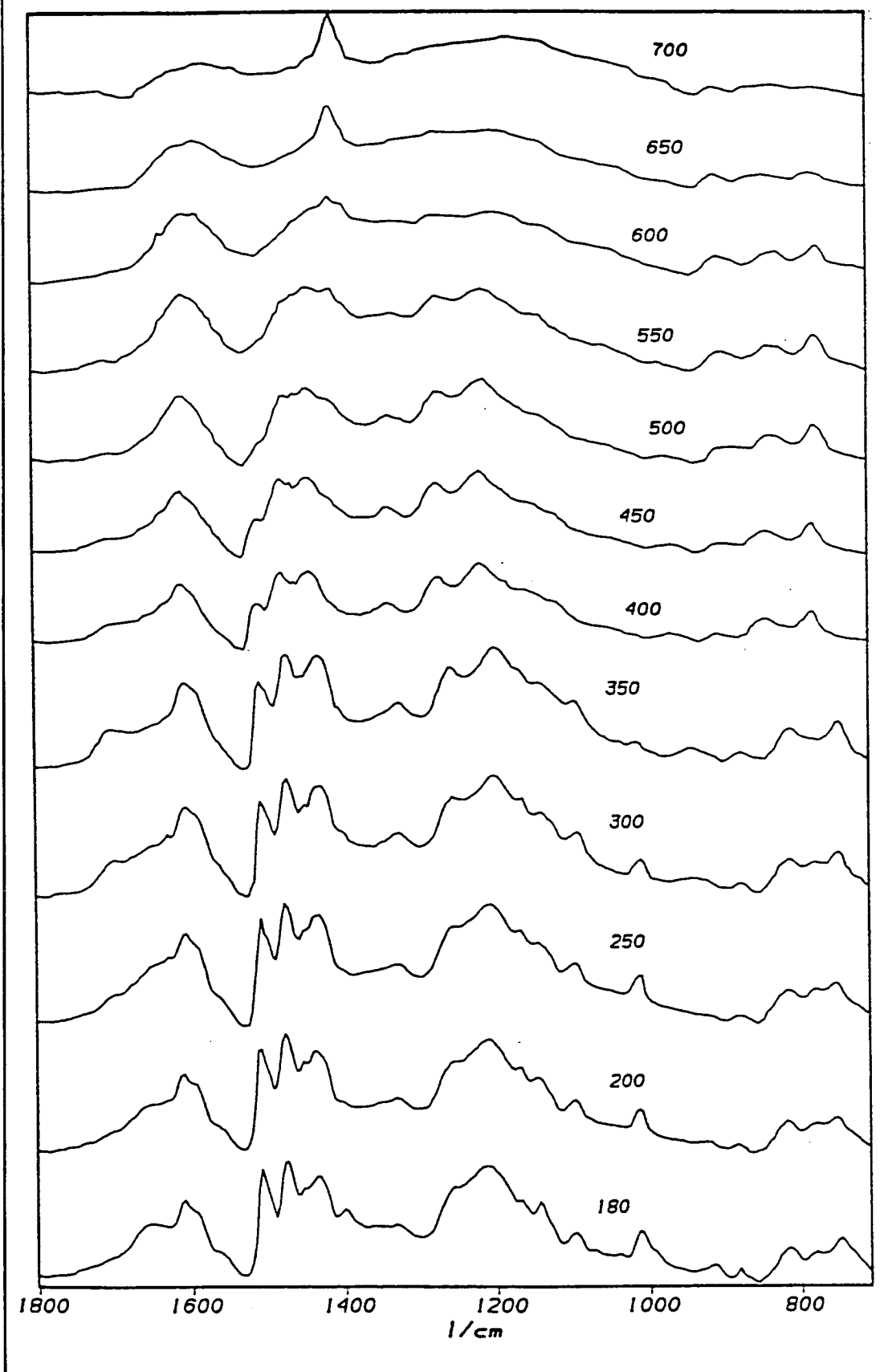
HFH

Figure 5.1 FTIR spectra for HFH over the heat treatment temperature range. The number for each spectrum indicates the temperature ($^{\circ}\text{C}$) to which the resin was heat treated.

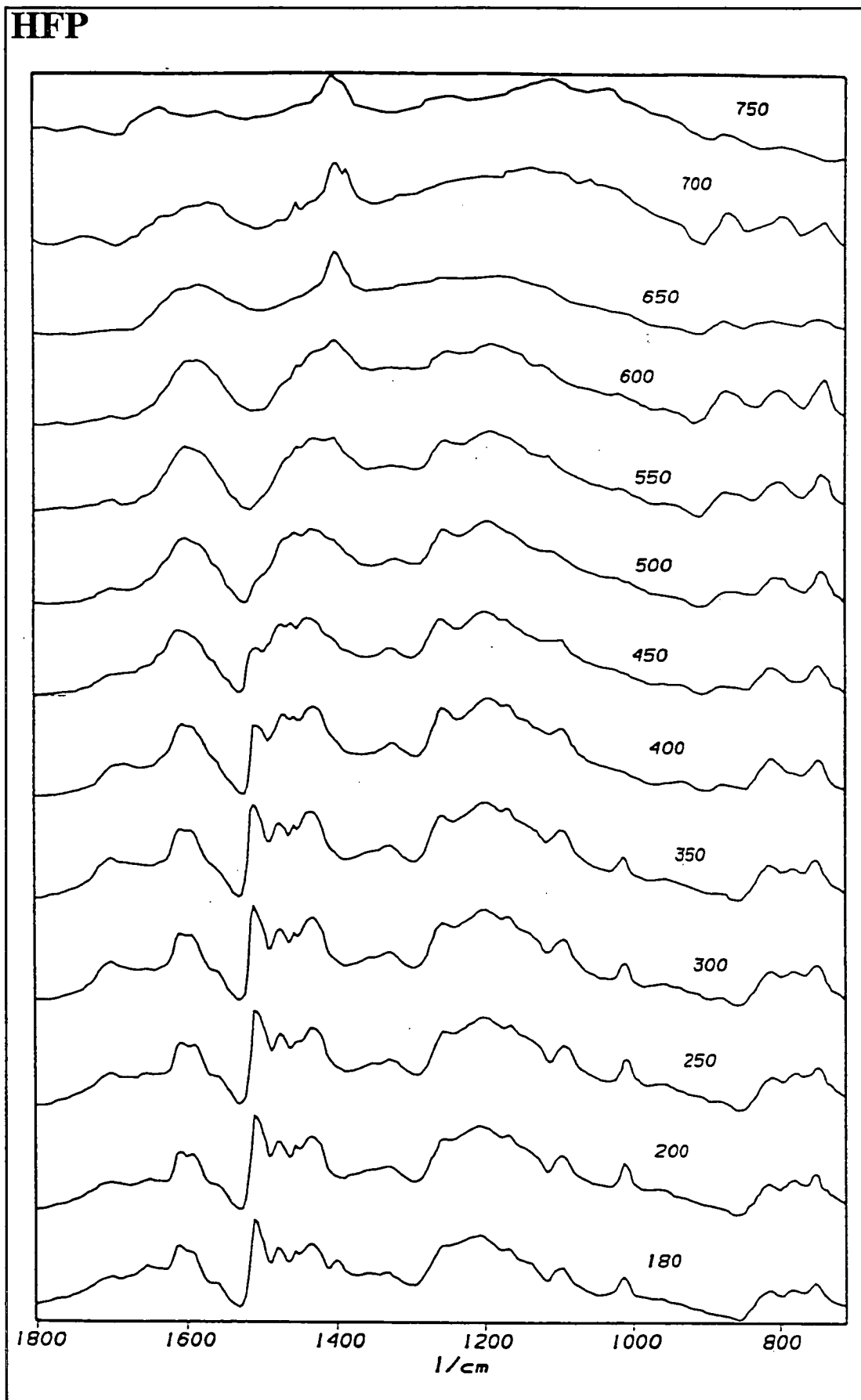


Figure 5.2 FTIR spectra for HFP over the heat treatment temperature range. The number for each spectrum indicates the temperature (°C) to which the resin was heat treated.

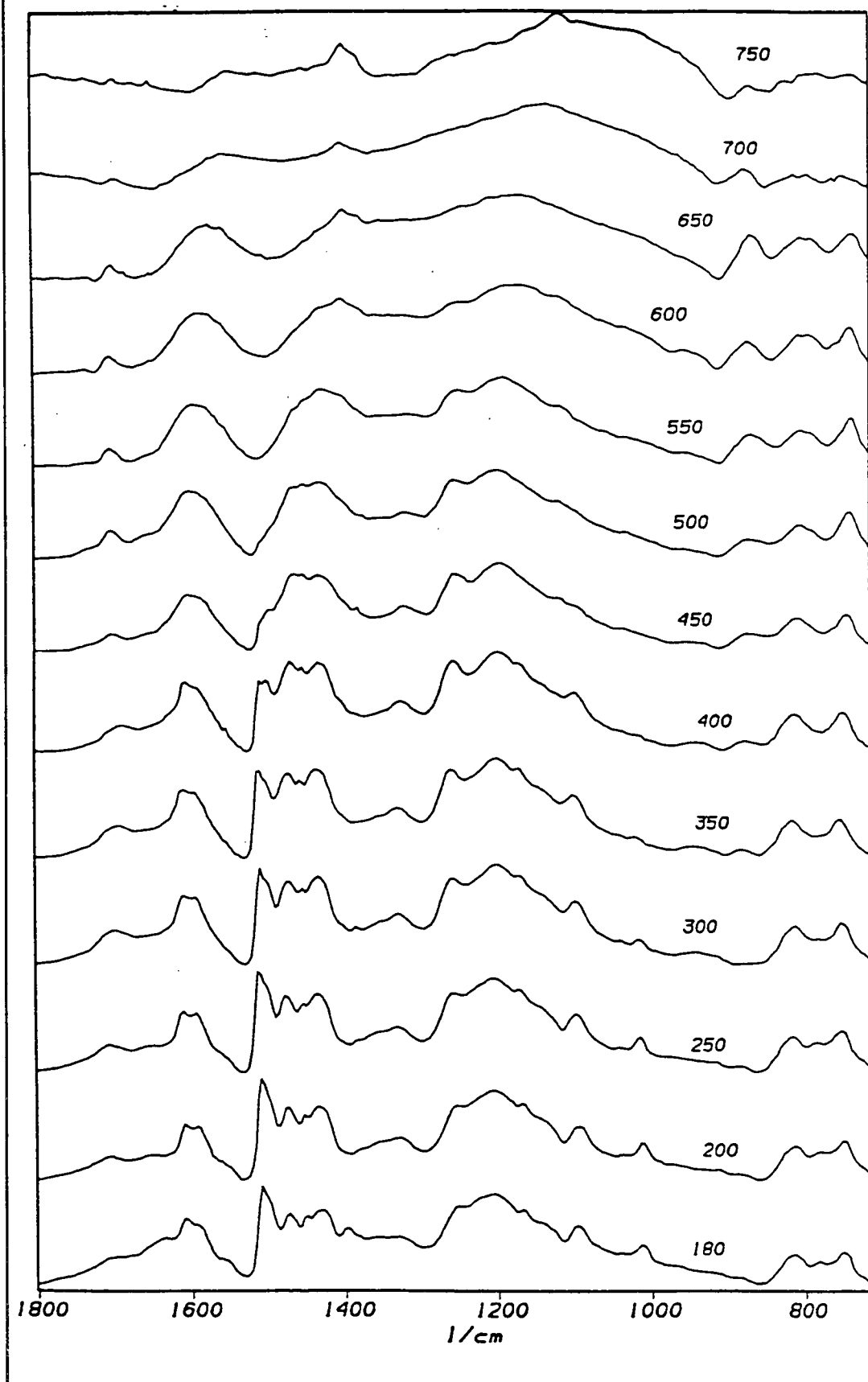
LFH

Figure 5.3 FTIR spectra for LFH over the heat treatment temperature range. The number for each spectrum indicates the temperature (°C) to which the resin was heat treated.

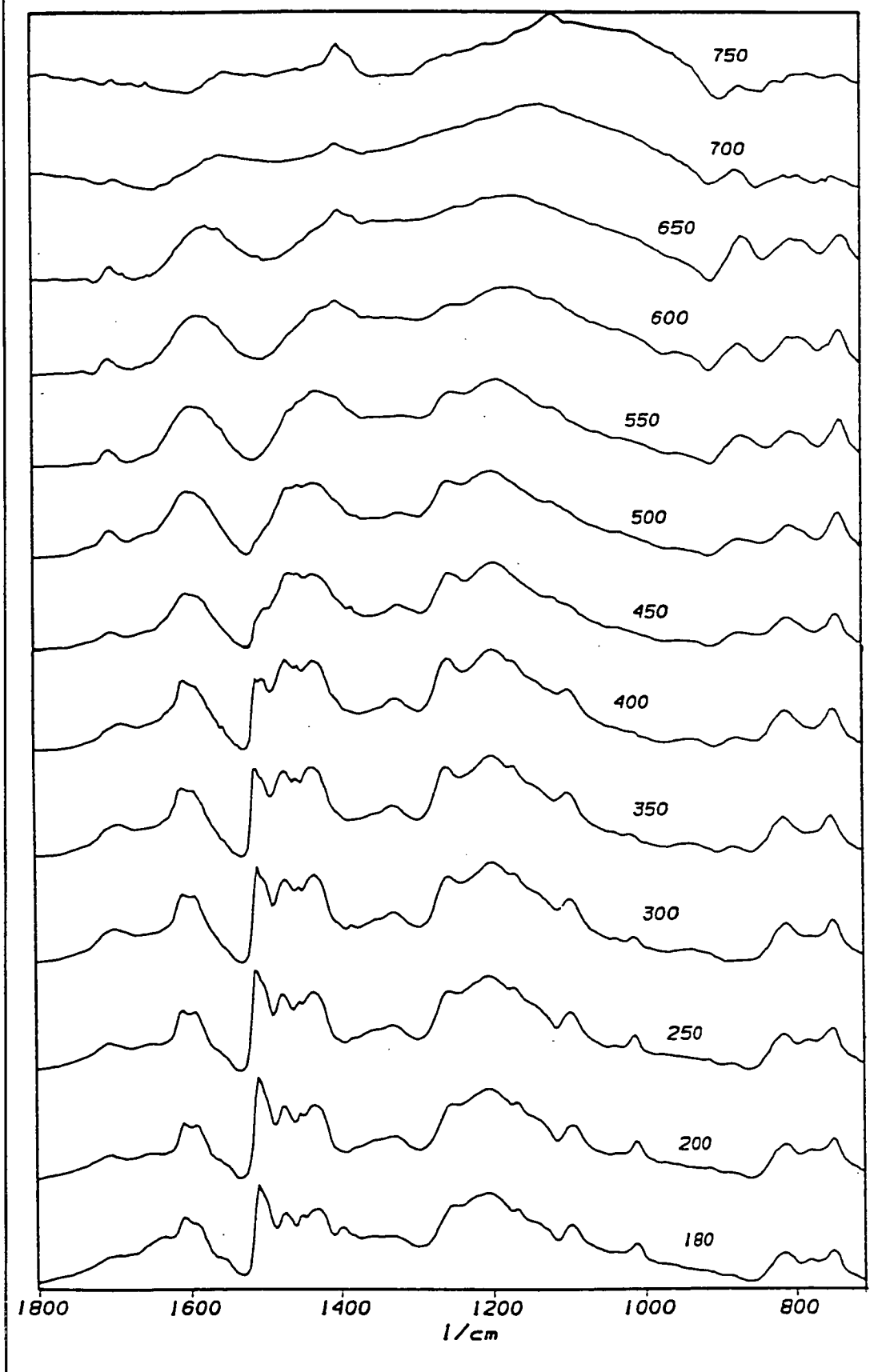
LFP

Figure 5.4 FTIR spectra for LFP over the heat treatment temperature range. The number for each spectrum indicates the temperature (°C) to which the resin was heat treated.

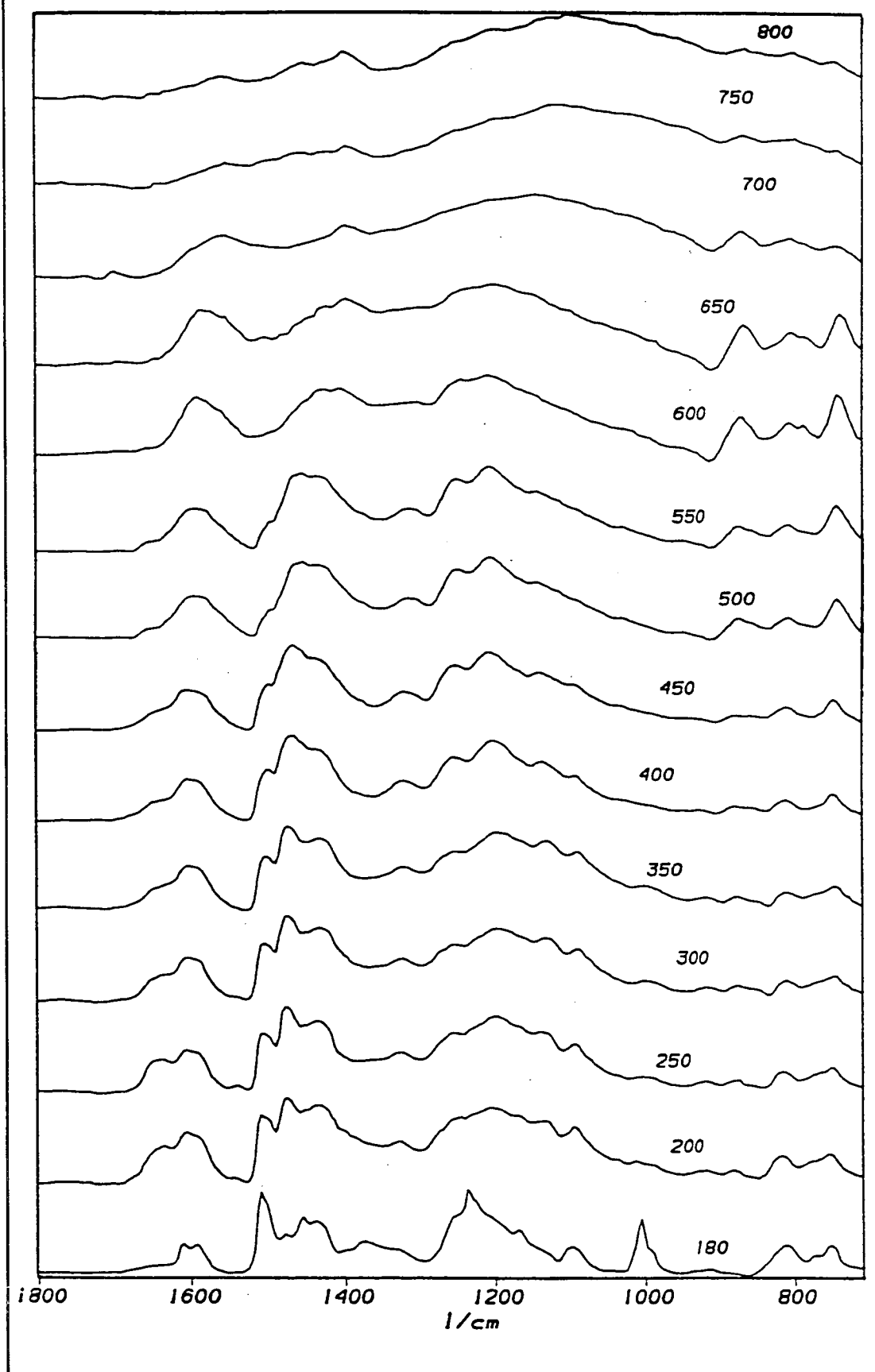
NFH

Figure 5.5 FTIR spectra for NFH over the heat treatment temperature range. The number for each spectrum indicates the temperature ($^{\circ}\text{C}$) to which the resin was heat treated.

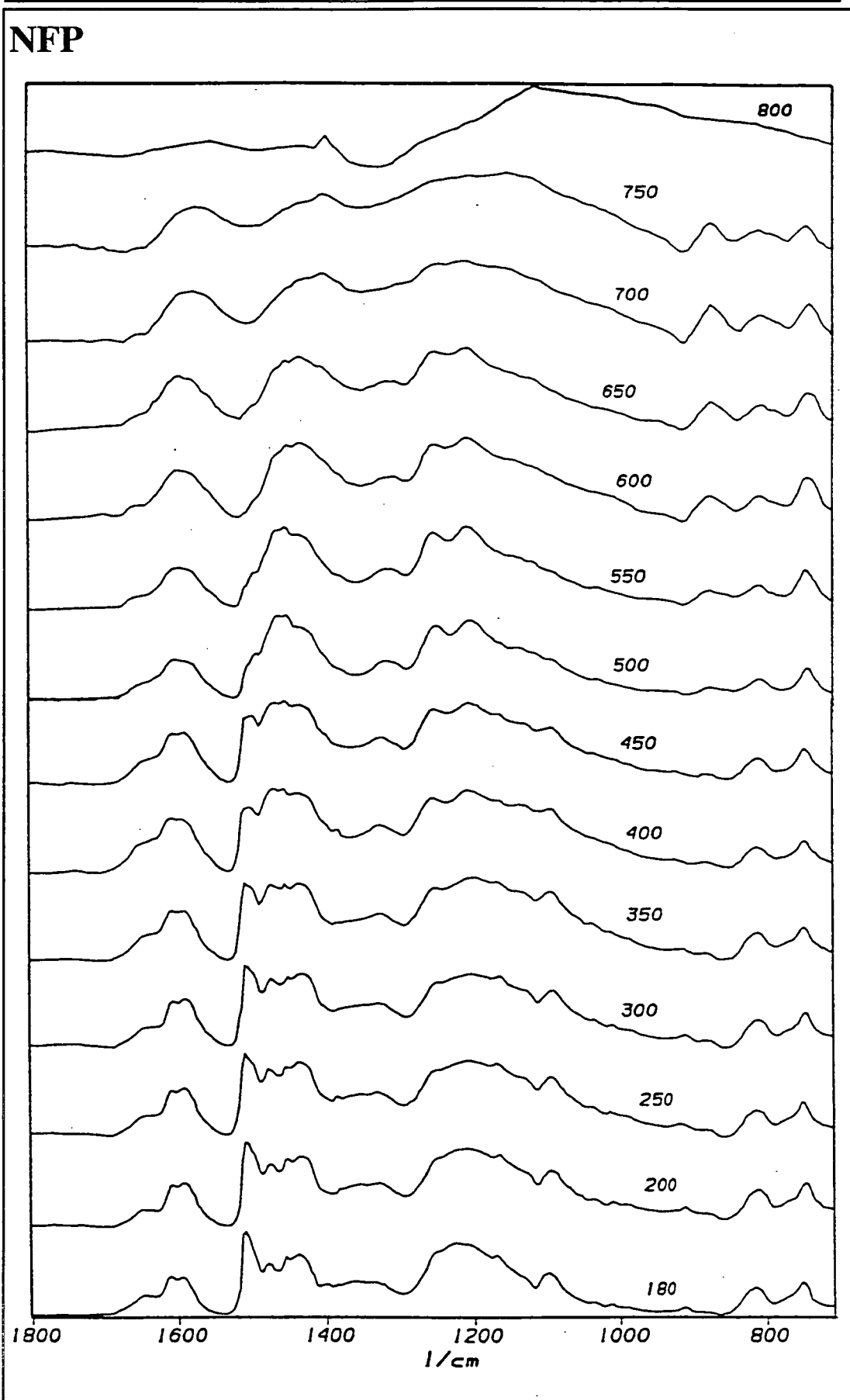


Figure 5.6 FTIR spectra for NFP over the heat treatment temperature range. The number for each spectrum indicates the temperature (°C) to which the resin was heat treated.

Band Centre (cm ⁻¹)	Character.	Assignment	Reference
3340	v.br.:v.s.	phenolic OH stretch	Morterra and Low
3060	w.	aromatic CH stretch	1985a
3020	w.	aromatic CH stretch	"
2930	m.	aliphatic CH stretch	"
2850	sh.	aliphatic CH stretch	"
1890	br.:w.	aromatic summation band	Colthup <i>et al</i> ,1975
1760	v.w.	aromatic summation band	"
1650	br.:m.	water scissor deformation	Camino <i>et al</i> ,1982
1618	d.:s.	"quadrant" ring stretch	Morterra and Low
1600	d.:s.	"quadrant" ring stretch	1985a
1510	v.s.	{	"
1480	w.	{ "semicircle" ring stretch	"
1455	d.:m.	{ and CH ₂ scissor bend	"
1440	d.:m.	{	"
1360	d.:s.	{ phenolic OH in-plane	"
1340	d.:s.	{ deformation	"
1270	sh.	{ aromatic CO stretch	"
1230	br.:v.s.	{	"
1110	s.	aromatic in-plane CH def.	Hummel and Scholl,
915	v.w.	aliphatic CH ₂ wag	1971
820	br.:s.	{ aromatic out-of-plane	Socrates,1980
775	d.:s.	{ deformations and ring	
760	d.:s.	{ out-of-plane vibrations	

Table 5.1 Infrared vibrational assignments of novolac phenolic resins (br. - broad; d. -doublet; m. - medium; s. - strong; sh. - shoulder; v. - very; w. - weak)

Each spectrum can be subdivided into several regions for the purpose of characterisation of functional groups and aromatic structures. These are summarised as follows.

The oxygen-hydrogen stretching region:

A broad absorption band between 3500 and 3100 cm^{-1} has been attributed to several oxygen-hydrogen stretching modes and has been used in other studies to measure the hydroxy content in coals [Painter *et al*,1981b]. In the case of phenolic resins it has been suggested that the O-H phenolic stretching band centred near 3340 cm^{-1} is also due to intermolecular hydrogen bonding, and therefore much of the broad O-H band must be ascribed to intense intermolecular OH-OH interactions [Morterra and Low,1985a; Casiraghi *et al*,1981]. These interactions are due either to the adjacent phenolic hydroxyl groups themselves, or to the presence of adsorbed water which can also be seen at 1650 cm^{-1} [Morterra and Low,1985a]. Not only do these phenomena cause quantification of the band to be difficult, but the band width also impedes accurate detection of the weak aromatic and aliphatic C-H stretching vibrations at approximately 3030 and 2900 cm^{-1} , respectively. Therefore, this region has not been considered as relevant in this study.

The 1750-1400 cm^{-1} region:

A band at 1709 cm^{-1} [Fitzer and Schaefer,1970] is reported as being indicative of the C-O-C bond of the furan ring in furfuryl-alcohol. This band was observed only in the spectra of HFP and LFP, the furfuryl-alcohol/paraformaldehyde cured resins, and to a small degree in the HFH resin, from the as-cured forms of the resins to their chars of at least 500°C. It is therefore possible that the absence of this band in LFH, and its low level in HFH, suggest that the hexamine contained in these two resins acts to collapse or destroy the furan ring in the resin prior to, or during curing. The band at 1639 cm^{-1} is suggested to indicate the ring stretch of the unsaturated carbons in the furan ring of furfuryl-alcohol [Conley and Metil,1963]. As this vibration is only seen strongly in HFP and LFP, together with

the other furan ring band at 1709 cm^{-1} , it is unlikely that the paraformaldehyde has a great effect on the furfuryl-alcohol in the initial resin formulation prior to pyrolysis. As water is quoted as having a scissor deformation at 1650 cm^{-1} , it is possible that the 1639 cm^{-1} band exists in HFH but is covered by the water vibration that can also be seen as a very broad band at or around 3200 cm^{-1} [Morterra and Low,1985a]. It is reasonable to assign the 1709 and 1639 cm^{-1} bands to the respective furan vibrations as neither of them are detected in the non furfuryl-alcohol cured resins NFH and NFP.

Two bands of relatively equal intensities are found at 1620 and 1590 cm^{-1} , which usually indicate 1,2- and 1,4 di-substitution of the benzene ring, respectively. A comparison of the height of these two bands can give an indication of degree of 1,4 substitution (cross-linking). The 1,2,6 and 1,2,4 configurations are also possible, as tri-substitutions are expected to be those most abundant in a cross-linked polymeric material [Morterra and Low,1985a]. The ratio of the 1620 to 1590 cm^{-1} band for each resin shows that the as-cured conditions of all the resins have a relatively equal degree of cross-linking. Also a strong and sharp band at 1510 cm^{-1} is indicative of 1,4- and/or 1,2,4- substitution. As this region is known to contain the CH_2 scissor bending vibration, the 1480 cm^{-1} component of the $1480\text{-}1440\text{ cm}^{-1}$ multiplet is likely to be caused by CH_2 deformations.

The 1300-900 cm^{-1} region:

The $1300\text{-}900\text{ cm}^{-1}$ region is indicative of C-O stretching vibrations. A band at 1260 cm^{-1} is present in all resins except NFH. It can be due to either the ether link in the furan ring of furfuryl-alcohol or the C-O vibration of paraformaldehyde. This vibration is poorly resolved in the low temperature spectra, and little weight will be placed upon it in the postulation of the resin structure. The same vibration assignment also indicates the existence of diphenylene-ether linkages at higher

temperatures, which are of more importance to this study.

The band at or near 1210 cm^{-1} is due to the C-O stretching vibration of the C-OH phenolic bond and, as expected, it is seen as a strong band in all resins. NFH shows two peaks at 1240 cm^{-1} and 1009 cm^{-1} which are of interest in consideration of the role of hexamine in the pyrolysis process. The sharp peak at 1240 cm^{-1} in the as-cured spectrum of NFH is also seen in a standard spectrum of a phenol-novolac/hexamine resin [Hummel,1984, *FTIR spectrum no. 2699*], but not in a standard spectrum of a simple phenol-novolac [Hummel,1984, *FTIR spectrum no. 2696*]. There is also a sharp peak in the as-cured spectrum of NFH at 1009 cm^{-1} which is also seen in the standard phenol-novolac/hexamine spectrum at 1010 cm^{-1} , and a standard hexamine spectrum [Pouchert,1985, *FTIR spectrum no. 378B*], but not in the standard simple phenol-novolac spectrum. The existence of these two bands, although unassigned, suggest that the hexamine in the as-cured form of NFH remains as a dissolved species within the phenol-formaldehyde resin, which is then shown by the higher temperature spectra to assist in cross-linking and further pyrolysis mechanisms. This also gives weight to the previous suggestion of a reaction between the hexamine and furfuryl-alcohol during curing, as these bands are greatly reduced in the spectra of the as-cured HFH and LFH resins. Given these considerations, it has been suggested by several workers in this field [Sojka *et al*,1979] that using FTIR assignments for the analysis of the hexamine curing of phenolic resins is difficult and inconclusive. A band at 915 cm^{-1} is indicative of an aliphatic CH_2 vibration, which is seen to exist in the standard spectrum of a simple phenol-novolac [Hummel,1984, *FTIR spectrum no. 2696*] and is seen to exist in all the as-cured resins of this study, except HFP and LFP.

The 850-700 cm⁻¹ region:

The 850-700 cm⁻¹ region contains the aromatic C-H wagging modes. A strong band near 820 cm⁻¹ indicates the existence of 1,4 and 1,2,4 substitutions and the 780-750 cm⁻¹ doublet suggests 1,2 and 1,2,6 substitutions. The as-cured conditions of all six resins suggest a relatively equal amount of cross-linking as the ratio of the above two bands remains relatively constant. The FTIR analyses of these resins can provide a qualitative pyrolysis reaction mechanism. Very few obvious changes occur in the i.r. spectra of the resins up to 400°C. In LFH, the peak at 1211 cm⁻¹ shifts to 1200 cm⁻¹ and simultaneously the band at 1252 cm⁻¹ shifts to 1260 cm⁻¹, increasing markedly in intensity. This behaviour is consistent with the formation of diphenyl ether or aryl-ether linkages and it is suggested that the main reaction mechanism at these low temperatures is the formation of the diphenyl-ether linkages by the elimination of H₂O [Morterra and Low, 1985a; Ouchi, 1966]. This is supported by the fact that the evolution of water, as shown in Figure 4.14, has a maximum for all resins between 350°C and 450°C. This phenomenon is seen in all the resins, but to a lesser degree in HFP, LFP, NFP and NFH, and in the case of LFP, only at 400°C, without the diphenyl-ether linkages remaining above this temperature.

The ratio of the CH₂ deformation band at 1480 cm⁻¹ to the 1,2,4 di-substituted ring stretching band at 1510 cm⁻¹ gives a good indication of the relative degree of linearity or *o-o'* polymerisation of the resins, and the change in cross-linking over temperature. Using LFH as a reference, it can be seen that the degree of linearity for this resin is relatively high initially, although it is seen to steadily decrease to 350°C. Resin LFP shows less linearity than LFH and this can be seen to change at 300°C, which is followed by the increased cross-linking and then 1,2,4,6-substitution at 400°C. In comparison, the as-cured form of NFH shows a low degree of linearity as concluded by the high intensity of the 1510 cm⁻¹ band relative to the 1477 cm⁻¹ band. The linearity is seen to increase suddenly, as the

200°C form of NFH shows a ratio of the two bands of the same order as LFH. The linearity of NFH is then seen to further increase and plateau at 250°C to 350°C, after which little cross-linking of the phenolic groups is seen to occur below 500°C until the development of the tetra-substituted rings, as seen by the substantial growth of the 880 cm⁻¹ band.

The linearity of NFP is seen to be reduced from a distorted chain system to a more cross-linked system at 350°C. The appearance of the band at 880 cm⁻¹ signals the growth of the highly cross-linked ring system. The polymeric network of HFP shows moderate linearity up to 400°C, where cross-linking at the previously vacant *para* positions on the ring is indicated by the relative rise of the 1593 cm⁻¹ band. The appearance of the 880 cm⁻¹ band for HFP at 450°C suggests the early condensation of this ring system to tetra-substitution, in comparison to the later ring condensation of the other resins.

The linearity and degree of cross-linking of HFH is shown to be of the same order as NFH, but less than LFH. This is shown by the differences in intensity ratios of the 1590 : 1510 : 1470 cm⁻¹ bands between the two resins. The two parameters for HFH are also seen to remain relatively unchanged up to 350°C, at which temperature the cross-linking increases and the development of the tetra-substitution condensation begins.

The complexity of the 1170-1100 cm⁻¹ region in all resins is likely due to the aromatic CH deformation bands, which are indicative of the unsubstituted carbons on the phenol ring. The band at 915 cm⁻¹ is suggested as an aliphatic CH₂ wagging vibration, and is seen to exist in all resins except the furfuryl-alcohol/paraformaldehyde as-cured HFP and LFP [Hummel and Scholl, 1971]. This could be due to a more complex cross-linking between furfuryl-alcohol and the phenolic rings, which may be hindered by the presence of hexamine in HFH and LFH. This is also seen by the evolution of free furfuryl-alcohol from HFH

and LFH (Figure 4.15), but not from HFP and LFP which suggests that the furfuryl-alcohol in the latter two resins is bound to the phenolic structure and therefore cannot be released at low temperatures. The 915 cm^{-1} band is seen to grow in HFP and LFP above 250°C which suggests the replacement, with methylene bridges, of the structure that attaches the furan-rings to the phenolic rings.

The pyrolysis mechanisms of the resins in the temperature range $400\text{--}550^{\circ}\text{C}$ are seen from the i.r. spectra to be relatively similar. These same mechanisms are delayed by approximately 100°C in NFH due to the retention of volatile species. The band at 1260 cm^{-1} , which is assigned to the CO stretch of diaryl-ethers, is seen to sharpen and increase at 400°C and then decrease at 600°C . This is paralleled by a shift of the 1220 cm^{-1} band to 1196 cm^{-1} which is possibly due to the loss of the phenolic hydroxyl groups and a condensation of the ring system to a xanthene type structure and then a diphenylene oxide structure. The diphenylene-ether linkage formation reaction described above is seen to end above 450°C , and these same structures appear to be largely destroyed by 550°C in all resins, which suggests that this process is independent of the starting chemistry of the resins. This is likely, as the joining of adjacent hydroxyl groups to form water and leave an ether link between the rings would be mainly independent of cross-linking of the ring systems.

The 1590 cm^{-1} band in all the resins is seen to remain constant relative to the decrease of the 1510 cm^{-1} band above 400°C , and therefore it is likely that there is an increase in cross-linking in the remaining phenolic units, which is closely followed by the appearance of a new out-of-plane CH deformation at 880 cm^{-1} , which is indicative of 1,2,4,6 tetra-substitution.

The decrease of observable features that are indicative of C-O-C in the $1080\text{--}1000\text{ cm}^{-1}$ range suggests that the branching mechanisms involving the reaction

between phenolic OH and methylene bridges, leading to aryl-alkyl ethers are unlikely. This mechanism must be supported by the fact that H_2 is released at temperatures higher than $500^\circ C$ [Fitzer and Schaefer, 1970]. It is thought that the mechanism postulated by Ouchi [1966], and supported by Morterra and Low [1985a], is more likely. In this reaction, which occurs at approximately the same temperature range as the diphenylene-ether reaction described above, the products of the reaction between the phenolic hydroxyl and adjacent methylene bridge groups are water, and a methine bridged triphenyl structure. This is supported by the shift of the 1475 cm^{-1} band to approximately 1460 cm^{-1} , as seen at approximately $450^\circ C$ in all six resins, which indicates the increased complexity of the aliphatic CH stretching band.

The growing complexity of the $900\text{-}700\text{ cm}^{-1}$ range, which is due to the wagging vibration of isolated aromatic CH groups, indicates that there is an increase in the poly-substitution of the rings. The growth of the 750 cm^{-1} band relative to the 820 cm^{-1} band suggests an increase in cross-linking due to an increase in 1,2,6-substitution relative to 1,2,4-substitution. This phenomenon is seen in all but HFH and HFP, which suggests that the high level of furfuryl-alcohol in these two resins causes a high level of cross-linking initially in the resins which is fixed until complete condensation of the rings to a pseudo-crystalline structure. In LFH, the degree of cross-linking remains unchanged up to $350^\circ C$, after which tri-substitution of the phenolic ring takes place to $500^\circ C$. In LFP the degree of substitution remains unchanged to $450^\circ C$, and is seen to increase to approximately the same level as that of LFH to $500^\circ C$. In NFH, as it has already been established, the cross-linking of the resin is low initially due to the dissolution of hexamine at approximately $180\text{-}200^\circ C$. Above this temperature, the availability of methylene groups from the hexamine is seen to facilitate extensive cross-linking at $250^\circ C$, which remains relatively constant to $400^\circ C$. Above $400^\circ C$ the polymeric lattice of NFH undergoes even further 1,2,6 substitution to a higher level than the LFP and LFH resins. This substitution is then replaced by tetra-

substitution at 550°C as indicated by the growth of the 875 cm⁻¹ band. NFP shows a similar pattern to LFH and LFP such that the degree of cross-linking remains constant up to 500°C, at a comparable level to that of the above mentioned resins. This resin then experiences a short period of increased cross-linking to 550°C.

It has been suggested [Conley and Bieron, 1963a, 1963b; Conley, 1965; Ouchi, 1966; Morterra and Low, 1985a] that the growth of a band at approximately 1650 cm⁻¹ at or around 550°C is indicative of the presence of a highly conjugated and possibly H-bonded carbonyl group. This new absorption is considered to never exceed that of a weak shoulder on the strong multiplet band in the 1630 - 1580 cm⁻¹ range, and its position is relatively variable as shown by the absorption of hydrogen-bonded benzophenones near 1630 cm⁻¹, and near 1670 cm⁻¹ for benzophenones not involved in intramolecular hydrogen-bonding [Hummel and Scholl, 1968]. The weakness of this band indicates that the auto-oxidative mechanisms for the methylene bridges, which are also represented by the observation of evolved water and are considered to be the primary degradation routes of Conley and Bieron [1963a, 1963b, 1965] and Ouchi [1966], do not represent important reaction pathways in the pyrolysis of novolac resins [Morterra and Low, 1985a]. The i.r. spectra of the resins considered here agree with this suggestion as all six resins show the existence of small shoulders around 1650 cm⁻¹ in the 500-550°C, temperature range but their presence is insignificant and the assignment of the band can only be considered as speculative.

The band multiplet in the 1630-1580 cm⁻¹ range becomes stronger, but less resolved, and broadens into a single symmetrical band centred at 1600 cm⁻¹ in the spectra of the resins above 550°C. This suggests the conversion of the ring stretch vibration of the 1,2- and 1,2,4- substitutions into the broader 1600 cm⁻¹ band found with all oxidised carbons [Morterra and Low, 1983, 1985b]. This band is considered due to the C=C stretching mode of the poly-aromatic system, which is made i.r. active by the existence of an oxidic layer [Morterra and Low, 1982]. This

process is seen to occur at 550°C for HFP, LFP, NFH, NFP, and although it occurs at approximately 50°C lower in HFH and LFH, there is no reason to suggest that this is caused by any particular difference in starting resin, as the actual process is seen to occur very gradually.

Above 550°C, the entire region of 1520-1000 cm^{-1} is seen to change for all resins as it broadens to reveal a single strong, and very broad, band centred at approximately 1130 cm^{-1} . At higher temperatures there is little spectral detail, as might be expected from a highly carbonised resin.

It is suggested that the i.r. spectra of the chars produced by novolac resins become indistinguishable above 560°C from those of intermediate temperature chars produced by the pyrolysis of other similar compound at comparable temperatures, e.g. the spectra of chars of cellulose materials [Morterra and Low, 1983, 1985a]. This appearance of a *standard* spectrum for all high temperature chars of this type of starting material is considered to be achieved along with the complete elimination, from a spectroscopic view point, of residual aliphatic groups. It has been reported by Morterra and Low [1985] that at the lower temperatures, oxygen bridges of the aryl-aryl ether type are thought not to interfere with the polycondensation process to a great extent such that they may either enter into the poly-nuclear system by being transformed into pyran and/or furan rings [Ouchi, 1966] or remain as oxygen bridges cross-linking the poly-aromatic domains, although the strong band of the single-bond (ether-like) CO become broader and more poorly resolved, which indicates a higher disorder of the poly-aromatic system formed as a result of the final collapse of the residual resin network.

The increase in the tetra-substituted aromatic CH deformation band at 880 cm^{-1} , in relation to the tri-substituted aromatic band at 750 cm^{-1} , indicates the increase in methylene bridge condensation of the poly-aromatic system above 600°C. As is

shown by the spectra of the six resins, NFH and NFP show the highest temperature for the commencement of the process, which again suggests that the absence of furfuryl-alcohol in the resins provides for less initial cross-linking and inhibits the release of volatiles, and delay such condensation processes to higher temperatures. From density measurements, it was suggested by Ouchi [1966] that the growth of condensed planar aromatic structures in phenolic resins does not take place significantly below 600°C, and the increase of substitution may be attributed to the possible formation of, for example, fluorene-type nuclei, or other disturbed network structures. This process is seen to be completed at 700 - 750°C for HFH, HFP, LFP and 750 - 800°C for LFH, NFH, NFP. Above 800°C it is assumed by the loss of spectral detail that a highly carbonised structure is formed.

A weak absorption, which is mainly seen as a shoulder of the broad band in the 1500-1000 cm^{-1} range in these resins, is found near 1440 cm^{-1} . It was shown that it cannot be assigned to the deformation modes of aliphatic CH groups which are no longer detectable because their stretching vibrations are so weak. It is suspected from the literature that in addition to the aliphatic CH_n deformation there were some other contributions to a weak band usually observed near 1440 cm^{-1} with intermediate temperature chars [Morterra and Low,1985a]. It was reported that this absorption was of such persistence in like chars up to and near 700°C that the following hypothesis was put forward. On poly-aromatic systems which still have short-range order and relatively short domain size, and provided that hydrogen is retained, which is indicated by the presence of aromatic CH at 900-750 cm^{-1} , some residual activity of the semicircle ring stretching modes may still present itself as a weakly resolved component on the high wave-number side of the broad ether-like band.

As the amount of hydrogen and oxygen in the resins is seen from elemental analysis (Figures 4.7 and 4.9) to be very low in each resin above 750°C (≈ 5 atomic%), it can be deduced that this removal of atoms from the system causes a

collapse of any polymeric order, and this is confirmed by the i.r. spectra of the resins of 750°C and higher temperatures failing to exhibit any residual structure in the 2000-500 cm^{-1} range. This does not differ appreciably from the obvious continuum absorption exhibited by other high temperature carbons [Delhaes and Carmona,1981].

Chapter Six

**The determination of specific
Phenolic Resin chemical and
structural modifications during
pyrolysis (25 - 750°C) by Solid State
¹³C Nuclear Magnetic Resonance
Spectroscopy**

¹³C Nuclear Magnetic Resonance

A detailed study of the solid pyrolysis products of the six carbons was conducted with the use of solid-state ¹³C nuclear magnetic resonance spectroscopy. The experiments were carried out on each of the six resins and their solid pyrolysis products up to heat treatments of 750°C. A spectrometer with a magnetic field-strength of 7.05 T was used with the combined line narrowing technique of cross - polarisation / magic - angle - spinning / high - power - proton - decoupling (CP/MAS/HPPD) in conjunction with a side-band suppression (TOSS) pulse sequence [Dixon,1982]. In this study, cross-polarisation dynamics in the resin chars have been investigated by means of variable contact time experiments and carbon distributions in the chars have been determined from the TOSS/DD spectral data. Additional structural parameters related to aromatic structures, namely the degree of substitution of the aromatic rings and the average aromatic cluster size, have been estimated. The values of relaxation time constants for the carbon species related to the cross-polarisation and dipolar dephasing experiments are reported. The relationship between the structural parameters and pyrolysis temperature of the resins are examined in view of the general structural features of the chars studied.

From Casiraghi *et al* [1981], a solution-state spectrum (in CD₃OD) of a highly *ortho* phenolic novolac resin is shown in Figure 6.1. The doublets at 115.78 and 120.7 ppm are suggested to be due to the two *ortho*-methine carbons of the aromatic end groups and the *para*-methine carbons, respectively. The two smaller peaks at 152.4 and 154.92 ppm are due to the aromatic hydroxyl substituted carbons of internal and external nuclei, respectively. The peaks between 127.8 and 131.2 ppm are the remaining aromatic carbons, and the presence of only one resonance at 31 ppm is due to the *ortho-ortho'* CH₂-bridges, which confirms that the resin of this particular study is all-*ortho* ordered [DeBreet *et al*,1977].

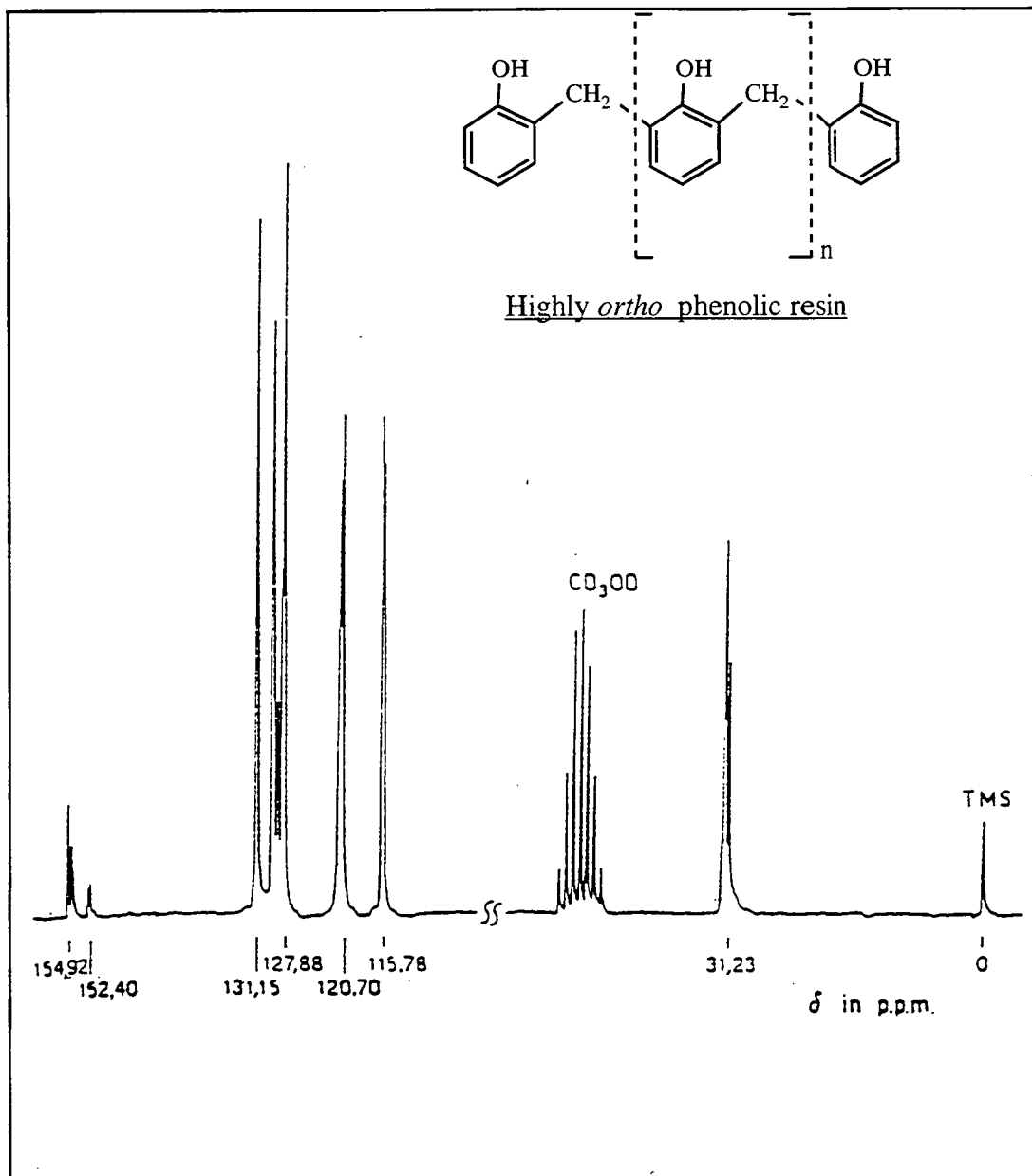


Figure 6.1 ^1H -decoupled ^{13}C nmr spectrum at 25.206 Mhz of a highly *ortho* phenolic resin [Casiraghi *et al*, 1981].

This is compared to the solid-state spectrum of the as-cured form of HFH in Figure 6.2. The normal TOSS ^{13}C nmr spectra (contact time, $t_{\text{cp}} = 2$ ms) for each of the six resins over the heat treatment temperature range are shown in Figures 6.2 to 6.7. Although the resolution of the solid-state TOSS spectrum is not as high as that of the solution spectrum, spectral detail is still present in the solid-state spectra.

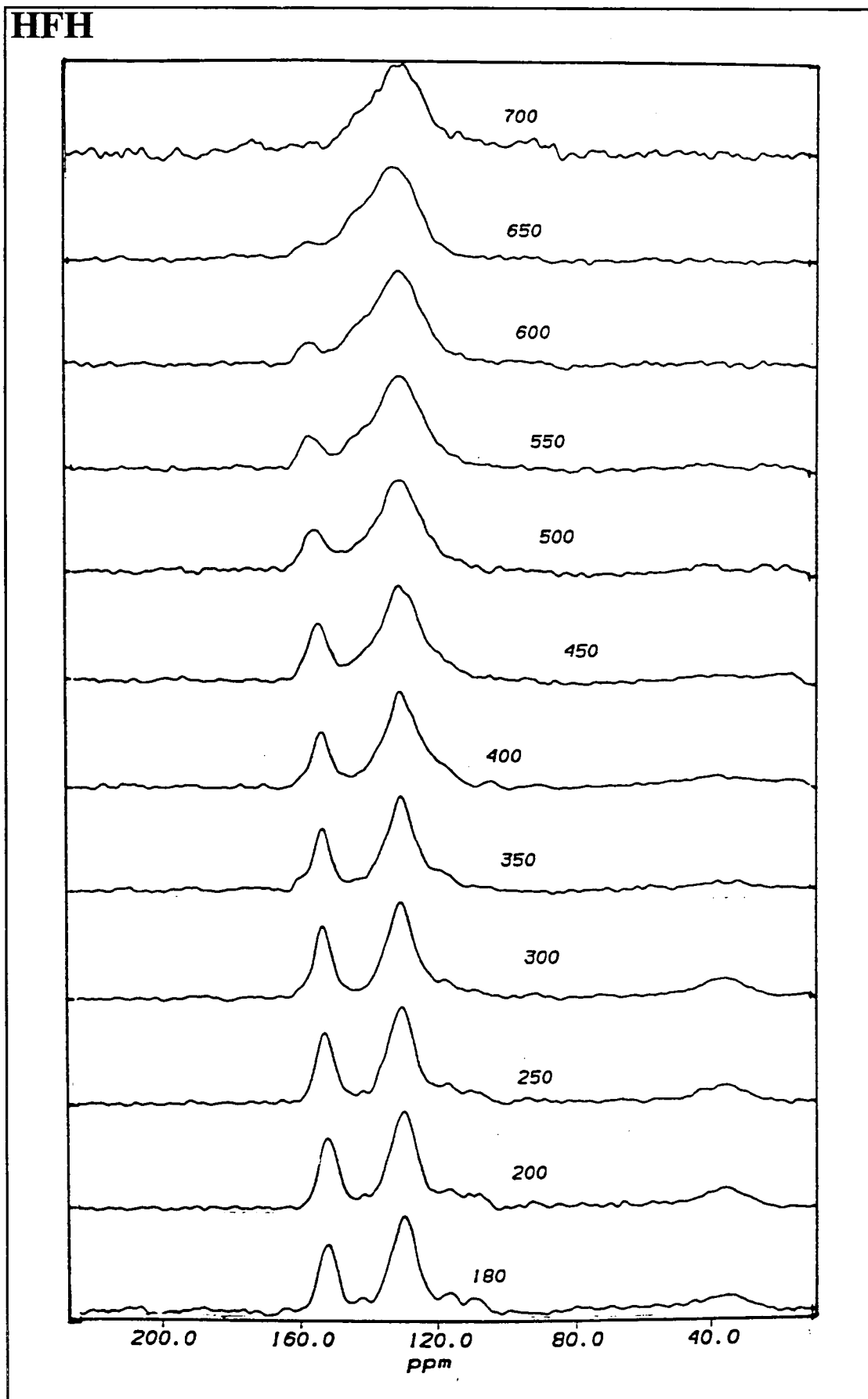


Figure 6.2 The normal TOSS ^{13}C nmr spectra ($t_{\text{cp}} = 2$ ms) for HFH over the heat treatment temperature range. The number for each spectrum indicates the temperature ($^{\circ}\text{C}$) to which the resin was heat treated.

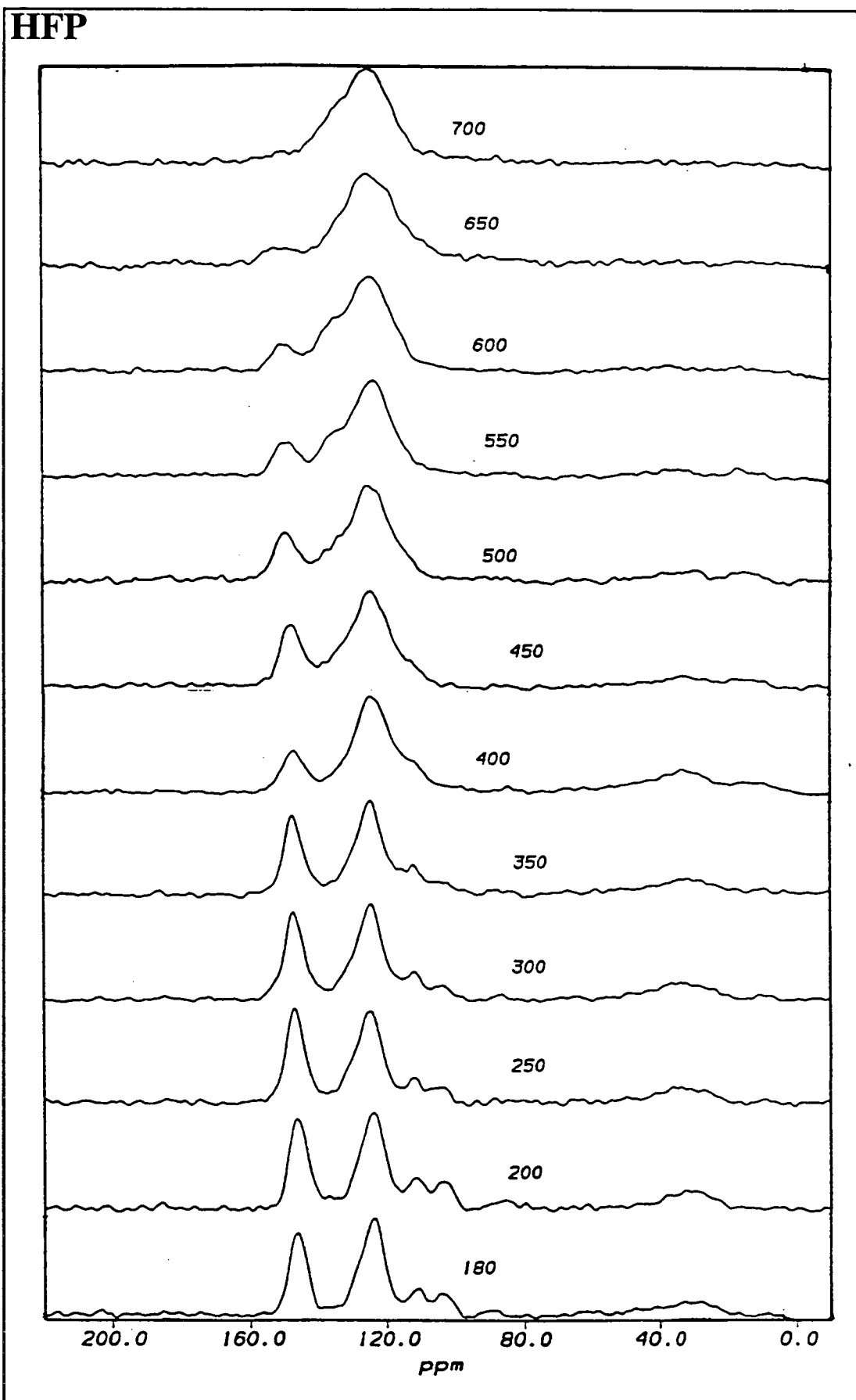


Figure 6.3 The normal TOSS ^{13}C nmr spectra ($t_{\text{cp}} = 2$ ms) for HFP over the heat treatment temperature range. The number for each spectrum indicates the temperature ($^{\circ}\text{C}$) to which the resin was heat treated.

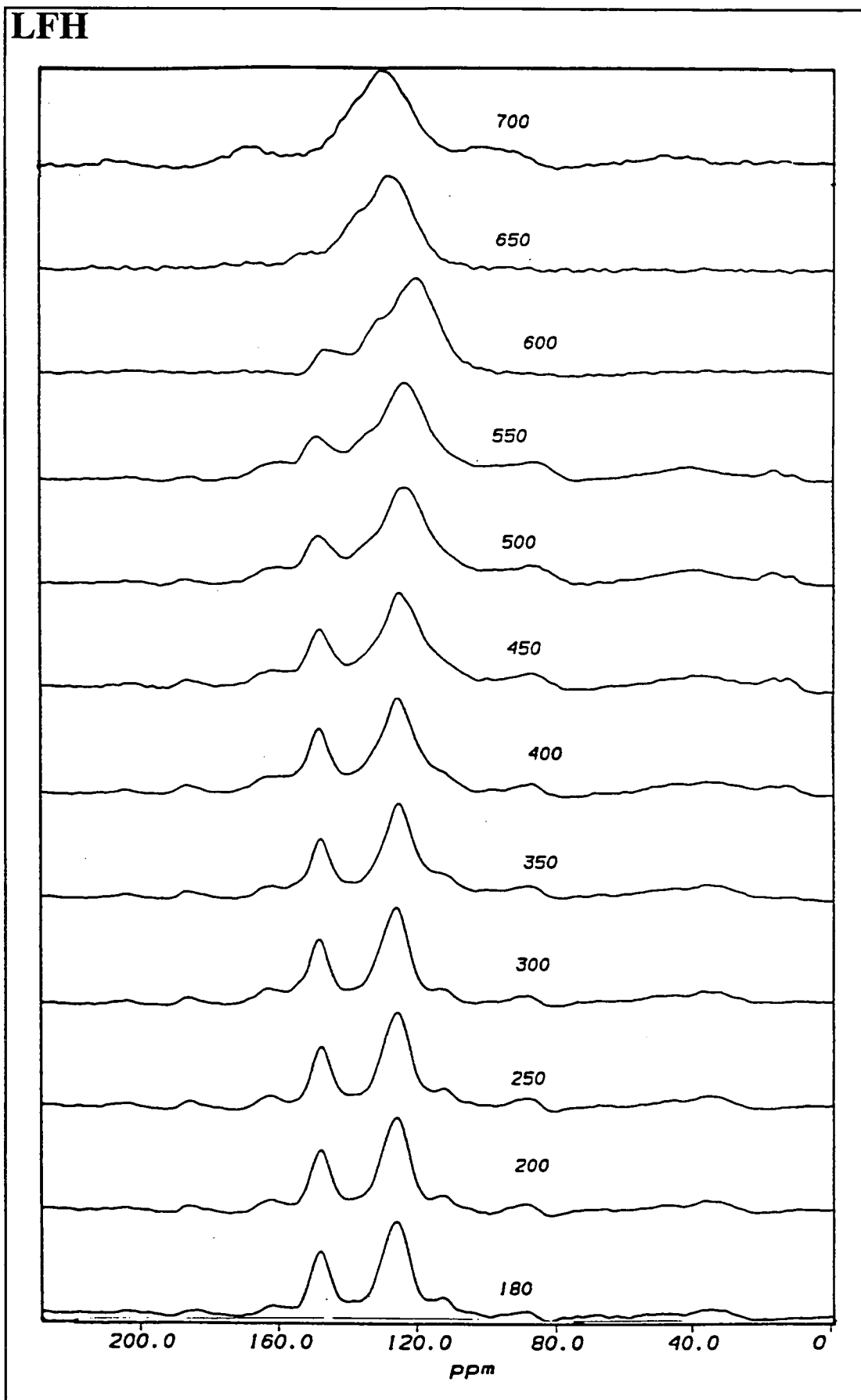


Figure 6.4 The normal TOSS ^{13}C nmr spectra ($t_{\text{cp}} = 2$ ms) for LFH over the heat treatment temperature range. The number for each spectrum indicates the temperature ($^{\circ}\text{C}$) to which the resin was heat treated.

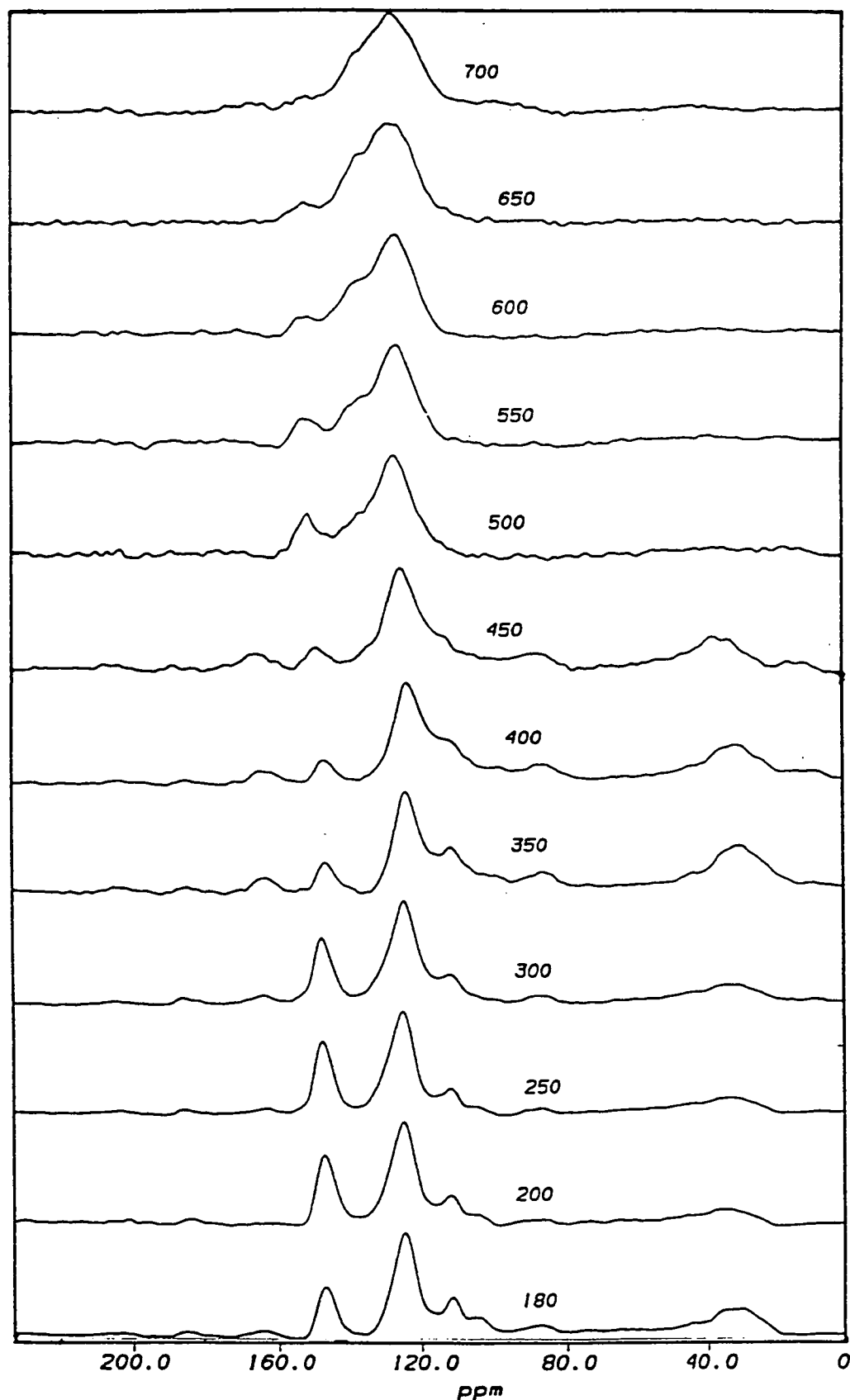
LFP

Figure 6.5 The normal TOSS ^{13}C nmr spectra ($t_{\text{cp}} = 2$ ms) for LFP over the heat treatment temperature range. The number for each spectrum indicates the temperature ($^{\circ}\text{C}$) to which the resin was heat treated.

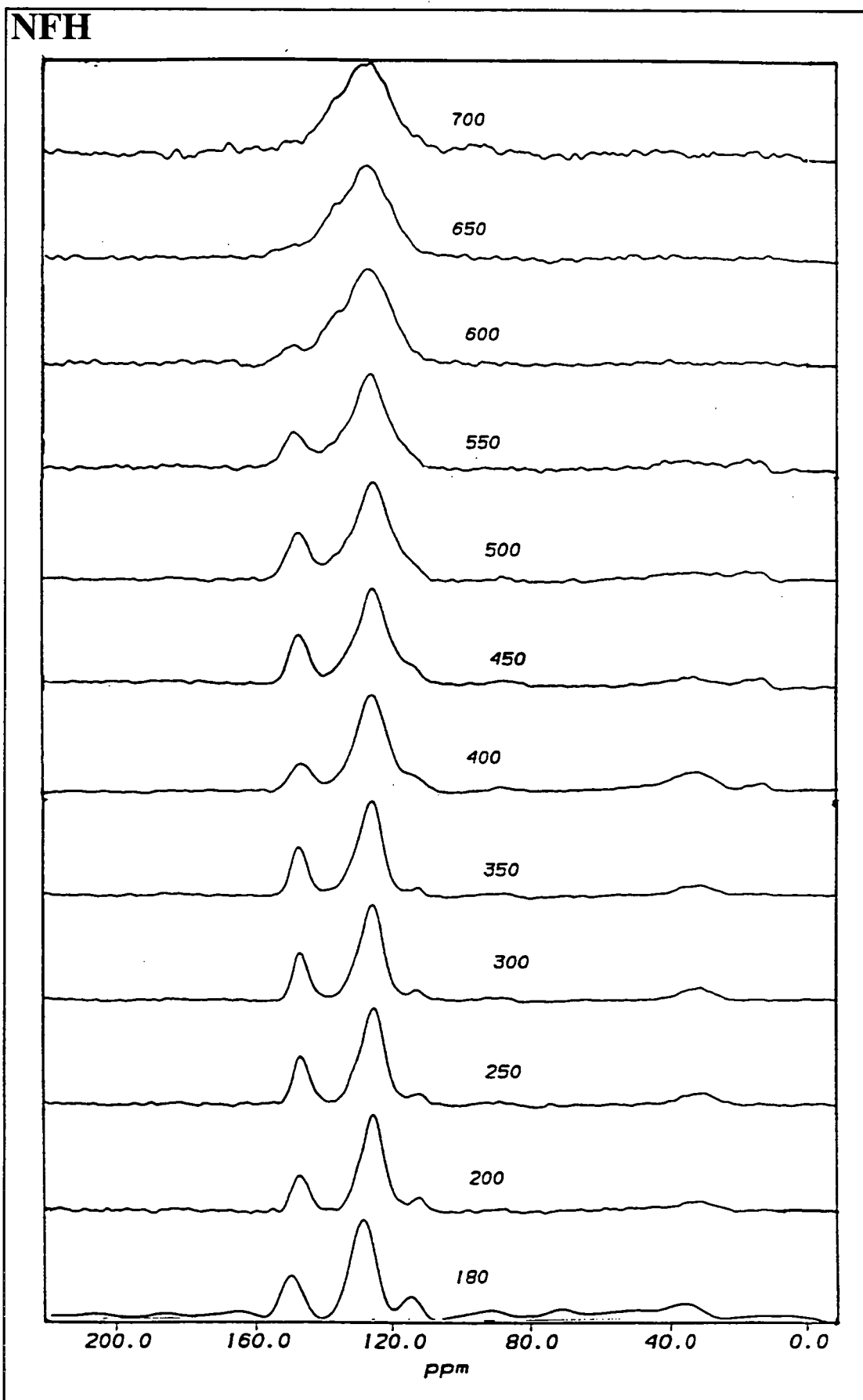


Figure 6.6 The normal TOSS ^{13}C nmr spectra ($t_{\text{cp}} = 2$ ms) for NFH over the heat treatment temperature range. The number for each spectrum indicates the temperature ($^{\circ}\text{C}$) to which the resin was heat treated.

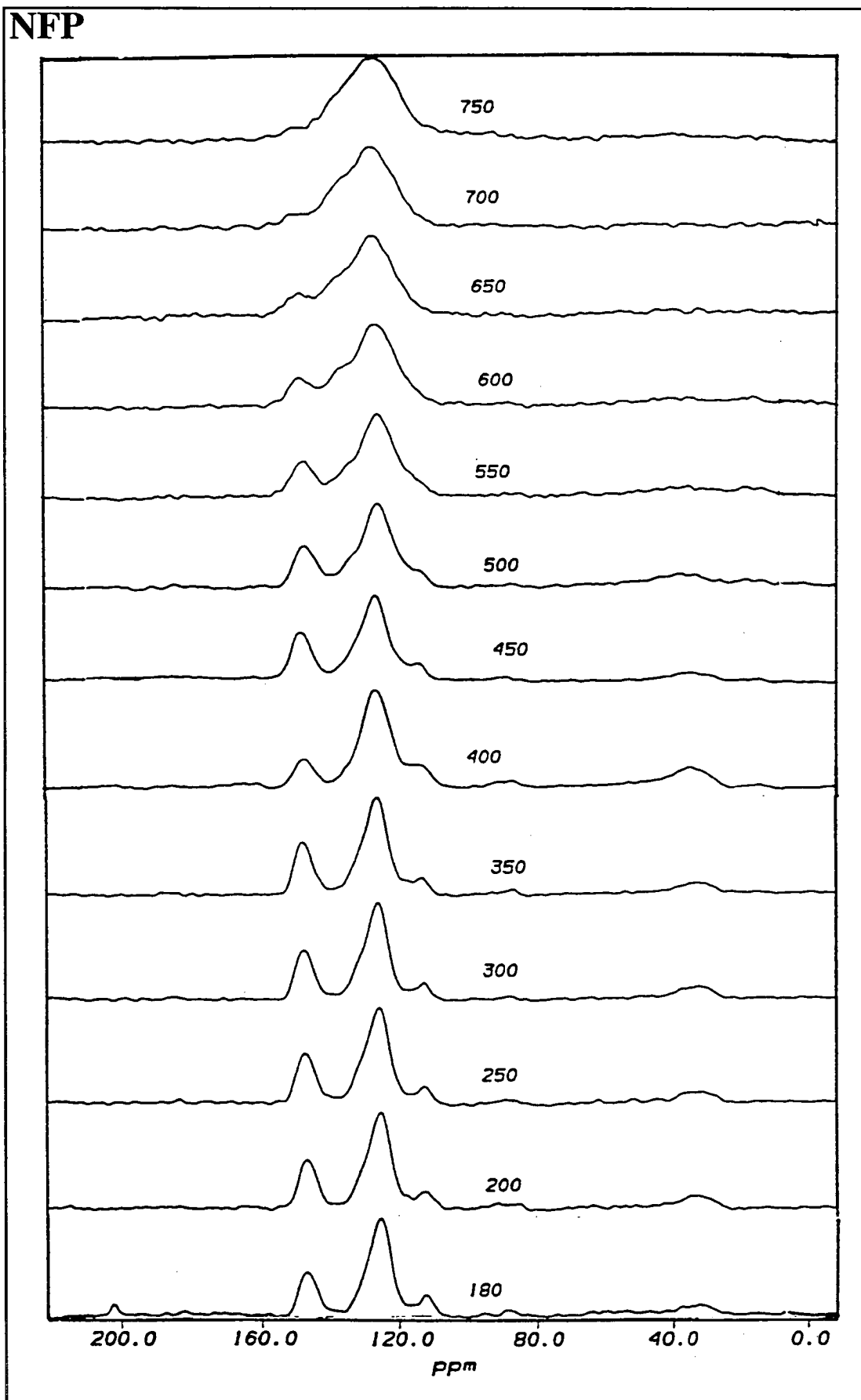


Figure 6.7 The normal TOSS ^{13}C nmr spectra ($t_{\text{cp}} = 2$ ms) for NFP over the heat treatment temperature range. The number for each spectrum indicates the temperature ($^{\circ}\text{C}$) to which the resin was heat treated.

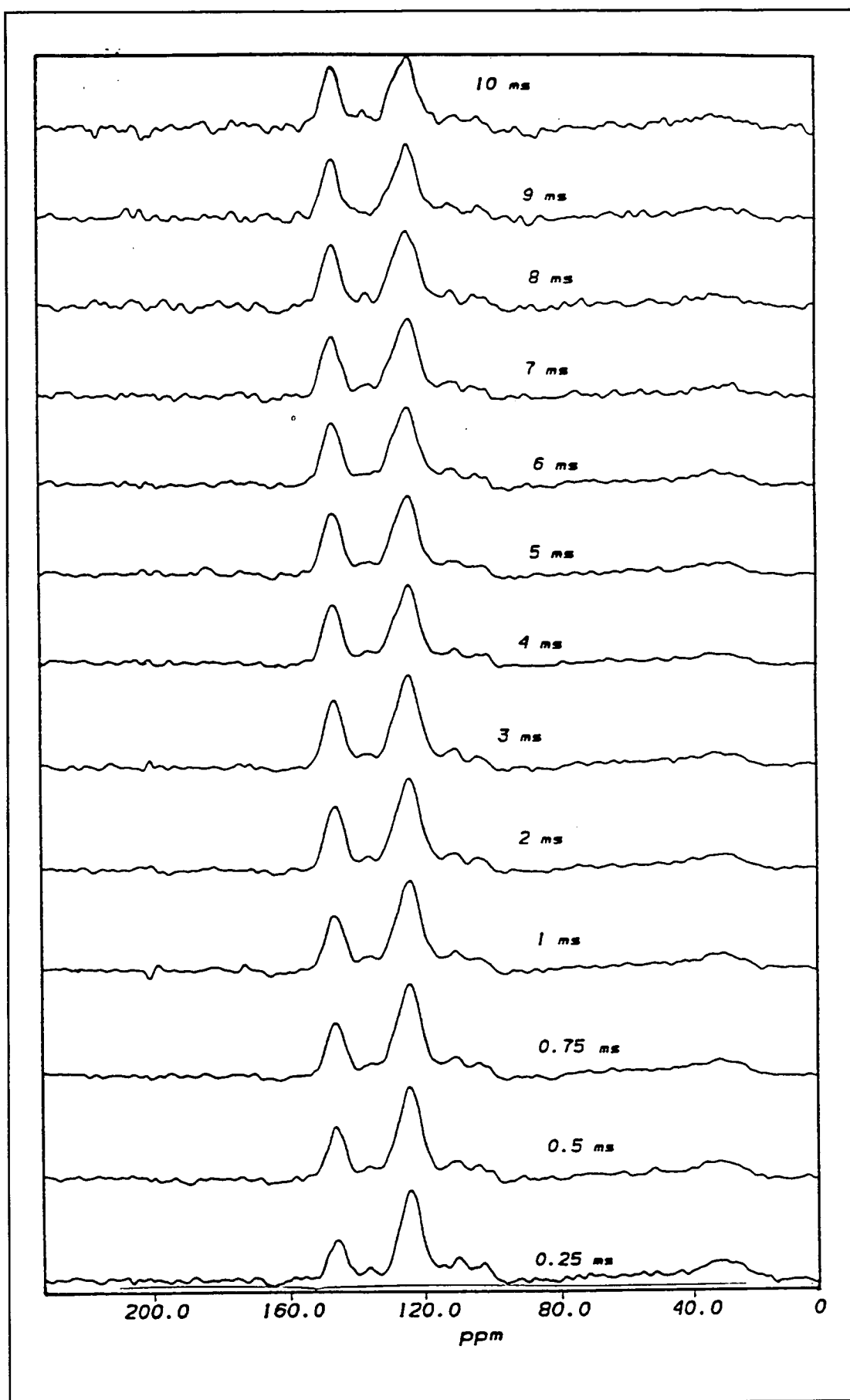


Figure 6.8 TOSS spectra at various contact times (ms) for the unpyrolysed resin HFH.

Cross-polarisation dynamics in the phenolic resins:

The ^{13}C - ^1H CP/MAS technique is based on the transfer of magnetisation from the proton system to that of carbon-13 under appropriate conditions [Yannoni,1982]. This transfer is governed, for a given carbon, by two important parameters; the cross-polarisation time, T_{CH} , of the observed carbon atom; and the spin-lattice relaxation time, $T_{1\rho}^{\text{H}}$, of the protons in the rotating frame. In general, T_{CH} is much shorter than $T_{1\rho}^{\text{H}}$ and the evolution of the ^{13}C -nmr integrated intensity M with the contact time, t_{cp} , between the two systems is dominated by T_{CH} at short t_{cp} and by $T_{1\rho}^{\text{H}}$ at long t_{cp} [Sullivan and Maciel,1982; Supaluknari,1989]. According to the spin-temperature model [Gerstein and Dybowski,1985; Mehring,1983] the ^{13}C magnetisation, $M(t_{\text{cp}})$, at any contact time, t_{cp} , is related to T_{CH} and $T_{1\rho}^{\text{H}}$ by the equation:

$$M(t_{\text{cp}}) = M_0 \cdot \lambda^{-1} \cdot [1 - \exp(-\lambda \cdot t_{\text{cp}}/T_{\text{CH}})] \cdot \exp(-t_{\text{cp}}/T_{1\rho}^{\text{H}}) \quad \text{.....(i)}$$

such that,

$$\lambda = (T_{1\rho}^{\text{H}} - T_{\text{CH}})/T_{1\rho}^{\text{H}} \quad \text{.....(ii)}$$

and M_0 is the maximum ^{13}C magnetisation. Under the condition that $T_{\text{CH}} \ll t_{\text{cp}} \ll T_{1\rho}^{\text{H}}$, λ can be assumed to approximate unity and therefore this equation was reduced to the following form [Amram and Laval,1989]:

$$M = M_0 \cdot [1 - \exp(-t_{\text{cp}}/T_{\text{CH}})] \cdot \exp(-t_{\text{cp}}/T_{1\rho}^{\text{H}}). \quad \text{.....(iii)}$$

Therefore, at short contact times ($< 10\mu\text{s}$) only the protonated CH and CH_2 carbon species are magnetised and appear on the spectrum. The CH_3 groups are more slowly magnetised because of their ability to rotate, and therefore are not obvious at the low t_{cp} . For a quantitative determination of the carbon species, the tail of the

variable contact time curve was fitted to a single decaying exponential in the region where $t_{cp} \gg T_{CH}$. By extrapolating this monoexponential to $t_{cp} = 0$, the value of M_0 , which is proportional to the number of carbons, was obtained.

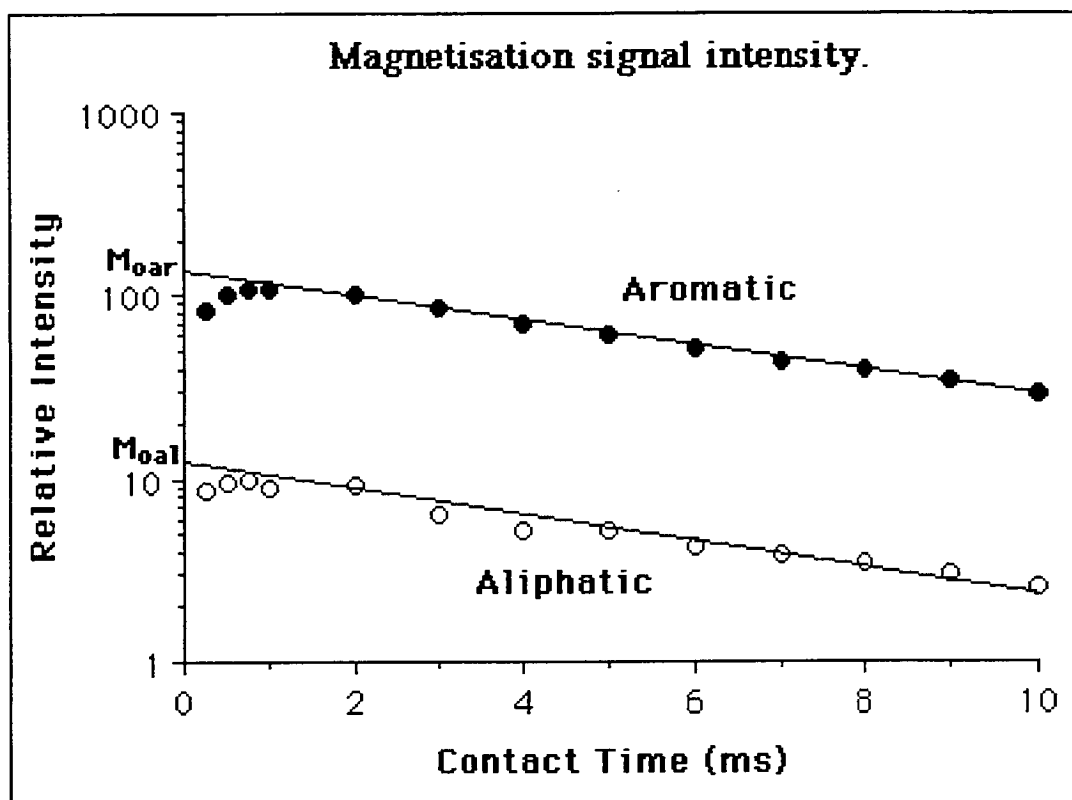


Figure 6.9 Variation in ^{13}C signal intensity with contact time, t_{cp} for the unpyrolysed resin HFH.

The aromatic fraction could then be calculated from the equation:

$$f_{ar} = M_{oar} / (M_{oar} + M_{oal}) \quad \dots\dots\dots(\text{iv})$$

where M_{oar} and M_{oal} are the extrapolated intensities of the aromatic and aliphatic carbons, respectively. The time constant, $T_{1\rho}^H$, of the single decaying exponential was also measured. For these calculations the relative integrated intensities of the aromatic region was taken at 169-95 ppm, and the aliphatic region at 95-0 ppm. The change in relative intensity for the two main aromatic carbon peaks with

varying contact time can be seen from the spectra taken for the as-cured HFH at different contact times, as shown in Figure 6.8. The integrated magnetisation profile of the two carbon types, aromatic and aliphatic, over contact time, can be seen in Figure 6.9. These decay profiles for the two carbon species are typical of those from other contact time experiments [Amram and Laval,1989].

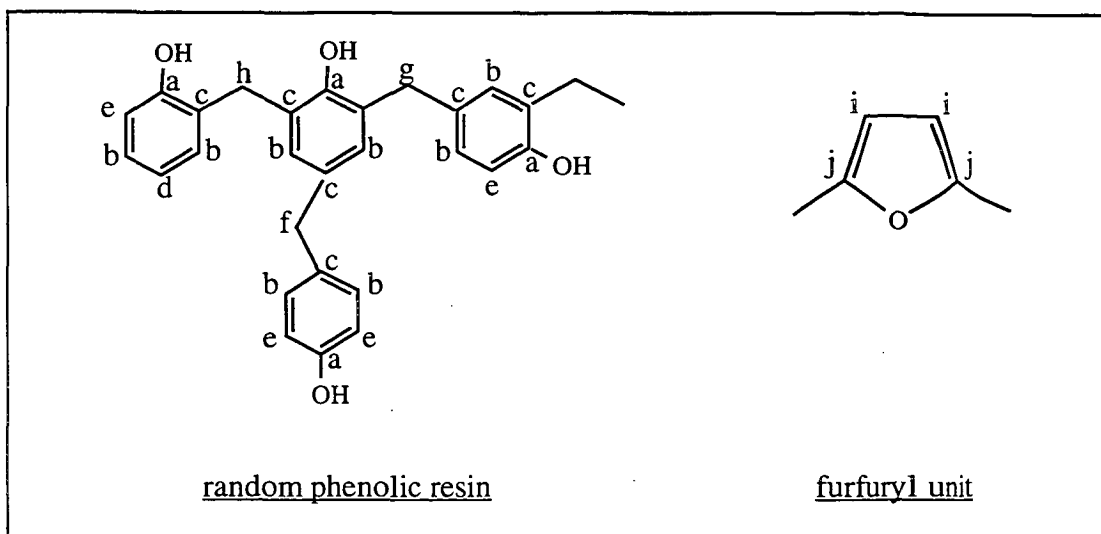
Dipolar-dephasing analysis and carbon distribution:

The dipolar dephasing experiment is similar to a conventional cross-polarisation experiment except for the introduction of a pulse delay time, t_d , between the contact time and the acquisition of the free induction decay (FID) signal, and this allows for the dephasing of the C-H spins. The strongest spin interaction for most carbons of complex molecules in the solid state during magnetisation is dipolar coupling to protons [Opella *et al*,1979]. The cross-polarisation of carbons from protons relies on this mechanism, while proton decoupling during data acquisition removes the dipolar broadening. The rate of dephasing of the ^{13}C signal is related to the ^{13}C - ^1H dipolar interaction, which has a $1/(r_{\text{CH}})^3$ dependence, where r_{CH} is the ^{13}C - ^1H internuclear distance [Yannoni,1982]. Therefore, the coupling is much greater for carbons bonded to protons ($r_{\text{CH}} \approx 1.1 \text{ \AA}$) as compared to those carbons with protons bonded only to nearest neighbour carbons ($r_{\text{CH}} > 2.0 \text{ \AA}$). Therefore, in the DD spectrum with a long dephasing delay ($> 40 \mu\text{s}$), the resonances observed are mainly of non-protonated and weakly coupled carbons that have long decaying times. The weakly coupled carbons also include carbons in the groups such as CH_3 that have free molecular motion which can partially average the ^{13}C - ^1H dipolar-interaction experienced by the carbon nuclei. In the resin chars of this study, the aromatic peaks due to protonated (CH) and quaternary carbons were studied by this method. The methine carbons relax rapidly, whereas the quaternary carbons relax more slowly. Therefore at long t_d ($> 60\mu\text{s}$) only the latter appear in the spectrum. Additionally, based on the dipolar-dephasing interpretation, and on

chemical-shift data of solid phenolic resins [Amram and Laval,1989; Bryson *et al*,1983; Dradi *et al*,1978; Fyfe *et al*,1983a,1983b; Maciel *et al*,1984; Siling *et al*,1977; Sojka *et al*,1979;] and solid furfuryl-alcohol resins [Chuang *et al*,1984; Maciel *et al*,1982], various carbon functionalities in the resin chars studied can be identified from the TOSS/DD spectra. These are shown in Table 6.1.

In addition to the expected band assignments of the various carbon species, the normal ^{13}C TOSS nmr spectra of each as-cured resin (2 ms contact time) in Figures 6.2 to 6.7 show small peaks either side of the central aromatic peaks positioned at approximately 80 ppm and above 160 ppm. As these peaks were seen to be shifted inward with decreased magic-angle-spinning rate, they were assigned as spinning side bands and so neglected from any integrations. Additionally, the absence of any clearly defined signals above 160 ppm suggests that there were no carbonyl or carboxylic carbons of any type in the as-cured resins. This theory is supported by the FTIR spectra which show no obvious carbonyl absorptions in the $1700 - 1800\text{ cm}^{-1}$ region. In the spectra of all six resins the strong resonance at approximately 150 ppm displays the well resolved band of the phenolic hydroxyl groups within the resin polymeric structure. As this peak is also indicative of the unsubstituted carbons of the furan ring in furfuryl-alcohol, it is possible that the greater integral value of this peak relative to the 125 ppm peak in HFH and HFP is representative of the higher furfuryl-alcohol content in both resins.

The unsubstituted *meta* aromatic carbons of the phenolic system are only seen as a weakly resolved peak centred at approximately 130 ppm, and this resonance is often overshadowed by the much stronger resonances at 150 and 125 ppm. The peak at 130 ppm is most obvious in the as-cured HFH, and least in LFH and LFP, where it does not appear as a shoulder on the 125 ppm peak. The 125 ppm peak, assigned to the methylene substituted aromatic carbon, is seen in all resins as very sharp and well resolved.



Chemical Shift (ppm) ^a	Carbon Position	Carbon Species ^b
150	a	hydroxy substituted aromatic
140-150	j	substituted furan ring carbon
130	b	unsubstituted <i>meta</i> aromatic
125	c	methylene substituted aromatic
120	d	unsubstituted <i>para</i> aromatic
115	e	unsubstituted <i>ortho</i> aromatic
110	i	unsubstituted furan ring carbon
40	f	<i>para-para</i> methylene bridge
35	g	<i>ortho-para</i> methylene bridge
30	h	<i>ortho-ortho</i> methylene bridge

^a Relative to tetramethylsilane.

^b *Ortho*, *meta* and *para* designations are relative to the hydroxy-substituted carbon.

Table 6.1 ¹³C-NMR Structure/Shift relationships for the referenced unpyrolysed resins [Amram and Laval,1989; Bryson *et al*,1983].

The unsubstituted *para* aromatic carbon is seen as a well resolved peak at approximately 120 ppm. This peak, which is strongly indicative of methylene bridge formation at the *ortho-ortho'* carbon sites (in addition to the *o-o'* CH₂-bridge carbons at 31 ppm) [Casiraghi *et al*,1981], is shown most strongly in LFP and NFH. The peak at 110 ppm is assigned as the unsubstituted carbon on the furan ring of furfuryl-alcohol. This is a reasonable assignment of these carbons, as this peak is only observed for HFH, HFP, LFP. It is possible, as has previously

been discussed in relation to the FTIR data, that the hexamine in LFH possibly reacts with the furan ring as it exists in furfuryl-alcohol, which leads to the absence of the 110 ppm peak in the spectrum of LFH. This peak is further enhanced in HFH and HFP, which is also evidence of its assignment as furfuryl-alcohol due to the higher proportion of this constituent in these two resins.

The fine structures in the aliphatic region (40 ppm - 0 ppm) show the existence mainly of *ortho-ortho'* and *ortho-para* bridge formation in the resins due to the prominence of the 30 ppm and 35 ppm peaks, respectively. From Supaluknari [1989], it was suggested that an oxygenated aliphatic carbon species exists in the range 95-75 ppm. As this band is poorly resolved within the spectra of the resin chars, these carbon types are not being considered as relevant within this study. A shoulder on the low-field side of the aliphatic band at 40 ppm is evidence of *para-para'* bridge carbons and can be an indicator of extensive tri-substitutional cross-linking.

There were no definite bands found in the 225-170 ppm region in any of the spectra, and so it was assumed that there were no carbonyl carbon types in the chars, even in those heat treated to 700°C. In all resins, except NFP, the spectra of the chars of pyrolysis temperatures above 700°C failed to give any recognisable peak signals due to the low atomic H/C ratios for those chars. Because the carbons need sufficient neighbouring hydrogen atoms for cross-polarisation, and therefore signal enhancement, it is found from elemental analyses results (Figure 4.7) that a char with a H/C ratio less than 1:5 fails to provide a resolvable ^{13}C nmr spectrum. As NFP retains more hydrogen than the other resins up to pyrolysis temperatures of 750°C ($\text{H/C}_{750} = 3/10$) it can provide a reasonably resolvable spectrum of its 750°C char. A normal TOSS experiment was conducted on a 750°C char of LFH to determine the possibility of signals being observable in the high temperature chars ($T > 700^\circ\text{C}$) with a sufficient number of scans. After 30000 scans there were no observable signals from the spectrum and so it was decided that these high

temperature chars above 700°C were fully carbonised.

For the unpyrolysed HFH resin a comparison of the TOSS and TOSS/DD experiments is shown spectrally in Figure 6.10 and the decay of signal intensity for the variable t_d experiment is shown in Figure 6.11. From the dipolar dephasing studies of Supaluknari [1989], the signal decay profiles of both aromatic and aliphatic carbon species, as a function of dephasing delay time, are shown to be composed of fast and slow components characterised by the time constants T'_{2f} and T'_{2s} respectively. The relative integrated intensity from the dipolar dephasing experiment, $I(t_d)$, of either the aromatic or aliphatic region was found after being fitted to the following equation:

$$I(t_d) = (I_0)_f \cdot \exp[-0.5 (t_d/T'_{2f})^2] + (I_0)_s \cdot \exp(-t_d/T'_{2s}) \quad \text{.....(v)}$$

where t_d is a dephasing delay and $(I_0)_f$ and $(I_0)_s$ are the relative intensities at $t_d = 0$ for the fast and slow components respectively. Although the full DD analysis is useful for the estimation of protonated and non-protonated carbons from $(I_0)_f$ and $(I_0)_s$ values, the experiment is time consuming, and can be made more convenient by using another approach [Wilson *et al*, 1984]. In this method only two spectra obtained at $t_d = 0$ and 50 μs were used to estimate the protonated aromatic carbon fractions of the resin chars.

The non-protonated carbons of the aromatic fractions, which are represented by the slow component of the aromatic signal decay, can be used to calculate protonated aromatic (tertiary) carbons by difference. Therefore, at long t_d ($> 50 \mu\text{s}$) only the non-protonated carbons appear in the DD spectrum and the evolution of the integrated intensity of the non-protonated carbons, I_s , is given by the following equation [Amram *et al*, 1989]:

$$I_s = (I_0)_s \cdot \exp(-t_d/T'_{2s}) \quad \text{.....(vi)}$$

Therefore by extrapolating the least squares linear regression of the $50\mu\text{s} < t_d < 100\mu\text{s}$ range of the DD plot to $t_d = 0$, the intensity of the slow, non-protonated carbons, $(I_0)_s$ can be determined as a fraction of the corresponding region from the normal TOSS spectrum. The proportion of protonated carbons can then be determined by difference. By using the integrated areas obtained from TOSS and $50\mu\text{s}$ TOSS/DD spectra and using the values of $(I_0)_s$ for the aromatic and aliphatic regions, the distribution of carbon-types in the resin chars can be estimated.

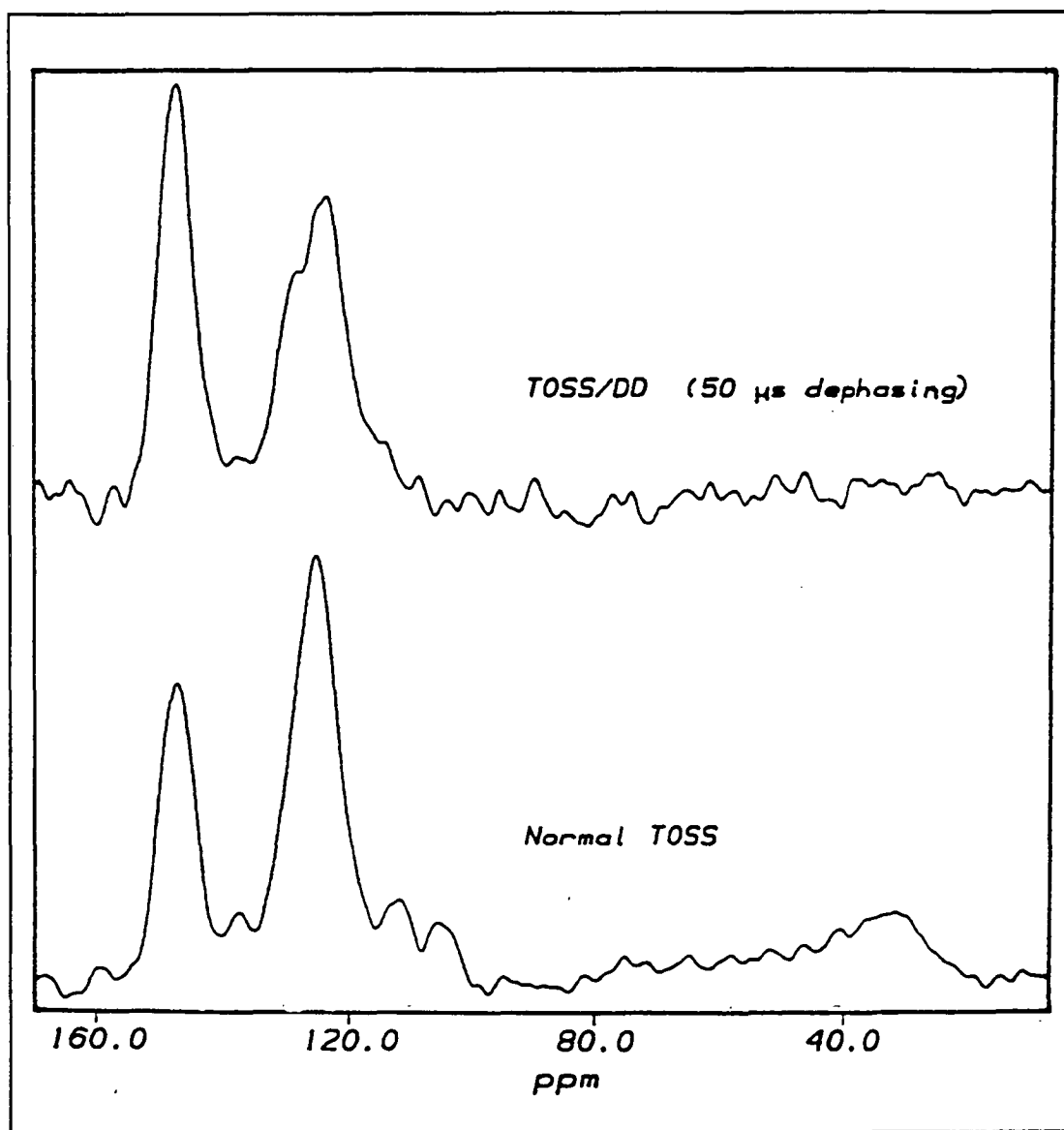


Figure 6.10 Normal TOSS and TOSS/DD spectra of unpyrolysed resin HFH.

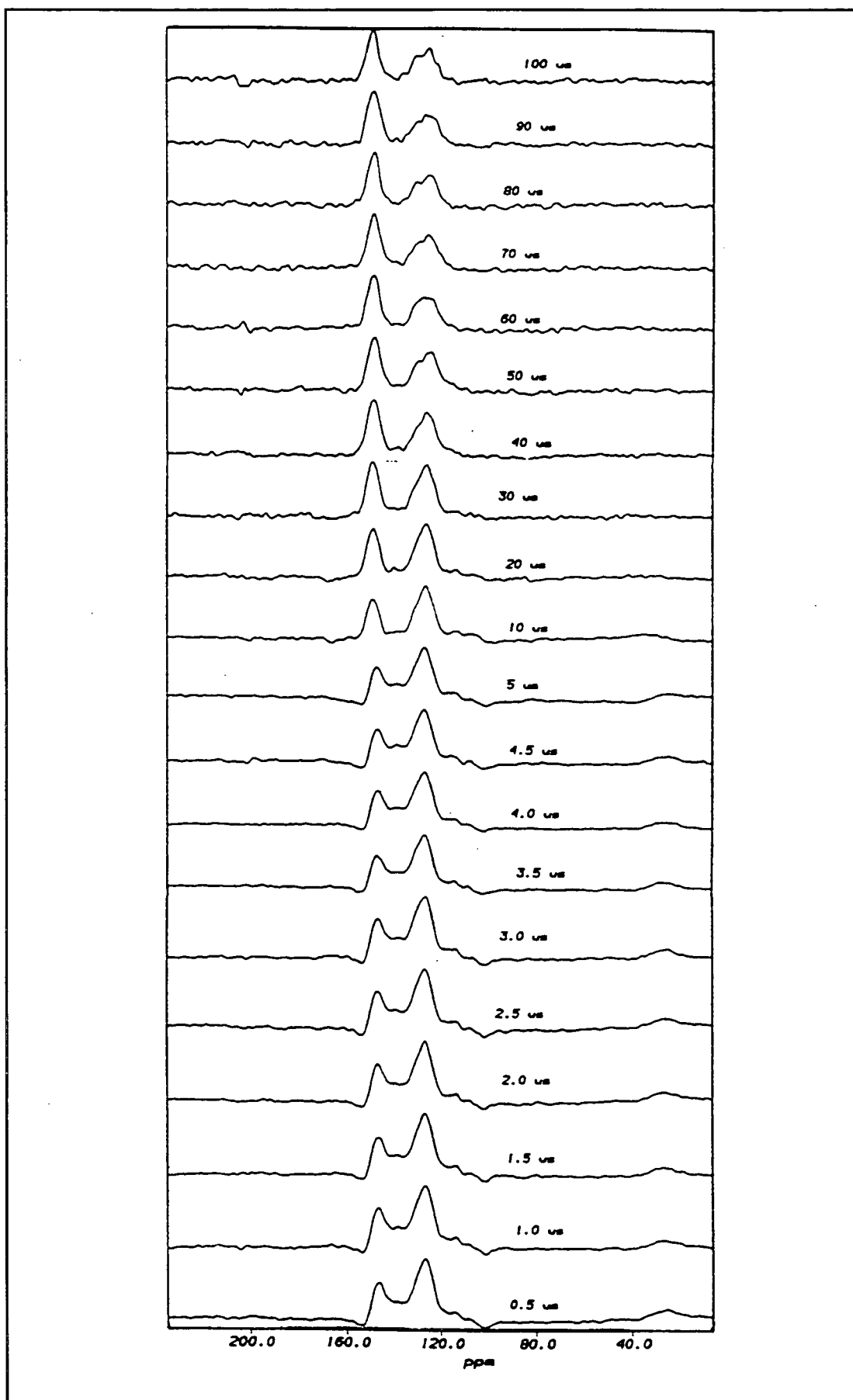


Figure 6.11 TOSS/DD spectra at various dephasing times for the unpyrolysed HFH resin.

For the aliphatic carbons, the value of $(I_0)_s$ was used to estimate the protonated carbon fractions by difference. To calculate the structural parameters of the resin chars, such as the proportion of aromatic unsubstituted *para* carbons, etc., the spectra from the normal TOSS experiment were deconvolved to reveal the presence of the various resonance bands associated with the different carbon species. The fractions of the various unsubstituted aromatic carbons were calculated in proportion to their relative intensities from the normal TOSS spectra and the proportion of protonated aromatic carbons. A similar method was used to calculate the proportions of the various methylene bridge types from the fraction of protonated aliphatics. The definitions of the various carbon fractions are given in Table 6.2. The two main parameters, f_{ar} and f_{al} , were calculated from the variable contact time experiments for the resin chars.

The TOSS experiment, which uses a series of four 180° carbon channel pulses to eliminate spinning sidebands, has been reported to be a source of some inaccuracy and in this study has shown some difficulty in actually suppressing spectral sidebands. It has been demonstrated [Axelson,1987] that for a limited range of coal samples the measurements from the TOSS technique were comparable to those obtained from normal ^{13}C nmr spectra. The f_{ar} results from a pyrolysed resol-type phenolic resin were measured by the normal ^{13}C nmr spectra obtained from a different spectrometer (Bruker CXP 90) operated at a lower magnetic field of 22.638 MHz [Amram and Laval,1989]. The f_{ar} value for the unpyrolysed resol resin (0.85) compared well with the f_{ar} values of the unpyrolysed resins of this study (0.8 - 0.93), and this shows encouragement for the application of the TOSS technique for phenolic resin chars.

The $T_{1\rho}^H$ values of the aliphatic and aromatic carbons in the resin chars are shown in Figure 6.12. It can be seen that the $T_{1\rho}^H$ values remain relatively constant over the pyrolysis temperature range to 600°C for both the aliphatic and aromatic carbons in the chars. Above 600°C there is a slight increase for the aromatic

carbons of the 700°C chars, which suggests that these carbons have increased in structural regularity because of the formation of a pseudo crystalline lattice during the carbonisation process [Amram and Laval,1989].

Carbon fraction	Definitions ^a	
Total aromatic (aromaticity)	f_{ar}	$= (I_{170-95}/I_{total})_0$
Protonated aromatic	f_{ar}^H	$= f_{ar} \cdot [1 - (I_0)_s^{ar}]$
Hydroxyl aromatic	f_{ar}^{OH}	$= f_{ar} \cdot (I_{150}/I_{ar})_0$
Bridgehead aromatic	f_{ar}^{ar}	$= f_{ar} - (\text{other aromatics})$
Total aliphatic	f_{al}	$= 1 - f_{ar}$
<i>o-o'</i> methylene bridge	f_{al}^{oo}	$= f_{al} \cdot [I_{30}/I_{95-0}]$
<i>o-p</i> methylene bridge	f_{al}^{op}	$= f_{al} \cdot [I_{35}/I_{95-0}]$
<i>p-p'</i> methylene bridge	f_{al}^{pp}	$= f_{al} - f_{al}^{oo} - f_{al}^{op}$

a. The subscript 0 denotes the data obtained from normal TOSS spectra. The subscript of I denotes the chemical shift range, or the centre of a fitted chemical shift peak; *al* and *ar* denote the aliphatic (95-0ppm) and aromatic (170-95ppm) regions respectively. *Total* indicates the full ppm range (170-0).

Table 6.2 The definitions of various carbon fractions.

The relatively constant $T_{1\rho}^H$ values over the pyrolysis temperature range below 700°C suggest rapid 1H spin diffusion in the chars due to a relatively high proton density [Maciel *et al*,1984]. As the proton density of the resin chars decreases with ring condensation, the average 1H spins are seen to slow dramatically.

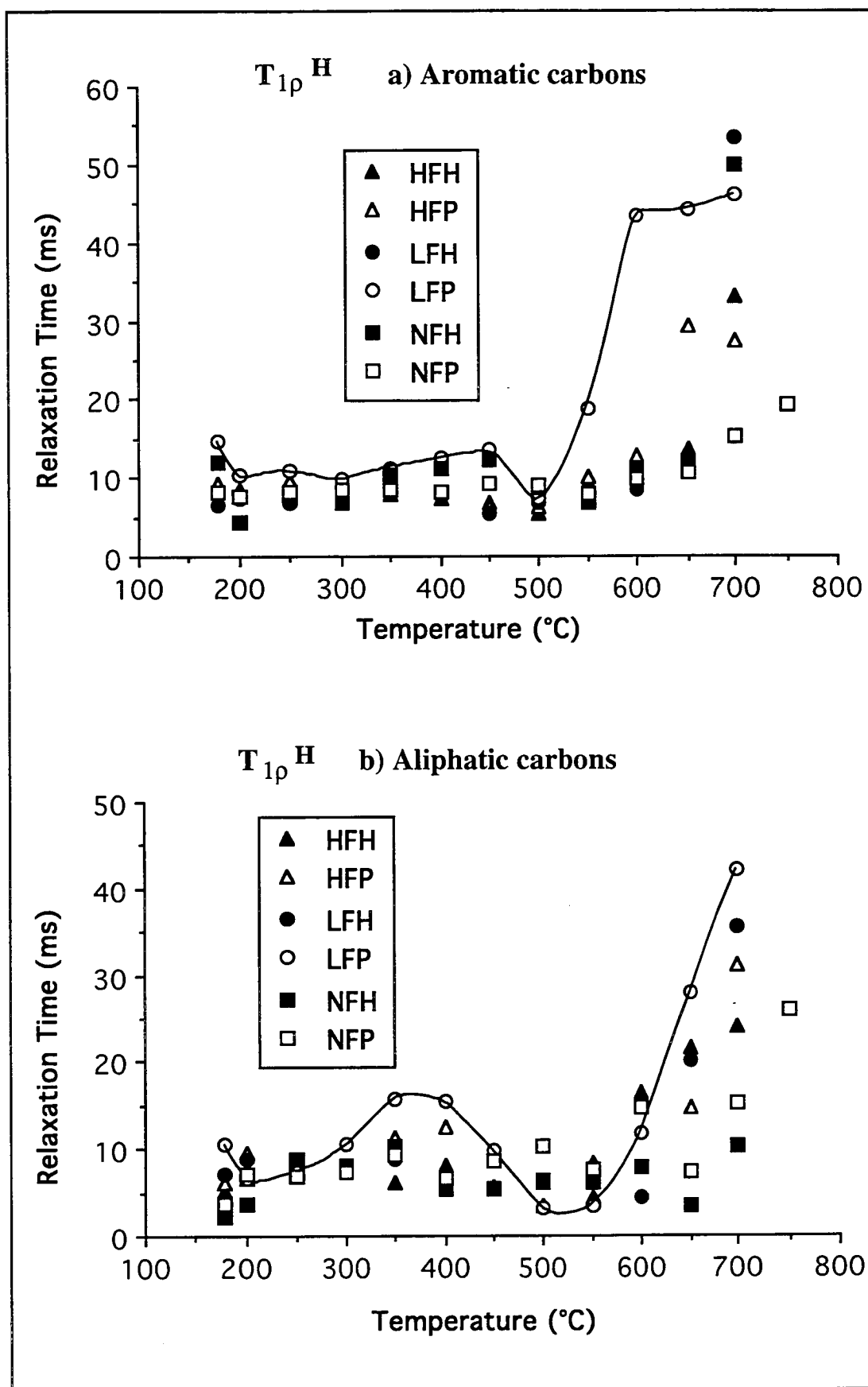


Figure 6.12 ^1H Spin-lattice relaxation time in the rotating frame, $T_{1\rho}^{\text{H}}$, for the **a) aromatic**, and **b) aliphatic** carbons of the six resins over the heat treatment temperature range.

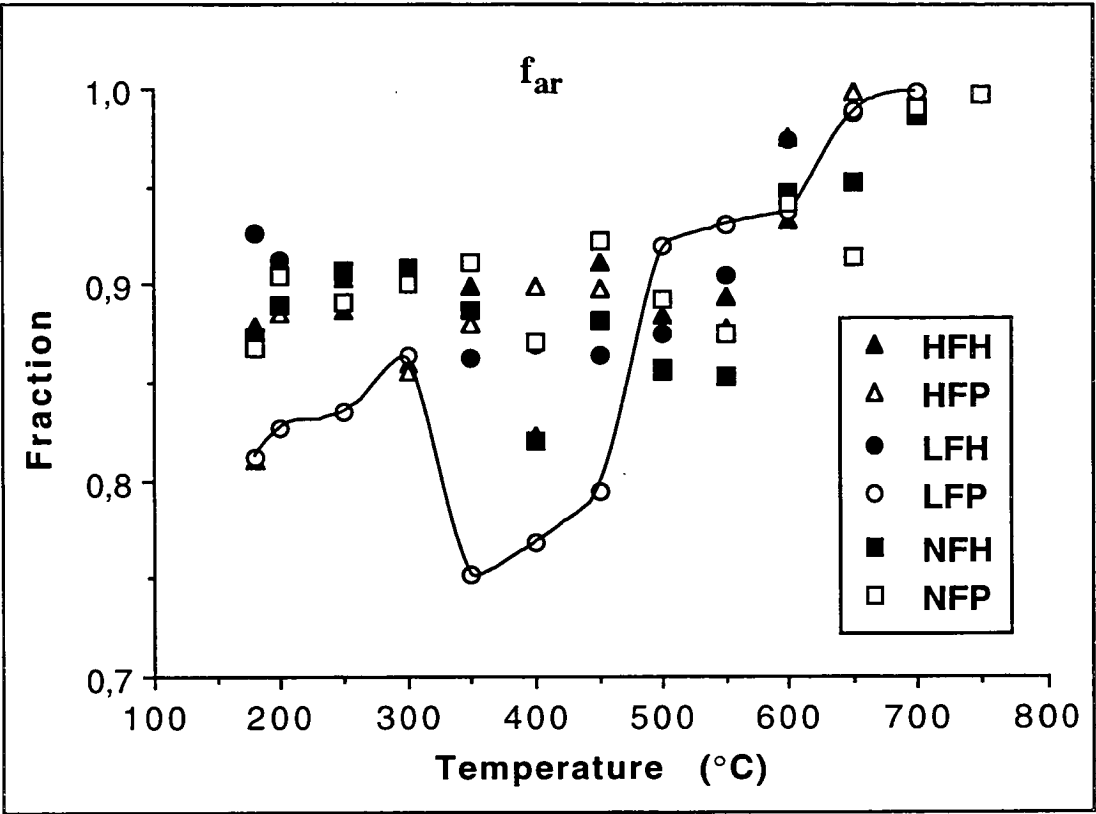


Figure 6.13 Aromatic fraction, f_{ar} , for the six resins over the heat treatment temperature range.

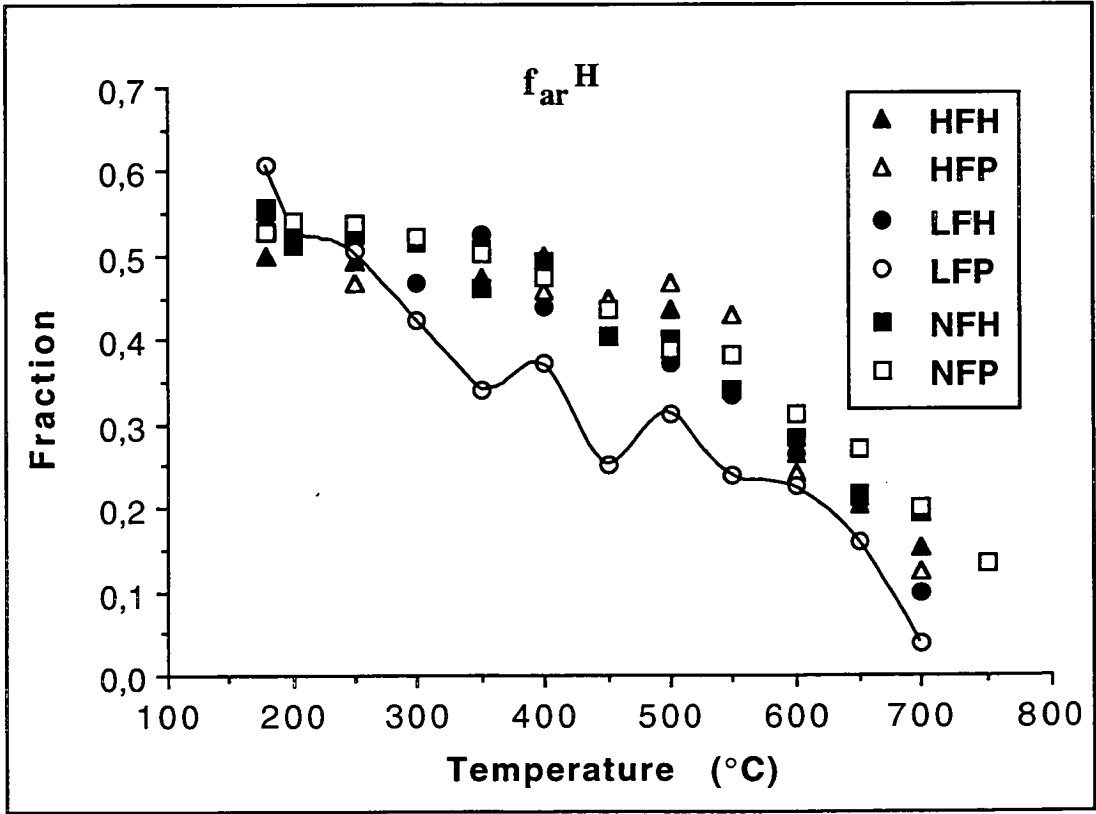


Figure 6.14 Fraction of protonated aromatic carbons, f_{ar}^H , for the six resins over the heat treatment temperature range.

In general, it can be shown from Figure 6.13 that the pyrolysis of all resins except LFP show f_{ar} values that remain relatively constant over the over the pyrolysis temperature up to 500°C. Above 500°C the f_{ar} values of HFH, HFP, LFH and LFP approach unity at 650°C, and those of NFH and NFP approach unity at 700°C. From these results it can be seen that all the resins achieve near complete aromatic ring condensation by approximately 700°C. NFH and NFP are seen to delay the complete condensation of the ring structure to 700°C, 50°C higher than the other four resins, due to their retention of aliphatic chains holding the aromatic ring clusters.

Theoretically, the f_{ar} value for a 1-dimensional phenolic chain, of either random or highly *ortho* orientation, is 0.857, and for a completely cross-linked phenolic polymeric structure is 0.8. From the f_{ar} results of the resin chars, it can be seen that HFH, NFH and NFP have structures that initially are of 1-dimensional polymerisation ($f_{ar} = 0.86 - 0.88$). NFP remains largely linearly polymerised to 550°C, after which rapid ring condensation occurs as previously suggested. Resins HFP and NFH are seen to increase in cross-linking of the polymeric structures to 400°C at a f_{ar} value of 0.82, after which the bridges are broken to facilitate ring condensation. The f_{ar} values of LFH show a structural change from a highly linear, short-chained polymeric structure ($f_{ar} = 0.93$) at 180°C, to a longer chained linear structure which undergoes only limited cross-linking ($f_{ar} = 0.86$) at 400°C, until ring condensation begins at 550°C. HFP is seen to be cross-linked initially ($f_{ar} = 0.81$), and then to have its structure linearised up to 300°C ($f_{ar} = 0.91$), followed by further cross-linking at 400°C to the same extent as HFP and NFH and finally the commencement of ring condensation at 550°C.

Resin LFP demonstrated quite different pyrolysis behaviour according to its aromaticity. The f_{ar} value of the unpyrolysed LFP shows reasonable cross-linking ($f_{ar} = 0.81$), which is followed by moderate linearisation of the polymeric structure up to 300°C, and then very extensive cross-linking throughout the polymer lattice

in the range 350-450°C ($f_{ar} \approx 0.77$). This is followed by a rapid ring condensation mode at 500°C ($f_{ar} = 0.92$), and then a slower ring condensation mode which parallels HFH, HFP and LFH from 600°C to 700°C.

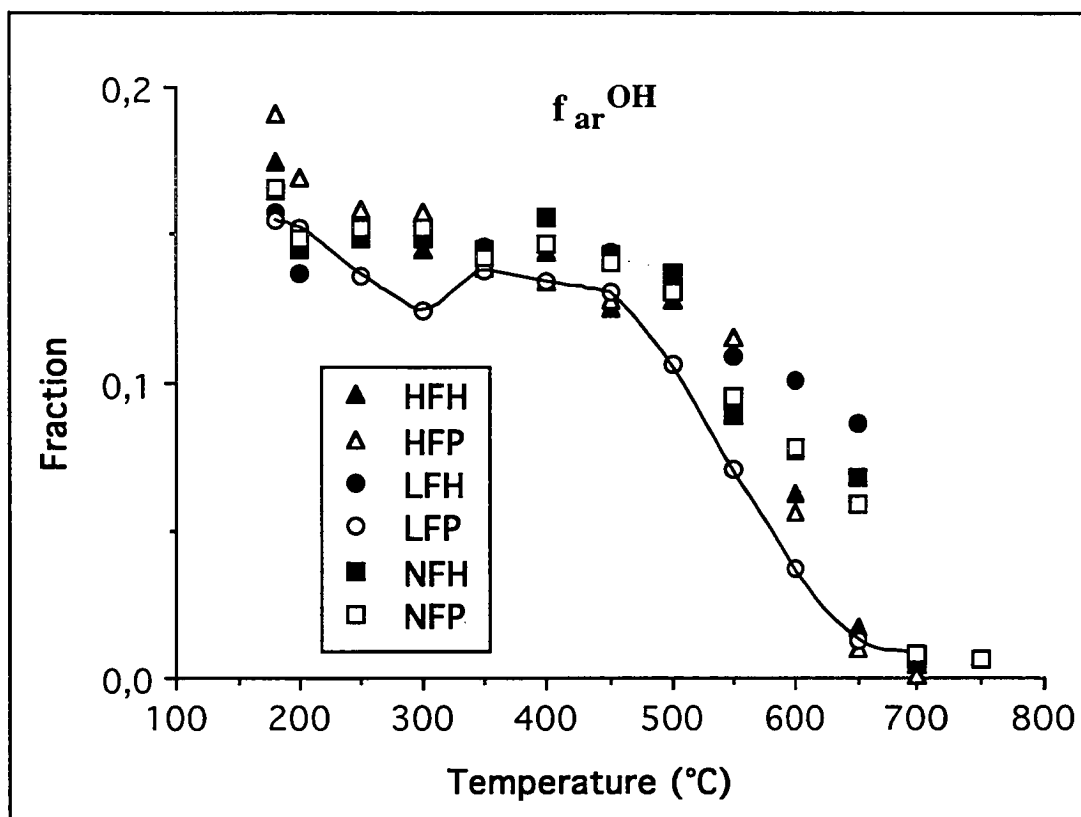


Figure 6.15 Fraction of hydroxyl aromatic carbons, f_{ar}^{OH} , for the six resins over the heat treatment temperature.

The fraction of protonated aromatic carbons, f_{ar}^H , is shown in Figure 6.14. As this parameter is more reliable for initial cross-linking than f_{ar} , it is considered from the theoretical values of f_{ar}^H ($f_{ar}^H = 0.428$ and 0.267 for a linear and cross-linked novolac resin respectively) that all the resins in the unpyrolysed form are seen to be largely linear to the same degree. The high f_{ar}^H values for the unpyrolysed resins ($f_{ar}^H \approx 0.55$) suggest that the resins as polymers are initially short chained and therefore contain a high proportion of un-bridged end groups. It is possible that in the case of the unpyrolysed LFP, the furan rings provide a large source of unsubstituted ring carbons, adding to its f_{ar}^H value, but also the paraformaldehyde contributes to the amount of aliphatic carbons available for later cross-linking at

higher temperatures. As the pyrolysis temperature increases, all the resins except LFP appear to exhibit a constantly low degree of substitution at the ring carbon sites to 400°C, at which temperature the f_{ar}^H fraction decreases, displaying continued cross-linking of the polymer chains, which is followed by the eventual formation of extensive aromatic C-C bonding due to ring condensation at 700°C. Again, NFH and NFP show the least degree of substitution at 700°C. LFP is seen to follow this pattern of aromatic substitution during pyrolysis, although to a much greater extent than the other resins, as can be seen from the curve in Figure 6.14. This suggests, again, that LFP is cross-linked to a greater degree than the other resins at lower temperatures due to the loss of the unsubstituted aromatic sites.

The fraction of hydroxyl aromatic carbons, f_{ar}^{OH} , is shown in Figure 6.15. Although this nmr resonance band lies in a region which contains other oxygenated aromatic carbon species (169-145 ppm), the curves in Figure 6.15 are assumed to be representative of hydroxyl carbons only because of the specific position of the 150 ppm peak in all the resin chars, and because it has been suggested in coal ^{13}C -nmr studies [Supaluknari,1989] that aromatic oxygen bonds are negligible in coals of such high aromaticity. Resin HFP is shown to display the highest level of f_{ar}^{OH} between 180 and 400°C, and as this resin contains a large proportion of furfuryl-alcohol initially, but releases very little of this free furfuryl-alcohol during pyrolysis, it is possible that the furfuryl hydroxyl groups attach themselves to the phenolic benzene rings upon their removal from the furfuryl group, and it is also likely that this process is aided by the presence of paraformaldehyde. The high amount of aromatic hydroxyl groups for the unpyrolysed HFH ($f_{ar}^{OH} = 0.175$ at 180°C) is also due to the greater proportion of furfuryl-alcohol present in these resin formulations, but the hydroxyl groups are seen to be quickly removed due to the absence of paraformaldehyde. The trend of the reduction of the f_{ar}^{OH} with increasing temperature closely follows the evolution of volatilised water from the polymers, and as the f_{ar}^{OH} values show that there is a sudden loss of aromatic hydroxyl groups from the unpyrolysed resins to

200°C, this trend is seen to provide further evidence of the formation of aromatic ether linkages from adjacent phenolic hydroxyl groups as suggested by Ouchi [1966] and Morterra and Low [1985a].in their FTIR studies.

The amount of aromatic hydroxyl groups is seen to remain relatively constant for all resins ($f_{ar}^{OH} = 0.13 - 0.16$) up to 500°C. Above 500°C ring condensation in association with rapid hydroxyl removal increases in LFP. The removal of hydroxyl groups from LFP at these high temperatures occurs to a greater extent than that from the other resins, and the lower f_{ar}^{OH} values agree with the greater cross-linking hypothesis for this resin at higher temperatures. It is likely that in LFP, the hydroxyl groups of the phenolic rings and the alcohols attached to the furan ring are replaced by aliphatic chains from the broken ether linkages of paraformaldehyde. This would lead to higher water evolution, although it can be seen from Figure 4.14 that there is little difference in water evolution for all the resins, given the level of accuracy of that particular experiment. Therefore, the f_{ar}^{OH} curves aren't considered to have an exact relationship with the trends for water evolution. It can be shown from Figure 4.15 that furfuryl-alcohol is not evolved from LFP so it can be inferred that the initial furfuryl-alcohol remains within the polymeric structure, possibly co-polymerising with the phenolic structure due to the replacement of the hydroxyl sites with aliphatic groups.

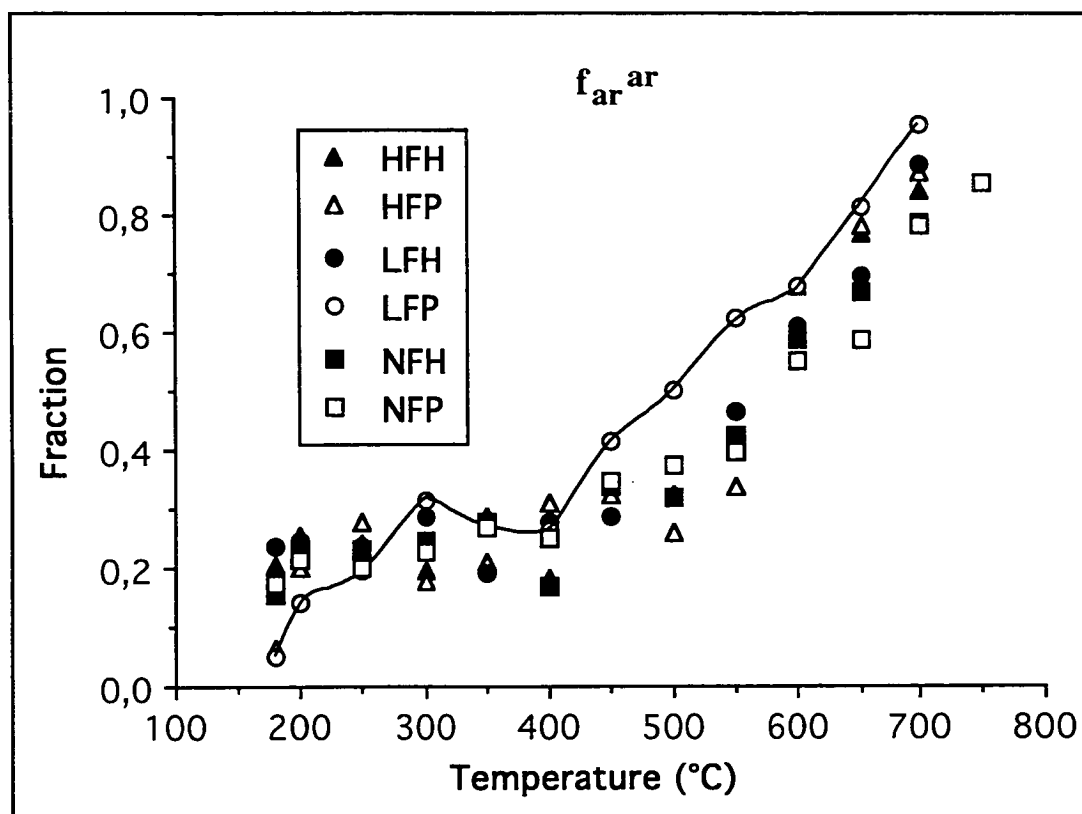


Figure 6.16 Fraction of bridgehead aromatic carbons, f_{ar}^{ar} , for the six resins over the heat treatment temperature range.

From Figure 6.16, the values of the fraction of bridgehead aromatic carbons, f_{ar}^{ar} , show a similar trend for the six resins. Theoretically, the f_{ar}^{ar} values for a linear and cross-linked novolac resin are 0.286 and 0.4 respectively, and therefore it can be seen that all the resins start to cross-link at 400-450°C, as the f_{ar}^{ar} values increase greatly with increased phenolic ring bridge formation. As HFP and LFP display low f_{ar}^{ar} values for their unpyrolysed forms ($f_{ar}^{ar} = 0.05$), it is possible that much of the reduced aromaticity of these resins is due to longer aliphatic chains between phenolic rings as produced by the paraformaldehyde, rather than by initial cross-linking. The f_{ar}^{ar} values for all of the resins remain constant between 200 and 400°C ($f_{ar}^{ar} \approx 0.2$). LFP is then seen to increase in bridgehead aromatic fraction to a greater extent than the other resins from 400 to 600°C which is indicative of increased cross-linking, and with the f_{ar} values, is indicative also of the breaking of longer aliphatic chains. Of the other resins, NFH and NFP show slightly lower bridgehead formation above 600°C, which is concurrent with their

retention of aliphatic groups to higher temperatures.

The fraction of aliphatic carbons over the heat treatment temperature range for the six resins are shown in Figure 6.17 and, as would be expected, are seen to be complementary to the fraction of aromatic carbon values. The importance of this parameter is in its use for calculating the specific fractions of the different *ortho-ortho'*, *ortho-para* and *para-para'* aliphatic carbon bridge orientations present in the phenolic chains. The theoretical values for these fractions are shown in Table 6.3 for various polymerisation modes of novolac resins.

It can be seen from Figure 6.18 that the fraction of *o-o'* aliphatic carbons, $f_{al^{oo}}$, is highest for HFP and LFP initially, and these values ($f_{al^{oo}} \approx 0.11$) suggest a relatively cross-linked structure with some randomly oriented linear polymerisation present. The lower $f_{al^{oo}}$ values of the other resins ($f_{al^{oo}} = 0.04 - 0.07$) suggest a mainly random orientation of the resins, particularly LFH. Resin LFP is seen to decrease in all aliphatic fractions to 300°C, with a very significant increase in $f_{al^{oo}}$ to 400°C. As this is paralleled by an increase in the fraction of *p-p'* bridges (Figure 6.19) it is confirmed that LFP shows an increase in cross-linked structure between 300 and 400°C. This is also confirmed by the very low proportion of *o-p* bridge formation for this resin over the 180 - 700°C pyrolysis temperature range (Figure 6.20).

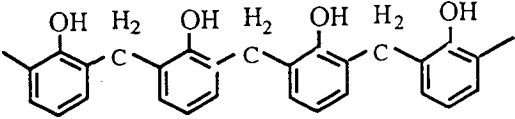
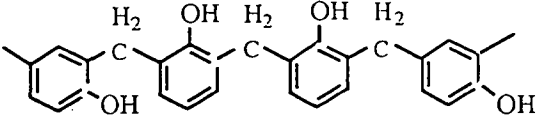
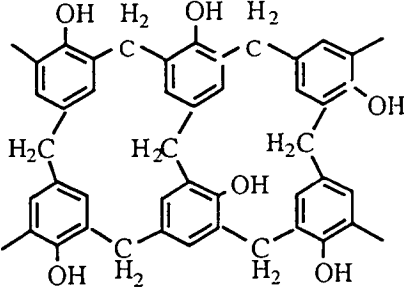
	<i>o-p</i>	<i>p-p'</i>	<i>o-o'</i>
 <p>Highly Ortho</p>	0.000	0.000	0.143
 <p>Random Linear</p>	0.041	0.061	0.041
 <p>Cross-Linked</p>	0.093	0.023	0.047

Table 6.3 Theoretical fractions of *ortho-para* (f_{al}^{op}), *para-para'* (f_{al}^{pp}), and *ortho-ortho'* (f_{al}^{oo}) aliphatic bridge carbons for the three major polymerisation modes of a novolac phenolic resin.

Resin LFH displays a similar pattern of increased f_{al}^{oo} to LFP, but also remains low in f_{al}^{pp} and f_{al}^{op} values, which suggests that LFH increases in *o-o'* linearity, but sustains limited cross-linking in comparison to the other resins. NFH and NFP show the lowest degree of *o-o'* linearisation and the highest degree of *o-p* bridge formation which suggests that these resins sustain the least cross-linked and most randomly oriented polymeric structure of the resins over the pyrolysis temperature range.

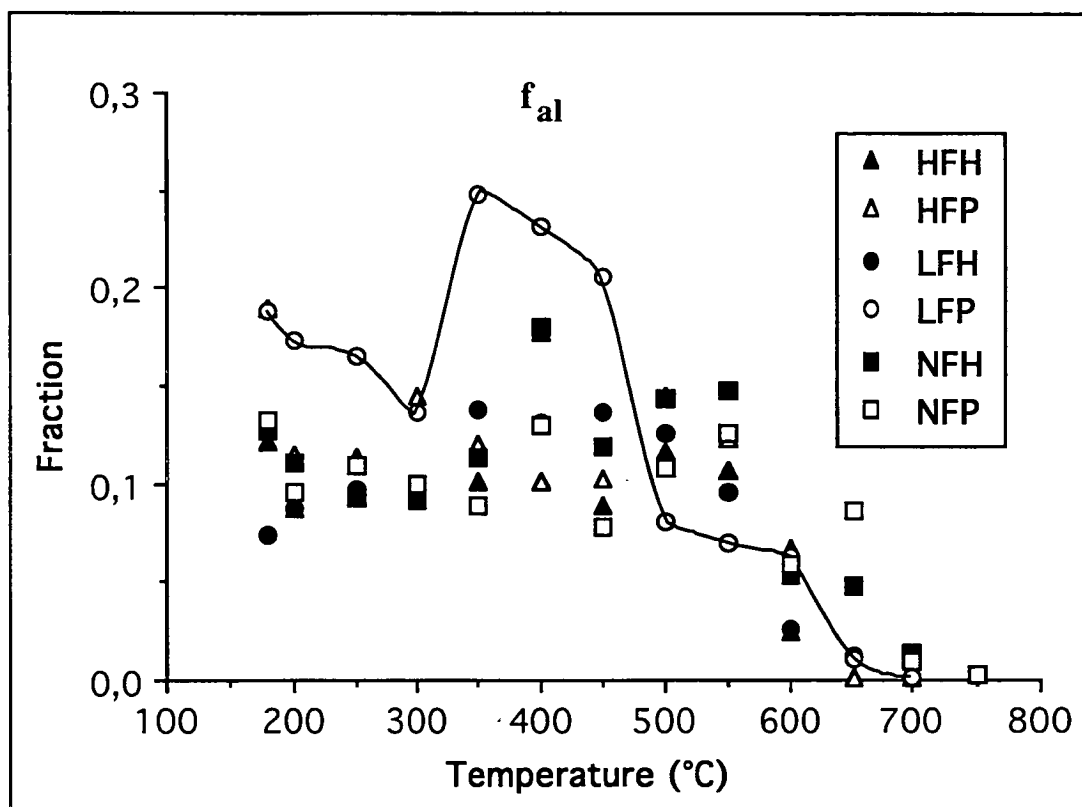


Figure 6.17 Fraction of aliphatic carbons, f_{al} , for the six resins over the heat treatment temperature range.

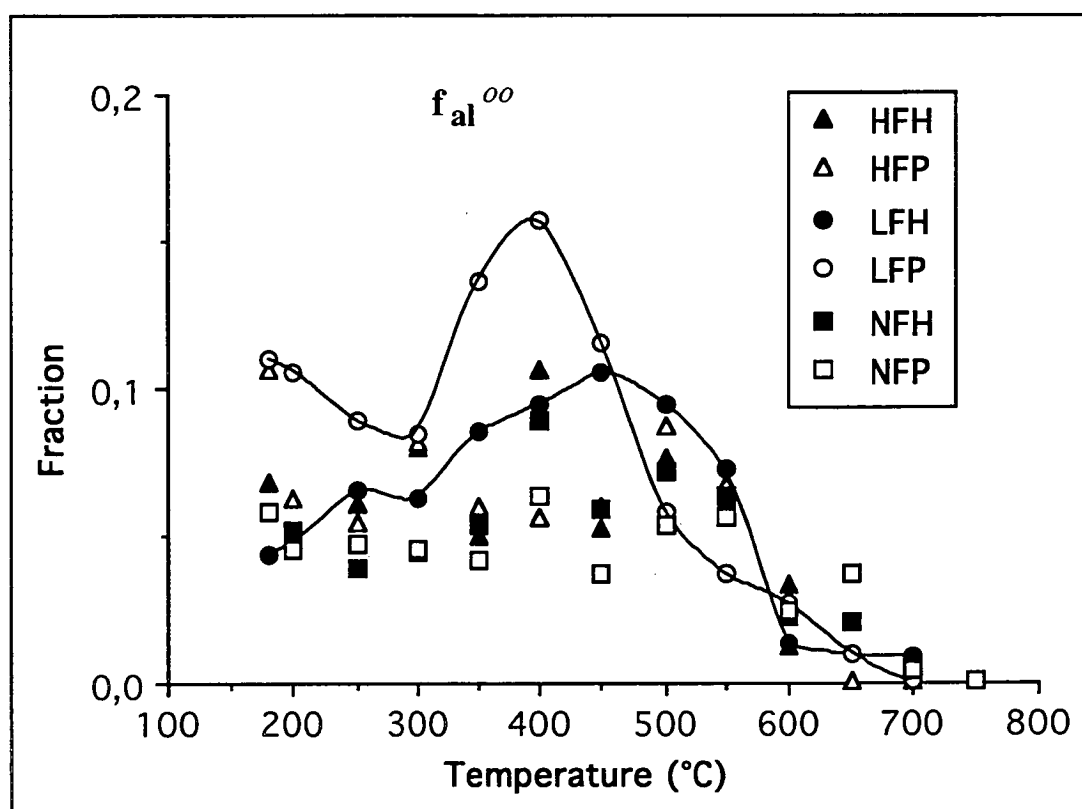


Figure 6.18 Fraction of *o-o'* bridge carbons, f_{al}^{oo} , for the six resins over the heat treatment temperature range.

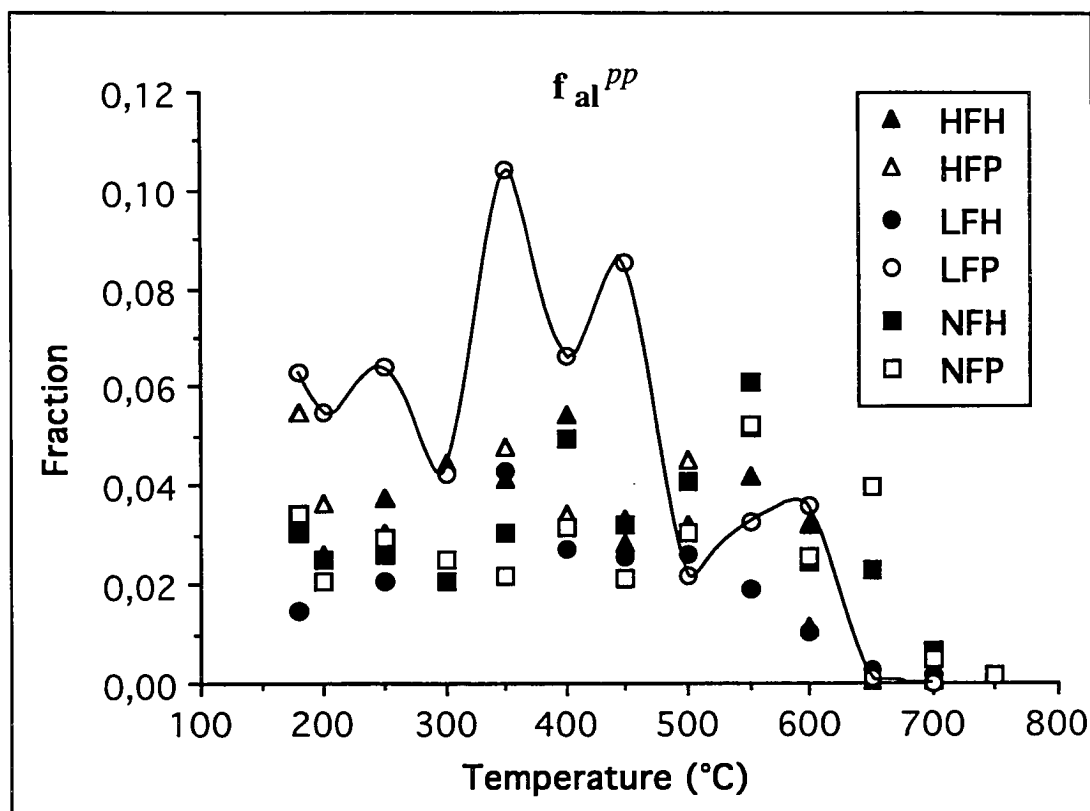


Figure 6.19 Fraction of $p-p'$ bridge carbons, f_{al}^{pp} , for the six resins over the heat treatment temperature range.

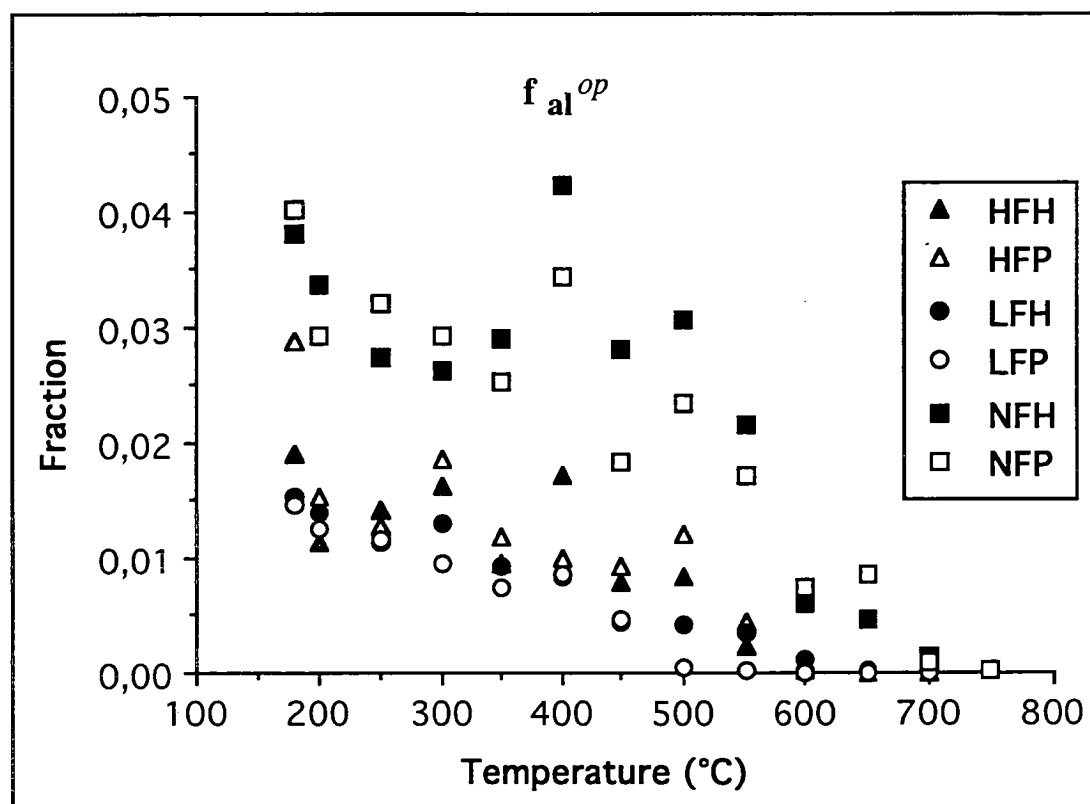


Figure 6.20 Fraction of $o-p'$ bridge carbons, f_{al}^{op} , for the six resins over the heat treatment temperature range.

Evaluation of Aromatic Ring Condensation:

The ratio of quaternary to tertiary aromatic carbons, $f_{q/t}$, is a parameter which is used to provide greater structural information about the change in cross-linking and condensation of the phenolic rings. The number $f_{q/t}$ is defined as the ratio of non-protonated to protonated carbons and can be calculated from the other parameters as follows;

$$f_{q/t} = (f_{ar}^{ar} + f_{ar}^{OH}) / f_{ar}^H \quad \text{.....(vii)}$$

As the nmr-measured parameter of aromatic fraction f_{ar} is quite high for all the chars, particularly those from the higher temperatures, $HTT > 500$, ($f_{ar} > 0.85$), an assumption was made that all of the carbon atoms of the pyrolysed resins, which can be characterised as high rank coals, were either tertiary or quaternary carbons ($f_{ar} = 1.0$) [Amram and Laval, 1989].

The $f_{q/t}$ values for all the resins are shown in Figure 6.21. From the graph the values for $f_{q/t}$ are seen to rise slowly from approximately 0.5 for the unpyrolysed form to approximately 1.5 for the 500°C char. Above 500°C the $f_{q/t}$ values are seen to increase markedly with temperature as a result of polymeric cross-linking and ring condensation. This can be seen from the relatively low values for NFH and NFP at 700°C ($f_{q/t} = 4$), to a higher value for LFH ($f_{q/t} = 9$), and a very high value for LFP ($f_{q/t} = 25$). The $f_{q/t}$ values for LFP are also seen to be slightly higher for all chars above 400°C.

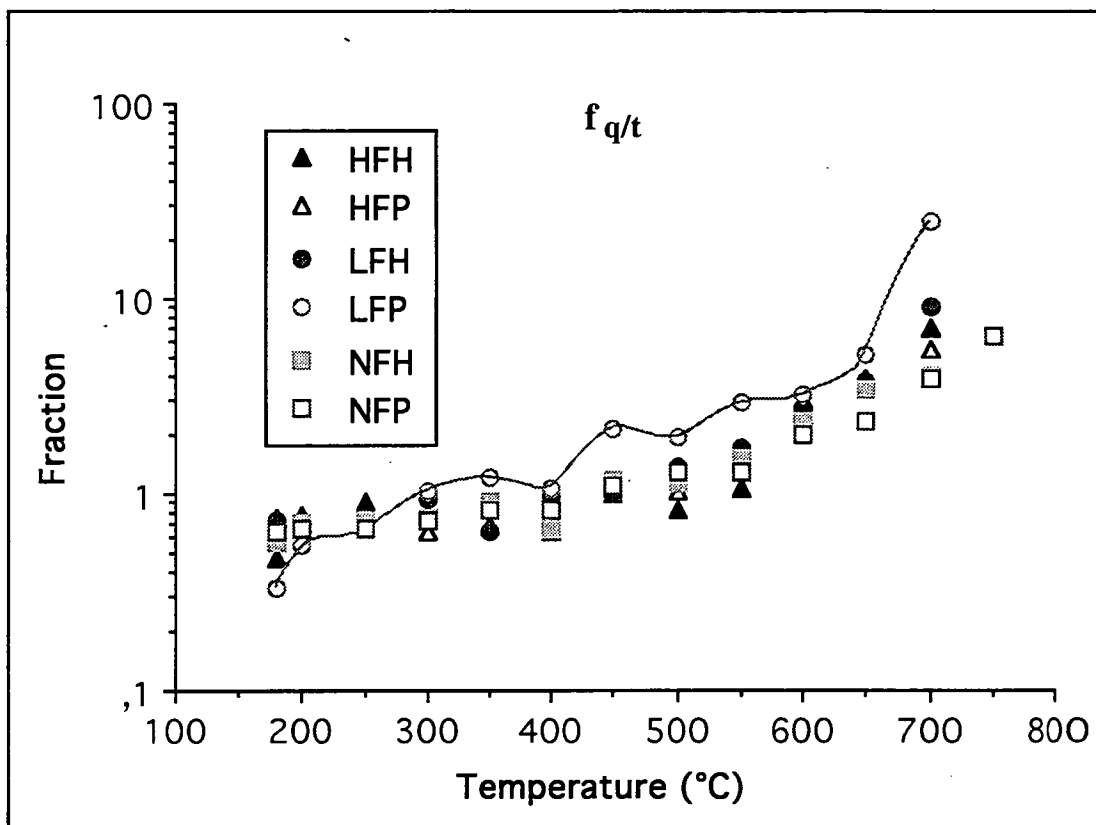


Figure 6.21 Fraction of quaternary to tertiary aromatic carbons, $f_{q/t}$, for the six resins over heat treatment temperature.

A two parameter model of pericondensed 2-dimensional sheets of aromatic rings was proposed to study the structure of anthracite coals [DuBois-Murphy *et al.*, 1982]. From this model, which requires the parameter $f_{q/t}$ calculated from the dipolar-dephasing CP/MAS ^{13}C -nmr experiment, and D , the average cluster diameter estimated from X-ray and electron microscopy data, the number of benzene rings in an aromatic cluster, and the size of the cluster, could be determined [Hirsch, 1954]. A one-parameter model to be used in this study assumes a 2-dimensional cluster growing isotropically during pyrolysis [Amram and Laval, 1989]. From this model, which is shown in Figure 6.22, an ordered ring structure is characterised only by its 2-dimensional growth, and therefore the stacking of the layers cannot be estimated by this method. According to this model, the aromatic ring cluster is characterised by only one parameter, n , the number of concentric clusters of benzene rings in the expanding lattice. For example the system depicted in Figure 6.22 has $n = 3$.

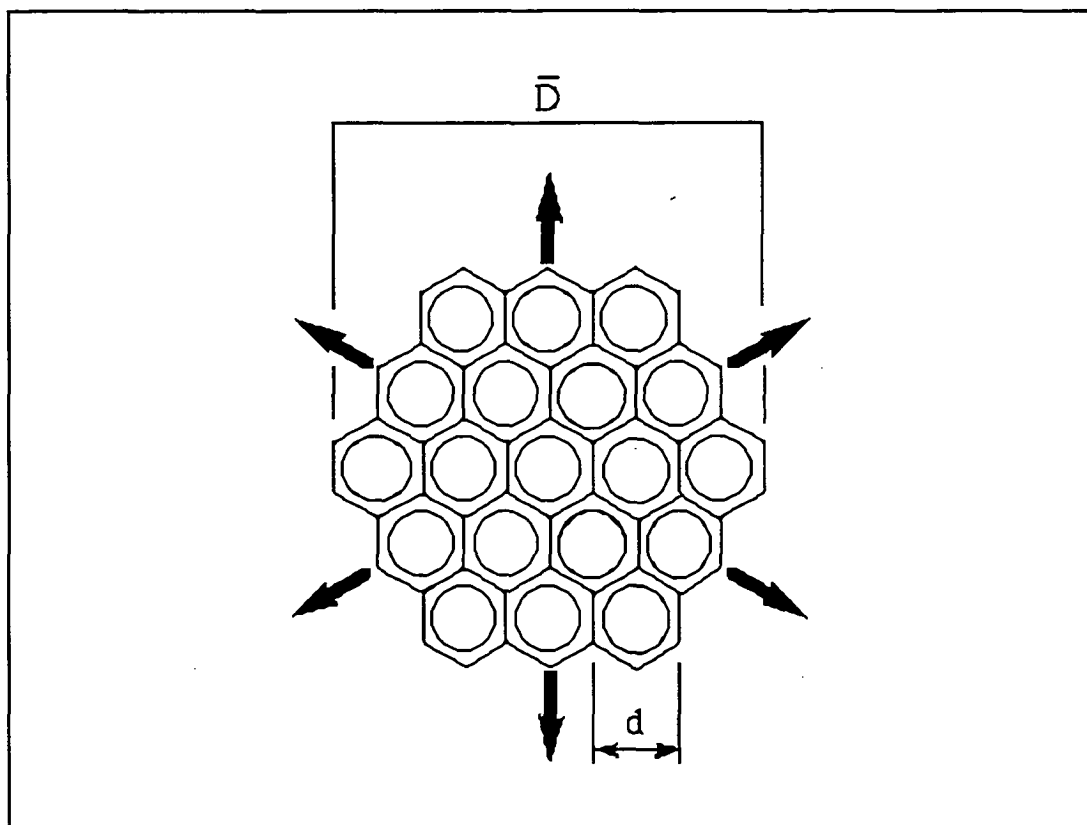


Figure 6.22 One parameter model for aromatic ring condensation [Amram and Laval, 1989]. \bar{D} represents the average diameter of the cluster; d is the pseudodiameter of a single ring.

The average diameter, D , and the number, r , of condensed rings can be written as functions of n :

$$D = (2n-1) \cdot d \quad \text{.....(viii)}$$

where d is the distance between two parallel bonds in a single ring (2.42 Å, when the carbon-carbon bond distance and the angle CCC are assumed to be 1.40 Å and 120° respectively). The number of condensed rings, r is calculated by;

$$r = 1 + 3n \cdot (n-1) \quad \text{.....(ix)}$$

The ratio of quaternary to tertiary aromatic carbons can now be written as a function of n ;

$$f_{q/t} = n-1. \quad \text{.....(x)}$$

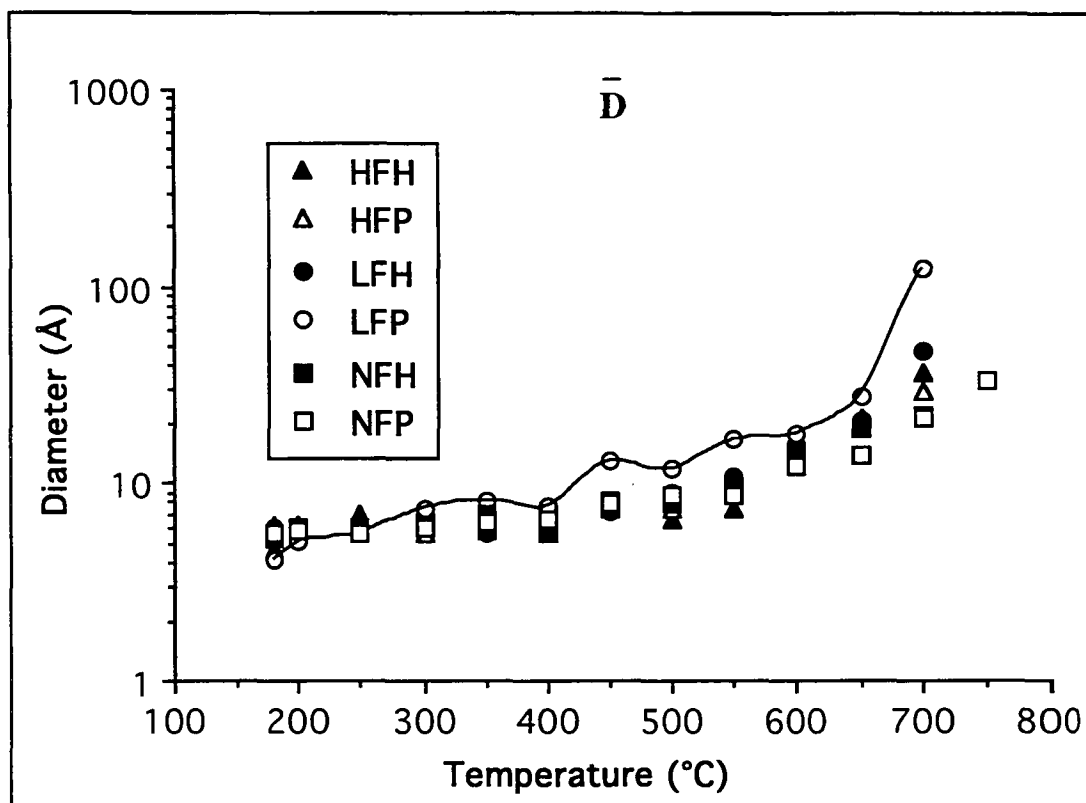


Figure 6.23 Aromatic ring cluster diameter, \bar{D} , of the resin chars over the heat treatment temperature range.

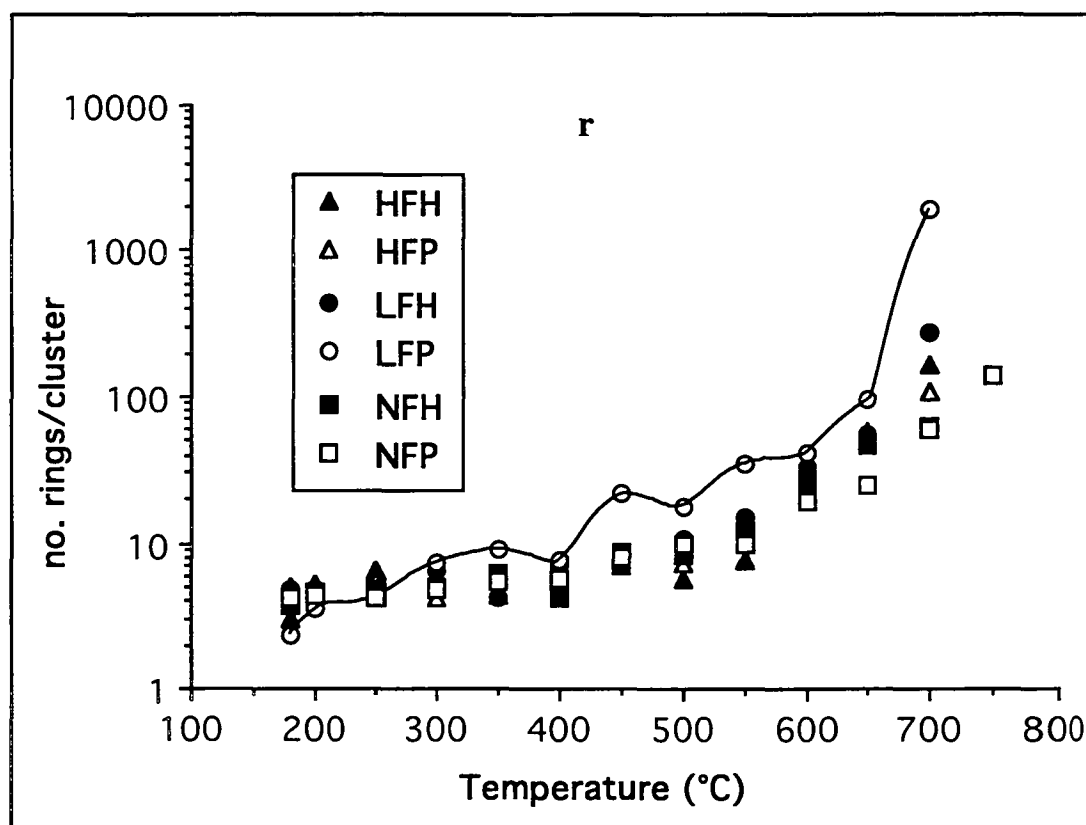


Figure 6.24 The number of aromatic rings per cluster, r , of the six resin chars over the heat treatment temperature range.

From these equations, the cluster diameter and average number of rings per cluster can be written as functions of $f_{q/t}$, as follows;

$$D = (2f_{q/t} + 1) \cdot d \quad \text{.....(xi)}$$

$$r = 1 + 3f_{q/t} \cdot [f_{q/t} + 1]. \quad \text{.....(xii)}$$

Therefore the determination of $f_{q/t}$ can directly provide the characteristics of the average aromatic carbon cluster. As the initial unpyrolysed resins are considered to be either linear or cross-linked polymers, or combinations thereof, the isotropic graphitisation / ring cluster growth model is seen as obscure, and therefore the results for these condensation parameters can only be considered as relevant for the chars when they are seen to change significantly at a particular temperature.

The change in ring cluster diameter, D , with pyrolysis temperature is shown in Figure 6.23. It can be seen that the trends within these curves very closely parallel the trends of $f_{q/t}$ for each of the resins, which would be expected considering the directly proportional nature of D with $f_{q/t}$. From the curves it is shown that the aromatic clusters for each resin do not increase significantly from 5 Å between 180 and 550°C, although above this temperature the size increases rapidly with condensation. This condensation model leads to aromatic cluster diameters at 700°C ranging from approximately 20 Å for NFH and NFP, to progressively larger clusters for the resins in the increasing order of NFH = NFP < HFP < HFH < LFH, and finally LFP with an aromatic ring cluster diameter of approximately 125 Å.

With these results, the number of aromatic rings per cluster, r , is shown for each resin as a function of pyrolysis temperature in Figure 6.24. As r is dependent on the $(f_{q/t})^2$, it is seen to vary more significantly with each resin, than with the parameter D . As is shown from the graph (Figure 6.23) there are approximately 2 - 6 aromatic rings per cluster for the unpyrolysed resins, and this figure is seen to

remain relatively constant up to 400°C, above which the r value increases substantially with temperature for each resin. Resin LFP particularly experiences a high degree of ring condensation above 400°C, which is shown by its r value to increase to approximately 2000; one order of magnitude greater than the next most condensed resin char, LFH, with an r value of approximately 250 rings per cluster.

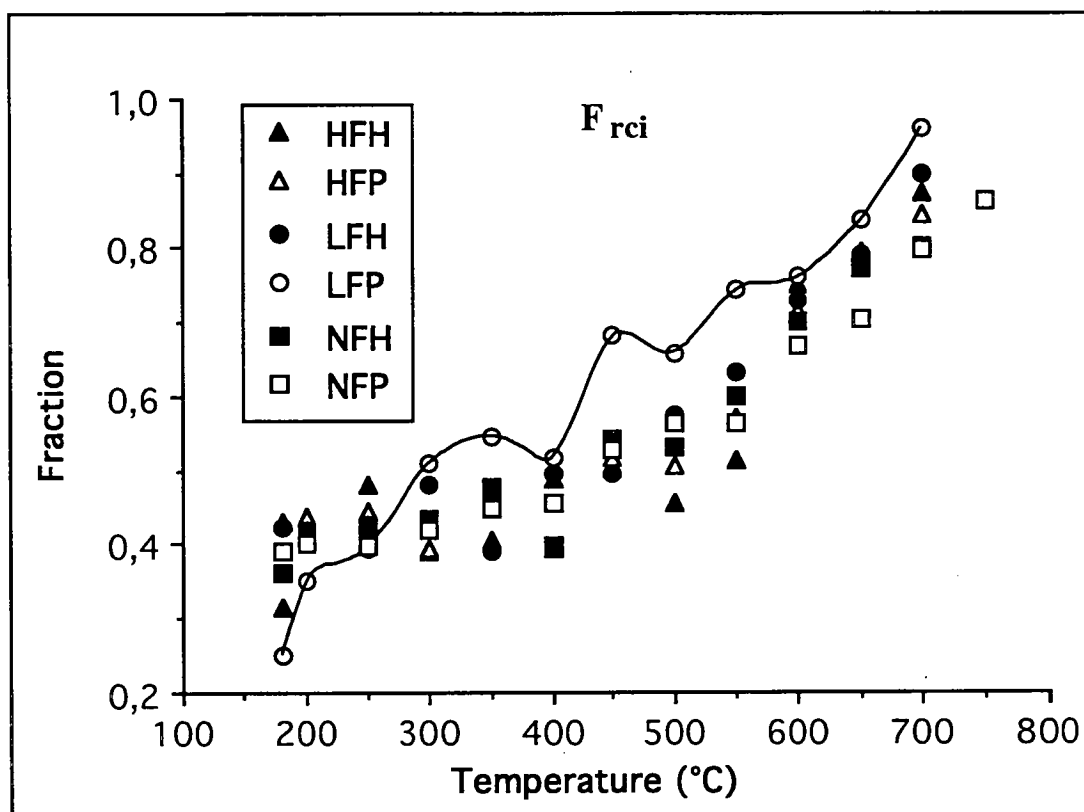


Figure 6.25 Ring condensation index [Van Krevelen,1961], F_{rci} , of the six resin chars over the heat treatment temperature range.

A final parameter which can be used to describe the chemically graphitic character of the chars is the ring-condensation index, F_{rci} , as described by Van Krevelen [1961]. This index, which by definition has a value of zero for benzene and unity for graphite, was calculated as follows;

$$F_{rci} = f_{q/t} / [1 + f_{q/t}] \quad \text{.....(xiii)}$$

This index for the resin chars of this study, as seen in Figure 6.25, shows that LFP shows the lowest value for its unpyrolysed form ($F_{rci} = 0.25$), but that the index is seen to increase almost linearly with temperature to approximately 0.98 at 700°C. The other resins show little change in their respective values of this index up to 400°C ($F_{rci} = 0.4$) and then their values increase approximately linearly with pyrolysis temperature up to 700°C.

It has been reported [DuBois-Murphy *et al*,1982] that the quaternary to tertiary ratio of a high ranked coal, as measured by the dipolar dephasing ^{13}C nmr experiment, experiences a major source of error from the DD spectrum when extrapolating from $t_d = 60\ \mu\text{s}$ to its apparent value at $t_d = 0\ \mu\text{s}$, and this error was estimated at 20%. As the parameters for the size and degree of condensation of the aromatic clusters, D and r respectively, are very sensitive to f_q/t it is expected that their values would be considerably varied.

In comparison with other data, X-ray scattering experiments [Hirsch,1954] showed that the average diameter of a sheet of condensed rings in an anthracite (high rank) coal (95 wt% C, 3 wt% H) is approximately 16 Å. A high resolution electron microscopy study of anthracites [Oberlin and Terriere,1975] concluded that the average cluster diameter is less than 10 Å, i.e. an area less than ten aromatic rings. It was also observed from infrared and X-ray methods [Amram and Laval,1989] that high rank coals may contain 10-20 fused rings. These results correlate to a char that has been heat treated to a pyrolysis temperature of 600°C for the resins of this study, which therefore corresponds to a carbon content of 85-90 wt%. This suggests that the resin chars heat treated at temperatures up to 600°C are suitable models for high rank coals, although pyrolysis above this temperature causes extensive condensation of the polymeric ring system in a novolac resin. The degree of condensation is likely to be dependent on the cross-linking and aromaticity of the original unpyrolysed resin, which in turn is dependent on the starting chemistry of the resin.

Chapter Seven

**The determination of crystallite
formation in the Phenolic Resin Chars
during pyrolysis (600 - 2200°C) by
Raman Spectroscopy.**

Raman Spectroscopy.

Raman vibrational modes in carbons:

The technique of Raman spectroscopy was used in this study to determine the alteration of the crystal microstructure of the phenolic resin chars over the heat treatment temperature range 600 - 2200°C. This technique relies on the ability of a chemical sample to reflect monochromatic radiation from a laser light source at a frequency shift of the incident monochromatic radiation, and to use this frequency shift as an indication of the molecular species present in the sample due to the particular vibrational modes of their molecular bonds. This method is particularly useful in detecting carbon-carbon vibrational modes. Therefore, the resin samples heat treated to temperatures below 600°C were incapable of analysis by this method due to the tendency of the organic functional groups present to thermally degrade and 'fluoresce', and therefore provide no useful Raman spectra.

The vibrational characteristics of carbon bond species in the Raman mode of spectroscopy allow for the identification of the distinct resonances from ordered and disordered regions of the material. Ordered graphitic layers show a resonance between 1580 and 1600 cm^{-1} , and the theoretical *graphitic* vibration is centred at 1580 cm^{-1} . Therefore, the more ordered (carbonised) the aromatic carbon lattice, the more the broad band at 1600 cm^{-1} is seen to narrow and shift to 1580 cm^{-1} . A second order Raman graphite vibration at 2700 cm^{-1} is seen only in very highly ordered graphites and therefore is not discussed in this study [Mernagh *et al*, 1984].

Two other vibration modes of interest, centred around 1350 and 1500 cm^{-1} respectively, are observed by the Raman spectra of the carbons in this study. As a

vibrational shift indicative of disorder in the carbon lattice the 1350 cm^{-1} band is attributed entirely to in-plane defects in the aromatic carbon structure, such as lattice distortions and vacancies [Edwards,1989; Rouzaud *et al*,1983]. This band was reported as being due to a vibration mode originating from the distorted hexagonal lattice near the crystal boundary, and can be observed for ordinary carbons containing various defective structures in the graphite layer planes [Tuinstra and Koenig,1970]. The 1500 cm^{-1} band is suggested as being due to hetero-atoms, such as residual hydrogen, between graphitic layers [Rouzaud *et al*,1983].

From the Factor Group Analysis of graphite [Bhagavantam and Venkatarayuda, 1939; Wychoff,1963] it is shown that the number of internal vibration modes belonging to each symmetry species, N_{int} , of the graphite unit cell is expressed as follows;

$$N_{\text{int}} = A_1 + B_1 + E_1 + E_2 \quad \dots\dots\dots(i)$$

From the C_{6v} character table it is shown that the A_1 and E_2 modes are Raman and infra-red active, and the B_1 mode is inactive in both effects [Bauman,1962]. From correlation with assignments made under space group D_{6h}^4 [Dresselhaus *et al*, 1977] the E_1 (Raman and infra-red active) and E_2 (Raman active only) modes under C_{6v}^4 symmetry are placed at 1588 and 1582 cm^{-1} respectively. Although it is not considered in this study, the totally symmetric A_1 mode is reported to exist at 48 cm^{-1} .

Raman analysis of carbonised phenolic resins:

In this study two series of Raman analyses were undertaken; one for the $3^\circ\text{C}/\text{min}$ heat treated resins, denoted as R3 chars, and another for the higher temperature

chars produced from the 1000°C carbon heated at 10°C/min, denoted as R10 chars. For the analysis of the 3°C/min resin chars, the carbonised products of the heat treatments to 600, 700, 800 and 900°C were analysed in addition to the 1000°C, 1600°C and 2200°C chars, for a more complete carbonisation model. Raman spectroscopy of the chars produced by the 10°C/min ramp rate were only conducted on the 1000°C, 1600°C and 2200°C chars as no chars were produced at a ramp rate of 10°C/min for pyrolysis temperatures of less than 1000°C.

The change in spectrum shape over the pyrolysis temperature range for the chars of the HFH resin is shown in Figure 7.1. From this figure the formation of the graphite E_{2g} ring band at or near 1580 cm^{-1} can be seen clearly. The final curve in Figure 7.1 is the spectrum of a typical highly oriented pyrolytic graphite which displays the narrow graphite E_{2g} peak at 1580 cm^{-1} , without any significant peaks corresponding to the ring and hetero-atom defect bands at 1350 or 1500 cm^{-1} .

For decomposition of the spectra, it was found that a three-band hypothesis [Beny-Bassez and Rouzaud,1985] gave the best fit, or lowest residual error between the composite fitted spectrum and the real spectrum, as opposed to a two band fitting model [Rouzaud *et al*,1983; Lespade and Marchand,1984; Cottinet *et al*,1988]. The bands chosen were the graphite band at 1580 cm^{-1} , and the defect bands at 1350 and 1500 cm^{-1} , which are shown in Figure 7.2. Additionally, another defect band at approximately 1600 cm^{-1} was capable of being fitted to the spectra of the 2200°C chars. This band is due to a similar defect vibration as that of 1350 cm^{-1} , i.e., associated with the non-planar zones of graphitic microstructural distortion, such as zones of curvature in the lattice [Mernagh *et al*,1984]. As this band was found only in the highest temperature chars, its existence wasn't considered important to this study, except as an additional defect band. Therefore only the 1350 , 1500 and 1570 cm^{-1} bands were studied. For every pyrolysis heat treatment temperature the peak full width at half maximum height (FWHM) was expressed as an index of the refinement of each particular vibration

mode in the lattice of the char of that heat treatment.

The other structural parameter of importance to the study of these chars is the ratio of the integral area of each of the 1350, 1500 and 1570 cm^{-1} band respectively to the sum of all the bands, i.e., the total area of the spectrum. These ratios were termed the "specific areas" of the respective bands, and are denoted as S_{1350} , S_{1500} and S_{1570} [Rouzaud *et al*,1983]. For each char sample three different spectra were taken from different sites on the sample surface. As the errors for the specific area values of each particular band were below 10% for each sample it was found that there was no particular spectral variation due to surface phenomena, and therefore, the pyrolysis temperature of the resins is considered to be the only parameter of significance for the changes in the three bands fitted from the Raman spectra.

In Figure 7.3, the change in specific area of the 1350 cm^{-1} band shows a relatively constant, but slightly increasing, degree of aromatic lattice distortions in the resin chars from 600 to 1000°C. This is likely as the pseudo-crystalline polymeric structure becomes distorted due to ring condensation. Following this, LFP shows the greatest reduction in lattice defect from 58% at 900°C to 43% at 1000°C, and then remaining relatively unchanged at approximately 45% to 2200°C. The other resins, except NHF, follow an equivalent pattern to that of LFP, with a sudden decrease from 900 to 1000°C, and with final values of between 38 and 45 %. For resin NFH, the S_{1350} values above 900°C are seen to decrease only a small amount to 1600°C, and then greatly decrease to 2200°C.

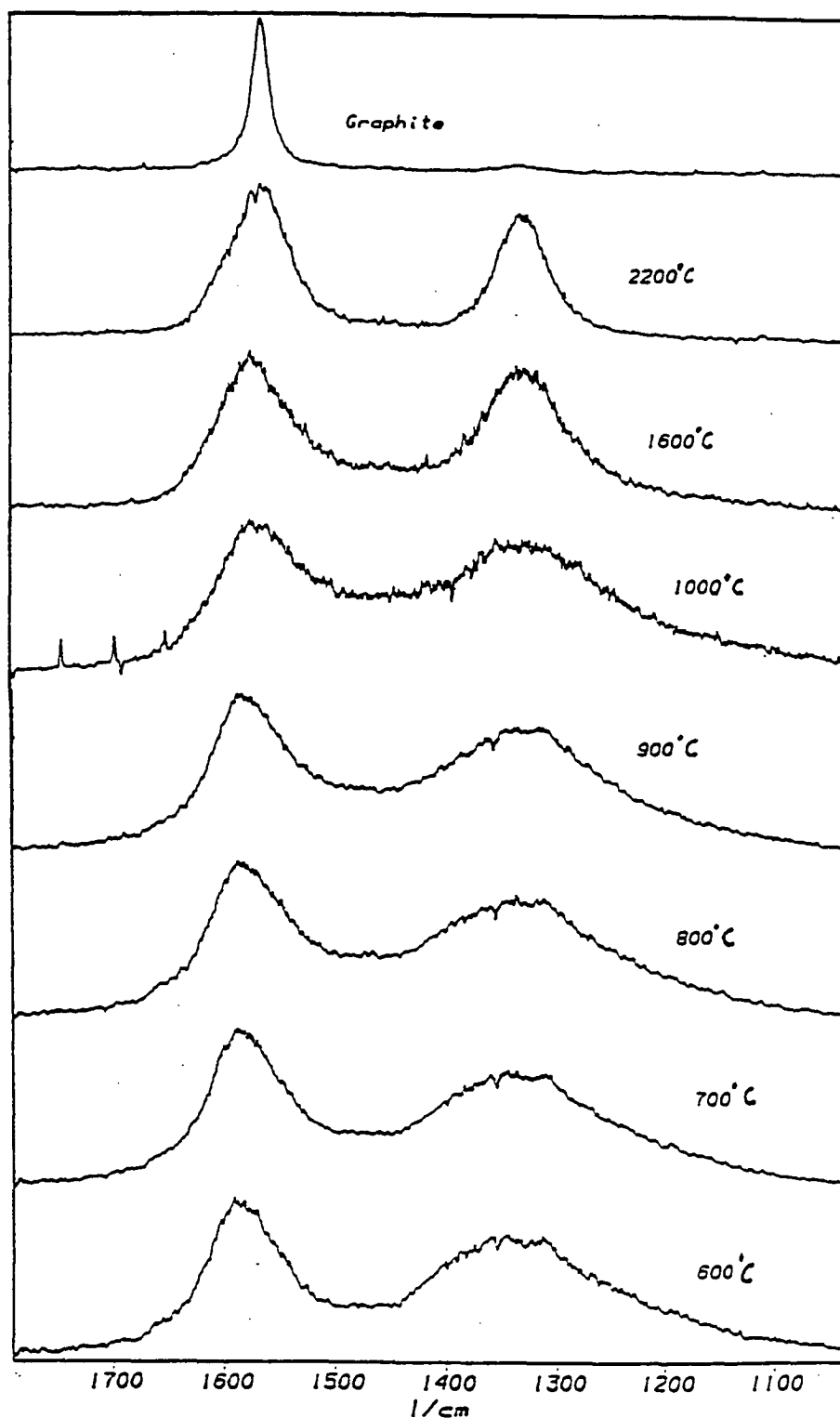
HFH

Figure 7.1 The evolution of Raman bands for resin HFH over the heat treatment temperature range. The numbers beside the spectra indicate the temperature to which the resin was heat treated.

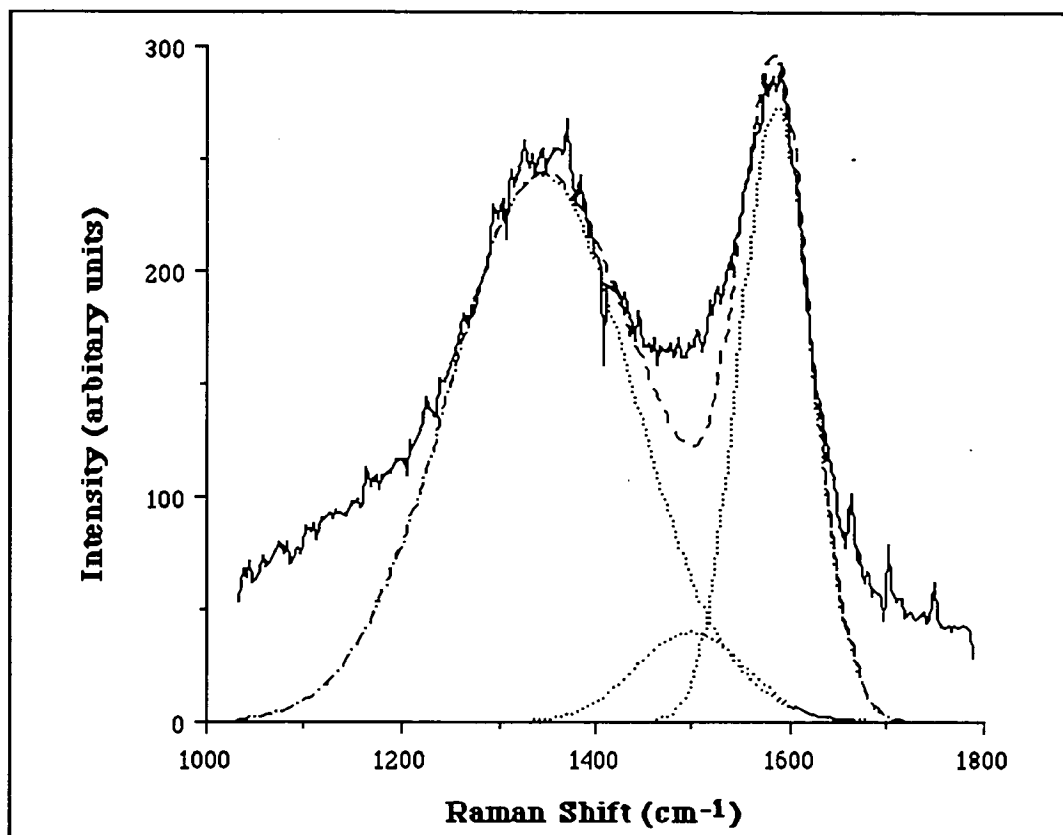


Figure 7.2 Deconvolution of the 1000°C char of resin HFH into bands at 1350, 1500 and 1570 cm⁻¹.

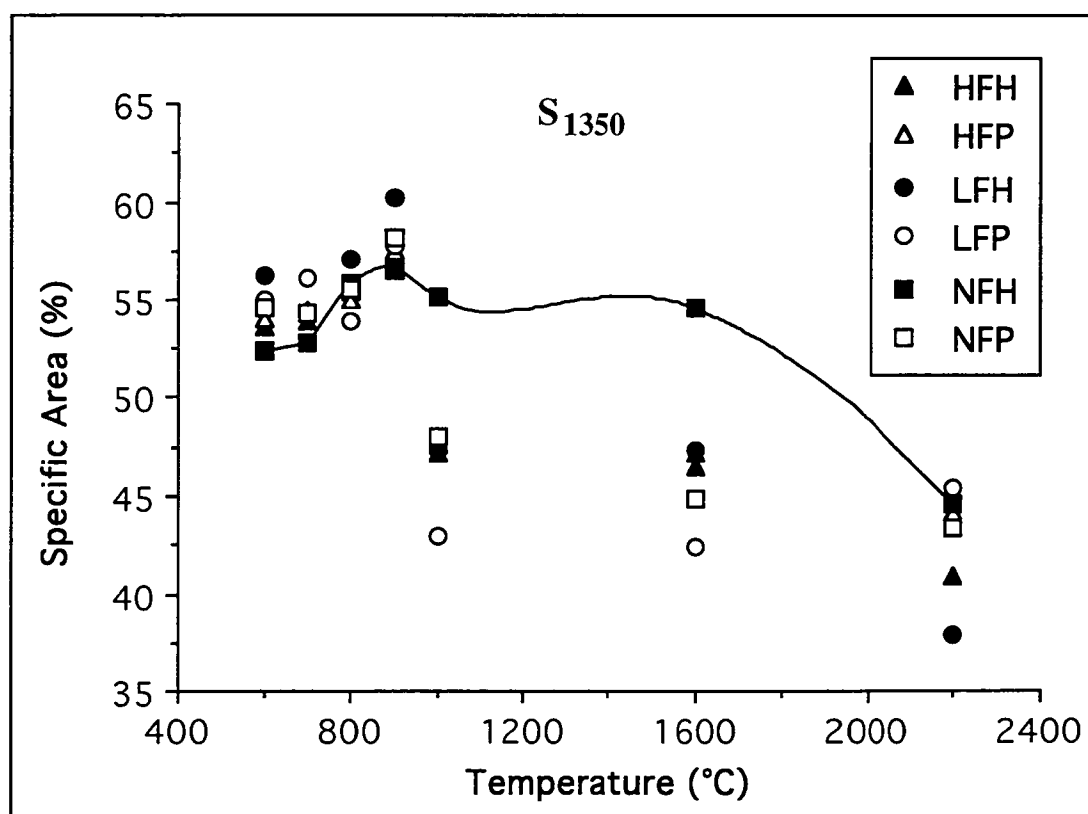


Figure 7.3 Evolution of the specific area of the 1350 cm⁻¹ band, S₁₃₅₀, for the six R3 resins over the heat treatment temperature range.

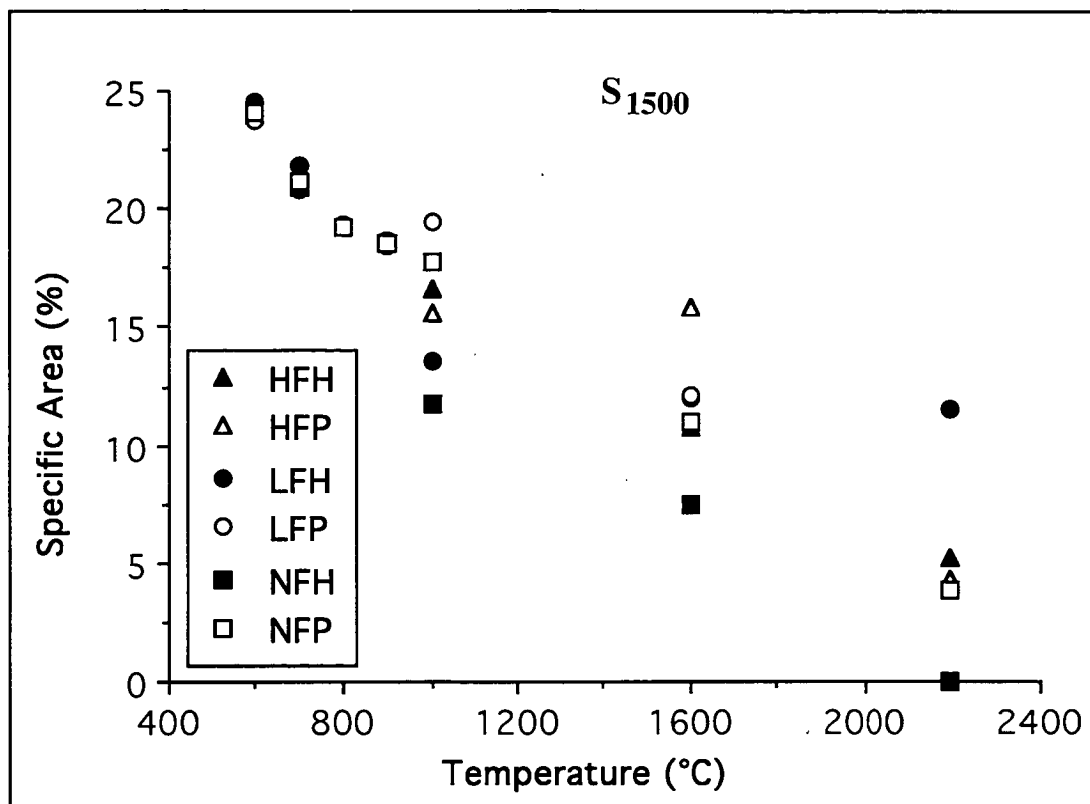


Figure 7.4 Evolution of the specific area of the 1500 cm^{-1} band, S_{1500} , for the six R3 resins over the heat treatment temperature range.

This suggests that the aromatic lattice of the LFP chars displays a greater tendency for an ordered orientation than the other resins above 900°C and up to 1600°C . Following this, it may be suggested that the higher degree of ring condensation of LFP to 900°C provides an aromatic lattice which avails itself to the removal of in-plane defects, such that the localised aromatic structural units, as shown by the ring condensation mechanism of the nmr data, are replaced above 900°C by stacks of semi-ordered layers with a large radius of curvature. Resin NFH displays the most distorted aromatic lattice above 900°C , which adds to the evidence of this resin providing the least degree of ring condensation. It is seen that the lack of suitably large aromatic clusters in NFH at the higher pyrolysis temperatures ($700 - 1000^{\circ}\text{C}$) causes a retention of lattice twisting, and other curvature distortions, which inhibit the growth of a suitably ordered lattice to 1600°C . Finally, it can be seen that the aromatic lattice structures for all the resins become similar in their degree of twisting and curved distortions at 2200°C ,

which suggests that lattice formation is similar for all the resins at this temperature.

The change in the specific area of the 1500 cm^{-1} band over the pyrolysis temperature range for the six resins is shown in Figure 7.4. The trend for the S_{1500} values is observed as a steady and equal decrease for all six resin chars from 24% at 600°C to 18% at 900°C . Above 900°C the values change for each resin to a range of 12 - 20 %, but with an equally decreasing trend for all the resins. Although NFH shows the least proportion of this mode of defect above 900°C , the close relationship of the curves of all the resins suggest that the defect mechanism is very similar for each resin, with no particular resin distinguishing itself.

The development of an ordered structure in these resin chars is best shown in the change in specific area of the 1570 cm^{-1} band (Figure 7.5). The formation of the ordered lattice is sharply increased from 900°C to 1000°C , and is then more gradually increased to 2200°C . Although the greatest degree of crystalline development is shown by LFP at 1600°C and NFH at 2200°C , the spread in results at each sample temperature suggest that the extent of crystallisation in the chars is equivalent for each resin above 900°C . Compared to the spectrum of the artificial graphite, which has an S_{1570} value of approximately 90%, the resin chars at 2200°C , with S_{1570} values of approximately 50%, are seen to have sufficient twisting and curvature to retain a defective lattice.

The variation in full width at half maximum heights for the 1350 , 1500 and 1570 cm^{-1} bands are designated as Γ_{1350} , Γ_{1500} and Γ_{1570} respectively. Figure 7.6 displays the Γ_{1350} values for the six resin chars over the pyrolysis temperature range. The range of values between 600 and 900°C suggests a variation in aromatic types, and a certain degree of sp^3 tetrahedral bonding between carbons, which gives a variety of distortion modes within the lattice. As the temperature is increased, the 1350 cm^{-1} band widths for all of the chars decrease and become

relatively equal, from approximately $\Gamma_{1350}=280\text{ cm}^{-1}$ at 900°C to $\Gamma_{1350}=80\text{ cm}^{-1}$ at 2200°C , with the greatest reduction between 900 and 1000°C . This suggests that the variation in carbon defect species is narrowed to represent the twisting, or curvature defects. This is particularly evident due to the sudden reduction in 1350 cm^{-1} band width corresponding to a temperature increase from 900 to 1000°C , which can be related to total ring condensation, and which negates the presence of any defects due to tetrahedral carbons or those involved in aliphatic bonding.

The Γ_{1500} values, as shown in Figure 7.7, are seen as scattered over the $600 - 2200^{\circ}\text{C}$ heat treatment temperature range, but with a trend to decrease between 1600 and 2200°C . The variation of the 1500 cm^{-1} band width suggests that there are different hetero-atoms present in the lattice at 600°C , which is confirmed by elemental analysis. As the Γ_{1500} values of all the resins remain relatively constant between 600 and 1600°C , it can be assumed that the proportion of hetero-atoms remains constant, i.e., there is little removal of any hetero-atoms between 600 and 1600°C . As the Γ_{1500} values are seen to decrease rapidly for heat treatments above 1600°C , it is likely that there is a sudden removal of hetero-atoms from the chars between 1600 and 2200°C .

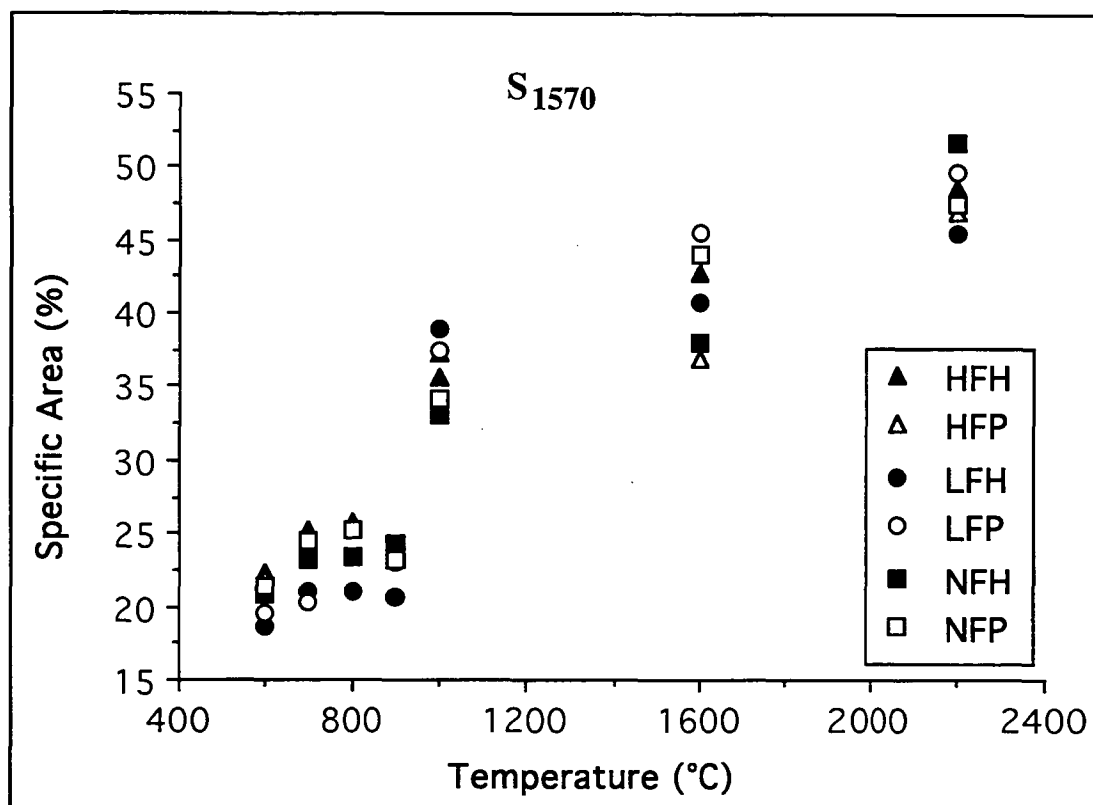


Figure 7.5 Evolution of the specific area of the 1570 cm^{-1} band, S_{1570} , for the six R3 resins over the heat treatment temperature range.

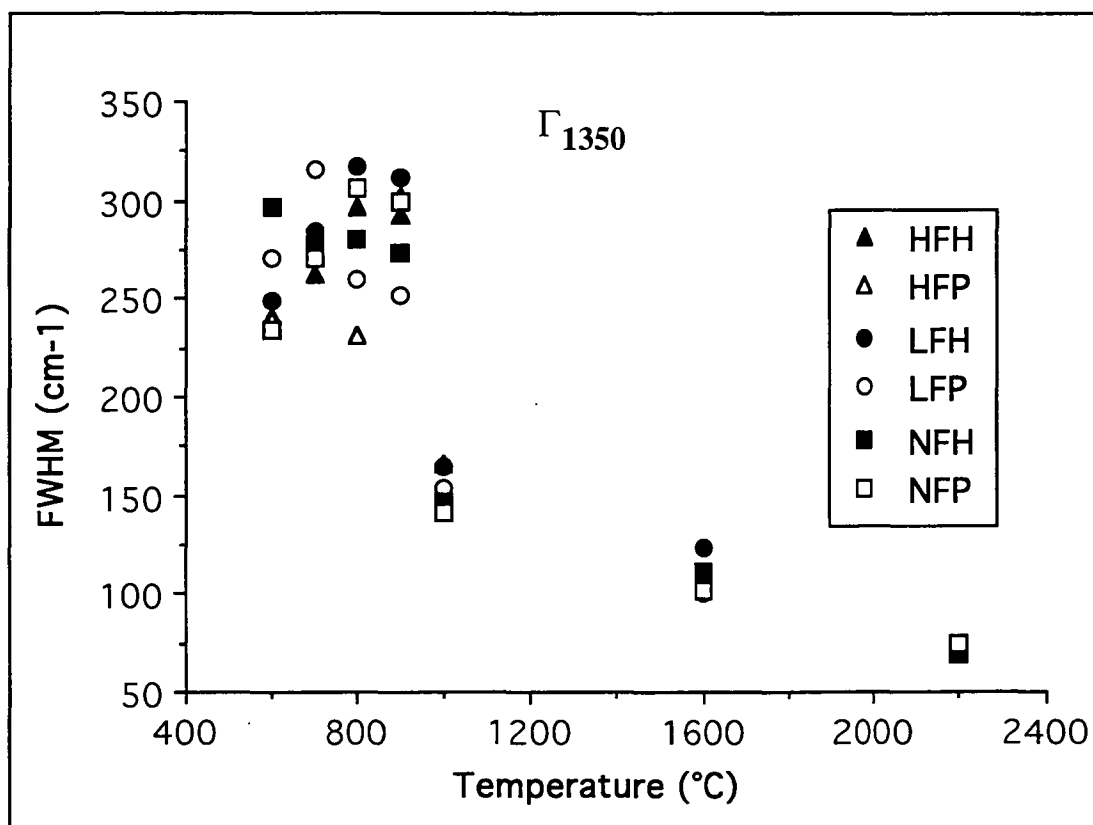


Figure 7.6 Evolution of the width of the 1350 cm^{-1} band, Γ_{1350} , for the six R3 resins over the heat treatment temperature range.

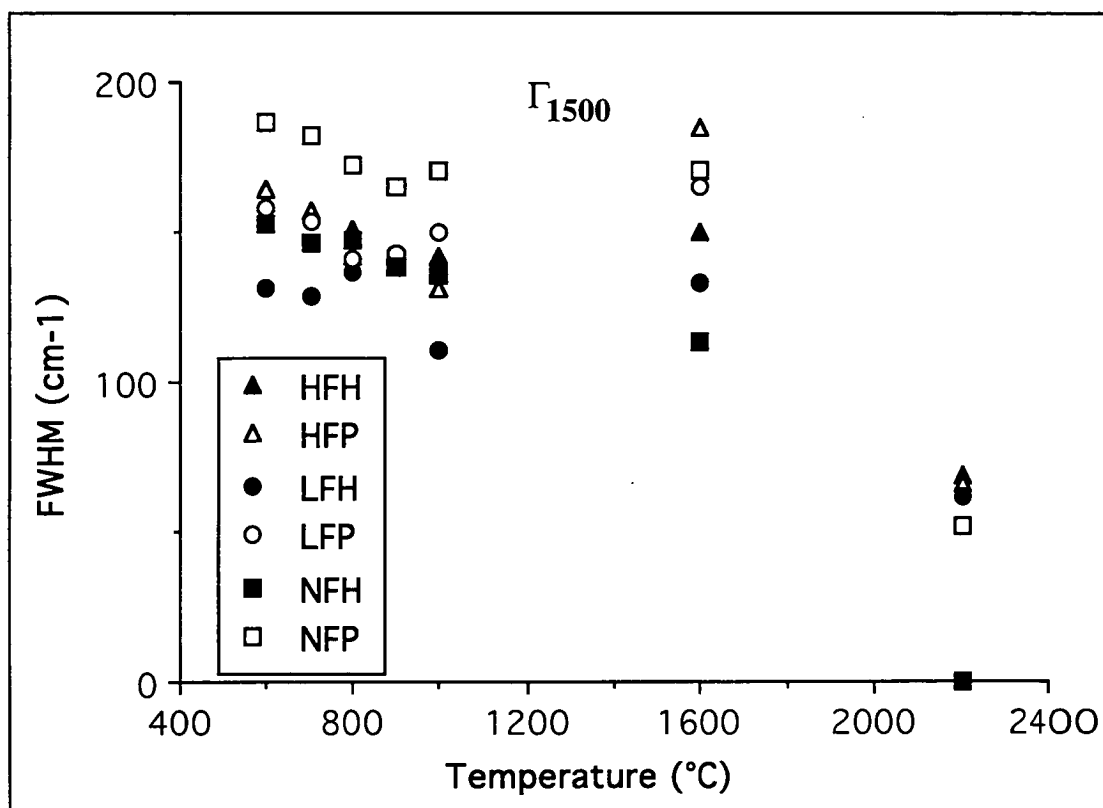


Figure 7.7 Evolution of the width of the 1500 cm^{-1} band, Γ_{1500} , for the six R3 resins over the heat treatment temperature range.

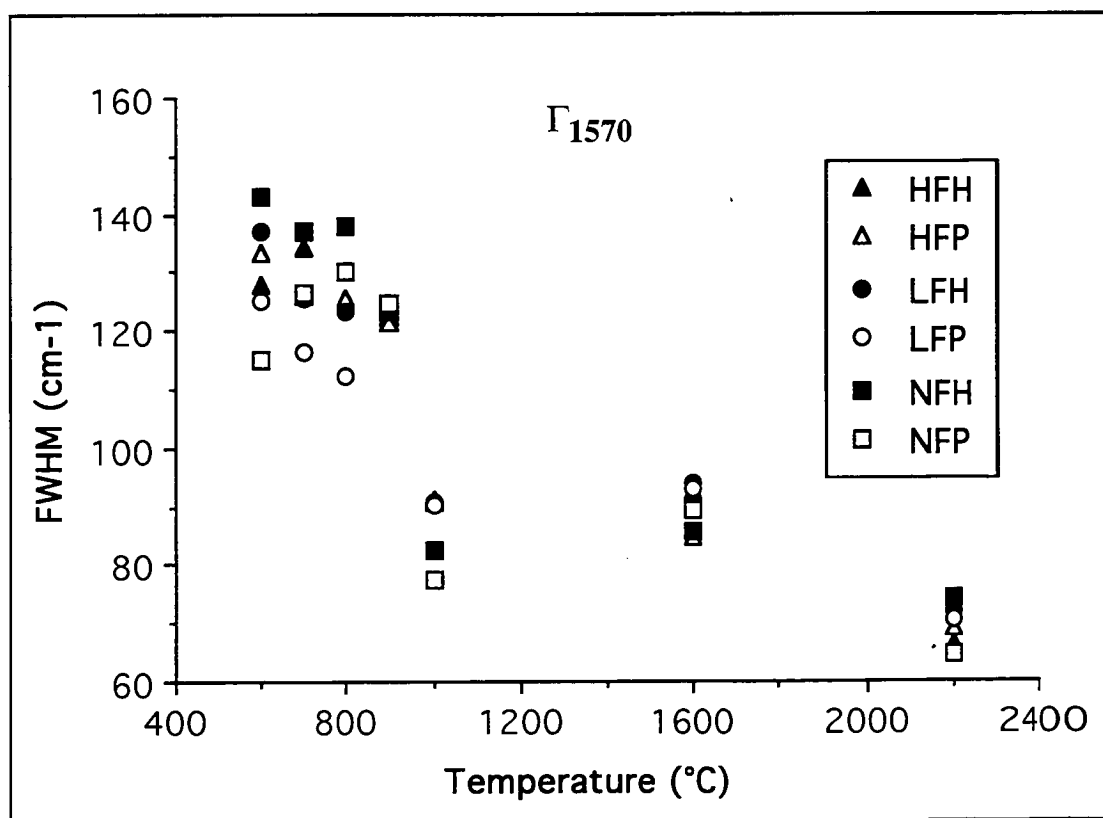


Figure 7.8 Evolution of the width of the 1570 cm^{-1} band, Γ_{1570} , for the six R3 resins over the heat treatment temperature range.

In figure 7.8, the Γ_{1570} values for the resin chars show that the spread of band widths is wide initially at the lower pyrolysis temperatures (600 - 900°C). It also shows that LFP exhibits the most narrow band width in this temperature range, which is to be expected considering that this resin is seen as having the greatest degree of ring condensation (from nmr data), and therefore the most refined crystalline lattice in this temperature range. For heat treatments above 900°C, the band widths, which are all approximately 125 cm⁻¹, decrease rapidly to values of $\Gamma_{1570} = 75\text{-}90$ cm⁻¹ at 1000°C. Above 1000°C, the 1570 cm⁻¹ band widths for the six resin chars remain relatively equal and constant to 2200°C. These results suggest that the lattice spacing, of which lattice order is a function, is quite varied amongst the chars between 600 and 900°C, due to the varying degree of ring condensation. As ring clusters grow to complete aromatisation in all resin chars above 900°C, the structural and defect differences between the resins are very minor, and the variation in lattice spacing of the crystal structure is reduced in each char to a more constant value. As the two indicators of the presence of defects, Γ_{1350} and Γ_{1500} , show a decreasing trend with temperature, and therefore a narrowing of defect distribution in the carbon lattice, the Γ_{1570} trend shows that these carbons achieve a certain degree of crystallisation and lattice spacing, which is equal in each char, beyond which further lattice refinement, and any subsequent pseudo-graphitic order, is not achieved below 2200°C due to the presence of these twisting defects. This supports the theory that these carbons are essentially non-graphitising [Marsh *et al*, 1989].

From other reported band width values [Beny-Bassez and Rouzaud, 1985] it was shown that the Γ_{1350} and Γ_{1570} values of saccharose- and anthracene- cokes are comparable to the phenolic resin chars of this study. For these cokes, the Γ_{1350} values remain relatively constant at approximately 250 cm⁻¹ to a heat treatment of 750°C, and then decrease rapidly to 100 cm⁻¹ at 1000°C, followed by a steady decrease to approximately 20-50 cm⁻¹ at 2000°C. The Γ_{1570} values of these cokes are seen to remain relatively constant at approximately 100 cm⁻¹ to 1000°C, and

then to decrease to approximately 50 cm^{-1} at 2000°C and remain at that value to a heat treatment of 3000°C .

The specific area of the 1350 cm^{-1} band, S_{1350} , for the anthracene and saccharose cokes shows similar values to the resin chars of this study to a heat treatment of 1500°C . Above 1500°C , the reported S_{1350} values for the cokes are seen to decrease to much lower levels ($\approx 10\%$) than the chars of this study. This suggests that the lattice structures and defect modes are similar between the three sources of carbon, although the degree of crystalline order in the phenolic resin chars of this study is lower than that of the anthracene and saccharose chars of other studies [Beny-Bassez and Rouzaud, 1985].

Carbons pre-baked at $10^{\circ}\text{C}/\text{min}$:

For the six resins pyrolysed to 1000°C at $10^{\circ}\text{C}/\text{min}$, denoted as R10 chars, the specific areas of the 1350 , 1500 and 1570 cm^{-1} bands are shown in Figures 7.9, 7.10 and 7.11 respectively. As there were no resins pyrolysed at $10^{\circ}\text{C}/\text{min}$ to heat treatment temperatures below 1000°C , only values for 1000 , 1600 and 2200°C are taken for the parameters derived from the Raman spectra.

The S_{1350} values in Figure 7.9 show a slight increase from 1000 to 1600°C , and then a moderate decrease to 2200°C , as compared to the same parameter values for the resins pyrolysed to 1000°C at $3^{\circ}\text{C}/\text{min}$ (R3 resins) whose chars showed a definite decreasing nature from 1000 to 1600 to 2200°C . The S_{1350} values for the R10 chars show more consistency between the resins, suggesting that all of the chars produced at higher ramp rates suffer a similar degree of aromatic condensation, and therefore a similar degree of defect propagation as they are heat treated between 1000 and 2200°C .

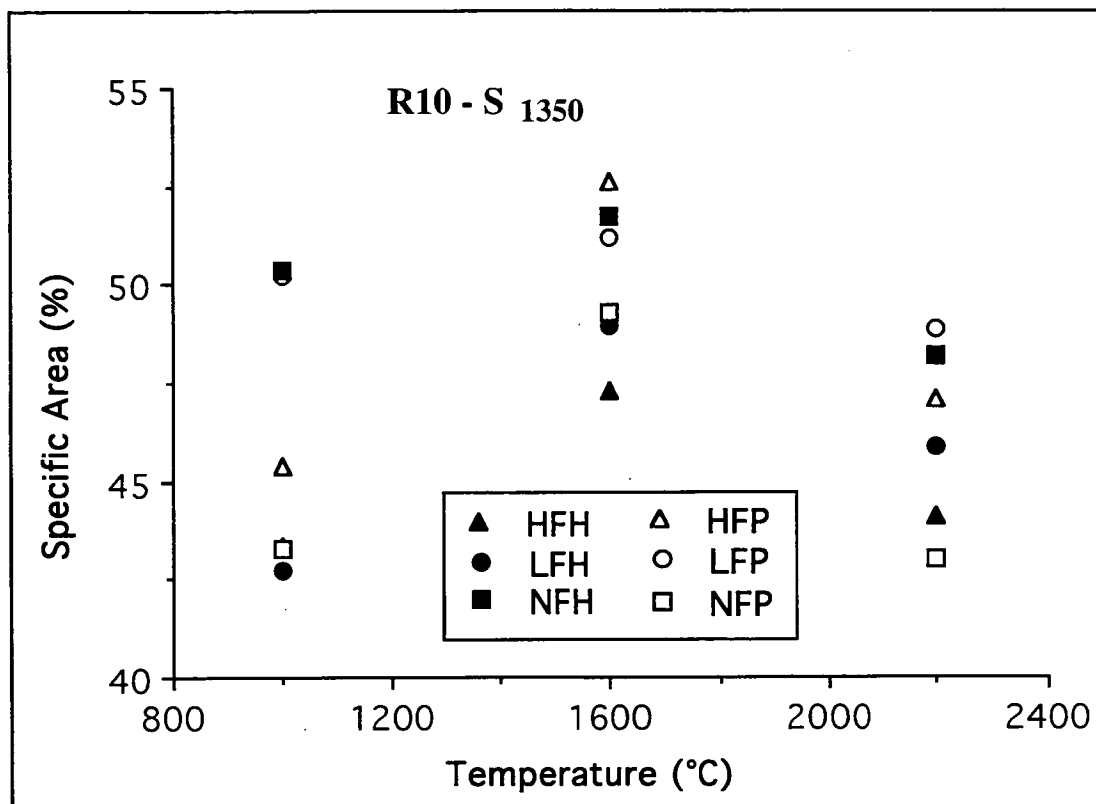


Figure 7.9 Evolution of the specific area of the 1350 cm^{-1} band, S_{1350} , for the six R10 resins over the heat treatment temperature range.

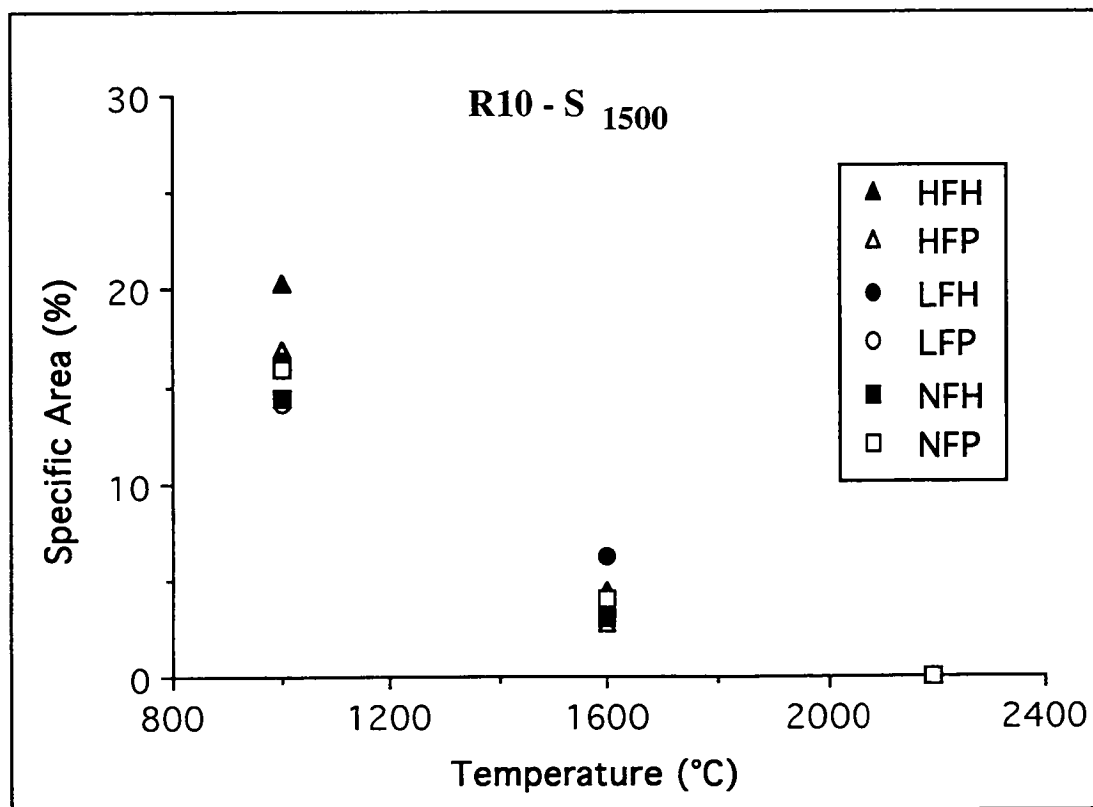


Figure 7.10 Evolution of the specific area of the 1500 cm^{-1} band, S_{1500} , for the six R10 resins over the heat treatment temperature range.

The S_{1500} values for the R10 chars, as shown in Figure 7.10, displays a similar decreasing trend to that of the R3 chars, as seen in Figure 7.4. The S_{1500} values for all of the R10 resin chars are very similar, with only a 5% spread between the chars at 1000 and 1600°C, and no 1500 cm^{-1} peak for all R10 chars of the six resins at 2200°C.

The S_{1570} values for the R10 chars, as shown in Figure 7.11, display a very similar nature to the R3 chars, with less spread of results at each temperature. These results suggest that the degree to which the resins increase in lattice order is largely independent of the pyrolysis heating rate in the range 3-10 °C/min. The defect mode of the higher temperature carbon lattice may be affected by heating rate as the structural (twisting) defect, indicated by the 1350 cm^{-1} band, remained relatively constant for the R10 chars between 1000 and 2200°C, whereas in the R3 chars it decreased. Conversely, the proportion of defects caused by hetero-atoms is significantly lower in the R10 than the R3 chars, and is negligible in the 2200°C R10 chars. It is therefore possible that the combination of the higher heating rate of 10°C/min to temperatures in the lower pyrolysis range of 25-1000°C causes a more homogeneous condensation mechanism between the resins, resulting in similar twisting defect modes.

The change in the 1350, 1500 and 1570 cm^{-1} band widths for the R10 chars are shown in Figures 7.12, 7.13 and 7.14 respectively. The Γ_{1350} and Γ_{1570} values are similar to those of the R3 chars, as both parameters are seen to decrease at similar rates for both families of resin chars.

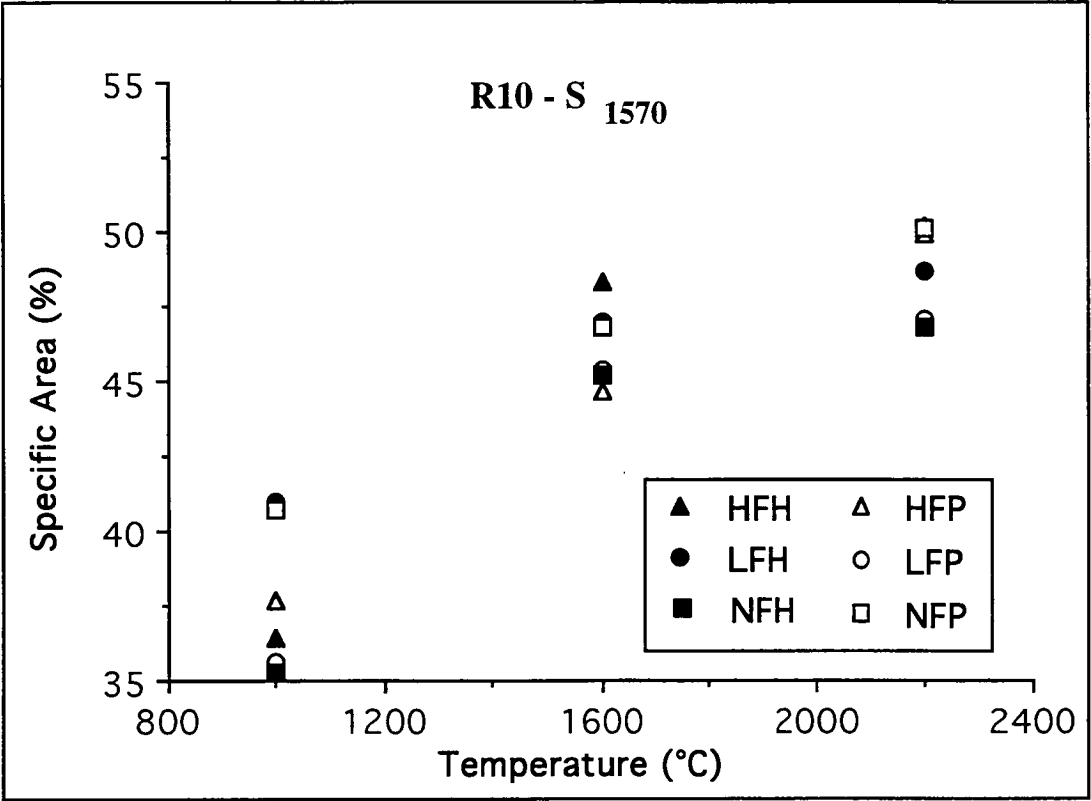


Figure 7.11 Evolution of the specific area of the 1570 cm⁻¹ band, S₁₅₇₀, for the six R10 resins over the heat treatment temperature range.

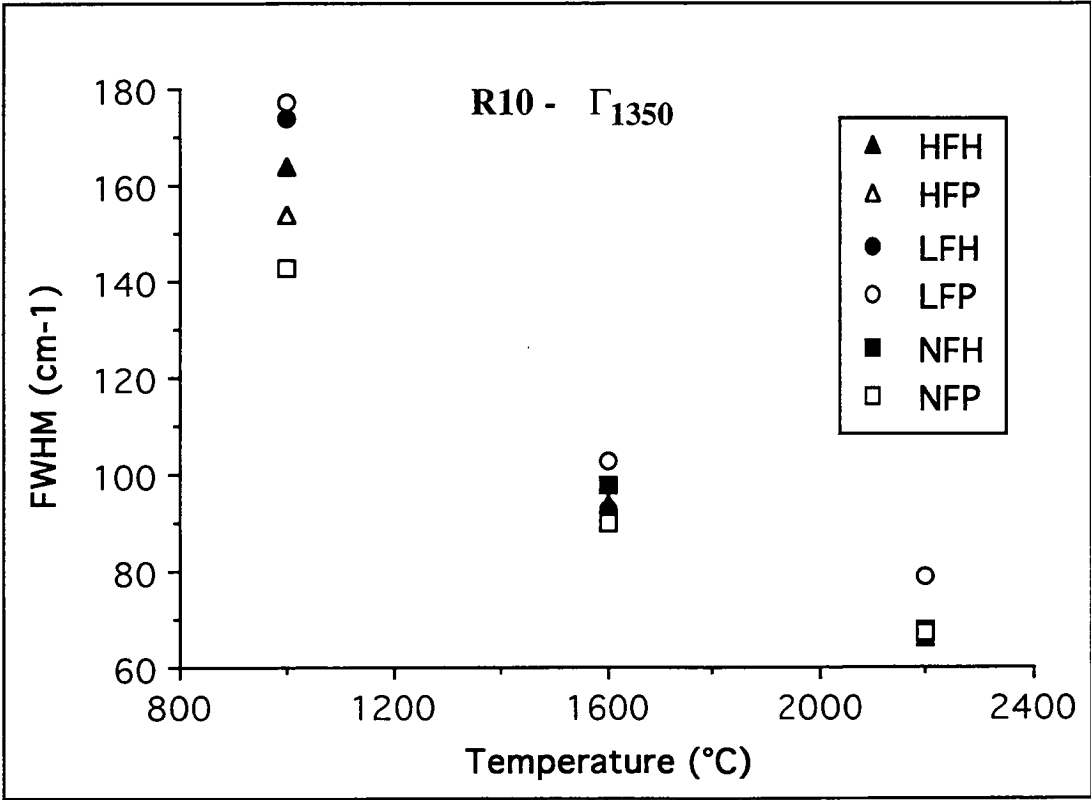


Figure 7.12 Evolution of the specific area of the 1350 cm⁻¹ band, Γ_{1350} , for the six R10 resins over the heat treatment temperature range.

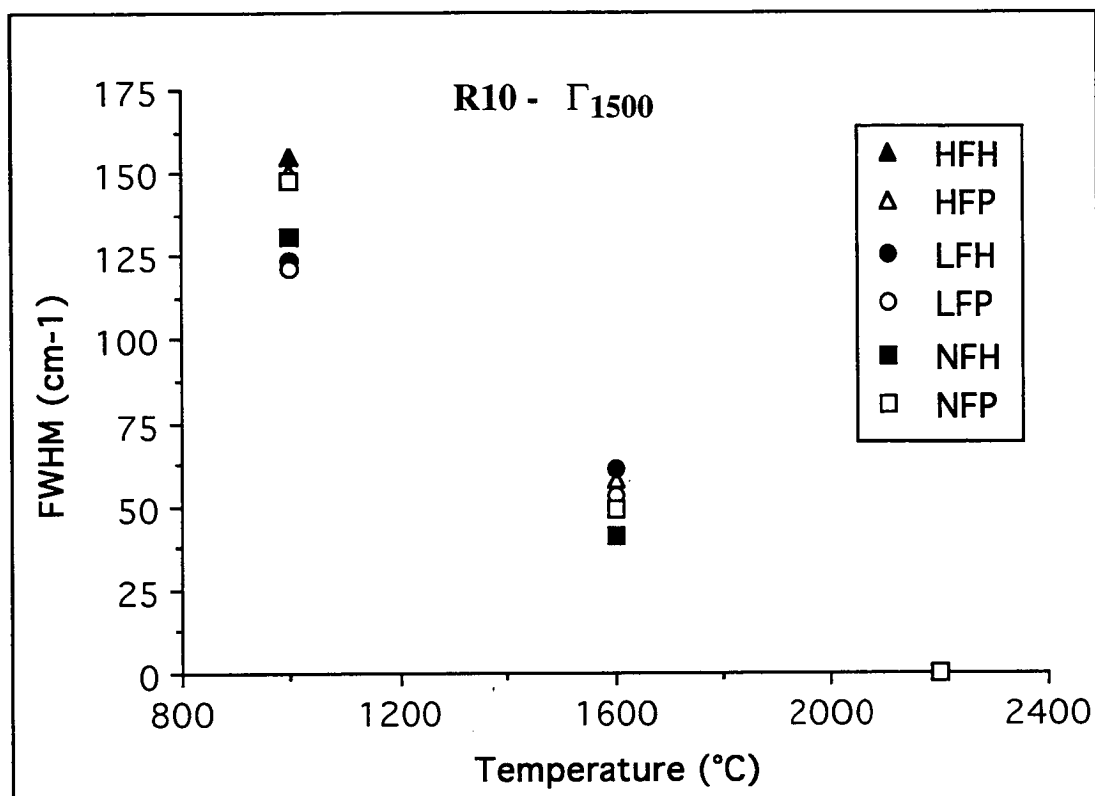


Figure 7.13 Evolution of the specific area of the 1500 cm⁻¹ band, Γ_{1500} , for the six R10 resins over the heat treatment temperature range.

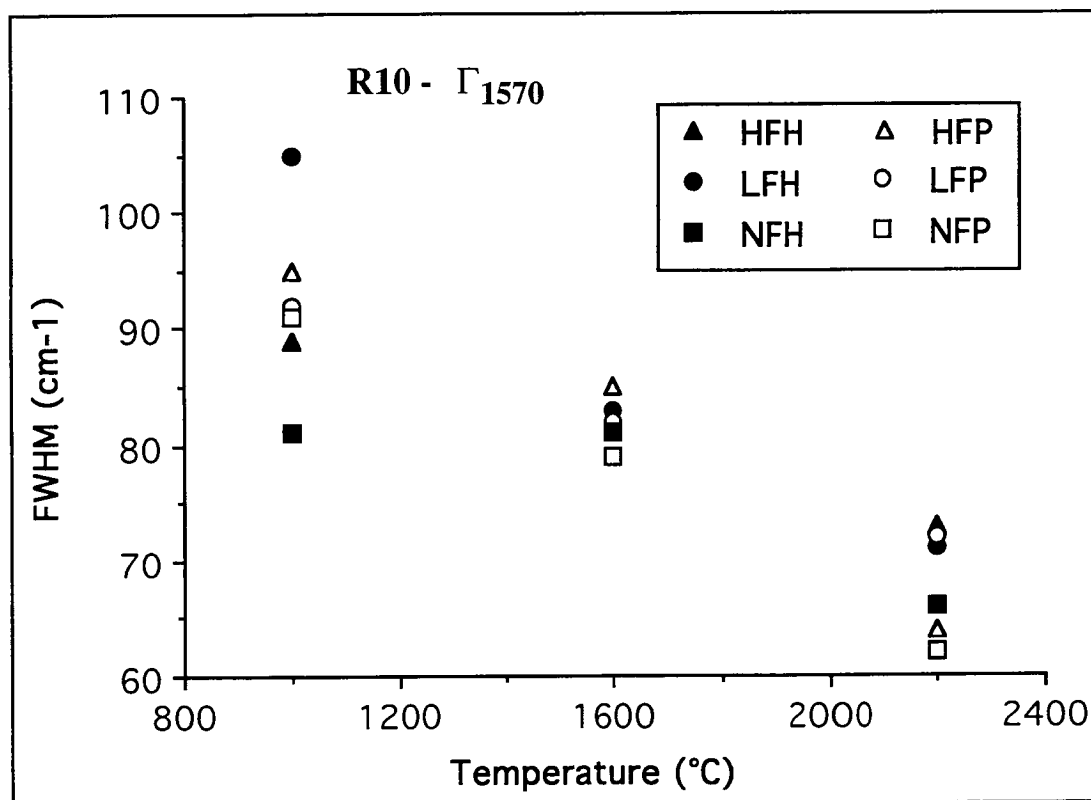


Figure 7.14 Evolution of the specific area of the 1570 cm⁻¹ band, Γ_{1570} , for the six R10 resins over the heat treatment temperature range.

The Γ_{1500} values (Figure 7.13) show a very narrow spread and a decreasing trend to zero for the R10 chars, whereas in the R3 chars (Figure 7.7) the results are highly spread, but constant, with a range of values of approximately 60 cm^{-1} at 1000 and 1600°C, and only decreasing from a mean value of 150 cm^{-1} at 1600°C to approximately 40 cm^{-1} at 2200°C. Therefore, it is possible that the higher ramp rate has little effect on the variation of twisting defects associated with the carbon lattice, but that the variation of defects due to hetero-atoms is less at the higher ramp rate. This suggests that the higher heating rate to 1000°C selectively removes one particular hetero-atom to a greater degree than the lower ramp rate.

Chapter Eight

**The observation of modifications
in the surface chemistry of the
Phenolic Resin Chars during
pyrolysis (25 - 1000°C) by
X-Ray Photoelectron
Spectroscopy.**

X-Ray Photoelectron Spectroscopy:

The technique of X-ray photoelectron spectroscopy was used in this study to determine changes in the surface chemistry of the resins as they are carbonised to 1000°C chars. Although the true shape of XPS lines are Lorentzian due to the distributions of the exciting radiation and electron emission being Lorentzian, the instrumental broadening factors tend to be Gaussian. Therefore the observed line shape is a convolution of all these contributions, and is considered to be resolved theoretically by a Voigt-type function [Briggs, 1978]. In general, most peaks can be seen to approximate a Gaussian distribution, which is sufficient in this study.

A C1s excitation peak for a graphite sample is shown in Figure 8.1. As can be seen from the spectrum a smooth and almost symmetrical peak exists, centred at 285eV, with a tail on the high binding energy side of the peak. This asymmetry at the base of the peak is due to a spread of energies of the electrons caused by several factors affecting the ejection of the electrons, including the number of collisions an electron suffers before escape, the angle of collision, the mass and vibrational state of the atom, etc. Because of area considerations, the greater proportion of these low kinetic energy photoelectrons become part of the background.

In addition to the spectral contribution of the electron collision energy, there is a satellite peak seen for the C1s line at a binding energy of approximately 275eV, i.e., at a shift of 10eV from the main carbon peak on its low binding energy side. Because the X-ray source for the spectrometer is not completely monochromatic, there is some contribution from bands other than the $K_{\alpha 1,2}$. The most important of these are the $K_{\alpha 3}$ and $K_{\alpha 4}$ lines at energies of 9.7 and 11.1eV higher than the other main $K_{\alpha 1,2}$ line. As these lines are of higher energy, the photoelectrons they produce will be of higher kinetic energy, corresponding to lower binding energies [Krause and Ferreira,1975]. The satellite peak is well separated from the main

peak, and can therefore be excluded completely from peak integration or fitting.

Because of the difficulty in establishing correct background due to the above mentioned perturbations of π - electrons, which lead to the inelastic loss tails, the baseline correction of the spectra was found initially by visual observation, and so it was both useful and sufficient to assume a linear sloping baseline for all C1s, O1s and N1s spectra, and then to use a computer program to interpolate a straight line between peak minima, and subtract this line from the peak [Wandass *et al*,1987]. This method has been reported in other studies [Aksela and Aksela,1974; Honda and Hirokawa,1976; Weightman,1976].

Determination of surface elemental concentrations of the resin chars:

The C1s, O1s and N1s spectra for the unpyrolysed HFH and the 1000°C LFH char pyrolysed at 3°C/min are shown in Figures 8.1, 8.2 and 8.3 respectively. Several chemical shifts have been reported for each of the three elemental species of carbon surfaces. Assignments for a high ranked coal sample showed four carbon bonding species as hydrocarbon ($\approx 285\text{eV}$), carbonyl ($\approx 287\text{eV}$), carboxyl (289eV) and the main graphite peak ($\approx 284\text{eV}$) respectively; the graphitic carbon being found at a binding energy of $284.3 \pm 0.2\text{eV}$ referenced to gold ($\text{Au}4f_{7/2}$, $E_b = 84.0\text{eV}$) [Brown *et al*,1981]. There is also support for the assignment of the C1s bands as aromatic or aliphatic hydrocarbon at 285eV , ether or hydroxyl carbons at 286.6eV , carbonyl carbons at 287.7eV , and carboxyl groups at 288.9eV [Gai *et al*,1989]. In the study of a raw high grade coal sample all the carbon peaks, except that of graphite, were lost after ashing of the sample up to 600°C [Brown *et al*,1981]. In the same study, a coal calcined at 600°C for 6 hours showed a decrease in the carbon bands except the main graphite peak which remained the same size as for the uncalcined sample. As the C1s peaks of the char samples in this study are shown to be mainly narrow graphitic bands with a small shoulder at a chemical shift of 5eV ,

it can be concluded from the study of Brown *et al* [1981] that the carbon surfaces of interest in this study are free of aliphatic hydrocarbons.

Apart from the graphite component of the C1s peak, there is also a carbonyl and carboxyl band at chemical shifts of 2.2eV and 4.2eV, respectively, relative to 284.6eV [Kozlowski and Sherwood,1986]. There is also an N1s peak centred between 401eV and 399eV that corresponds to either amine/amide or cyano/pyridine type structures produced after surface treatment with ammonia. From this it was suggested that there would also be a corresponding C1s peak at a chemical shift of 2.0eV [Kozlowski and Sherwood,1986]. The existence in a polyimide polymer of an aromatic carbon peak at 284.6, analogous to the graphitic peak, and a peak of C \equiv N type bonding at 286.0eV has also been reported [Hu *et al*,1988]. In comparison, the same polymer heat treated to 2100°C showed only a graphitic peak, with no oxidic carbons. Different C1s band chemical shifts (from the graphite peak) are as follows; CH_x +0.8eV, C-O +2.1eV, C=O +3.5eV [Wandass *et al*,1987]. As these differ from other assignments [Brown *et al*,1981; Gai *et al*,1989; Kozlowski and Sherwood,1986] and on the basis of a lack of sufficient resolution within the spectra of this study, it was decided to consider the band at ca. +4eV shifted from the main C1s peak as a 'carbon-oxide' peak of either C-O or C=O bonding.

Due to the lack of high resolution within the spectra, and a relatively high degree of error (\approx 10%) inherent in this method of experimentation [Gasser,1985], the conclusions reached from the data collected in this study should only be considered as an approximate guide to the surface chemistry of these chars. The best XPS surface data of carbons come from those samples electrolytically treated to enhance the effect of surface oxidation, i.e., the spectra representing the C1s and O1s binding energy distributions [Brown *et al*,1981; Gai *et al*,1989; Hu *et al*,1988; Kozlowski and Sherwood,1986; Wandass *et al*,1987]. Within the limitations of the present data, it is possible to demonstrate an oxidative effect on the surface of these

chars, and to show a mechanism of nitrogen loss for the hexamine containing resins.

A deconvolution of the 1000°C HFH resin is shown in Figure 8.4. As the C1s peak is seen to contain at least two bands representing the graphitic (elemental) and oxidic carbon, Gaussian curves were fitted to these peaks using the Marquard Non-Linear Least Squares [Marquard,1963] algorithm in a Fortran computer program modified by the author especially for these spectra. From the surface chemistry studies of oxidised graphite it is suggested that the peak centres and widths of the C1s band be constrained when using iterating peak fitting techniques due to the independent knowledge of the surface chemistry of the samples [Wandass *et al*,1987]. However, as the chars in this study are primarily of partially-ordered non-graphitic carbons, all parameters (centre, FWHM, height) were varied for the two bands, but the initial choice of peak position of the graphitic C1s peak as 284.6eV remained constant, for all spectra, and to estimate the initial values of the parameters of the carbon oxide band by visual observation of each spectrum.

The O1s peaks for all spectra were found to show only one relatively symmetrical band centred at 531-532eV (Figure 8.2). Therefore deconvolution of the O1s peak was not required, and a Fortran program was written to simply baseline correct the spectra after locating peak minima, and then to locate the peak centre, height and FWHM. This program was also used for the N1s spectra, (Figure 8.3) which also contained only one prominent peak in the spectra of the hexamine containing resins (HFH, LFH and NFH), which were centred mainly at 398-400eV. The non hexamine containing resins presented no resolvable N1s peaks, and therefore it is assumed that there was no air contamination of the samples, and that all the detected surface nitrogen and oxygen originated from the bulk samples themselves.

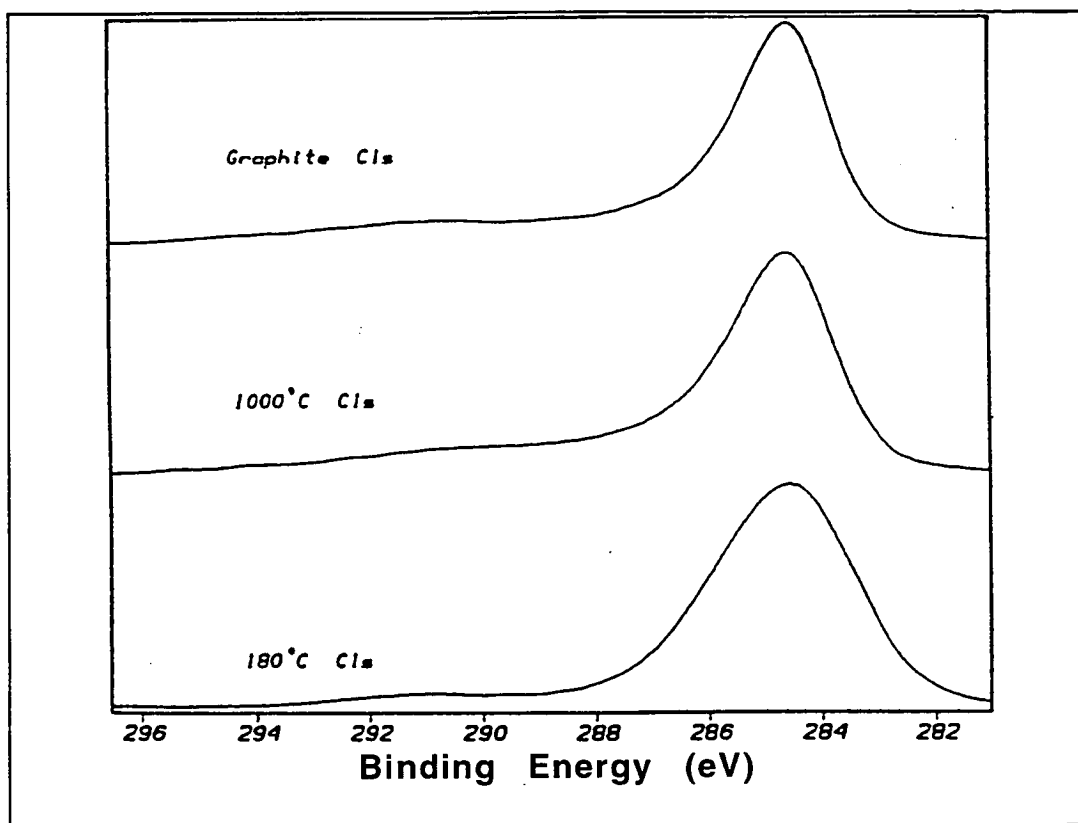


Figure 8.1 The C1s XPS spectra of a graphite sample, unpyrolised HFH resin and 1000°C (3°C/min) HFH resin char surface.

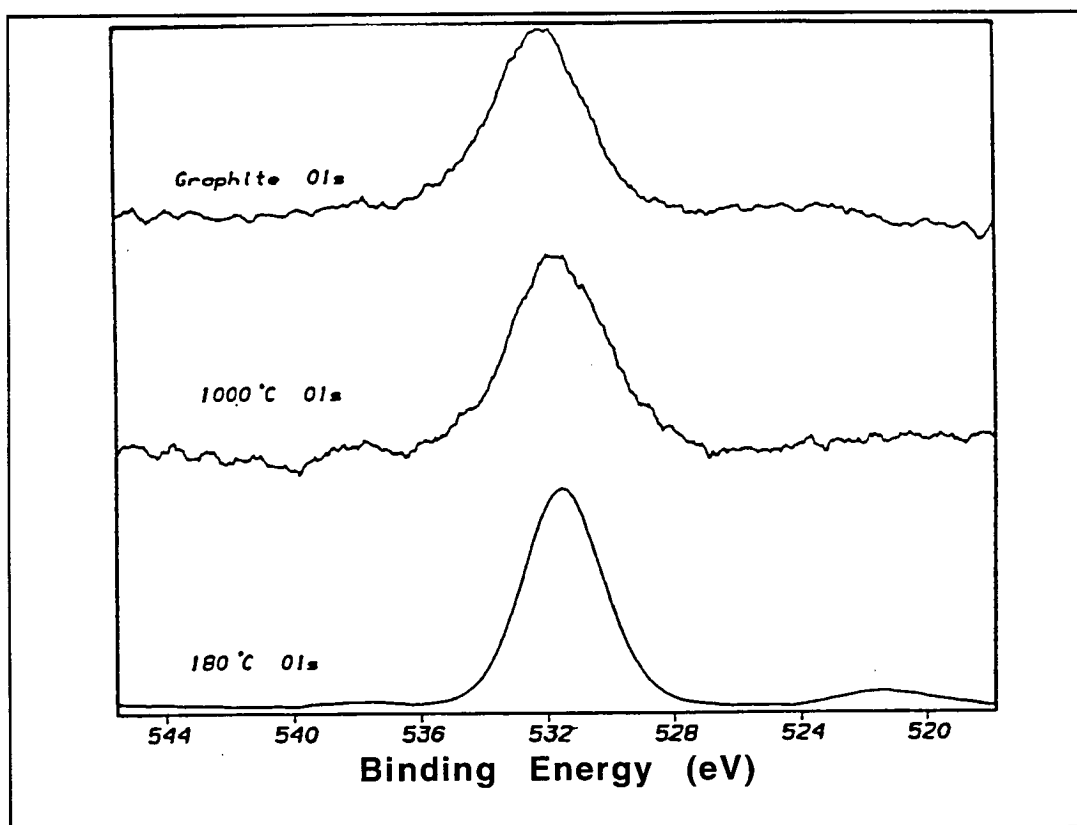


Figure 8.2 The O1s XPS spectra of a graphite sample, unpyrolised HFH resin and 1000°C (3°C/min) HFH resin char surface.

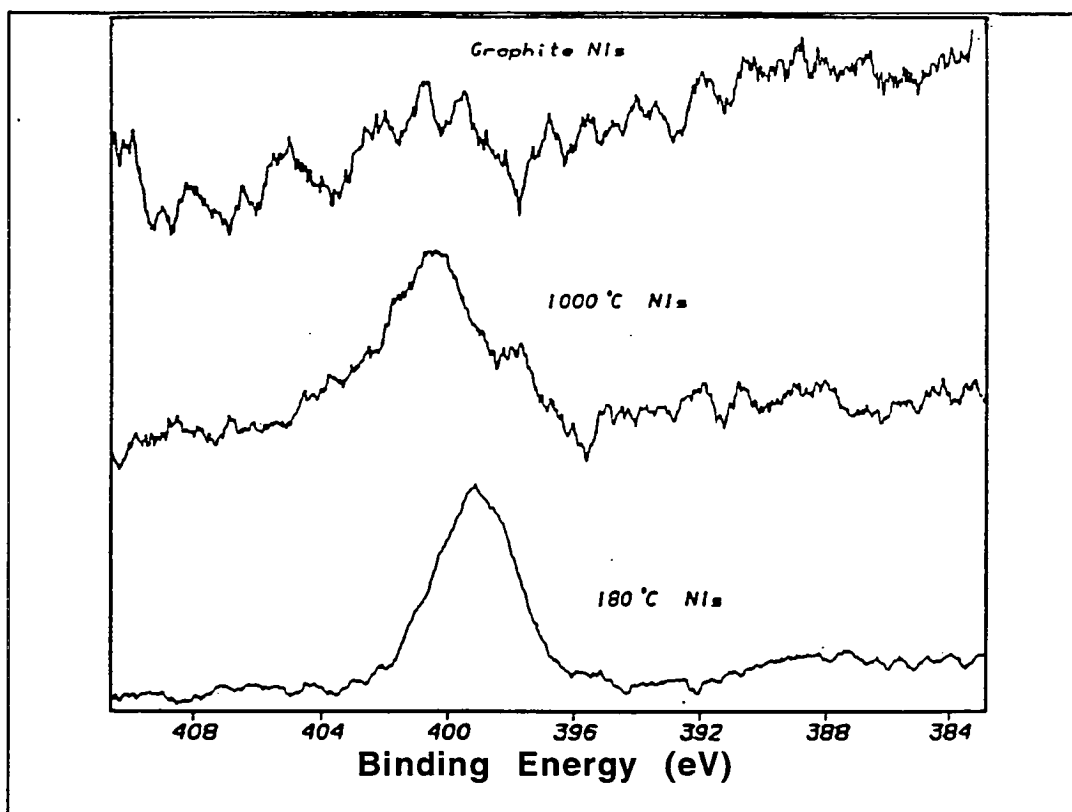


Figure 8.3 The N1s XPS spectra of a graphite sample, unpyrolised HFH and 1000°C (3°C/min) HFH char surface.

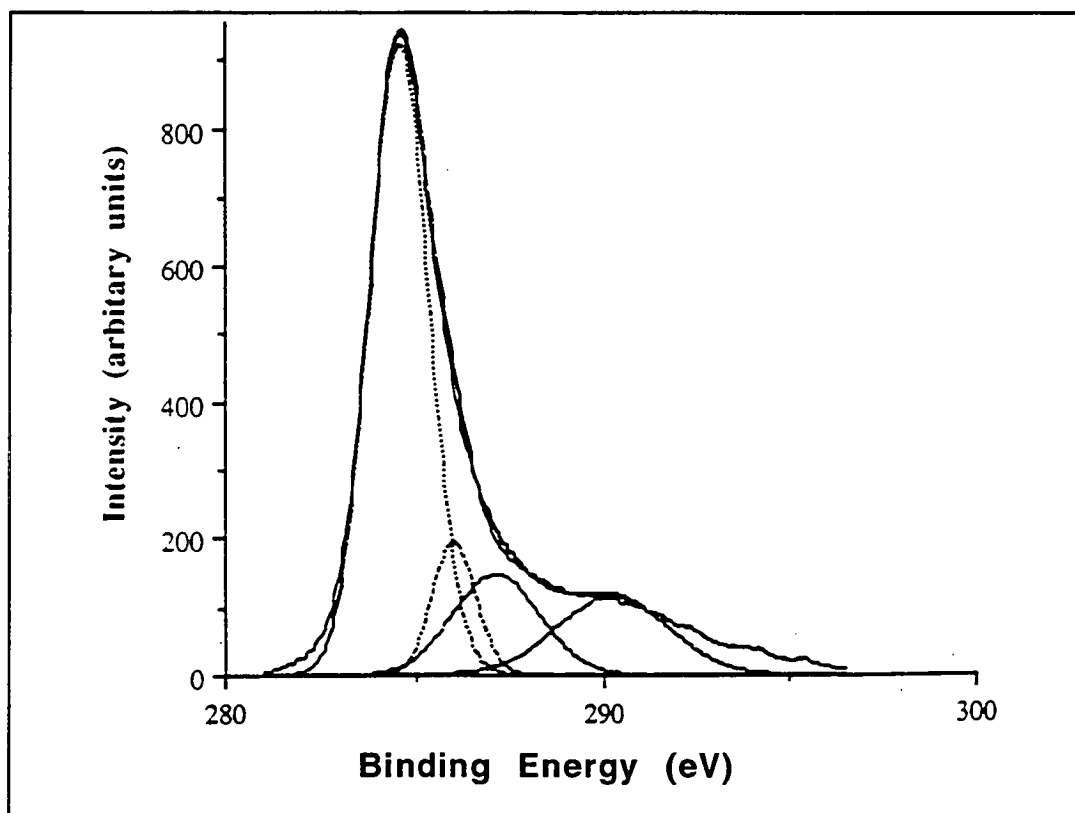


Figure 8.4 Deconvolution of C1s XPS spectrum of HFH 1000°C char surface.

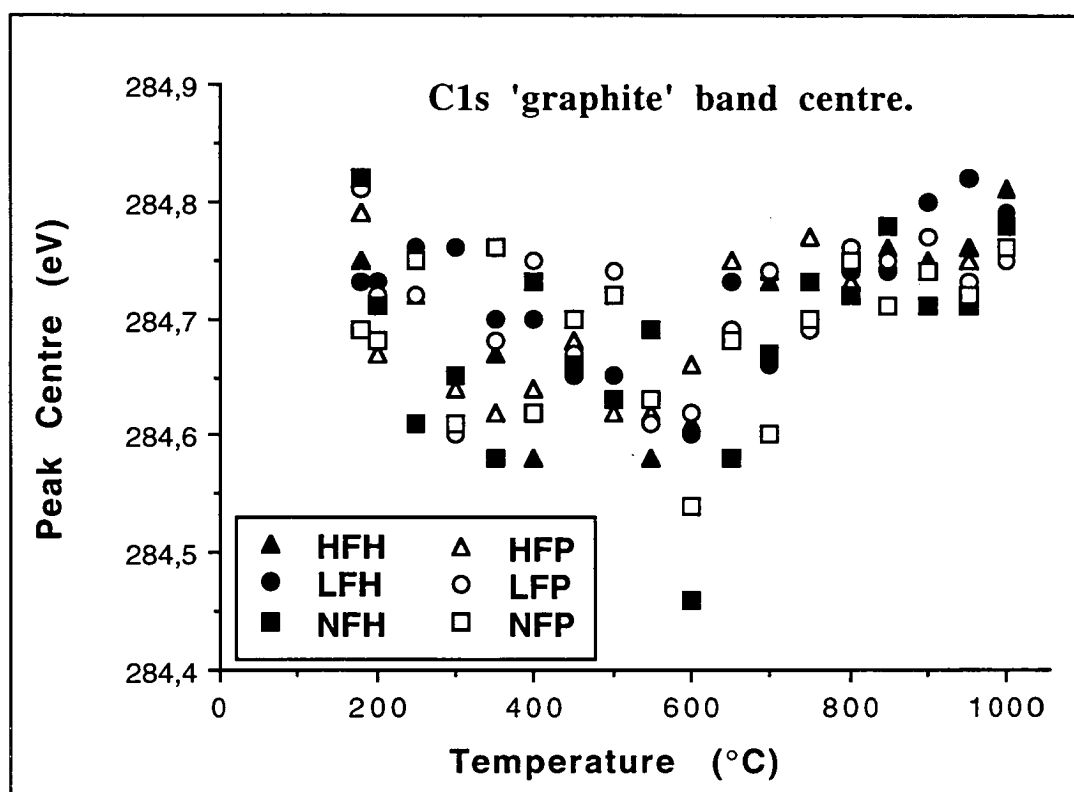


Figure 8.5 The shift in the main 'graphite' band centre for the six resin chars over the heat treatment temperature range.

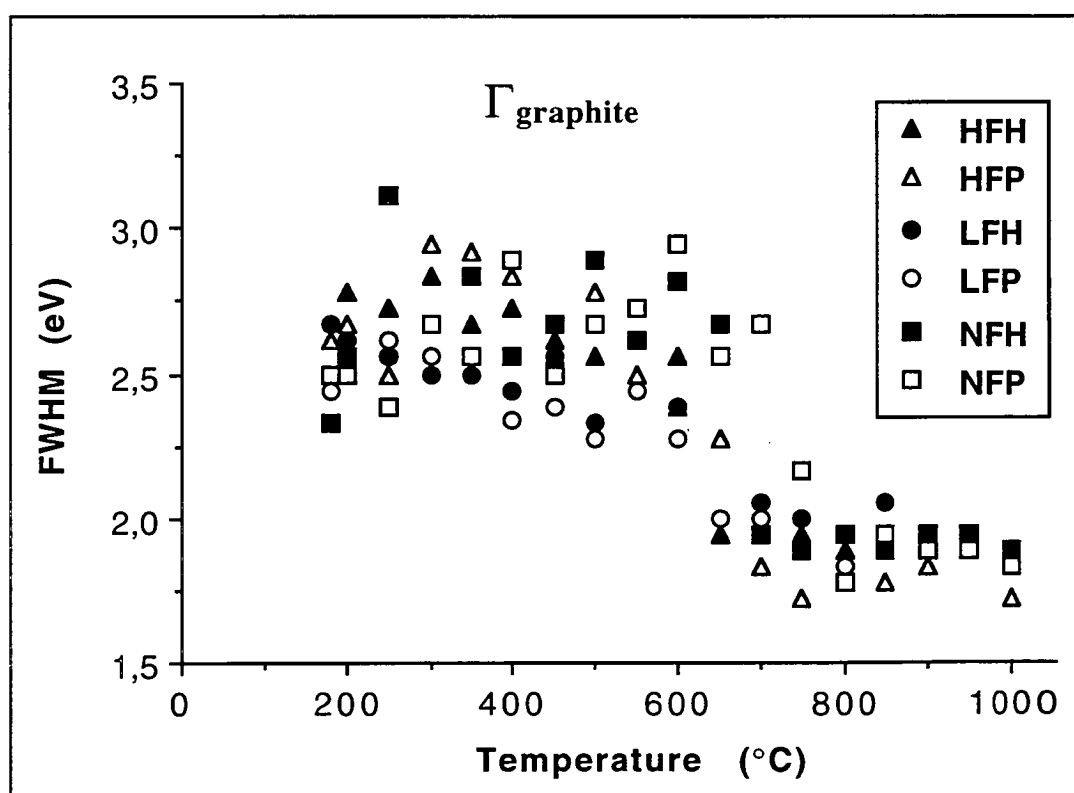


Figure 8.6 Variation of the width of the main graphite band, Γ_{graphite} , for the six resin chars over the heat treatment temperature range.

oxygen species exists at a chemical shift of 531.8eV, whereas the double bonded oxygens are seen at 533.3eV [Kozlowski and Sherwood,1986]. Therefore, it was assumed that the majority of the oxide species on the carbons were single bonded C-O groups. As has already been suggested, the assignment of the N1s peak at 399-401eV was also reported as amine/amide or cyano/pyridine groups [Kozlowski and Sherwood,1986]. The lack of a corresponding carbon band at a chemical shift of ca. 2eV to the main graphite peaks puts doubt on the existence of triple bonded carbon - nitrogen groups, and the lack of an O1s C=O peak also rules out the existence of any amide groups, which suggests the possibility of either simple amine groups on the char surfaces, or chemisorbed nitrogen.

The uncertainty of the nature of the nitrogen species causes the results of the surface nitrogen spectra to simply provide an indication of the migration or loss of nitrogen from the sample surface. This can be seen as a parallel to the loss of nitrogen from the bulk sample.

From Figure 8.5, the shift in centre of the main 'graphitic' band is shown for the six resin char surfaces over the pyrolysis temperature range. Although the scatter in values for the entire temperature range is seen to lie within the suggested error of $\pm 0.2\text{eV}$ from the theoretical 284.6eV, the combination of a general shift in centre from the scattered values around 284.7eV ($\pm 0.2\text{eV}$) up to a heat treatment of 700°C, and then a refinement in centre position at 284.75eV with a reduction in scatter between chars to 0.05eV, indicates a refinement of the aromatic carbon surface. This is supported by the ^{13}C nmr and Raman spectroscopy results of this study, which show, respectively, that the aromatic carbons up to 700°C can be bonded to either a hydrogen, oxygen or other carbon, and that the carbons above 700°C are mostly bonded to other aromatic carbons in a pseudo crystalline structure.

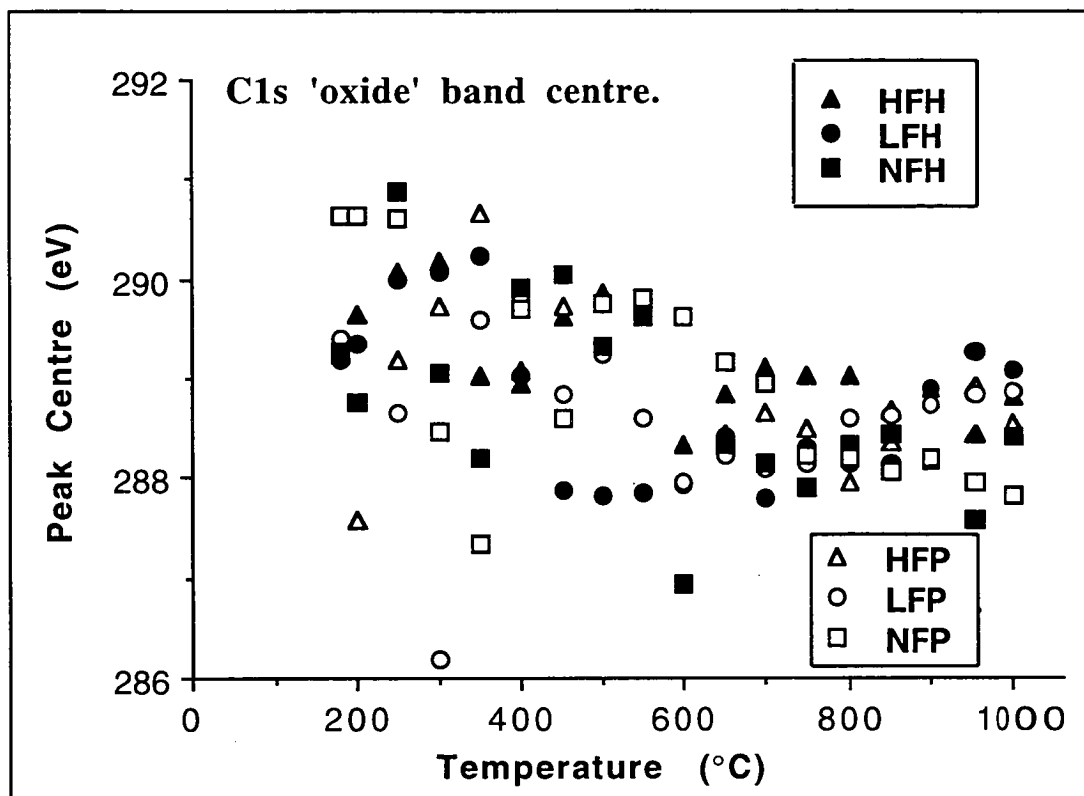


Figure 8.7 The shift in the C1s 'oxide' band centre for the six resin chars over the heat treatment temperature range.

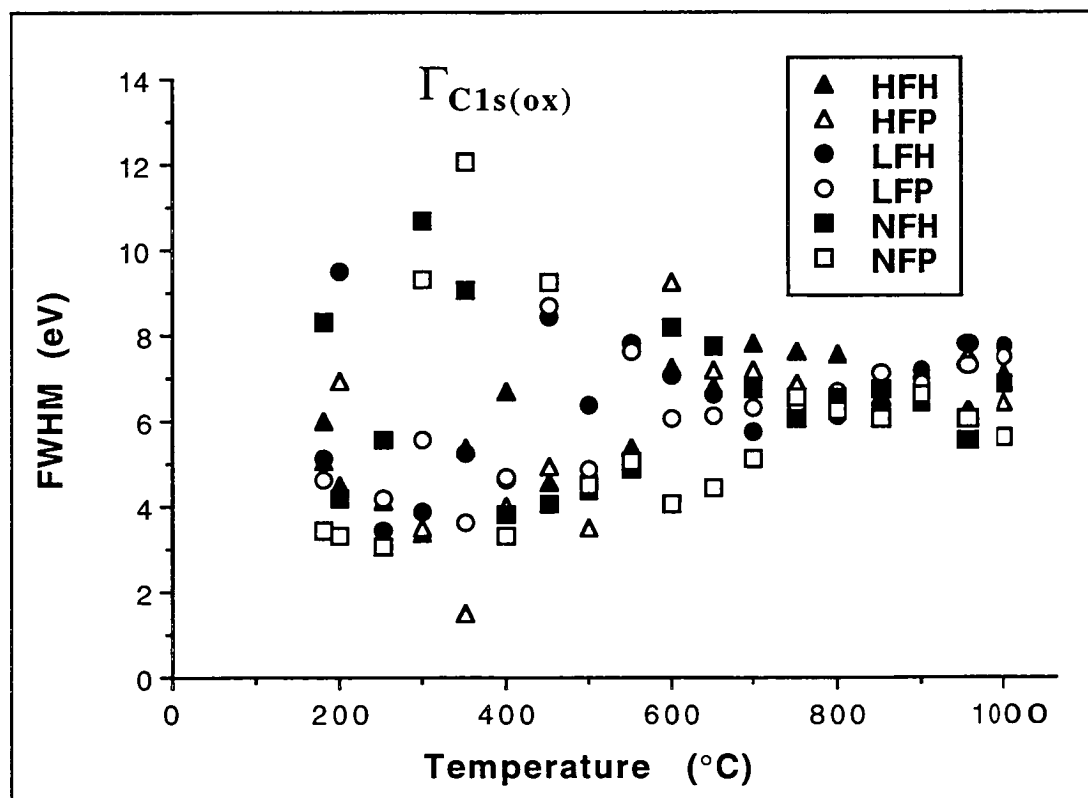


Figure 8.8 Variation of the width of the C1s oxide band, $\Gamma_{C1s(ox)}$, for the six resin chars over the heat treatment temperature range.

the temperature range are shown in Figure 8.6. From these data it is obvious that the initially broad peaks, with a large range of width values around 2.6eV, are seen to narrow rapidly at heat treatments between 650 and 750°C to widths of ca. 1.85eV (± 0.15 eV) and which remain constant to 1000°C. Again, this supports the theory that the nature of the surface C-C bonds are being more refined to those of an ordered nature, as a narrowing of the main C1s band is associated with the reduction of the variety of carbon bonding environments (defects, etc.) as it approaches the theoretical graphitic band width of 1.7eV [Galuska *et al.*,1988]. It is also possible that the C1s band due to CH_x bonding, which is very close to the main graphite peak, is seen to disappear at 700°C, which correlates to the almost complete loss of hydrogen at that temperature. The depletion of the CH_x band would also narrow the main graphitic peak.

From the variation of centres for the fitted C1s oxide band of the char surfaces over the pyrolysis temperature range, as shown in Figure 8.7, it can be seen that the scatter of centre values is wide up to 700°C, and is then narrowed to an average value of 288.5 ± 0.6 eV. Combined with the FWHM values for the C1s oxide band from Figure 8.8, which also show a wide scatter to 700°C, and then become relatively constant at ca. 7 ± 1 eV, it can be seen that a wide selection of carbon-oxygen species exists initially, and then these are refined to a single bond type above 700°C. The variation of the centre positions are initially in the range 286-291eV, with a mean at ca. 289eV. This suggests the presence mainly of C-O bonds, which are likely due to the phenolic hydroxyl groups. Carboxyl groups have also been assigned to this region and this may be the cause for the initial variation in centre positions as the resin is heated. Because of the changing resin chemistry up to 700°C it is likely that carbonyl and amide groups do exist, providing a multitude of bands which would cause the great variation in peak centres and widths. Above 700°C the distribution of carbon-oxygen bonding types is reduced to the C-O, or possibly a carboxyl group, as shown by the narrowing of the bands to a constant width.

From Figure 8.9, it can be seen that the specific area of the C1s oxide band, $S_{C1s(Ox)}$, (the C1s(ox) area divided by the total C1s envelope) shows great variation but with a tendency to increase up to 700-750°C, and then remain relatively constant at 0.3 - 0.35 for chars of heat treatments greater than 750°C. This shows that the proportion of surface carbons bound to oxygen increases with temperature for all the resins up to 700°C, but that the change in nature of the C-O surface types with temperature causes a great fluctuation in the amount of the oxide species, which is also affected by the presence of CH_x species. Above 700°C, and 750°C for NFP, the proportion of carbon oxides is seen to become constant and relatively equal for all the resins which suggests that, with the removal of hydrogen from the sample, and the narrowing of the distribution of oxide species to the one type, it is possible that all the available oxygens are bound to the surface, and no further surface oxidation takes place.

The variation of O1s peak centres over the temperature range, which is displayed in Figure 8.10, displays a scatter of results around $531.5 \pm 1\text{eV}$, which remain relatively constant for heat treatments from 25 to 1000°C. This constant position suggests mainly single bond oxygen species, although the O1s band widths, as shown in Figure 8.11, display a wide range of oxygen envelope widths suggesting a wide distribution of oxygen bonding environments, or possibly a change in effect from the *shake-off* process of the electrons [Briggs, 1978]. The shift in the N1s peak position over the pyrolysis temperature range (Figure 8.12) exhibits a relatively constant centre for the N1s peaks of HFH and LFH, but a great variation of those from NFH above 400°C. The trend shown in Figure 8.13 for the N1s band widths is similar, such that the changes in band width over the pyrolysis temperature range for HFH and LFH are relatively smooth. The parameter Γ_{N1s} for LFH increases from 500 to 1000°C, indicating an increase in variation of nitrogen bonding species, which suggests the existence of N-O bonding at the char surface. Like that of the N1s peak position, the trend of the variation in N1s band width for NFH is seen to be very widely scattered above 400°C.

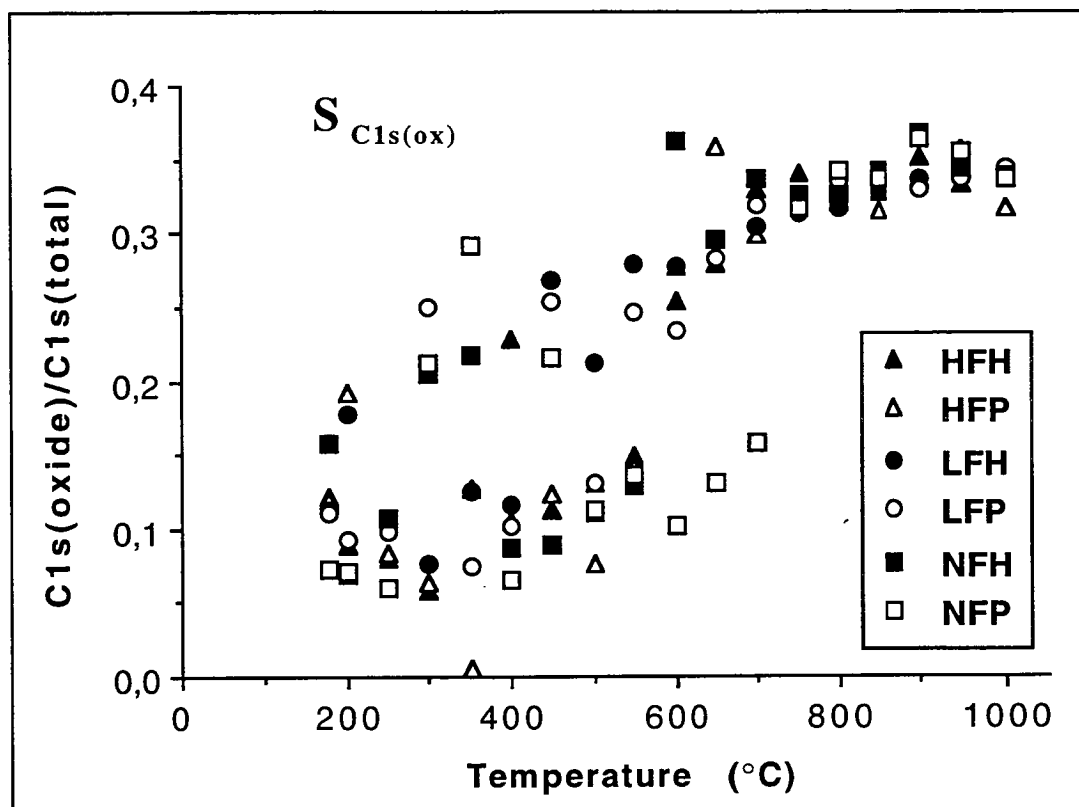


Figure 8.9 Variation of the specific area of the C1s oxide band, $S_{C1s(ox)}$, for the six resin chars over the heat treatment temperature range.

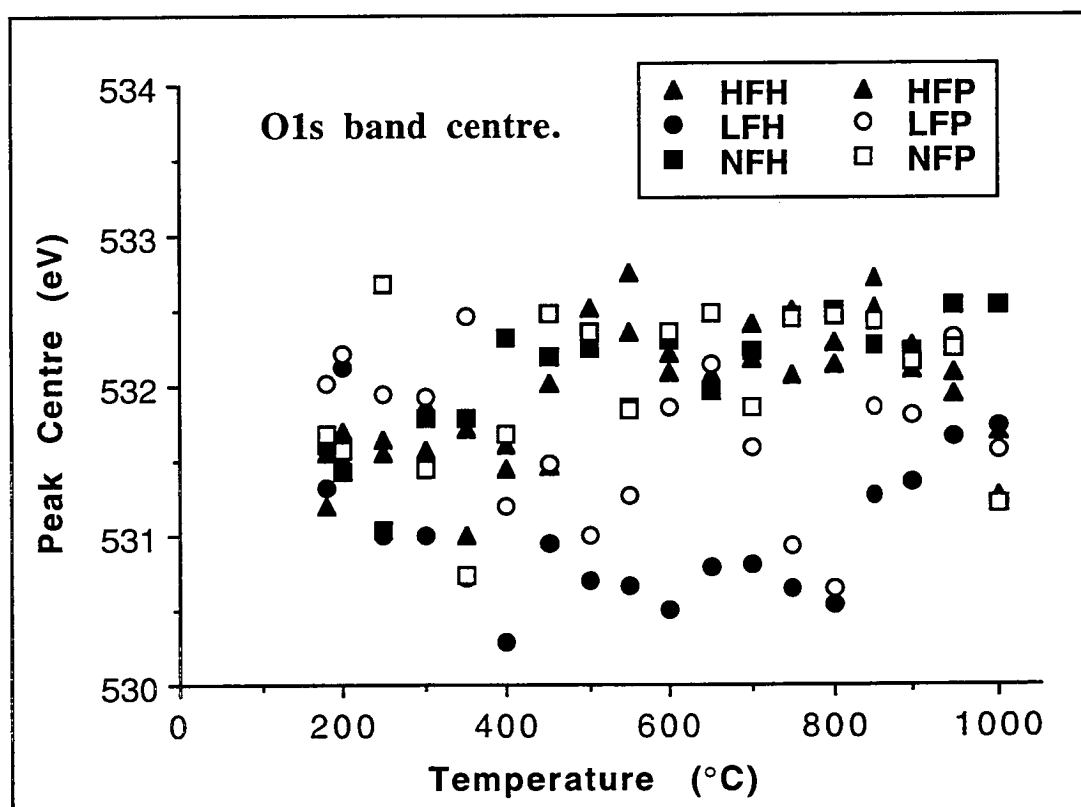


Figure 8.10 The shift in the O1s band centre for the six resin chars over the heat treatment temperature range.

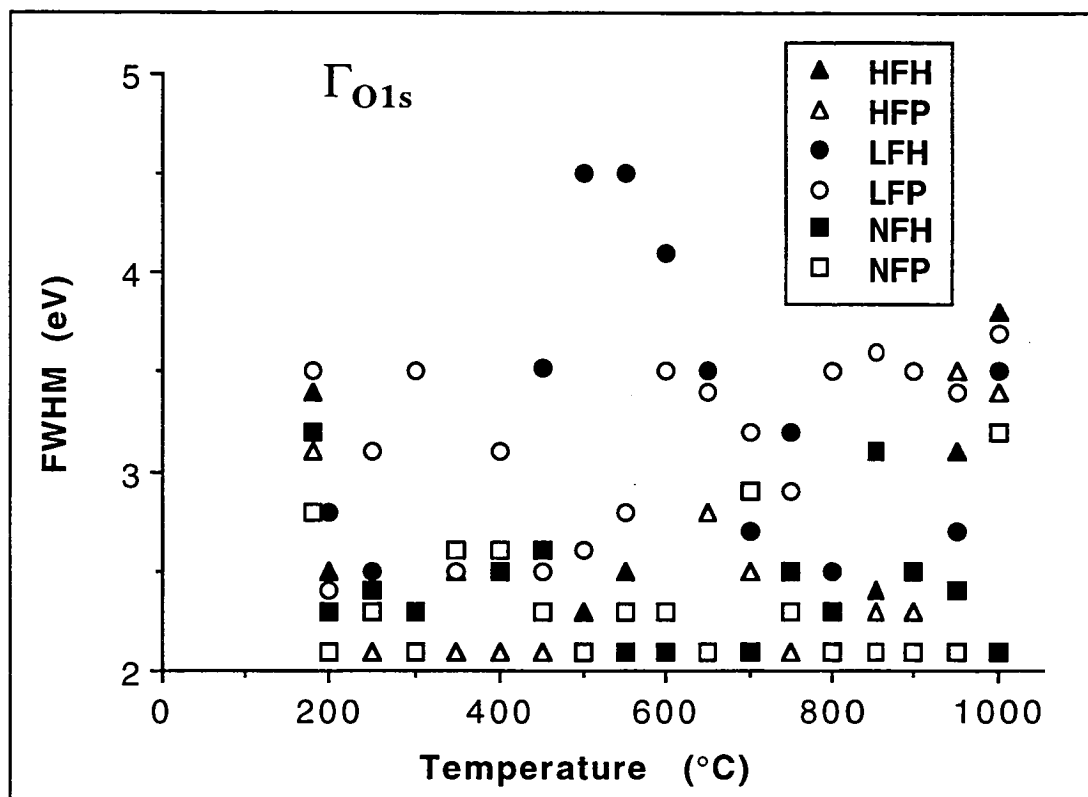


Figure 8.11 Variation of the width of the O1s band, Γ_{O1s} , for the six resin chars over the heat treatment temperature range.

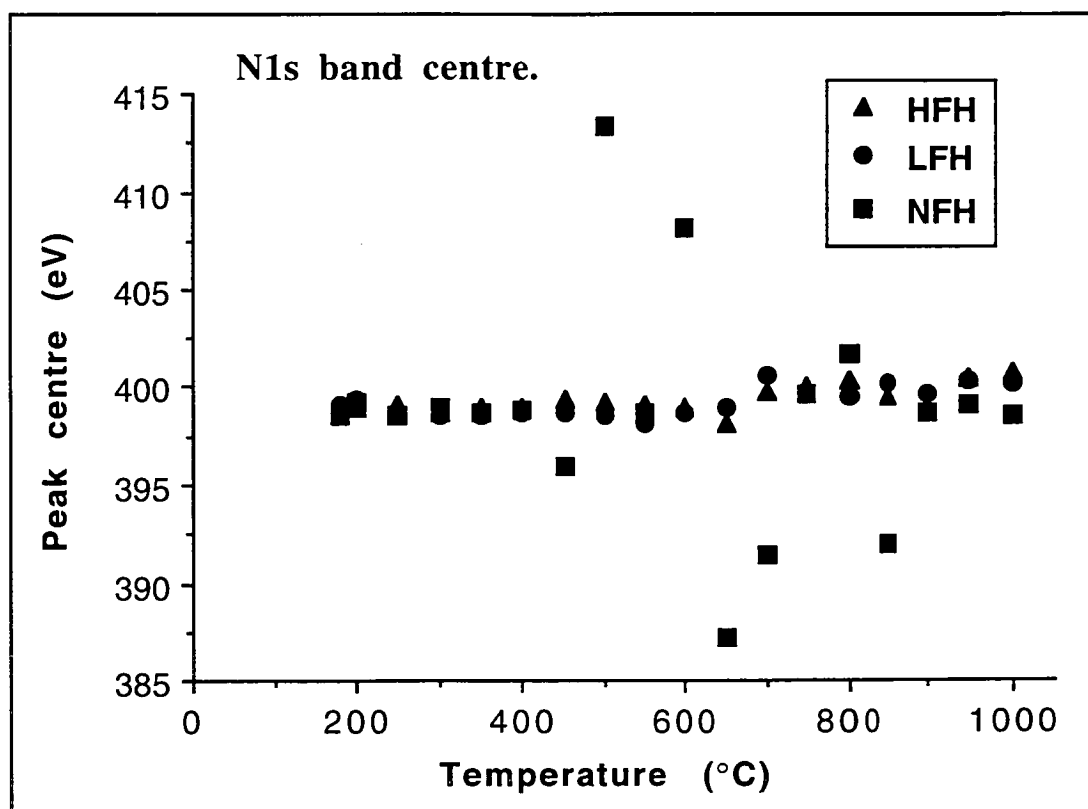


Figure 8.12 The shift in the N1s band centre for the six resin chars over the heat treatment temperature range.

The nitrogen bearing resins HFH, LFH and NFH all show differing degrees of surface nitrogen removal. From the change in surface N/C ratio for the chars over the pyrolysis temperature range (Figure 8.14) the proportion of surface nitrogen species for NFH is very rapidly reduced by an order of magnitude and approaching a negligible level from the unpyrolysed resin to the 400°C char. This is paralleled by the bulk removal of nitrogen from this resin during pyrolysis, as shown by the rapid decrease in bulk atomic % nitrogen to a heat treatment of 400°C (Figure 4.8). Therefore, the wide scatter of centre and width values for the N1s bands of the NFH chars' surfaces are due to the very small N1s peaks being difficult to be sufficiently resolved by the deconvolution algorithm. Therefore, the centre and width values for these peaks can be disregarded as insignificant above the NFH heat treatment temperature of 400°C. The constant centre and increase in width of the N1s peak for HFH and LFH (and the low temperature NFH), suggest that the range of nitrogen surface species present on these chars remains relatively constant, but with a small increase in distribution.

The total surface nitrogen content decreases for all the nitrogen bearing resins during pyrolysis. In the case of NFH the nitrogen surface species are completely removed at 400°C, and for HFH and LFH the relationship between surface N/C ratio and temperature exhibits a linear, but decreasing, trend, suggesting a moderate loss of surface nitrogen in these resins. As this phenomenon parallels the removal of nitrogen from the resins' bulk, it is unlikely that there would be a significant collection of nitrogen on the char surfaces during the pyrolysis process.

The change in surface O/C ratio for the resins over the temperature range (Figure 8.15) shows a trend of overall loss for the surface oxygen species, with a generally large scatter of results over the entire range, particularly for heat treatments above 600°C. The larger proportion of surface oxygen at the lower temperatures is indicative of the surface hydroxyl groups which would exist due to the phenol and furfuryl-alcohol groups.

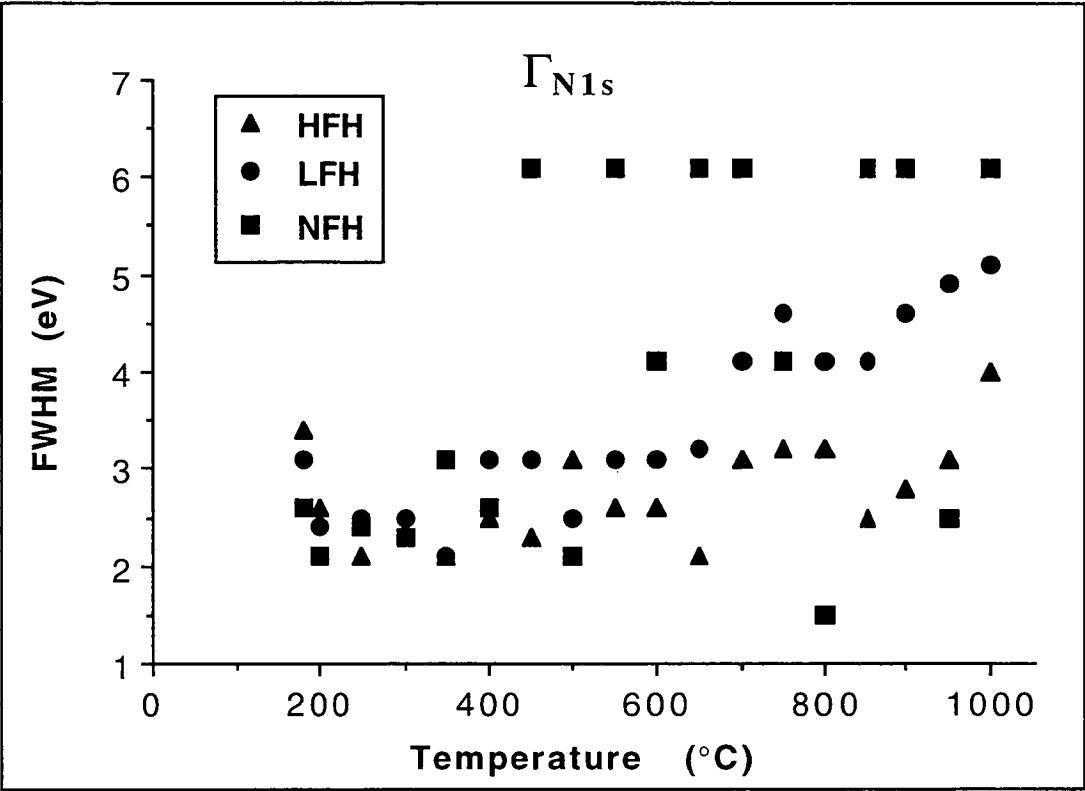


Figure 8.13 Variation of the width of the N1s band, Γ_{N1s} , for the six resin chars over the heat treatment temperature range.

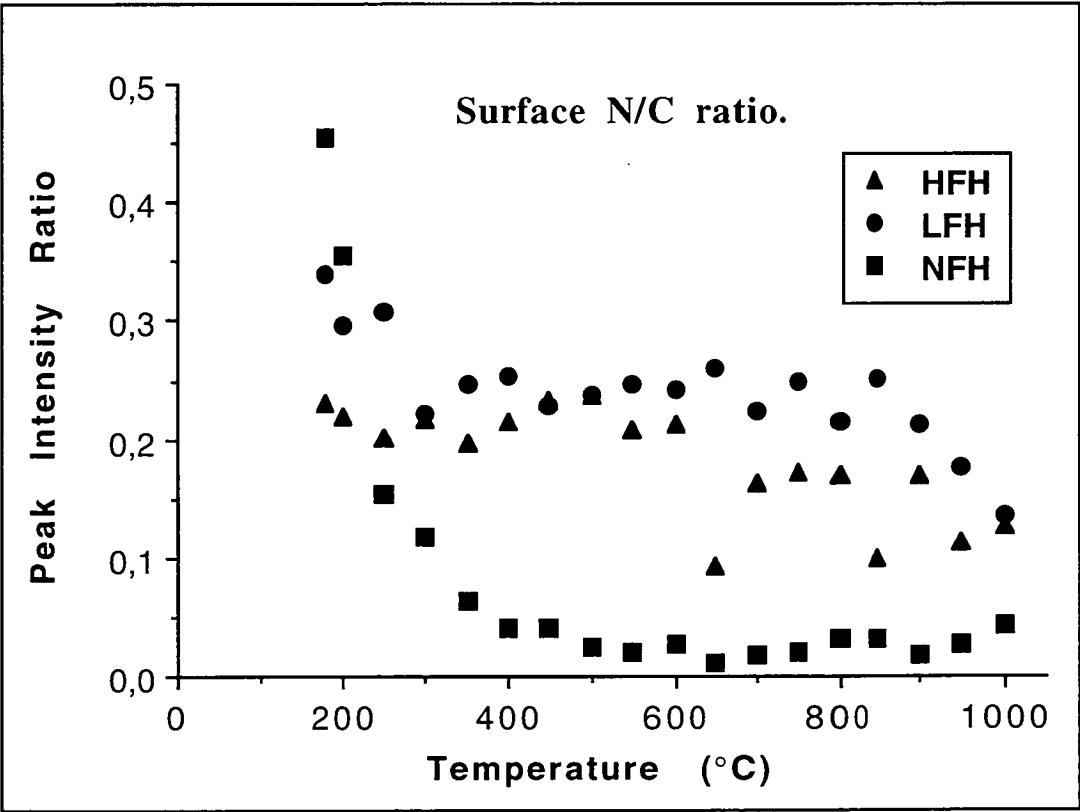


Figure 8.14 Surface N/C ratio of the six resin chars over the heat treatment temperature range.

can only be used to describe all the resins as they are pyrolysed to 1000°C. It is therefore suggested from these results that each unpyrolysed resin contains a range of carbon and oxygen bond species at the surface. As the resins pass through their heat treatment a greater proportion of the surface carbons become bonded to oxygen atoms in one particular mode with a decreasing proportion of the surface carbons being bonded to hydrogens. As the chars reach 700°C, the surface CH_x bonds are almost completely removed and C–O is the most prominent. Although the carbon oxides are seen to increase proportionally to the total amount of surface carbon due to the loss of other carbon species, the total amount of oxygen is seen to decrease with temperature, suggesting the failure of the carbon to retain oxygen at the surface.

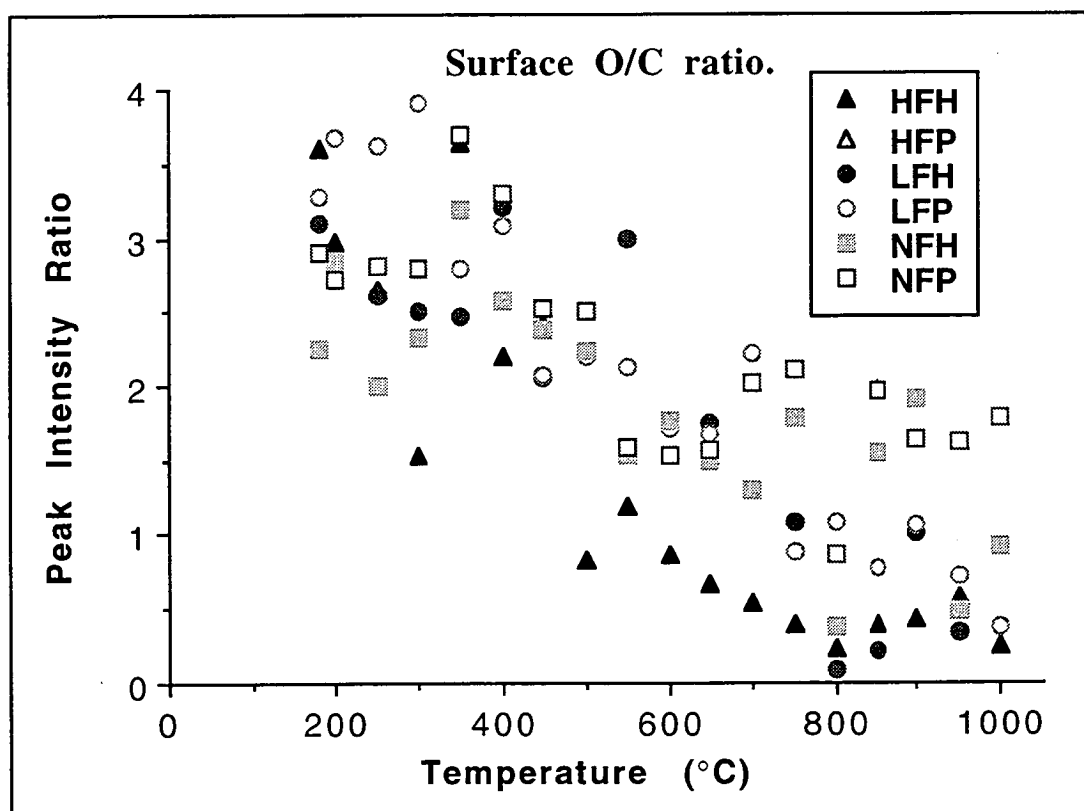


Figure 8.15 Surface O/C ratio of the six resin chars over the heat treatment temperature range.

As the changes in surface elemental analyses of the chars are very similar to the changes of those of the bulk sample, it is likely that there is little change in the surface chemistry of the chars that is independent of the changes of the bulk sample chemistry. Therefore, unlike activated carbons, or those graphites electrolytically treated to enhance the effects of surface oxidation [Brown *et al*,1981; Galuska *et al*,1988; Kozlowski and Sherwood,1986; Marsh and Menendez,1989], these carbons act with the characteristics of glassy carbons, where the surface remains largely inert and unaffected by the release of the volatiles from the bulk of the sample.

Chapter Nine

The comparison of experimental data for the determination of the Phenolic Resin carbonisation reaction mechanism.

Pyrolysis Reaction Mechanism of Novolac Phenolic Resins

A pseudo pyrolysis reaction mechanism may be established for each of the six resins in the 180 - 1000°C heat treatment temperature range based on the experimental results shown in this study. A further model of crystalline development of the six resin chars up to 2200°C can be put forward from the results of the Raman spectroscopy analyses. The overall pyrolysis mechanism of these novolac phenolic resins can be considered as involving the following four temperature ranges; post-cure (180°C) - 350°C, 350 - 750°C, 750 - 1000°C and 1000 - 2200°C. As the curing process requires the resins to be baked to 180°C, this temperature will be considered the starting temperature of the pyrolysis cycle. For the TGA experiments, which rely on the initial condition of room temperature, these experiments will be considered as having commenced at 25°C. Therefore, each particular pyrolysis mechanism will be discussed in reference to the temperature range in which it occurs.

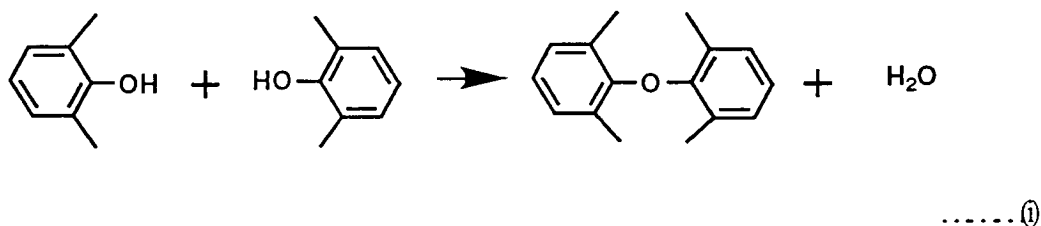
Pyrolysis Mechanism 25 - 350°C.

Polyphenol-formaldehyde (phenolic) resins can be considered as being only partially cross-linked initially, and as giving only broad exothermic differential thermal analysis (DTA) peaks due to curing (further cross-linking) [Dollimore and Heal,1967]. The furfuryl-alcohol present in the resin can also exhibit exothermic decomposition and the double bonds within the furan ring can be used for further cross-linking within the resin system [Riesz and Susman,1960]. From the TGA results in Figures 4.1 and 4.2, it is shown for both R3 (3°C/min) and R10 (10°C/min) ramp rates that HFH experiences a prominent weight loss of 5% in the 100 - 200°C range, whereas the other five resins lose little of their initial mass up to 200°C. These five resins (not HFH) slowly lose material to a 5% weight loss up to 350°C for both ramp rates. The DTG curves (Figures 4.3 and 4.4) also exhibit for both R3 and R10 ramp rates the presence of a peak at 200°C for HFH and no peak at

this temperature for the other resins. This would suggest a major reaction initially for HFH. The DTGA curve in Figure 5.5 also shows this phenomenon, which suggests that the model conditions in the TGA experiment were also well modeled in the laboratory pyrolysis reaction tube of this study.

From the elemental analyses (Figures 4.6 - 4.9) it is shown that carbon and hydrogen are removed from each resin in a stoichiometric ratio that remains constant and equal for each resin up to 350°C. In contrast, the nitrogen content is seen to remain constant for HFH and LFH up to 350°C, but all of the nitrogen in NFH is removed in the 180 - 350°C temperature range. As the atomic % oxygen shows a small loss of oxygen for the resins to 300°C, it is possible that the nitrogen from NFH is removed as a nitro-oxide.

The residual atomic compositions of the resins show that 20% of their initial carbon and hydrogen content, and 30% of their initial oxygen is lost to 350°C. Combining this data with the large water evolution peak (Figure 4.14) and furfuryl-alcohol loss peak (Figure 4.15) at 200°C for HFH suggests that the main reaction mechanism for this resin is the release of water and furfuryl-alcohol up to 300°C. Moderate H₂O evolution is also shown for the other resins up to 350°C, and as no other major organic volatile species are detected as being released below 350°C, H₂O production is considered to be the main reaction for the all resins in the low temperature range. This hypothesis is also shown by FTIR, as the loss of hydroxyl peaks and the shifting of a diphenyl-ether vibration gave indication of the following reaction (i) [Morterra and Low,1985a; Ouchi,1966; Yamashita and Ouchi,1981]:



This reaction mechanism is seen to occur in all resins between 200°C and 350°C and is complemented by a reduction of aromatic OH (Figure 6.15) in the range 180 - 250°C.

In addition to the evolution of H₂O, the mechanism of cross-linking between phenolic chains is considered important in each resin in the 180 - 350°C temperature range. From the FTIR analysis resins HFP and LFP exhibit high initial *ortho-ortho'* linearity at 180°C, HFH exhibits moderate *o-o'* linearity and LFH a low degree of *o-o'* phenolic bridge formation at 180°C. Resin HFP retains the highest degree of *o-o'* linking to 350°C, whereas LFP and NFP are seen to experience some *para* substitution. Resins HFH and LFH are further reduced in *o-o'* linearity with increasing temperature to 350°C, and that of NFH is greatly reduced to 200°C, and then further reduced to 350°C.

When combined, the nmr and FTIR results yield the following information. Resins HFP and LFP both display the highest proportion of *o-o'* chain linking initially, and in both cases the proportion decreases with increasing temperature to 350°C. Resin NFP shows conflicting results between the two analytical methods, although it is likely that the *o-o'* linking would be low due to the nmr results (Figures 6.17 - 6.20) which exhibit low *para-para'* and high *ortho-para* linking, but low initial cross-linking in this resin. In resins HFP and LFP the proportion of all the aliphatic carbons is seen to decrease (Figure 6.17), with a particularly rapid decrease in the *o-p* and *p-p'* aliphatic linkages, and this is accompanied by an increase in cross-linking to 350°C. Resin NFP exhibits a similar decrease in the high proportion of *o-p* aliphatics with a constant level of *p-p* substitution to 350°C, and the low initial cross-linking of this resin is increased to its heat treatment of 350°C.

Resins HFH and LFH both exhibit a further reduction of their initial low levels of *o-p* linking, whereas NFH exhibits a reduction in its initially high level of *o-p* and low level of *o-o'* linking with increasing temperature to 350°C. In addition, resins

HFH and LFH initially exhibit moderate levels of cross-linking, which increase with temperature, whereas NFH exhibits the lowest level of cross-linking of all the resins at the start of the pyrolysis process, with only a small increase in cross-linking to 350°C.

From these results it is suggested that the combination of furfuryl-alcohol and paraformaldehyde in the novolac resin provide for *ortho-ortho'* bridge formation in the phenolic chains and a highly cross-linked *para-para'* structure between the chains. This extensively cross-linked polymerisation is enhanced by the paraformaldehyde which provides the aliphatic chain linkages between phenolic units. The furfuryl-alcohol present in the resin is important in providing a certain degree of *o-o'* linking although it is more important in creating a highly cross-linked structure. The level of furfuryl-alcohol has little effect on the initial degree of cross-linking, particularly as much of the furfuryl-alcohol is volatilised from HFH around 200°C. The detection of furfuryl-alcohol removal from only the furfuryl-alcohol/hexamine bearing resins suggests that in the furfuryl-alcohol/paraformaldehyde bearing resins there is a chemical reaction during curing and up to 300°C which effectively incorporates the furfuryl-alcohol and paraformaldehyde into the phenolic network of the resin. Although paraformaldehyde is shown as a more effective agent than hexamine for cross-linking and *o-o'* linearisation, a total lack of furfuryl-alcohol from either type of resin causes poor cross-linking overall.

In the 180 - 350°C temperature range, the degree of lattice ordering cannot be determined from Raman Spectroscopy due to the problem of fluorescence in complex organic systems such as low temperature resins. This structural complexity also presents a large range of single bonded carbon oxide surface species. The nitrogen surface species are relatively constant in their composition to 400°C, and are likely to be either amine/amide or cyano/pyridine structures. The surface O/C and N/C ratios show that the surface chemistry for the resins, during the low

temperature pyrolysis process, is similar to their bulk chemistry, suggesting that there is little surface activity of the resins to 350°C. In particular, NFH shows a total loss of surface nitrogen in the 180 - 350°C temperature range, at a rate that parallels the loss of nitrogen from the bulk sample in the same temperature range. This suggests that none of the nitrogen removed from the bulk sample remains on the surface of the sample for NFH. Resins HFH and LFH show little nitrogen loss to 350°C. This observation provides for the hypothesis that the combination of furfuryl-alcohol and hexamine aids both resin additives in their incorporation to the resin system. The lack of furfuryl-alcohol in NHF causes the under-utilised hexamine to leave the system as NH or an NO species, and the hexamine fails to provide cross-linking in the resin structure at higher pyrolysis temperatures.

Pyrolysis Mechanism 350 - 750°C.

From the TGA results (Figures 4.1 and 4.2), the main pyrolysis mass loss mechanisms take place in the 350 - 750°C temperature range for both the 3°C/min and 10°C/min heating rates. The greatest rate of mass loss is shown to be at 450°C for all resins except NFH which shows a delayed reaction mechanism, such that the greatest rate of mass loss (DTG) for NHF takes place at 550°C. This phenomenon is shown to occur regardless of the heating rate.

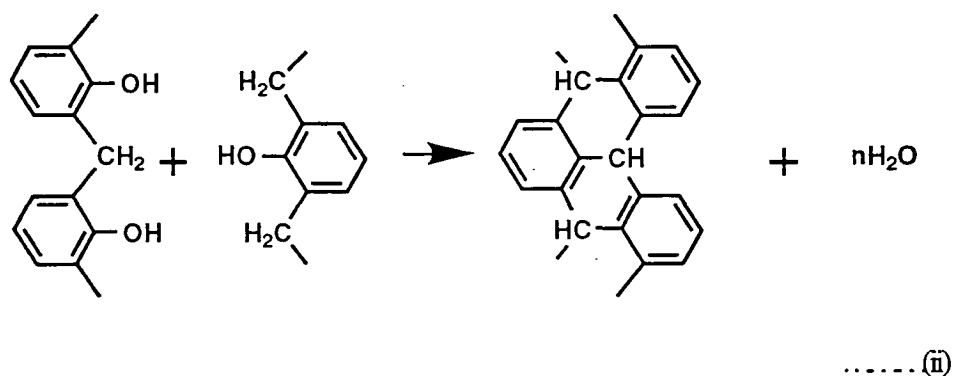
The four furfuryl-alcohol containing resins show similar mass-loss patterns such that they lose approximately 45% of their mass in the 350 -750°C temperature range for both the R3 and R10 resins. The non furfuryl-alcohol containing resins show a lower degree of mass loss in this temperature range, with NFP losing 32% of its mass at 3°C/min and 35% at 10°C/min, and NFH losing 30% for both ramp rates. Resin NFH also exhibits a greater maximum mass loss rate for R3 than R10, suggesting that the slower heating rate allows for faster pyrolysis reaction kinetics. Resin NFP exhibits two DTG peaks at 400°C and 550°C at both heating rates,

suggesting that two major mass loss mechanisms exist for this resin in the 350 - 750°C temperature range.

The change in atomic % carbon over this heat treatment region exhibits a steady linear increase in carbon proportion, which is equivalent for all the resins from 50% at 350°C to an average of 80% at 750°C. The change in carbon residual atomic % shows little absolute carbon loss from the NFH system in the 350 - 750°C temperature range, although there is a sharp increase in carbon loss from the other five resins between 300 and 600°C, which is accompanied by an increase in the degree of hydrogen and oxygen loss from the resins. In this temperature range HFH and LFH lose little nitrogen, whereas almost all of the nitrogen present in resin NFH has been removed to 350°C and therefore this resin can have no further nitrogen removal above this temperature. It is therefore likely that NFH loses only H₂ and H₂O as its main volatilised products above 350°C.

From liquid volatiles analysis (Figures 4.14) it is shown that the main pyrolysis product in the 350 - 750°C temperature range is H₂O. The main water evolution occurs at 450°C for all resins except NFH, which exhibits a main water evolution at 550°C. This phenomenon parallels the TGA results which again suggest that water evolution is the main reaction process occurring in these resins. Accompanied by FTIR data, it is shown that the main reaction in the pyrolysis process of these resins is the production of H₂O as shown by the mechanism in Scheme (ii) which is most prominent at 400 - 450°C, but is seen to continue to 550°C [Morterra and Low, 1985a; Ouchi, 1966; Yamashita and Ouchi, 1981]. This reaction is seen to occur following the reaction in Scheme (i) as described previously. The mechanism of Scheme (ii) indicates the commencement of poly-aromatic condensation. This ring condensation continues as the hydrogens are removed from the bridge methine groups, and later from the rings themselves. No further furfuryl-alcohol loss is observed for HFH and LFH above 350°C, although the loss of more complex

organic material by volatilisation (although much less than the degree of water loss) shows interesting results between the resins.



The evolution of phenol and cresol species (Figures 4.16 - 4.20) occurs predominantly between 450 and 500°C. The double ring xanthene species, which is indicative of ring fusion and poly-aromatic structural formation, are fully released at 550°C (Figures 4.21, 4.22 & 4.23). The single ring phenol and cresol species are shown to evolve from NFH at temperatures of 100°C higher than the other five resins, to levels lower than those of the other resins, and no bis-cresol is observed to have evolved from resin NFH. Resin NFP exhibits a loss of phenol twice that of LFH and LFP, and 4 times that of the other resins at 450°C, which suggests that the lack of furfuryl-alcohol allows for easy breaking of phenolic end groups from the chains with replacement by methylene groups from the paraformaldehyde chains. In NFH it is likely that the evolution of phenols and other organic volatiles is impeded by the formation of a glassy char due to the transformation of this resin to a molten mesophase at 200°C.

The evolution of methylated phenol (cresol) species is greatest from LFH and LFP, and as these phenolic chain fragments are indicative of 2,4,6 substitution it is likely that LFH and LFP undergo the greatest degree of cross-linking. Resin NFP is shown to release less of the phenolic molecules as these ring species increase in degree of methyl substitution, i.e., more phenol is evolved from NFP than cresol,

which exhibited a greater evolution than methyl-cresol. Therefore, as it is shown that an increase in furfuryl-alcohol in the resin allows for an increase in the evolution of mono- and di- methyl substituted phenols, it is likely that furfuryl-alcohol acts to a large part as a methylating agent for the phenolic groups in the chain structure, thereby aiding in cross-linking of the chains. This methylation is aided by the availability of methyl groups from paraformaldehyde, and to a lesser extent, hexamine.

The release of bis-cresol from the three paraformaldehyde containing resins during pyrolysis in the 350 - 750°C temperature range suggests that extensive cross-linking is most prominent in LFP and NFP, and to a lesser extent HFP. Again, this indicates that the combination of furfuryl-alcohol and paraformaldehyde are important for providing CH₂ groups for cross-linking. As NFP evolved little methyl-bis-cresol, it gives further evidence for the role played by furfuryl-alcohol in the cross-linking process, due to the ability of this molecule to provide hydroxyl groups that are either incorporated into the structure or lost as water. The evolution of the xanthene species provides further evidence that the level of evolution of each fused ring species from NFP decreases by a factor of 2 for each additional methylene group substitution. This adds to the theory that furfuryl-alcohol assists in methylating and cross-linking the phenolic groups as the condensed aromatic regions extend themselves.

The evolution of simple xanthene groups from NFP in the 350 - 750°C temperature range suggests that crystalline development by ring condensation can begin in these resins at temperatures as low as 450°C, as fused ring organic species such as xanthenes are indicators of such phenomena. From the FTIR and nmr data it is shown that the degree of *o-o'* linearity for NFP remains constant to 550°C and then decreases rapidly. This pattern is also found in the change in *p-p'* linearisation, except for LFP where both *o-o'* and *p-p'* bridge formations are seen to decrease as the temperature is increased above 350°C.

The extent of cross-linking of LFH and LFP is found to increase further to 500°C, whereas that of the other resins remains constant at a moderate level. The FTIR analysis shows the start of C=C formation at 550°C, and as CH and CH₂ bridges are removed by 600°C, polycondensation occurs. The results from nmr analyses show that the fraction of aromatic carbons, f_{ar} , increases slowly with temperature from a moderate level for all resins (except LFP with its low f_{ar} at 350°C) to 550°C where the f_{ar} of all resins is then increased rapidly to 700°C. Polycondensation is seen to have occurred for all the resins at 700°C, providing a pseudo-crystalline lattice structure.

The residual atomic % carbon (Figure 4.10) shows that the process of carbon loss from all of the resins ceases at 600°C, with oxygen loss ceasing at 600°C for NFH and LFH, and at 700°C for the other four resins. This latter loss of oxygen at 700°C for the paraformaldehyde cured resins and HFH is attributed to continued water evolution up to 700°C due to the loss of OH groups as they are stripped from the phenolic rings prior to poly-aromatic condensation. This phenomenon is also shown by the continued reduction of the level of hydroxyl aromatic carbons, f_{ar}^{OH} , (Figure 6.15) from a moderate level at 500°C to $\approx 0\%$ at 700°C for all resins. Resin LFP is seen to lose OH groups at lower temperatures which suggests that the stripping of OH groups allows for more extensive cross-linking in this resin at lower temperatures in the pyrolysis process.

The level of protonated aromatic carbons, f_{ar}^H , continues to decrease to $\approx 0\%$ above 700°C for all resins, except LFP, in whose resin char the aromatic hydrogens have already been removed due to cross-linking below 700°C. This phenomenon is evident due to the loss of atomic hydrogen, as shown by the continued decrease of residual atomic % hydrogen (Figure 4.11) to 800°C. Therefore, as the phenolic rings begin to condense at 500 - 550°C, the OH groups are stripped due to cross-linking, and this process continues with ring condensation to 700°C. At this

temperature the protons from the unsubstituted ring sites are removed from the structure while simultaneously releasing H₂ gas [Ouchi,1966].

In terms of poly-aromatic lattice growth it is shown (Figures 6.23 & 6.24) that ring fusion is negligible in the 180 - 400°C temperature range according to the definitions of the two aromatic cluster size parameters; D, the aromatic ring cluster diameter; and r, the number of aromatic rings per cluster. Using D as a model for lattice growth lattice formation is initiated by the nucleation of a poly-aromatic centre, followed by lattice growth due to the condensation of neighbouring phenolic groups into the structure. The lattice growth is slow between 400°C and 550°C due to the presence of protons and OH groups on the unbridged aromatic carbon sites. Poly-aromatic lattice growth is accelerated above 550°C, and as occurs with the OH groups, unsubstituted aromatic protons and aliphatic bridge protons are removed, and the neighbouring cross-linked polymeric networks can join the already condensed structures to form larger regions of the pseudo-crystalline lattice. According to this model, and using LFP as an example, the combination of furfuryl-alcohol and a sufficient level of paraformaldehyde creates a highly cross-linked structure early in the pyrolysis process of these resins. As this allows for a lattice *skeleton* at lower temperatures, a more extensively formed poly-aromatic lattice exists in LFP than in the other resins at 700°C, i.e., $D_{700} \approx 125 \text{ \AA}$ for LFP, $D_{700} \approx 50 \text{ \AA}$ for LFH, and $D_{700} \approx 20 - 40 \text{ \AA}$ for HFH, HFP, NFH and NFP. As many functional groups are retained in NFH and NFP, the poly-aromatic nuclei of these particular resins are observed as being small and poorly formed.

Raman spectroscopy shows only a moderate increase in lattice order from 600 to 750°C, and this is mainly caused by the removal of hetero-atoms rather than by lattice alignment. Therefore, at these relatively low temperatures the poly-aromatic lattice is still too defective to allow crystalline development. It is also shown that the variety of carbon species present in the lattice between 600°C and 750°C causes a variety of distortion modes within the lattice.

The surface chemistry of the chars shows that with the loss of hydrogen, the surface carbon species are refined to those of a more ordered nature at 700°C. The proportion of surface C-O groups is increased to 700°C which suggests that many of the surface carbons are oxidised. In contrast, the surface O/C ratio (Figure 8.15) is decreased almost linearly with temperature to 700°C. This suggests that although the surface carbons are mostly refined to ideal crystalline carbons in parallel with the carbons of the bulk sample, there is a proportion of surface carbons that are oxidised as the temperature is increased to 700°C. As this phenomenon ceases at 700°C, it is possible that this oxidation of surface carbons occurs by a reaction with evolved H₂O, with a possible further production of C-OH surface groups. From the surface O/C ratio, it is shown that oxygen is removed from the surface at approximately the same rate as that of the oxygen from the bulk sample, which suggests that surface oxidation is a minor phenomenon below 700°C.

The surface N/C ratios (Figure 8.14) for HFH, LFH and NFH show that there is no surface nitrogen present in NFH above 400°C. The surface nitrogen of LFH is seen to remain constant between 350°C and 750°C, whereas that of HFH is seen to decrease in this temperature range. The band widths of the N1s peak from the spectra of HFH shows that there is no increase in the variation of surface nitrogen species in the 350 - 750°C temperature range, whereas that of LFH exhibits an increase in the selection of surface nitrogens from 500 to 750°C. The loss of bulk nitrogen from NFH is paralleled by the complete removal of surface nitrogen, suggesting that there were no specific surface reactions involving nitrogen for the NFH resin. This is indicated as also being true for HFH, whereas LFH, which may contain nitrogen species in the bulk due to reactions with furfuryl-alcohol, provides for a proportion of these nitrogen bearing species in the bulk to remain bound to the char surface upon volatilisation.

Pyrolysis Mechanism 750 - 1000 °C.

The major pyrolysis chemical reactions are considered to have been completed below 750°C, and this is shown by the negligible mass loss for both R3 and R10 resins above 750°C. The two furfuryl-alcohol free resins, NFH and NFP, exhibit less overall weight loss due to the lack of cross-linking at lower temperatures, allowing for the production of a molten meso-phase (as discussed previously) which subsequently impedes the release of the organic volatile species. The main mass loss mechanism above 750°C is that of the release of aromatic protons, which allows for rapid and extensive increase in aromatic ring condensation and increased ordering of the lattice. The release of nitrogen from HFH and LFH is observed, as is the evolution of minor amounts of water between 750 and 800°C, although no organic species are evolved in this temperature range. This lack of chemical activity is also demonstrated by the termination of useful nmr data above 700°C (750°C for NFP) due to the lack of protons available for cross-polarisation of the carbon nuclei in the magnetic field of the spectrometer. Also, in this study FTIR spectroscopy data exhibited little practical use for resins heat treated to temperatures above 700°C due to the almost complete degree of C=C functionality in the aromatic network. Therefore, from the nmr data of resins heated to 700°C, the lattice is considered to be of a near complete ring structure (no aliphatic carbons) for all six resins above heat treatments of 750°C. The results of Raman spectroscopy show that the resins increase in lattice twisting and structural defects between 700 and 900°C, although this is countered by a reduction in the proportion of defects due to hetero-atoms, which gives little overall change in lattice order in this temperature range.

It is shown from the variation of the 1350 cm⁻¹ Raman band width over the 750 - 1000°C temperature range (Figure 7.6) that the structural defects are refined to being mainly those of lattice ring twisting between 900 and 1000°C, as the tetrahedral and aliphatic carbons are converted to poly-aromatic ring carbons. This is complemented by a refinement in structural order as the graphite (1575 cm⁻¹) band width is greatly

reduced between 900 and 1000°C (Figure 7.8). Little refinement of the hetero-atom defects is shown in this temperature interval. It can therefore be suggested that this defect mode may be due to only one hetero-atom type, which in this case is most likely to be oxygen as there is little difference in the 1500 cm⁻¹ band width between NFH (which completely lacks nitrogen at these high temperatures) and the nitrogen bearing HFH and LFH chars.

There is a sharp reduction in structural defects between heat treatments of 900 and 1000°C in all resins except NFH, which is possibly due to the residual functional groups present in this resin at these higher pyrolysis temperatures. Resin LFP exhibits the greatest reduction in proportion of structural defects between 900 and 1000°C. This phenomenon is reversed for the proportion of defects due to hetero-atoms, such that the level of these latter defect-types exhibits little reduction for LFP in the 900 - 1000°C temperature range but that the other resins exhibit a reduction in this defect, the greatest of which is shown in NFH. The respective levels of the two defect types are balanced such that there is a very sharp rise in degree of lattice ordering for all six resins from 900 to 1000°C.

The alteration of surface chemistry of these resins presents the elemental graphitic carbon as the predominant surface species, which varies little in proportion in the 750 - 1000°C temperature interval. The proportion of surface carbon oxides also remains constant for all resins in this temperature range. The variation in band width of the N1s peak for LFH and NFH (Figure 8.13) shows that the variety of different surface nitrogen species increases between 850 and 1000°C. The surface N/C ratio (Figure 8.14) shows that the amount of surface nitrogen for HFH remains constant, but that for LFH it is reduced in this temperature range to the same level as that of HFH. The surface O/C ratios for all the resins (Figure 8.15) exhibit a relatively constant level of surface oxygen above 800°C, which approximately parallels the constant level of C-O oxide species between 800 and 1000°C. This cessation in surface oxidation above 750°C, combined with a minimal level of nitrogen surface

activity in respect to the bulk chemistry of the resins, suggests that the carbons formed by the pyrolysis of these resins to 1000°C are primarily of a glassy nature [Marsh and Menendez,1989], which, unlike activated carbons, show little chemical surface activity.

Pyrolysis Mechanism 1000 - 2200°C.

The only evidence in this study of any carbon lattice alteration above 1000°C for the six resins is exhibited by Raman spectroscopy. For the R3 resins (those pyrolysed at a heating rate of 3°C/min) ordering in the lattice structure is seen to increase linearly from an average S_{1570} of 35% at 1000°C to 47% at 2200°C (Figure 7.5). A similar pattern is shown for the S_{1570} values of the R10 (10°C/min) resins, although the increase in lattice order of these resins from 1600 to 2200°C is slowed after a rapid increase in lattice refinement between 1000 and 1600°C (Figure 7.11). The greater degree of lattice ordering for the R10 resins is likely to be due to their greater removal of organic functional groups in the 350 - 750°C temperature range (Figures 4.1 and 4.2). The exception to this theory is resin LFP, which exhibits an equivalent degree of lattice development for its R3 and R10 chars at 1600°C. The degree of lattice ordering is equal for all six resins and for both the R3 and R10 heating rate at 2200°C, which suggests that pyrolysis heating rate or initial phenolic resin formulation has little effect on lattice order at this temperature. The proportion of defects due to lattice distortion in the R3 resins remains relatively constant over the 1000 - 2200°C temperature range, except for the S_{1350} values of NFH, which remain high at 1000°C due to the residual organic functionalities remaining in the lattice of this resin. These distortions remain in NFH to 1600°C, above which they are reduced to the same level as those of the other resins at 2200°C (Figure 7.3).

The S_{1350} values for the R10 resins demonstrate that these resins undergo a slight increase in the proportion of distortion defect present in their lattice structures from

1000 to 1600°C, followed by a decrease to a level higher than that of the R3 resins at 2200°C. In the 1000 - 1600°C temperature range the S_{1500} values demonstrate that the removal of hetero-atoms, and the lattice defects that they produce, is similar for both R3 and R10 resins, although at 2200°C there are no hetero-atom defects in any of the R10 chars (Figure 7.10), whereas some level of defect remains for the R3 chars of HFH, HFP, LFH and NFP (Figure 7.4).

It is possible that the pyrolysis at 10°C/min removes a greater amount of hetero-atoms in the lower pyrolysis temperatures (180 - 1000°C), although this higher heating rate also fails to allow sufficient time for aromatic ring lattice development in the 600 - 1000°C temperature range, whereas the slower 3°C/min heating rate provides sufficient time at each temperature range for rearrangement of the poly-aromatic carbon structure to form an ordered lattice. This trend is also shown in the variation of the various Raman band widths, where the half-width of the 1500 cm^{-1} band, Γ_{1500} , exhibits a higher degree of refinement of the variety of hetero-atom defects for the R10 resins up to 2200°C, whereas the range of variation of this defect is quite wide in the R3 resins between 1000 and 1600°C, and to a lesser extent to 2200°C.

In general, the crystalline development of the chars progresses at a relatively constant level to 2200°C. As the pyrolysis heating rate is increased for the 180 - 1000°C heat treatment of the resins, their lattice development below 1600°C is facilitated to a greater extent by the removal of hetero-atoms than by structural ordering due to the realignment of areas of distortion and twisting. Very little difference is shown in the level of lattice order of these resins to 2200°C, and therefore their crystalline development to this temperature is suggested as being independent of heating rate in the 3 - 10 °C/min range. The crystalline development of these resins above 1600°C is also independent of the level of furfuryl-alcohol in the resin formulation, or whether the co-curing agent is paraformaldehyde or hexamine.

Further Study and Experimentation

As has been shown by the results of Raman spectroscopy analysis the differences in lattice structure of these resins are mainly detected between 750 and 1000°C, although by using the degree of ring condensation and poly-aromatic cluster growth as the parameters for the determination of lattice development, the most important temperature range to be studied for these resins is of their pyrolyses between 350 and 750°C. The main pyrolysis chemical reactions have been shown to occur in this temperature range, and therefore such measurements as the removal of methylene bridges, hydroxyl groups and aliphatic (bridge) and aromatic (ring) protons from the resins are very important when studying these resins in terms of their ability to form partially-ordered pseudo-crystalline carbon structures to heat treatment temperatures of 1000°C

Important further experimentation would include the detection and measurement of evolved H₂O, CO, CO₂, small alkane and alkene hydrocarbons, H₂ and nitrogen bearing volatiles such as NH₃ during the 180 to 1000°C resin heat treatment. These evolved volatiles could be selectively analysed by Mass Spectrometry or a combination of Gas-Chromatography/Mass-Spectrometry during pyrolysis of the resins by directly analysing the off-gas stream from the outlet of the pyrolysis reactor vessel. From these analyses a better determination of the important reactions could be established during carbonisation of the resins, especially in the 350 - 750°C temperature range.

Bibliography

- Aksela H. and Aksela S., (1974), "M_{4,5}N_{4,5}N_{4,5} and M_{4,5}O₁ Auger Electron Spectra from Cadmium Vapour.", *J. Phys. B.*, **7**, 1262.
- Amelinckx S., Dlavignette P. and Heerschap M., (1965), *Chemistry and Physics of Carbon* (ed. Walker P.L.), Marcel-Dekker, New York.
- Amram B. and Laval F., (1989), "Graphitisation Studies of Cured Phenolic Resins by High-Resolution ¹³C-Cross-Polarisation Magic Angle Spinning Solid-State NMR Spectroscopy.", *J. Appl. Polymer Sci.*, **37**, 1.
- Andrew E.R., (1971), "The Narrowing of NMR Spectra of Solids by High-Speed Specimen Rotation and the Resolution of Chemical Shift and Spin Multiplet Structures for Solids.", *Prog. Nucl. Magn. Reson. Spectr.*, **8**, 1.
- Aranguren M.I., Borrajo J. and Williams R.J.J., (1982), "Some Aspects of Curing Novolac with Hexamethylenetetramine.", *J. Polym. Sci.: Polym. Chem. Ed.*, **20**, 311.
- Axelsson D.E., (1987), "Spinning Sideband Suppression and Quantitative Analysis in Solid State ¹³C NMR of Fossil fuels.", *Fuel*, **66**, 195.
- Bancroft G.M., Brown J.R. and Fyfe W.S., (1979a), "Advances in, and Application of, X-ray Photoelectron Spectroscopy (ESCA) in Mineralogy and Geochemistry.", *Chem. Geol.*, **25**, 227.
- Bancroft G.M., Gupta R.P., Hardin A.H. and Ternan M., (1979b), "Quantitative Electron Spectroscopy for Chemical Analyses of Bitumen Processing Catalysts.", *Anal. Chem.*, **51**, 2102.
- Bansal R.C. and Dhama T.L., (1980), "Surface Characteristics and Surface Behaviour of Polymer Carbons. (IV). Adsorption Isotherms of Organic Vapours.", *Carbon*, **18**, 137.
- Bauman R.P., (1962), *Adsorption Spectroscopy*, Wiley, New York, pp 585.
- Beeman D., Silverman J., Lynds R. and Anderson M.R., (1984), "Modeling Studies of Amorphous Carbons.", *Phys. Rev.*, **B31**, 870.
- Beny-Bassez C. and Rouzaud J.N., (1985), "Characterization of Carbonaceous Materials by Correlated Electron and optical Microscopy and Raman Microspectroscopy.", *Scanning Electron Microscopy*, **I**, 119.
- Bhagavantam S. and Venkatarayuda I., (1939), "The Raman Effect in Relation to Crystal Structure.", *Proc. Indian Acad. Sci.*, **9A**, 224.
- Bloch F., (1959), "Theory of Line Narrowing by Double Frequency Irradiation.", *Phys. Rev.*, **111**, 841.
- Botto R.E. and Winans R.E., (1983), "Characterization of Whole Coals by ¹³C CP/MAS Spectroscopy at High Field.", *Fuel*, **62**, 271-273.

- Bowling R.J., Packard R.T. and McCreery R.L., (1989), "Activation of Highly Ordered Pyrolytic Graphite for Heterogeneous Electron Transfer: Relationship Between Electrochemical Performance and Carbon Microstructure.", *J. Am. Chem. Soc.*, **111**, 1217.
- Brillson L.J., Burstein E., Maradudin A.A. and Stark T., (1971), *J. Phys. Chem. Solids Suppl.*, **32**, 187.
- Briggs D, *Handbook of X-ray and Ultraviolet Photoelectron Spectroscopy*. Heydon; London, Philadelphia, (1978) xiii, 398 pages.
- Brown J.R., Kronberg B.I. and Fyfe W.S., (1981), "Semi-quantitative ESCA Examination of Coal and Coal Ash Surfaces.", *Fuel*, **60**, 439.
- Bryson R.L., Hatfield G.R., Early T.A., Palmer A.R. and Maciel G.E., (1983), "¹³C NMR Studies of Solid Phenolic Resins Using Cross Polarisation and Magic-Angle Spinning.", *Macromolecules*, **16**, 1669.
- Camino G., Luda M.P., Costa L. and Trossarelli. E., (1982), "Thermal Analysis.", *12th Intern. Conf. Thermal Analysis*, **II**, 1137.
- Casiraghi G., Sartori G., Bigi F., Cornia M., Dradi E. and Casnati G., (1981), "A novel synthetic route to all-ortho Novolac Resins.", *Makromol. Chemie*, **182**, 2151.
- Chiu K.S. and Biemann K., (1984), "Structural Characterisation of Polycyclic Aromatic Compounds by combined Gas Chromatograph/Mass Spectrometry and Gas Chromatography/Fourier Transform Infrared Spectrometry.", *Anal. Chem.*, **56**, 1610.
- Christu N., Fitzer E., Kalka J. and Schaefer W., (1969), "Carbonisation of Organic Compounds and Polymers.", *J. Chim. Phys.*, **50**.
- Chuang I., Maciel G.E and Myers G.E., (1984), "¹³C NMR Study of Curing in Furfuryl Alcohol Resins.", *Macromolecules*, **17**, 1087.
- Colthup N.B., Daly L.H. and Wiberley S.E., (1975), *Introduction to Infrared and Raman Spectroscopy*, Academic Press, New York.
- Conley R.T., (1965), "Oxidative Degradation of Phenol-Formaldehyde Polycondensates Initial Degradation Reactions.", *J. Appl. Polymer Sci.*, **9**, 1117.
- Conley R.T., (1970), *Thermal Stability of Polymers*., Chapter 11, Marcel-Dekker, New York.
- Conley R.T. and Bieron J.F., (1963a), "A Kinetic Study of the Oxidative Degradation of Phenol-Formaldehyde Polycondensates using Infrared Spectroscopy.", *J. Appl. Polymer Sci.*, **7**, 171.
- Conley R.T. and Bieron J.F., (1963b), "A Study of the Oxidative Degradation of Phenol-Formaldehyde Polycondensates using Infrared Spectroscopy.", *J. Appl. Polymer Sci.*, **7**, 103.
- Conley R.T. and Metil I., (1963), "An Investigation of the Structure of Furfuryl Alcohol Polycondensates with Infrared Spectroscopy.", *J Appl. Polymer Sci.*, **7**, 37.

- Cottinet D., Couderc P., Saint-Romain J.L. and Dhamelin court P., (1988), "Raman Micropore Study of Heat-Treated Pitches.", *Carbon*, **26**, 339.
- Coughlin R.W., Ezra F.S. and Tan R.N., (1968), "Influence of Chemisorbed Oxygen in Adsorption onto Carbon from Aqueous Solution.", *J. Colloid Interface Sci.*, **28**, 386.
- Czuchajowski L., (1961), "Infrared Spectra of Carbonised Coals and Coallike Materials and Some Adsorption Changes During Subsequent Oxidation.", *Fuel*, **40**, 361.
- DeBreet A.J.J., Dankelman W., Huysmans W.G.B. and DeWit J., (1977), "¹³C-NMR Analysis of Formaldehyde Resins.", *Die Ange. Makromol. Chem.*, **62**, 7.
- Delhaes P. and Carmona F., (1981), "Physical Properties of Noncrystalline Carbons.", *Chem. Phys. Carbon*, **17**, 123.
- Dillon R.O., Wollam J.A. and Katkanant V., (1984), *Phys. Rev. B*, **29**, 3482.
- Dixon W.T., (1981), "Spinning-Sideband-Free NMR Spectra.", *Magnet. Reson.*, **44**, 220.
- Dixon W.T., (1982), "Spinning-sideband-free and Spinning-sideband-only NMR Spectra in Spinning Samples.", *J. Chem. Phys.*, **77**, 1800.
- Dixon W.T., Schaefer J., Sefcik M.D. and McKay R.A., (1982), "Total Suppression of Sidebands in CPMAS C-13 NMR." *J. Magnet. Reson.*, **49**, 341.
- Doll G.L., Sakya R.M., Nicholls J.T., Speck J.S., Dresselhaus M.S. and Engle G.B., (1988), "Electronic and Structural Studies of Carbon/Carbon Composites.", *Synth. Metals*, **23**, 481.
- Dollimore D. and Heal G.R., (1967), "The Degradation of Selected Polymers to Carbons in an Inert Atmosphere.", *Carbon*, **5**, 65-72.
- Dradi E., Casiraghi G., Sartori G. and Casnati G., (1978), "The Design of a Versatile Synthesis of *Ortho-Ortho'* Methylene-Bridged Polyphenols. ¹³C NMR Investigation of "All-Ortho" Oligomers.", *Macromolecules*, **11**, 1295.
- Dresselhaus M.S., Dresselhaus G., Eklund P.C. and Chung D.D.L., (1977), "Graphite Intercalation Compounds: Electronic Properties in the Dilute Limit.", *Materials Sci. & Eng.*, **31**, 141.
- DuBois-Murphy P., Cassady T.J. and Gerstein B.C., (1982), "Determination of the Apparent Ratio of Quaternary to Tertiary Aromatic Carbon Atoms in an Anthracite Coal by ¹³C-¹H Dipolar Dephasing NMR", *Fuel*, **61**, 1233.
- Earl W.L. and Vanderhart D.L., (1979), "Observations in Solid Polyethylenes by Carbon-13 Nuclear Magnetic Resonance Spectroscopy with Magic Angle Sample Spinning.", *Macromolecules*, **12**, 762.
- Edwards I.A.S., (1989) in *Introduction to Carbon Science* (ed. Marsh H.), Butterworths, London.

- Evans E.L., Lopez-Gonzalez J., Martin-Rodriguez A. and Rodriguez-Reinoso F., (1975), "Kinetics of the Formation of Graphitic Oxide.", *Carbon*, **13**, 461.
- Fitzer E., Mueller K. and Schaefer W., (1971) in *Chemistry and Physics of Carbon*. (ed. Walker P.L.) pp 268, Marcel-Dekker, New York.
- Fitzer E., Schaefer W. and Yamada S., (1969), "The Formation of Glasslike Carbon by Pyrolysis of Polyfurfuryl Alcohol and Phenolic Resin.", *Carbon*, **7**, 643.
- Fitzer E. and Schaefer W., (1970), "The Effect of Crosslinking on the Formation of Glasslike Carbons from Thermosetting Resins.", *Carbon*, **8**, 353.
- Frost D.C., Leeder W.R. and Tapping R.L., (1974), "An X-ray Photoelectron Spectroscopic Investigation of Coal.", *Fuel*, **53**, 206.
- Frost D.C., Leeder W.R., Tapping R.L. and Wallbank B., (1977), "An XPS [X-ray Photoelectron Spectroscopy] Study of the Oxidation of Pyrite and Pyrites in Coal.", *Fuel*, **56**, 277.
- Fyfe C.A., Lyster J.R., Volsken W. and Yannoni C.S., (1979), "High-resolution ^{13}C nmr Studies of Polymers in the Solid-state. Aromatic polyesters.", *Macromolecules*, **12**, 757.
- Fyfe C.A., Lyster J.R. and Yannoni C.S., (1978), "High-Resolution ^{13}C Nuclear Magnetic Resonance Spectra of Frozen Liquids Using Magic Angle Spinning.", *J. Am. Chem. Soc.*, **100**, 5635.
- Fyfe C.A., McKinnon M.S., Rudin A. and Tchir W.J., (1983a), "High-resolution ^{13}C CP/MAS Solid-State NMR Spectroscopic Investigation of the Thermal Decomposition of Cured Phenolic Resins.", *J. Polymer Sci., Polym. Lett. Ed.*, **21**, 249.
- Fyfe C.A., McKinnon M.S., Rudin A. and Tchir W.J., (1983b), "Investigation of the Mechanism of the Thermal Decomposition of Cured Phenolic Resins by High-Resolution ^{13}C CP/MAS Solid-State NMR Spectroscopy.", *Macromolecules*, **16**, 1216.
- Fyfe C.A., Rudin A. and Tchir W.J., (1980), "Application of High-Resolution ^{13}C NMR Spectroscopy Using Magic Angle Spinning Techniques to the Direct Investigation of Solid Cured Phenolic Resins.", *Macromolecules*, **13**, 1320.
- Gai P.L., Billinge B.H.M. and Brown A.M., (1989), "Microstructure of Carbons.", *Carbon*, **27**, 41.
- Galuska A.A., Madden H.H. and Allred R.E., (1988), "Electron Spectroscopy of Graphite, Graphite Oxide and Amorphous Carbon.", *Appl. Surf. Sci.*, **52**, 253-271.
- Gasser R.P.H., (1985), *An Introduction to Chemisorption and Catalysis by Metals.*, Clarendon Press.
- Gerstein B.C. and Dybowski C.R., (1985), *Transient Techniques in NMR of Solids.*, Academic Press, Orlando.

Given P.H. and Hill L.W., (1969), "Analysis of Surface Groups on Carbon Blacks.", *Carbon*, **7**, 649.

Hartmann S.R. and Hahn E.L., (1962), "Nuclear Double Resonance in the Rotating Frame.", *Phys. Rev.*, **128**, 2042.

Hirsch P.B., (1954), "X-ray Scattering from Coals.", *Proc. Royal Soc. Lon.*, **226A**, 143.

Honda F. and Hirokawa K., (1976), "A Photoelectron Spectroscopic Observation of Iron Surfaces Exposed to Nitrogen, Nitrous Oxide, Nitric Oxide, Nitrogen Dioxide and Air at 200 torr or 1 atm.", *J. Electron. Spectros.*, **8**, 199.

Honda H. and Ouchi K., (1955a), "Structure of Amorphous Carbon. (IV). Density of Bakelite carbon.", *J. Chem. Soc. Japan, Pure Chem. Sect.*, **76**, 148.

Honda H. and Ouchi K., (1955c), "Structure of Amorphous Carbon. (VI). Temperature Dependence of Magnetic Susceptibilities of Bakelite Carbons.", *J. Chem. Soc. Japan, Pure Chem. Sect.*, **76**, 154.

Honda H. and Ouchi K., (1955d), "Structure of Amorphous Carbon. (VII). Change of Magnetic Susceptibilities of Bakelites During the Course of Carbonisation.", *J. Chem. Soc. Japan, Pure Chem. Sect.*, **76**, 361.

Honda H. and Ouchi K., (1955e), "Structure of Amorphous Carbon. (VIII-IX). Change of Electrical Resistance of Bakelites During the Course of Carbonisation.", *J. Chem. Soc. Japan, Pure Chem. Sect.*, **76**, 364.

Honda H. and Sanada Y., (1957), "Magnetochemistry of Coal. (I) Magnetic Susceptibility of Coal.", *Fuel*, **36**, 159.

Hu C.Z., Feng L. and Andrade J.D., (1988), "Surface Structure of Pyrolyzed Polyimide.", *Carbon*, **26**, 543.

Hummel D.O., (1984), *Atlas of Polymer and Plastics Analysis*, Verlag Chemie, Cologne.

Hummel D.O. and Scholl F., (1968), *Atlas of Polymer and Plastics Analysis*, Verlag Chemie, Munich.

Hummel D.O. and Scholl F., (1971) in *Infrared Analysis of Polymers, Resins and Adhesives.*, Wiley-Interscience, New York, pp 115.

Ianniello R.M., Wieck H.J. and Yacynych A.M., (1983), "Characterisation of Chemically Modified Carbonaceous Electrode Materials by Diffuse Reflectance Fourier Transform Infrared Spectrometry.", *Anal. Chem.*, **55**, 2067.

Ishida S., Tsutsumi Y. and Kaneko K., (1981), "Studies of the Formation of Thermosetting Resins. (XII). Computer Simulation of the Reactions of Phenols With Formaldehyde.", *J Appl. Polymer Sci.*, **19**, 1609.

Jackson W.M. and Conley R.T., (1964), "High-temperature Oxidative Degradation of Phenol-formaldehyde Polycondensates.", *J. Appl. Polymer Sci.*, **8**, 2163.

- Jewell R.A. and Sykes G.F., (1977) in *Chemistry and Properties of Crosslinked Polymers* (ed. Labana S.S.), Academic Press, New York, pp 97-106.
- Kamide K. and Miyakawa Y., (1978), "Limiting Viscosity Number-Molecular Weight Relationships for Phenol-Formaldehyde Resin in Solution.", *Makromol. Chem.*, **179**, 359.
- Keutgen W.A., (1968), *Phenolic Resins*, Wiley, New York, pp 176-208 .
- Kinoshita K., (1988), *Carbon: Electrochemical and Physicochemical Properties*, John Wiley and Sons, New York.
- Knight D.S. and White W.B., (1989), "Characterisation of Diamonds and Diamond Films by Raman Spectroscopy.", *J. Mat. Res.*, **4**, 385.
- Knop A. and Pilato L., (1985) in *Phenolic Resins, Chemistry, Applications and Performance* . Springer-Verlag, Heidelberg, pp 5-58 .
- Knop A. and Scheib W., (1979)
Chemistry and Application of Phenolic Resins., Springer-Verlag, New York.
- Kozlowski C. and Sherwood P.M.A., (1986), "X-ray Photoelectron Spectroscopy studies of carbon fibre surfaces VII-electrochemical treatment in Ammonium Salt electrolytes.", *Carbon*, **24**, 357.
- Kraus M.O. and Ferreira J.G., (1975), *J Phys. B*, **8**, 2007.
- Kumar A., Kulshershta A.K. and Gupta S.K., (1980), "Modeling of the phenol-formaldehyde polymerisation reaction.", *Polymer*, **21**, 317.
- Laupretre F., (1990), "Applications of High-Resolution Solid-State Carbon-13 NMR to Polymers.", *Prog. Polymer Sci.*, **15**, 425.
- Lausevic Z. and Marinkovic S., (1986), "Mechanical Properties and Chemistry of Carbonisation of Phenol Formaldehyde Resin.", *Carbon*, **24**, 575-580.
- Lespade P. and Marchand A., (1984), "Characterization of Carbon-containing Materials by Raman Micro-Spectrometry. (Caracterisation de Materiaux Carbones par Microspectrometrie Raman).", *Carbon* **22**, 375.
- Levy R.L., (1967), "Trends and Advances in Design of Pyrolysis Units for Gas-Chromatography.", *J. Gas Chromatography*, **5**, 107.
- Lindberg J.J., Brotherus V. and Era V.A., (1975), "Infrared Spectroscopic Investigations on Phenol-Formaldehyde Foams.", *Die Ange. Makromol. Chem.*, **45**, 77.
- Lochte H.W., Strauss E.L. and Conley R.T., (1965), "The Thermo-Oxidative Degradation of Phenol-Formaldehyde Polycondensates: Thermogravimetric and Elemental Composition Studies of Char Formation.", *J. Appl. Polymer Sci.* **9**, 2799.
- Lubenfeld A., (1977), *Analysis of surfaces by Electron Spectroscopy.*, MSc. Thesis, Monash University.

- Lyerla J.R. and Yannoni C.S., (1982), "Chemical Applications of Variable-Temperature CPMAS NMR Spectroscopy in Solids.", *Acc. Chem. Res.*, **15**, 208.
- Maciel G.E, Chuang I. and Gollob L., (1984), "Solid-State ^{13}C NMR Study of Resol-Type Phenol-Formaldehyde Resins.", *Macromolecules*, **17**, 1081.
- Maciel G.E, Chuang I. and Myers G.E., (1982), " ^{13}C NMR Study of Cured Furfuryl Alcohol Resins Using Cross Polarization and Magic-Angle Spinning.", *Macromolecules*, **15**, 1218.
- Maciel G.E., Bartuska V.J. and Miknis F.P., (1979), "Characterisation of Organic Material in Coal by Proton-Decoupled Carbon-13 Nuclear Magnetic Resonance Spectroscopy with Magic Angle Spinning.", *Fuel*, **58**, 391.
- Madorsky S.L., (1964), *Thermal Degradation of Organic Polymers*, Interscience-Wiley, New York.
- Marquardt D.W., (1963), "An Algorithm for Least-squares Estimation of Nonlinear Parameters.", *J. S.I.A.M.* **11**, 431.
- Marsh H. and Griffiths J., (1982), "Extended Abstracts", *International Symposium on Carbon*., 81.
- Marsh H. and Menendez R., (1989) in *Introduction to Carbon Science*, (ed. Marsh, H.), Butterworths, London, pp 37-42.
- Martin R.W., (1956), *The Chemistry of Phenolic Resins*, Wiley, New York.
- Mattson J.S., Mark H.B., Malbin M.D., Weber W.J. and Crittenden J.C., (1969), "Surface Chemistry of Active Carbon Specific Adsorption of Phenols.", *J. Colloid Interface Sci.* **31**, 116.
- Medalia A.I. and Rivin D., (1976), *Characterisation of Powder Surfaces*, Academic Press, New York.
- Megson N.J.L., (1958), *Phenolic Resin Chemistry*, Academic Press, New York.
- Mehring M., (1983), *Principles of High Resolution NMR in Solids*, Springer-Verlag, Heidelberg.
- Meiler W. and Meusinger R., (1991) in *Annual Reports on NMR Spectroscopy*, Academic Press, New York, pp 375-409.
- Meldrum B.J. and Rochester C.H., (1990), "Fourier Transform Infrared Study of Surface Species on Carbon Mixed With KBr and Reacted with CO_2 , O_2 and CO .", *J. Chem. Soc. Faraday Trans.*, **86**, 3647.
- Mernagh T.P., Cooney R.P. and Johnson R.A., (1984), "Raman Spectra of Graphon Carbon Black.", *Carbon*, **22**, 39.
- Morterra C. and Low M.J.D., (1982), "The Nature of the 1600 cm^{-1} Band of Carbons.", *Spectrosc. Lett*, **15**, 689.
- Morterra C. and Low M.J.D., (1983), "I.R. Studies of Carbons-II. The Vacuum Pyrolysis of Cellulose.", *Carbon*, **21**, 283.

- Morterra C. and Low M.J.D., (1985a), "I.R. Studies of Carbons-VII. The Pyrolysis of a Phenol-Formaldehyde Resin.", *Carbon*, **23**, 525.
- Morterra C. and Low M.J.D., (1985b), "An Infrared Spectroscopic Study of Some Carbonaceous Materials.", *Mater. Chem. Phys.*, **12**, 207.
- Mukoyama Y. and Tanno T., (1973), "Analyses of Synthetic Resins by Application of ^{13}C NMR.", *J. Polymer Sci.*, **11**, 3193.
- Nakamizo M., Kammereck R. and Walker P.L., (1974), "Laser Raman Studies on Carbons.", *Carbon*, **12**, 259.
- Nemanich R.J., Glass J., Lucovsky G. and Shroder R.E., (1988), "Raman Scattering Characterisation of Carbon Bonding in Diamond and Diamond-like Thin Films.", *J. Vacuum Sci. Tech.*, **A6**, 1783.
- Nemanich R.J. and Lucovsky G., (1977), "Infrared Active Optical Vibrations of Graphite.", *Solid State Commun*, **23**, 117.
- Oberlin A. and Terriere G., (1975), "Graphitisation Studies of Anthracites by High-Resolution Electron Microscopy.", *Carbon*, **13**, 367.
- Olejniczak E.T., Vega S. and Griffin R.G., (1984), "Multiple pulse NMR in Rotating Solids.", *J. Chem. Phys.*, **81**, 4804.
- Opella S.J., Frey M.H. and Cross T.A., (1979), "Selection of Nonprotonated Carbon Resonances in Solid-State Nuclear Magnetic Resonance.", *J Am. Chem. Soc.*, **101**, 5854.
- Ouchi K., (1955), *Rep. Resources Res. Inst., Japan*, 31.
- Ouchi K., (1966), "Infra-red Study of Structural Changes During the Pyrolysis of a Phenol-Formaldehyde Resin.", *Carbon*, **4**, 59.
- Ouchi K. and Honda H., (1956), "Structure of Amorphous Carbon. (X). X-ray studies on the carbonisation of Bakelite.", *J. Chem. Soc. Japan, Pure Chem. Sect*, **77**, 147.
- Ouchi K. and Honda H., (1959), "Pyrolysis of Coal I - Thermal Cracking of Phenolformaldehyde Resins Taken as Coal Models.", *Fuel*, **38**, 429.
- Painter P.C., Rimmer S.M., Snyder R.W. and Davis A., (1981), "A Fourier Transform Infrared Study of Mineral Matter in Coal: The application of a Least Squares Curve-Fitting program.", *Appl. Spectrosc.*, **35**, 102.
- Painter P.C., Snyder R.W., Starsinic M., Coleman M.M., Kuehn D.W. and Davis A., (1981), "Concerning the Application of FT-IR to the Study of Coal: A Critical Assessment of Band Assignments and the Application of Spectral Analysis Programs.", *Appl. Spectrosc.*, **35**, 475.
- Pattabiraman P., Rodriguez N.M., Jang B.Z. and Baker R.T.K., (1990), "A study of the Interaction of Atomic oxygen with Various Carbonaceous Materials.", *Carbon*, **28**, 867.

- Perkins R.M., Drake G.L. and Reeves W.A., (1966), "Differential Thermal Analysis and Thermogravimetric Analysis Studies of Flame Resistant Fabrics.", *J. Appl. Polymer Sci.*, **10**, 1041.
- Pines A., Gibby M.G. and Waugh J.S., (1973), "Proton-enhanced NMR of Dilute Spins in Solids.", *J. Chem. Phys.*, **59**, 569.
- Pouchert C.J., (1985), *The Aldrich Library of FT-IR Spectra.*, Aldrich Chemical Company, Milwaukee.
- Ramsteiner M. and Wagner J., (1987), "Resonant Raman Scattering of hydrogenated Amorphous Carbons: Evidence for π -bonded Carbon Clusters.", *Appl. Phys. Lett.*, **51**, 1355.
- Resing H.A., Garroway A.N. and Hazlett R.N., (1978), "Determination of the Aromatic Hydrocarbon Fraction in Oil Shale by Carbon-13 NMR Spectroscopy with Magic-Angle-Spinning.", *Fuel*, **57**, 450.
- Retcofsky H.L. and Vanderhart D.L., (1978), "Carbon-13-Proton Cross-Polarisation Nuclear Magnetic Resonance Spectra of Macerals from Coal.", *Fuel*, **57**, 421.
- Riesz C.H. and Susman S., (1960), *Proceedings of the Fourth carbon Conference.*, Pergamon Press, London, pp 609 .
- Rivin D. and Illinger J.L., (1969), "Desorption of Organic Adsorbates From Carbon. I. Chemisorbed Acetone on Carbon Black.", *J. Colloid Interface Sci.*, **31**, 85.
- Rouzaud J.N., Oberlin A. and Beny-Bassez C., (1983), "Carbon Films: Structure and Microtexture (Optical and Electron Microscopy, Raman Spectroscopy).", *Thin Solid Films*. **105**, 75.
- Schaefer J., Stejskal E.O. and Buchdahl R., (1977), "Magic-Angle ^{13}C NMR Analysis of Motion in Solid Glassy Polymers.", *Macromolecules*, **10**, 384.
- Schaefer J. and Stejskal E.O., (1976), "Carbon-13 Nuclear Magnetic Resonance of Polymers Spinning at the Magic Angle.", *J. Am. Chem. Soc.*, **98**, 1031.
- Schmidt D.L., (1971) *Ablative Plastics*, Dekker, New York.
- Secrest P.J., (1965), "Infrared Studies of Phenolic Resins", *Off. Digest, Fed. Paint Technol.*, **37**, 187.
- Segal C.L., (1967), *High Temperature Polymers*, Dekker, New York.
- Shulman G.P. and Lochte H.W., (1966), "Thermal Degradation of Polymers. II. Mass Spectrometric Thermal Analysis of Phenol-Formaldehyde Polycondensates.", *J. Appl. Polymer Sci.* **10**, 619.
- Siling M.I., Urman Y.G., Adorova I.V., Alekseyeva S.G., Matyukhina O.S. and Slonim I.Y., (1977), "Structural Characteristics of Phenol-Formaldehyde Novolak Oligomers.", *J Polymer Sci.*, **19**, 358.

Simitzis J., (1991), "Composites of Furfuryl Alcohol-formaldehyde Resins and Olive Stones for Production of Activated Carbons.", *Die Ange. Mak. Chem.*, **184**, 41.

Siperko L.M., (1990), "Scanning Tunneling Microscopy and Raman Spectroscopy of Pyrolytic Graphite Electrodes.", *J. Electrochem. Soc.*, **137**, 2791.

Slade P.E. and Jenkins L.T., (1966), *Thermal Analysis*, Marcel-Dekker, New York.

Socrates G., (1980), *Infrared Characteristic Group Frequencies.*, Wiley, New York.

Sojka S.A., Wolfe R.A., Dietz E.A. and Dannels B.F., (1979), "Carbon-13 Nuclear Magnetic Resonance of Phenolic Resins. Position Isomers of Bis(hydroxybenzyl)phenols and Bis(hydroxyphenyl)methanes.", *Macromolecules* **12**, 767.

Solomon P.R. and Carangelo R.M., (1988), "FTIR Analysis of Coal. 2. Aliphatic and aromatic hydrogen concentration.", *Fuel* **67**, 949.

Sullivan M.J. and Maciel G.E., (1982), "Spin Dynamics in the ^{13}C Nuclear Magnetic Resonance Spectrometric Analysis of Coal by Cross Polarisation and Magic-Angle Spinning.", *Anal. Chem.*, **54**, 1615.

Supaluknari S. *Structural Characterisation of Australian Coals by FTIR and Solid-State ^{13}C NMR Spectroscopies.*, PhD Thesis, University of Tasmania, 1989.

Supaluknari S., Burgar I. and Larkins F.P., (1990), "High-resolution Solid-State ^{13}C NMR Studies of Australian coals.", *Org. Geochem.*, **15**, 509.

FTang M.M. and Bacon R., (1964), "Carbonisation of Cellulose fibres. (I). Low Temperature Pyrolysis. (II). Physical Property Study.", *Carbon*, **2**, 211.

Theriault Y. and Axelson D.E., (1988), "Solid state ^{13}C NMR Dipolar Dephasing Study of Canadian Coals.", *Fuel*, **67**, 62.

Tither D., Dehbi A., Holiday P., Matthews A., Fitzgerald A.G., Henderson A.E., Storey B.E., Dines T.J., John P. and Wilson J.I.B., (1990), "The Characterisation of Ultra-hard Carbon Films Produced From Pre-processed Carbon Powder in a Hybrid Physical Vapour Deposition System.", *Carbon*, **28**, 641.

Tuinstra F. and Koenig J.L., (1970), "Raman Spectrum of Graphite.", *J. Chem. Phys.*, **53**, 1126.

Van Krevelen D.W., (1961), *Coal*, Elsevier, Amsterdam.

Vidano R.P., Fischbach D.B., Willis L.J. and Loehr T.M., (1981), "Observation of Raman band Shifting With Excitation Wavelength for Carbons and Graphites.", *Solid State Comm.*, **39**, 341.

Wandass J.H., Gardella J.A., Weinberg N.L., Bolster E. and Salvati L., (1987), "X-ray Photoelectron and Scanning Auger Electron Spectroscopic Studies of Oxidised Graphite Electrode Surfaces.", *J. Electrochem. Soc., Electrochem. Sci. & Tech.*, **134**, 2734.

- Wehrli F.W. and Wirthlin T., (1976), *Interpretation of Carbon-13 NMR Spectra.*, Heyden, London.
- Weightman P., (1976), "Relaxation processes Accompanying Cadmium $M_{4,5}N_{4,5}N_{4,5}$ Auger Transitions.", *J. Phys. Chem.*, **9**, 1117.
- Wendlandt W., (1964), *Thermal Methods of Analysis*, Interscience-Wiley, New York.
- Whitehouse A.A.K., Pritchett E.G.K. and Barnett G., (1967), *Phenolic Resins*, Iliffe, London.
- Wilson M.A., Pugmire R.J., Karas J., Alemany L.B., Woolfenden W.R., Grant D.M. and Given P.H., (1984), "Carbon Distribution in Coals and Coal Macerals by Cross-Polarisation Magic Angle Spinning Carbon-13 Nuclear Magnetic Resonance Spectrometry.", *Anal. Chem.*, **56**, 933.
- Winkler E.L. and Parker J.A., (1971), "Molecular Configuration and Pyrolysis Reactions of Phenolic Novolaks.", *J Macromol. Sci., Revs. Macromol. Chem.*, **5**, 245.
- Wychoff R.W.G., (1963), *Crystal Structures*, Wiley-Interscience, New York.
- Yamashita Y. and Ouchi K., (1981), "A study on Carbonisation of Phenol-Formaldehyde Resin with Deuterium and ^{13}C .", *Carbon* **19**, 89.
- Yannoni C.S., (1982), "High-resolution NMR in Solids: The CPMAS Experiment.", *Acc. Chem. Res.*, **15**, 201.
- Yoshida A., Tanahashi I. and Nishino A., (1990), "Effect of Concentration of Surface Acidic Functional Groups on Electric Double-layer Properties of Activated Carbon Fibers.", *Carbon*, **28**, 611.
- Young P.R. and Chang A.C., (1988), "FTIR Characterization of Thermally Cycled PMR-15 Composites.", *3rd Intern. SAMPE Symp.*, 538.
- Zinke A., (1951), "The Chemistry of Phenolic Resins and the Processes Leading to Their Formation.", *J. Appl. Chem.*, **1**, 257.